Chapter 1

Introduction

1.1Background

Vibration refers to mechanical oscillations with respect to an equilibrium position [1]. In most cases, vibration is undesirable creating noise and potentially harmful response. According to these detrimental effects, engineers are motivated to find approaches to control vibration levels.

Vibration control measures can be classified into passive vibration control, semi-active vibration control and active vibration control. Passive vibration control is typically achieved by changing the mass, stiffness or damping [2]. The latter is applicable for resonance behaviour and energy dissipation, whilst changing the mass or stiffness will change the natural frequencies which might be of benefit. It is usually simple to implement, reliable and cost efficient, but its successful application requires a thorough understanding of the excitation and the vibration problem in hand [2]. Semi-active vibration control can be broadly defined as a passive vibration control measure in which the systems mechanical properties, such as stiffness and damping, can

be adjusted in real time by the application of a control signal [3, 4]. The semi-active system can possess the reliability of passive control using a small amount of energy to tune the system. It also supplies the versatility and effective performance at high frequencies [3, 5]. Its main disadvantage is its inherent nonlinearity and complicated engineering design. Fully active vibration control augments the system with actuators, sensors and some form of electronic controller together with signal conditioning devices to achieve the modification of the characteristics of the vibrating system [4]. The active systems require external energy to drive active devices continuously. However, its practical applications are limited due to the cost, stability and energy consumption [4].

In some cases, e.g. for harmonic excitation, then the use of tuned passive devices such as vibration absorbers [2] might be applicable and is the passive control method in this study. It is not feasible to use active controllers for vibration control in many practical applications. The reasons include the cost, added weight or required external power supply. For typical harmonic vibration control, passive vibration control system can also make for a relatively simple analytical approach. Hence, designs are sought, based on passive vibration control, for harmonic excitation and response [6].

This chapter briefly introduces the literature on the vibration response for linear and nonlinear vibration absorbers. The following chapters will present the absorber dynamic characteristics of a nonlinear absorber system under harmonic and random excitations.

1.2 Dynamic vibration absorbers

Dynamic vibration absorbers (DVAs), also sometimes called tuned mass dampers or vibration neutralizers, consist of mass, stiffness and damping elements. They are usually used in two distinct and different ways; the dynamic vibration absorber is tuned to a troublesome resonance of the host structure to which it is applied and the neutraliser is tuned to a problematic excitation frequency [2]. The purpose of a dynamic vibration absorber is to reduce the structural vibration at the resonance frequency, and the purpose of the vibration neutralizer is to add a large mechanical impedance to the host structure to minimize the structural vibration at a single frequency of excitation [7].

Dynamic vibration absorbers are important practical devices used for vibration reduction in structures (cf. Figure 1.1-1.2 [8, 9]). When connected to a structure or machine, the dynamic vibration absorbers are capable of absorbing the vibrational energy. Therefore, these devices have been used extensively in the vibration reduction of machinery and are typically applied when structures are excited near their resonance frequencies. Consequently, a structure can be protected from excessively high vibration levels [10]. Thus, the problem of how to improve the effectiveness of the vibration reduction using a dynamic vibration absorber, which occurs at frequencies around which it is tuned, and its optimal design are important research topics in the field of structural dynamics.

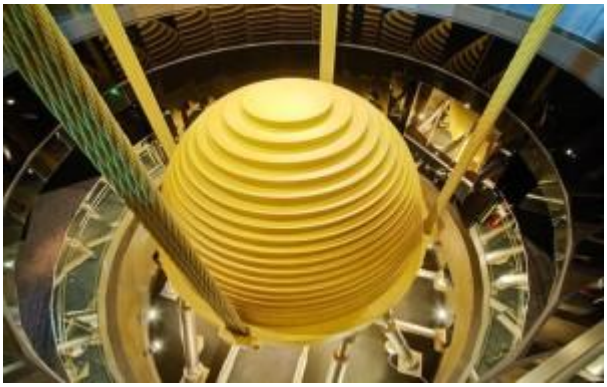

Figure 1.1 Dynamic vibration absorber is installed to the Taipei 101 to counteract vibrations in the building [8].

Figure 1.2 Multiple dynamic vibration absorbers are installed to a bridge [9].

1.3 The linear dynamic vibration absorber

Passive vibration mitigation of mechanical structures is often associated with the dynamic vibration absorber developed by Den Hartog [11]. The passive linear absorber is well-known and has been extensively studied [2, 7]. In its simplest form it consists of a mass supported by a linear elastic spring acting in parallel with a viscous damper. The design of this absorber relies on a solid theoretical basis, and the absorber possesses very well known properties (e.g., its capability to mitigate the response in one mode of the primary structure, the trade-off between performance and robustness and the introduction of a second resonance frequency). As will be described below, it appears that their performance is dependent upon the choice of the system properties and typically they act over a narrow band of frequencies. Den Hartog has presented the design formula for the optimal linear absorber [11]. In his book one can find the detailed investigation of optimal tuning and damping parameters. However, the vibration reduction bandwidth of *Den Hartog's optimal criterion* is different compared to that presented in the following section. Den Hartog's optimal criterion presents the vibration response to pass through two invariant points in the frequency response curve for the primary system, where its response amplitude is independent of the damping of the absorber system. The stiffness value that results in equal amplitudes at the invariant points is taken to be optimal [11-13].

1.3.1 Vibration reduction bandwidth

Ormondroyd and Hartog [14] derived the mathematical treatment of the linear absorber suppressing the vibration response of an undamped single-degree-of-freedom primary system. The model is shown in Figure 1.3 where k_s and m_s are the linear spring constant and mass of the primary system under harmonic external force $F\cos(\omega t)$; x_s is the displacement of the primary system. For the absorber, it has a mass m, a viscous damper c and a linear spring k_1 with x the displacement of the absorber mass. The mathematical expression for the non-dimensional terms as used by Den Hartog [11] are the mass ratio $\mu = m/m_s$, the damping ratio of the absorber $\zeta = c/2m\omega_1$, the linear tuned frequency ratio $\omega_0 = \omega_1/\omega_s$ and the excitation frequency ratio $\Omega = \omega/\omega_s$. The variables used for inspecting the performance of the absorber are the maximum amplitude X_s, which is the displacement amplitude of the primary system, X_0 the static displacement amplitude of the primary system due to a static force of magnitude F, given as $X_0 = F/k_s$.

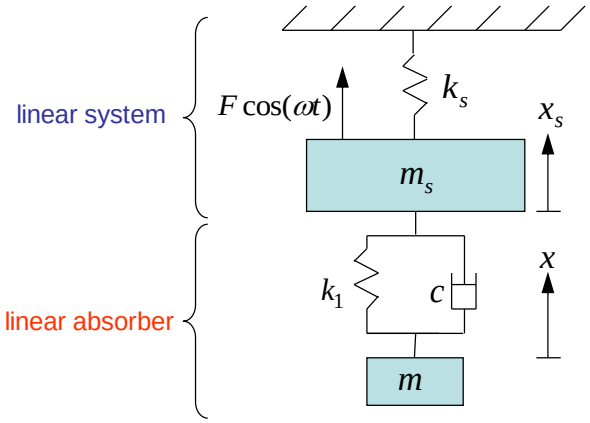

Figure 1.3 A linear dynamic vibration absorber (DVA) attached to an undamped single degree-of-freedom primary system.

The primary system frequency response, the amplitude ratio of the response normalized by the static displacement for a static force of equal amplitude to the excitation force, X_s / X_0, is shown in Figure 1.4. The effect of a damped vibration absorber is beneficial vibration attenuation around the structures resonance frequency range compared to the linear system without an absorber.

The effectiveness of the nonlinear absorber was first quantified and defined by Roberson [15] who introduced the concept of a "Vibration reduction bandwidth". The Vibration reduction bandwidth of an absorber is produced when the amplitude ratio is less than unity, i.e. $\left|X_s / X_0\right| \le 1$, i.e. a dynamic response reduction compared to a static response level is achieved, which is shown by a thin horizontal solid line in Figure 1.4. The vibration reduction bandwidth is then to be determined such that $\left|X_s / X_0\right| \le 1$ in that the frequency range. The frequency range is $\Omega_L \le \Omega \le \Omega_R$, where Ω_L and Ω_R are the lower and upper frequency bounds for the vibration reduction bandwidth range respectively. The "Vibration reduction bandwidth" is restricted to discussion on the frequency values between the resonance peaks of the frequency response curves. This frequency bandwidth can be determined as $\Omega_B = \Omega_R - \Omega_L$, and the width of this band has been compared for both linear and nonlinear stiffness absorbers [15, 16].

The vibration attenuation amplitude is used to examine the effectiveness of the linear absorber. The vibration attenuation is determined by the ratio between the vibration amplitude at the tuned frequency with an absorber and the amplitude of the primary system without an attached absorber. The analytical expression for the vibration attenuation of a linear absorber has been obtained [7]. However, the analytical expression for the vibration attenuation of the nonlinear absorber could be difficult to derive, due to the complexity of the mathematical algebraic relationships. The detailed derivation of the solution in the latter case will be presented in chapter 3.

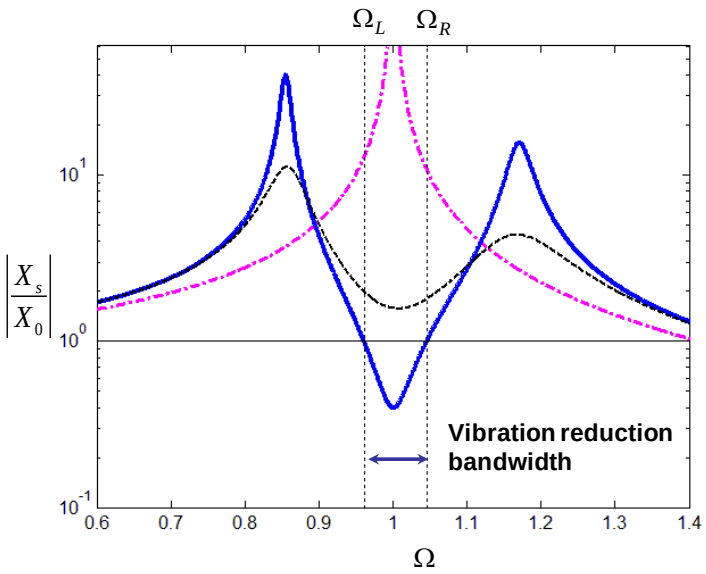

Figure 1.4 The frequency response curves of the normalised displacement on the primary system $|X_s / X_0|$ as a function of the non-dimensional excitation frequency $\Omega = \omega/\omega_s$ showing the vibration reduction bandwidth for a system with a linear vibration absorber attached ($\mu = 0.1$, $\omega_0 = 1$). The response for the single system without an absorber is given by the dashed-dotted line. For the linear absorber, the solid line is the low damping case with the absorber damping given by $\zeta = 0.02$ and the dashed line is the high damping absorber with $\zeta = 0.08$.

1.4 The nonlinear dynamic vibration absorber

There are some known limitations with the linear vibration absorber, for which a passive nonlinear absorber might have some advantages. Whatever nonlinear device is considered, it will preferably need both analytical study and experimental validation. The structure vibrates as a result of periodic excitation such as unbalanced rotating machines [17]. It is important to analyse the effects and behaviour of such excitations on vibrating systems to understand the foundation for the analysis of more general types of excitation [2, 11, 17, 18]. The periodic motion provides a basis of characterization of more complicated dynamic motions. Random vibration is non-deterministic motion where the response can be described on the basis of probabilistic and statistical approaches [18-20]. Many structures respond dynamically to random environmental loads such as an automobile driving across a rough road and ground motion due to an earthquake [20, 21]. The response to broadband random vibration of a nonlinear system is likely to be more complicated dynamic behaviour.

A linear absorber has a major drawback, it is limited in that it reduces vibration over a very narrow frequency range. This range is typically not large enough to cope with practical cases that correspond to changes in the excitation frequency, i.e. in speed for a rotating unbalanced source due to load, motor power supply or source variations [15]. To overcome this problem, the linear absorber can be designed to act as a wideband device by adding mass to the absorber. However, it is undesirable for the absorber mass to be too large in many applications because additional static loading of the primary system will occur. As a result, the absorber mass is typically restricted to a factor equivalent of about 10% or less of the primary system mass. In addition, the potentially large size and weight in structural applications are significant limitations [2].

In the light of some of the limitations, interest has arisen in the use of a nonlinear dynamic vibration absorber (NDVA). A technical benefit of the NDVA has been hypothesized that it can operate efficiently over a broader range of forcing frequencies.

1.4.1 The nonlinear dynamic vibration absorber under periodic excitation

The vibration bandwidth problem was first investigated by Roberson [15] who used the impractical case of an undamped absorber comprising a mass supported by a linear plus nonlinear spring acting in parallel. The nonlinear spring was chosen to produce a restoring force which is proportional to its extension and compression raised to a power of three (subsequently termed a cubic spring). The first approximation of a nonlinear system is obtained by the Duffing Iteration Method which investigates the effect of the parameters of the system. Pipes [22] used a hyperbolic sine spring with a hardening characteristic which followed Roberson's method. The characteristic of a hardening spring is that as the restoring force increases, then the difference in the displacement of the spring will be decreased. The benefit of a hardening spring is that it does not produced an unstable response [23]. In addition, Arnold [24] later confirmed Roberson's results.

Hunt and Nissen [16] presented a practical NDVA with a softening spring composed of a stack of Belleville washers to demonstrate double vibration bandwidth compared to a linear absorber. The response of the system is obtained by a numerical integration solution (Runge-Kutta-Nystrom method). The main inherent disadvantage of a softening spring is an unstable phenomenon which is produced due to large displacement over a critical value [23]. The unstable behaviour can change very suddenly and dramatically [25]. Nissen *et al.*[26] studied the optimal parameters of a NDVA and considered the technical aspects for realisation. Rice *et al.* [27] presented the nonlinear vibration absorber incorporating an asymmetric nonlinear element (a linear plus cubic springs) with hardening or softening behaviour and a solution by the harmonic balance method. Investigation of the system parameters, for a selection of spring types for narrow-band absorption applications, showed results that are up to 50% better than the linear absorber. It was found that a hardening absorber is equally as good as a softening one for maximizing the bandwidth.

Vibration reduction response has been reported using solutions obtained by the averaging method for a nonlinear vibration absorber [28], but no comparison of its efficiency has been performed. Zhu *et al.*[29] studied the system with nonlinear damping and nonlinear springs using the averaging method. They found that vibration reduction can be obtained by adjusting the parameters of the nonlinear dampers and the nonlinear spring stiffness from an examination

of the frequency response. It has also been demonstrated [30-33] that the primary phenomena behind the energy pumping produced, which refers to energy from a primary subsystem to a nonlinear attachment, is due to resonant interactions between coupled linear and nonlinear components. Sun *et al*. [34] investigated the response attenuation of a hardening Duffing oscillator utilizing a nonlinear absorber, a semi-active absorber and a multiple absorber consisting of the two in parallel. The multiple absorber was found to effectively reduce the steady state response. Some studies designed a practical oscillator with different components producing the nonlinear stiffness characteristics experimentally. Examples of such components are the pneumatic spring [35], magnets [36-38], Belleville washers [16, 26] and springs [6, 39-42].

Miller and Gartner [35] presented measurements on a pneumatic spring absorber with hardening characteristics and provided a detailed design of a prototype. Yamakawa et al. [36] presented a absorber consisting of magnets with hardening characteristics using different material of the magnets to investigate the vibration reduction. Kojima and Nagaya [37] analyzed a magnetic torsional dynamic vibration absorber with softening characteristics to investigate the optimum absorbing effect. Hunt *et al.* [16] and Nissen *et al.* [26] provided dynamic vibration absorbers with softening springs (Belleville washers) to demonstrate wider vibration reduction bandwidth compared to a linear absorber. Nissen *et al.* [26] provided guidance on the design of the Belleville washer as an absorber spring.

Rice [40] has presented the nonlinear vibration absorber (bow-type spring) incorporating an asymmetric nonlinear element (a linear plus cubic springs) with hardening or softening behaviour. The experimental data was investigated for a selection of the parameters for the absorber and its vibration reduction. Nayfeh [41] and Balachandran [42] investigated experimentally systems with a nonlinear element (a quadratic spring) which exhibited quasiperiodic and chaotic regimes at certain frequency. The undesirable responses could only be eliminated by careful tuning of the systems' frequencies. It is not a desirable way for a practical passive absorber.

Jiang *et al.*[6] investigated a nonlinear energy sink (a cubic spring) with hardening characteristics attached to a linear primary structure under sinusoidal excitation both theoretically and experimentally. They presented the energy absorption by the nonlinear energy

sink, realised a more broad frequency range, producing a which effective frequency range. Gatti *et al*.[39] designed a hardening oscillator (a linear plus cubic springs) to investigate the dynamic responses at the resonance frequencies of a nonlinear two degrees-of-freedom system. However, the result could not produce vibration reduction of the primary system as the mass of the nonlinear system was much smaller compared to the mass of the primary system.

The nonlinearity considered can present a stability problem for the primary and absorber system. It will affect significantly the vibration effectiveness of the absorber. Instability should be avoided by choice of the nonlinear absorber design. The instability characteristics refer to the system undergoing amplitude changes very suddenly and dramatically [25]. Many studies presented the stability characteristics for different forms of nonlinear stiffness characteristics [28, 43-47]. Rice [43] investigated the combinational instability using a perturbation method for the nonlinear absorber design. It was found that the nonlinearity will present an undesirable response for the almost-periodic response. Shaw *et al*. [44] found that the presence of nonlinearities introduced dangerous instabilities using the method of multiple scales. In some cases, the nonlinearity may lead to response amplification rather than vibration reduction. For this reason, for the design of an efficient NDVA it is necessary to develop a completely analytical procedure, which in addition to predicting the steady state responses also analyzes their stability characteristics. Stability here refers to the system undergoing smooth changes in their response [25]. Natsiavas [28] analyzed the stability characteristics of a nonlinear response and periodic steady state solutions were located and identified. By proper selection of the system parameters the resulting solutions avoided the dangerous consequences of instability. Malatkar and Nayfeh [46, 47] analyzed the stability characteristics of the steady-state vibration response for the nonlinear oscillator attached to the linear subsystem. It might cause increasing response in the linear subsystem when the damping of linear subsystem is low.

1.4.2 The nonlinear dynamic vibration absorber under transient excitation

Transient response occurs for a dynamical system excited by a suddenly nonperiodic excitation, such as when sudden load changes are initiated. For transient excitation studies, some researchers [6, 48-50] published data showing that a nonlinear absorber uses a smaller mass than a linear absorber to produce the same vibration reduction and effectively reduces the transient response of the primary structure. Similarity, Sun *et al*.[34] investigated the vibration

reduction of a hardening Duffing oscillator using the multiple absorber. The multiple absorber was found to be effective in reducing the transient response compared to a nonlinear vibration absorber.

1.4.3 The nonlinear dynamic vibration absorber under random excitation

Random vibration is a vibration phenomenon under an excitation satisfactorily modelled by a stochastic process [20]. The excitation and the system response can be described on the basis of probabilistic and statistical approaches. Many researchers present the development of the theory for random vibration [51, 52]. Applications of random vibration vary widely from aerospace industries, random road inputs in vehicles to the collapse of structures due to random loading [53]. These problems involve the structural responses due to random loading and nonlinear response resulting from large motions [53]. Many practical dynamic systems are also exposed to wide band frequency excitations, rather than single frequency excitation. A linear absorber is insufficient for such cases [54].

Lee [55] investigated a primary system coupled with a pendulum absorber under random excitation for autoparametric response, in which the absorber region improves as the damping increases. The autoparametric response is the varying of the parameters drives the system. Examples of parameters that may be varied are its resonance frequency and damping [56]. Rüdinger [57] investigated the performance of nonlinear viscous damping for a nonlinear absorber attached to a SDOF primary system excited by white noise. It was found that damping has a slight effect on the optimal parameters for a nonlinear absorber. In addition, the optimal linear and nonlinear absorbers have approximately the same effect in terms of vibration reduction.

The experimental investigation of nonlinear system is to validate the analytical results and to provide physical insight into complex response characteristics [58, 59]. Some studies have been conducted on the nonlinear vibration absorber using different components attached to a primary structure for autoparametric response system. Examples of such components are beam-type systems [59, 60] and pendulum-type systems [54]. Cuvalci [60] investigated experimentally an autoparametric system comprising a nonlinear absorber attached to the primary system under both sinusoidal and random excitations. The absorption region for the nonlinear absorber was

defined and the performance investigated as a function of the parameters of the vibration absorber. Cicek [54] determined the energy transfer between a beam, representing a primary structure, and a NDVA represented by a pendulum for autoparametric response system. This work provided the scope and limitations of the beam–pendulum oscillator as a potential vibration absorbing device.

1.5 Motivation for this study

From the review of the existing literature presented, the nonlinear absorber produces complex nonlinear dynamic responses. The nonlinear absorber is still not fully explored for its potential usage. An objective was to analyze the richness and complexity of nonlinear system in order to improve the design of vibration absorber. In addition, it can be seen that experimental results for the nonlinear absorber have not been widely published and sporadic attempts not supported by analytical predictions. Due to the somewhat limited work and understanding of the nonlinear absorber, then there is still a need for some further fundamental research. The aim of this thesis is to partially fill this gap and to investigate the benefits of using additional cubic nonlinearity in the elastic element of the vibration absorber in order to improve the effectiveness of such a nonlinear device.

1.6 Objectives and contributions

Given the fairly limited literature concerning the nonlinear dynamic vibration absorber (NDVA), this project was conceived. The specific objectives of the study were as follows:

- To develop a complete analytical expression and verify the numerical solutions that describe the performance of the particular NDVA under harmonic excitation. Subsequently, investigate the response and its sensitivity to the various physical parameters of the absorber namely the absorber mass, damping and stiffness. The latter possesses restoring force contributions which are both linear and nonlinear cubic powers of the displacement.
- To analyze the bifurcation and stability characteristics of the periodic steady state response and identify when, under periodic excitation, the response is not periodic.

- Determine whether the NDVA under harmonic excitation suffers from the problem of amplification and resonances outside the controlled bandwidth. Also, determine the bandwidth for control in comparison to the linear case.
- To investigate the performance of the various parameters of the NDVA under random excitation.
- To provide experimental validation for the vibrational characteristics of the NDVA and compare the results with the predictions.

The **original contributions** presented in this thesis are as follows:

For harmonic excitation

- An original derivation and formulation of approximate analytical expressions for the steady state response of a simple MDOF system (primary system with attached NDVA) using the harmonic balance method.
- Presentation of an in-depth analysis and interpretation of the parameters which affect the bifurcation and stability characteristics of the periodic steady state response.
- Presentation of an in-depth analysis and interpretation of the parameter range which affects the vibration response and determines the vibration reduction bandwidth.

For random excitation

- Presentation of an in-depth analysis and interpretation of the parameter range which affects the vibration response in the primary system has been produced using numerical simulations.

Experimental Validation

- An original design for a nonlinear absorber rig, for which the nonlinear stiffness and mass of absorber can be easily changed, has been provided.
- The implementation of the practical nonlinear absorber under harmonic excitation shows a broader vibration reduction frequency bandwidth, supporting and validating the theoretical predictions.
- The implementation of a practical nonlinear absorber under random excitation; the measurement provided a vibration response behaviour to support and validate the theoretical predictions.

1.7 Outline of the thesis

This study is concerned with the passive nonlinear dynamic absorber attached to a linear primary structure. The problem is first studied here analytically, to determine the most important features, before an experimental design is presented, implemented and its behaviour presented and discussed. The structure of this thesis is shown in Figure 1.5 and the contents of Chapters 2 to 6 are briefly described as:

Chapter 2: A mathematical model of the system is developed. Next, an approximate periodic solution of the system is determined using the Harmonic Balance Method (HBM). In addition, the bifurcation and stability of the steady-state solution is analyzed.

Chapter 3: The effect of the nonlinear absorber's physical parameters on the frequency response curve is investigated. In particular, the linear tuned frequency of the nonlinear absorber, the effect of damping, the amount of stiffness nonlinearity and the absorber mass ratio are considered and the subsequent effects on the response are produced and examined in detail.

Chapter 4: Statistical techniques for investigating the response under random excitation and the frequency response analysis is briefly described before application to numerical simulations investigating the dynamic behaviour of a system with an attached nonlinear vibration absorber. Control parameters (e.g., random input amplitude, nonlinear stiffness, damping ratio and mass ratio) are considered at different levels and the random response related to the effectiveness of the absorber is considered.

Chapter 5: Design, experimental implementation and measurement on a nonlinear absorber which is used to validate the model under both harmonic and random excitation cases.

Chapter 6: Conclusions of the current research work are presented and recommendations made for future investigations and projects.

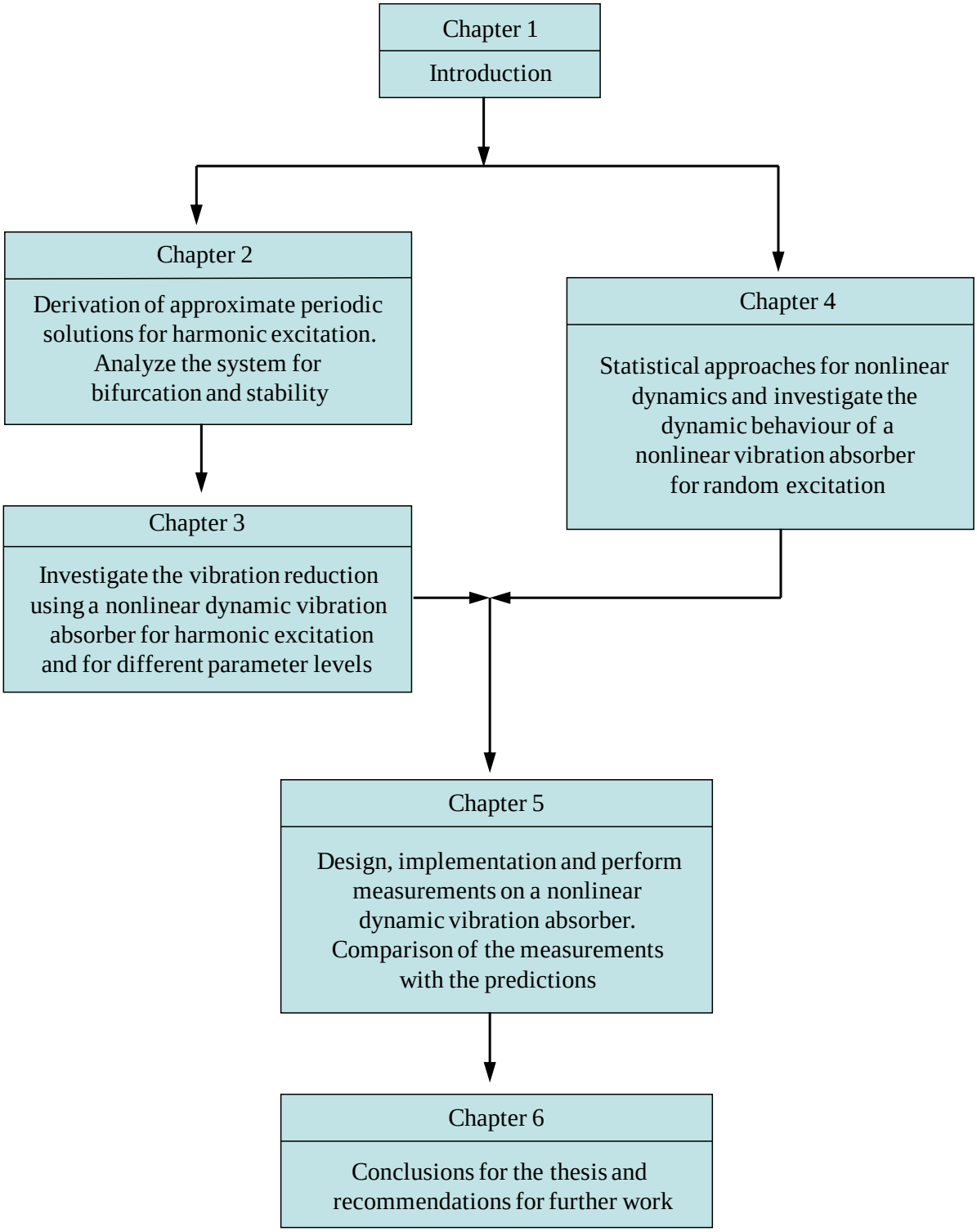

Figure 1.5 Structure of the thesis.

Chapter 2

Analysis of a single degree of freedom system with an attached nonlinear absorber under harmonic excitation

In order to produce the stiffness property of the nonlinear absorber, the system is selected to have symmetric stiffness properties i.e., the stiffness characteristic is the same when the spring is in compression or in tension, then the restoring force is an odd function in the displacement [23]. The combination of a linear plus cubic spring acting in parallel can be designed to have linear behaviour for low response levels and strongly nonlinear cubic behaviour for higher response [16, 24, 28, 39, 45, 61-63]. The characteristic of a hardening spring is that as the restoring force increases, then the difference in the spring displacement will be decreased. The benefit of a hardening spring is that it does not produced an unstable response [23]. However, in contrast the main inherent disadvantage of a softening spring is an unstable phenomena which is produced due to large displacement over a critical value [23]. The form considered in this study is only the case of a symmetric and hardening vibration absorber (linear plus positive cubic spring).

A primary purpose of this chapter is to derive the equations of motion of the entire dynamic system (i.e., the single degree-of-freedom mass-spring-damper primary structural system installed with a NDVA). This nonlinear absorber is designed to behave as the modelled

hardening vibration absorber. The mathematical expressions for calculating the frequency response curves of the primary structural system are determined for the harmonic steady state response at the harmonic excitation frequency. The nonlinear differential equations of motion are solved using the Harmonic Balance Method (HBM); simple approximate formulae for the description of the vibration are subsequently derived and produced. The detailed procedures are presented in the following sections. The investigation presented is focused on producing analytical expressions that describe the performance of the NDVA, i.e. its vibration reduction effectiveness and frequency bandwidth compared with a linear DVA. Achieving this might help to improve the design of a NDVA.

To obtain these approximate expressions, there is a need to establish an analytical relationship between the response amplitude and the frequency of excitation. It is the vibration reduction of the primary system at the excitation frequency that is the main component of interest in many practical problems for harmonic excitation. As far as possible, the equations and expressions obtained can be expressed in terms of non-dimensional parameters that will be introduced. The procedure which analyzes the bifurcation and stability characteristics of the identified periodic and harmonic steady state solutions are also presented separately. In some situations a non-harmonic response will occur and this is also considered.

2.1 Derivation of the governing equations of motion

As shown in Figure 2.1, the NDVA is attached to a linear single degree-of-freedom mass-spring-damper primary structural system. In the figure, k_s, c_s and m_s are the linear spring constant, viscous damping coefficient and mass of the primary structural system respectively; x_s, $\dot{x}_s$ and $\ddot{x}_s$ are the displacement, velocity and acceleration of the primary structural system respectively. For the NDVA, it has a mass m, a viscous damper c and a nonlinear spring with a nonlinear restoring force given by a general function $f(x) = k_1 x + k_3 x^3$, where x is the displacement across the spring, which has linear and nonlinear stiffness terms k_1 and k_3 respectively. The sign of k_3 denotes the nonlinear stiffness behaviour; a positive value means that the system is hardening and is considered in this study. x, $\dot{x}$ and $\ddot{x}$ are the displacement, velocity and acceleration of the mass m of the NDVA respectively.

Figure 2.2 shows the typical static restoring force function versus the displacement of the spring for the linear and linear plus cubic combination. The tangent to the force versus deflection curve is known as the tangent stiffness and the hardening characteristic corresponds to an increasing tangent stiffness for the nonlinear spring modelled and plotted.

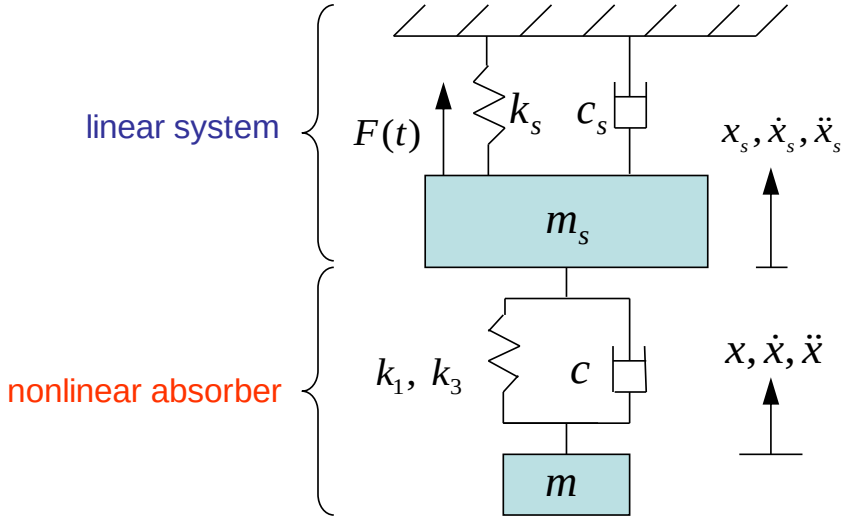

Figure 2.1 A nonlinear dynamic vibration absorber (NDVA) attached to a single degree-of-freedom spring-damper-mass primary system.

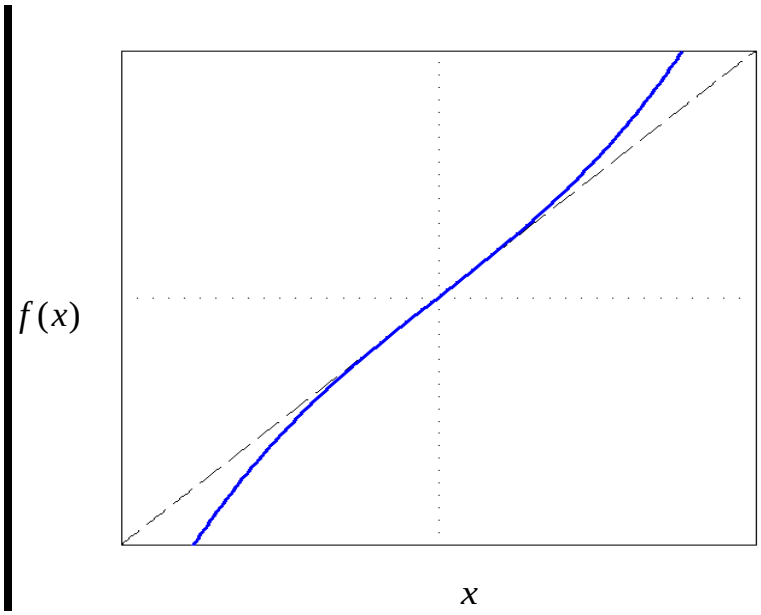

Figure 2.2 Spring force–displacement characteristic of the linear and nonlinear hardening spring types in non-dimensional form. Linear spring: $f(x) = k_1 x$ (dashed line), hardening spring: $f(x) = k_1 x + k_3 x^3$ (solid line), where $k_1 = 1$ and $k_3 = 0.5$.

The total kinetic energy of the entire vibrating system shown in Figure 2.1 is given by

$$E_k = \frac{1}{2} m_s \dot{x}_s^2 + \frac{1}{2} m \dot{x}^2 \tag{2.1}$$

The total potential energy of the entire vibrating system is given by

$$V = \frac{1}{2} k_s x_s^2 + \frac{1}{2} k_1 (x_s - x)^2 + \frac{1}{4} k_3 (x_s - x)^4 \tag{2.2}$$

The generalized forces Q_s and Q including the linear viscous damping forces are:

$$Q_s = -c(\dot{x}_s - \dot{x}) - c_s \dot{x}_s + F(t) \tag{2.3a,b}$$

$$Q = -c(\dot{x} - \dot{x}_s)$$

Equations (2.1)-(2.3a,b) are then substituted into the following Lagrange's equations of motion [64]

$$\frac{\partial}{\partial t}\left(\frac{\partial T}{\partial \dot{x}_s}\right) - \frac{\partial T}{\partial x_s} + \frac{\partial V}{\partial x_s} = Q_s \tag{2.4a,b}$$

$$\frac{\partial}{\partial t}\left(\frac{\partial T}{\partial \dot{x}}\right) - \frac{\partial T}{\partial x} + \frac{\partial V}{\partial x} = Q$$

The equations of motion are subsequently given by Nayfeh and Mook [65] for the case of harmonic excitation applied to the primary mass

$$m_s \ddot{x}_s + c_s \dot{x}_s + k_s x_s + c(\dot{x}_s - \dot{x}) + k_1 (x_s - x) + k_3 (x_s - x)^3 = F\cos(\omega t) \tag{2.5a,b}$$

$$m\ddot{x} - c(\dot{x}_s - \dot{x}) - k_1 (x_s - x) - k_3 (x_s - x)^3 = 0$$

where the excitation is periodic in time t with frequency ω and amplitude F.

It is convenient to write equations (2.5a,b) in non-dimensional form as

$$(w'' + y'') + 2\zeta_s (w' + y') + (w + y) + 2\mu\zeta\omega_0 w' + \mu\omega_0^2 w + \mu\gamma w^3 = \cos(\Omega\tau) \tag{2.6a,b}$$

$$y'' - 2\zeta\omega_0 w' - \omega_0^2 w - \gamma w^3 = 0$$

where the substitutions for the non-dimensional parameters are given below.

$$y_s'' = \frac{\ddot{x}_s}{\omega_s^2 x_0},\ y_s' = \frac{\dot{x}_s}{\omega_s x_0},\ y_s = \frac{x_s}{x_0};\ y'' = \frac{\ddot{x}}{\omega_s^2 x_0},\ y' = \frac{\dot{x}}{\omega_s x_0},\ y = \frac{x}{x_0}$$

$$w'' = \frac{\ddot{z}}{\omega_s^2 x_0},\ w' = \frac{\dot{z}}{\omega_s x_0},\ w = \frac{z}{x_0};\ \omega_s^2 = \frac{k_s}{m_s},\ \omega_1^2 = \frac{k_1}{m},\ \tau = \omega_s t$$

Here x_0 is the static extension of the linear spring k_s due to a static force of amplitude F, defined as $x_0 = F/k_s\big|_{k_1=0, k_3=0, \omega=0}$, $(\bullet)' = \frac{\mathrm{d}}{d\tau}(\bullet)$ is the derivative with respect to non-

dimensional time in which $\tau = \omega_s t$ is non-dimensional time, ω_s is the natural frequency of the primary system and $z = x_s - x$ is the extension of the nonlinear spring (equivalent to the relative displacement of the primary mass to the NDVA mass). It is noteworthy that ω_1 is not the natural frequency of the nonlinear system but is a characteristic frequency which is the natural frequency of the linearised nonlinear vibration absorber (setting k_3 to zero or a very low value such that the nonlinearity is negligible).

In equations (2.6a,b), the non-dimensional terms μ, γ, ζ_s, ζ, ω_0 and Ω are, respectively, the mass ratio, a nonlinear stiffness parameter, the linear damping ratio of the primary system, the linear damping ratio of the absorber, the linear tuned frequency ratio and the excitation frequency ratio which are all given by the following algebraic expressions respectively:

$$\mu = \frac{m}{m_s},\ \gamma = \frac{k_3 x_0^2}{k_s \mu},\ \zeta_s = \frac{c_s}{2 m_s \omega_s},\ \zeta = \frac{c}{2 m \omega_1},\ \omega_0 = \frac{\omega_1}{\omega_s},\ \Omega = \frac{\omega}{\omega_s}$$

When simplified equations (2.6a,b) become

$$y_s'' + 2\zeta_s y_s' + y_s + 2\mu\zeta\omega_0 w' + \mu\omega_0^2 w + \mu\gamma w^3 = \cos(\Omega\tau) \qquad \text{(2.7a,b)}$$

$$w'' + 2\zeta\omega_0 w' + \omega_0^2 w + \gamma w^3 = y_s''$$

Equation (2.7b) is multiplied by the mass ratio term μ and substituted into equation (2.7a) yielding

$$(1+\mu) y_s'' + 2\zeta_s y_s' + y_s - \mu w'' = \cos(\Omega\tau) \qquad \text{(2.8a,b)}$$

$$w'' + 2\zeta\omega_0 w' + \omega_0^2 w + \gamma w^3 = y_s''$$

These are still coupled and nonlinear, but the nonlinear term (cubic) just occurs in one of these equations.

It is noted that the other non-dimensional parameters (damping ratio, mass ratio and linear tuned frequency) remain constant, a change in the non-dimensional nonlinear parameter γ is only caused by a change in the nonlinear stiffness k_3 or in the amplitude of the excitation F and hence x_0 [39, 45]. The other absorber parameters (damping ratio, mass ratio and linear tuned frequency) that affect the vibration effectiveness to these parameters are examined using separate variations in just one parameter at a time. These simulation results will be presented in chapter 3. If the system parameters remain constant, a change in the excitation level F could result in the system having nonlinear behaviour as reported by others [39, 45, 66].

In general, the solutions of nonlinear differential equations are obtained either by numerical integration or approximate closed-form expressions. However, the approximate solution of nonlinear differential equations are not always obtained straightforwardly and can be complex using mathematical techniques [65].

There are some different procedures using the averaging, perturbation and multiple scales methods to obtain approximate solutions. However, these methods have some common features and limitations [65, 67]. The applicability of those methods are available for periodic excitation, transient and random excitations. The solution is found by applying small nonlinear perturbations to the linearised equation, but the implementation of these methods is restricted to weakly nonlinear systems. A weakly nonlinear system is one where its motion is described by a differential equation that can be separated into one part containing linear terms and a part with nonlinear terms which are small relatively to the linear ones [65]. In addition, complicated mathematical expressions for higher order terms will be produced [28, 29, 43].

The Harmonic Balance Method (HBM) has been applied within this thesis for harmonic excitation [65]. The reason that the HBM has been chosen to find the approximate solution of the nonlinear differential equation is described rather clearly by Worden [68]. ”The purpose of applied mathematics is to describe and elucidate experiment. Theoretical analysis should yield information in a form which is readily comparable with observation. The method of the harmonic balance conforms to this principle beautifully as a means of approximating the Frequency Response Functions of nonlinear systems.”

Furthermore, as stated by Hamdan *et al.* [69] it is not restricted to weakly nonlinear problems and, for smooth systems, the assumed harmonic solutions always converge to the exact solution. The mathematical analysis can be conducted relatively easily due to it not producing complicated mathematical expressions for higher order terms. However, the HBM has some limitations in accuracy. In the interpretation considered here, one chooses just to use the response at the excitation frequency, i.e., by assuming that sub and super harmonics are negligible compared to the fundamental harmonic and that the system is only under periodic excitation. In addition, the stability characteristics require a separate analysis.

2.2. An approximate periodic solution

To investigate the dynamic behaviour of the primary system with the nonlinear absorber attached, the HBM is used, as this enables mathematical expressions to be derived and the analysis to be conducted relatively easily. The fundamental assumption in the HBM approach used for the first order solution is that the response of the primary system and the absorber is predominantly harmonic at the harmonic excitation frequency. Applying the HBM, it is assumed that a solution exists of the form

$$y_s = Y_s \cos(\Omega\tau + \varphi_s) \qquad (2.9a,b)$$
$$w = W\cos(\Omega\tau + \varphi)$$

exists where Y_s and W are the real response amplitudes, φ_s and φ the phase of the responses with respect to the harmonic excitation force.

Non-dimensional time derivatives of equations (2.9a,b) yields

$$y_s' = -\Omega Y_s \sin(\Omega\tau + \varphi_s),\ y_s'' = -\Omega^2 Y_s \cos(\Omega\tau + \varphi_s) \qquad (2.10a,b)$$
$$w' = -\Omega W \sin(\Omega\tau + \varphi),\ w'' = -\Omega^2 W \cos(\Omega\tau + \varphi)$$

Substituting equations (2.9a,b)-(2.10a,b) into equations (2.8a,b) gives

$$\begin{aligned}&(1+\mu)(-\Omega^2 Y_s \cos(\Omega\tau + \varphi_s)) - 2\zeta_s\Omega Y_s \sin(\Omega\tau + \varphi_s)\\ &+ Y_s \cos(\Omega\tau + \varphi_s) - \mu(-\Omega^2 W\cos(\Omega\tau + \varphi)) = \cos(\Omega\tau)\end{aligned} \qquad (2.11a,b)$$

$$\begin{aligned}&-\Omega^2 W\cos(\Omega\tau + \varphi) - 2\zeta\Omega\omega_0 W\sin(\Omega\tau + \varphi)\\ &\quad + \omega_0^2(\mathrm{W}\cos(\Omega\tau + \varphi)) + \gamma(\mathrm{W}\cos(\Omega\tau + \varphi))^3 = -\Omega^2 \mathrm{Y}_s\cos(\Omega\tau + \varphi_s)\end{aligned}$$

By neglecting harmonics of order higher than 1, one can simplify these equations using the trigonometric identity

$$\cos^3(\Omega\tau + \varphi) \equiv \frac{1}{4}(3\cos(\Omega\tau + \varphi) + \cos 3(\Omega\tau + \varphi)) \approx \frac{3}{4}\cos(\Omega\tau + \varphi) \qquad (2.12)$$

Substituting equation (2.12) into equation (2.11b) and simplifying gives

$$\begin{aligned}&\Omega^2\mu W\cos(\Omega\tau + \varphi) - 2\zeta_s\Omega Y_s\sin(\Omega\tau + \varphi_s)\\ &\qquad + \left[1 - \Omega^2(1+\mu)\right]Y_s\cos(\Omega\tau + \varphi_s) = \cos(\Omega\tau)\end{aligned} \qquad (2.13a,b)$$

$$-2\zeta\Omega\omega_0 W\sin(\Omega\tau + \varphi) + \left[\omega_0^2\mathrm{W} - \Omega^2\mathrm{W} + \frac{3}{4}\gamma\mathrm{W}^3\right]\cos(\Omega\tau + \varphi) = -\Omega^2\mathrm{Y}_s\cos(\Omega\tau + \varphi_s)$$

To separate the components the orthogonality conditions for the trigonometric functions are used. Equation (2.13a) is multiplied by the terms $\cos(\Omega\tau)$ and $\sin(\Omega\tau)$ separately and integrated over one period of the excitation to yield

$$\int_0^{2\pi/\Omega}\begin{pmatrix}\Omega^2\mu W\cos(\Omega\tau+\varphi)-2\zeta_s\Omega Y_s\sin(\Omega\tau+\varphi_s)\\+\left[1-\Omega^2(1+\mu)\right]Y_s\cos(\Omega\tau+\varphi_s)\end{pmatrix}\cos(\Omega\tau)d\tau$$

$$=\int_0^{2\pi/\Omega}\left(\cos(\Omega\tau)\right)\cos(\Omega\tau)d\tau \qquad (2.14a,b)$$

$$\int_0^{2\pi/\Omega}\begin{pmatrix}\Omega^2\mu W\cos(\Omega\tau+\varphi)-2\zeta_s\Omega Y_s\sin(\Omega\tau+\varphi_s)\\+\left[1-\Omega^2(1+\mu)\right]Y_s\cos(\Omega\tau+\varphi_s)\end{pmatrix}\sin(\Omega\tau)d\tau$$

$$=\int_0^{2\pi/\Omega}\left(\cos(\Omega\tau)\right)\sin(\Omega\tau)d\tau$$

Equation (2.13b) is multiplied by the terms $\cos(\Omega\tau)$ and $\sin(\Omega\tau)$ separately and integrated to yield

$$\int_0^{2\pi/\Omega}\left(-2\zeta\Omega\omega_0 W\sin(\Omega\tau+\varphi)+\left[\omega_0^2\mathrm{W}-\Omega^2\mathrm{W}+\frac{3}{4}\gamma\mathrm{W}^3\right]\cos(\Omega\tau+\varphi)\right)\cos(\Omega\tau)d\tau$$

$$=\int_0^{2\pi/\Omega}\left(-\Omega^2\mathrm{Y}_s\cos(\Omega\tau+\varphi_s)\right)\cos(\Omega\tau)d\tau$$

(2.14c,d)

$$\int_0^{2\pi/\Omega}\left(-2\zeta\Omega\omega_0 W\sin(\Omega\tau+\varphi)+\left[\omega_0^2\mathrm{W}-\Omega^2\mathrm{W}+\frac{3}{4}\gamma\mathrm{W}^3\right]\cos(\Omega\tau+\varphi)\right)\sin(\Omega\tau)d\tau$$

$$=\int_0^{2\pi/\Omega}\left(-\Omega^2\mathrm{Y}_s\cos(\Omega\tau+\varphi_s)\right)\sin(\Omega\tau)d\tau$$

Thus produces four algebraic equations (2.14a,b,c,d)

$$\Omega^2\mu W\cos\varphi-2\zeta_s\Omega Y_s\sin\varphi_s+\left[1-\Omega^2(1+\mu)\right]Y_s\cos\varphi_s=1 \qquad (2.15a,b,c,d)$$

$$-\Omega^2\mu W\sin\varphi-2\zeta_s\Omega Y_s\cos\varphi_s-\left[1-\Omega^2(1+\mu)\right]Y_s\sin\varphi_s=0$$

$$-2\zeta\Omega\omega_0 W\sin\varphi+\left[\omega_0^2\mathrm{W}-\Omega^2\mathrm{W}+\frac{3}{4}\gamma\mathrm{W}^3\right]\cos\varphi=-\Omega^2\mathrm{Y}_s\cos\varphi_s$$

$$-2\zeta\Omega\omega_0 W\cos\varphi-\left[\omega_0^2 W-\Omega^2 W+\frac{3}{4}\gamma W^3\right]\sin\varphi=\Omega^2\mathrm{Y}_s\sin\varphi_s$$

The frequency response function can be calculated by squaring and adding equations (2.15c,d) to give

$$\left(-2\zeta\Omega\omega_0 W\right)^2+\left(\omega_0^2 W-\Omega^2 W+\frac{3}{4}\gamma W^3\right)^2=\left(\Omega^2\mathrm{Y}_s\right)^2 \qquad (2.16)$$

Equation (2.16) can be expanded and rearranged as

$$\frac{9}{16}\gamma^2 W^6 + \frac{3}{2}\gamma W^4(\omega_0^2 - \Omega^2) + (\Omega^4 + 4\zeta^2\Omega^2\omega_0^2 + \omega_0^4 - 2\Omega^2\omega_0^2)W^2 - \Omega^4 Y_s^2 = 0 \qquad (2.17)$$

From equation (2.17)

$$Y_s^2 = \frac{1}{\Omega^4}\left(\frac{9}{16}\gamma^2 W^6 + \frac{3}{2}\gamma(\omega_0^2 - \Omega^2)W^4 + (\Omega^4 + 4\zeta^2\Omega^2\omega_0^2 + \omega_0^4 - 2\Omega^2\omega_0^2)W^2\right) \qquad (2.18)$$

To eliminate Y_s from equation (2.15a,b), one can use equations (2.15c,d) to eliminate $Y_s \sin\varphi_s$ and $Y_s \cos\varphi_s$ in equation (2.15a,b) to obtain

$$\left(2\zeta_s\Omega\left[\omega_0^2 W - \Omega^2 W + \frac{3}{4}\gamma W^3\right] + 2\zeta\Omega\omega_0 W\left[1 - \Omega^2(1+\mu)\right]\right)\sin\varphi$$
$$= \left(-\Omega^4\mu W - 2\zeta_s\Omega\left(2\zeta\Omega\omega_0 W\right) + \left[1 - \Omega^2(1+\mu)\right]\left[\omega_0^2 W - \Omega^2 W + \frac{3}{4}\gamma W^3\right]\right)\cos\varphi + \Omega^2$$
$$\left(-\Omega^4\mu W - 2\zeta_s\Omega\left(2\zeta\Omega\omega_0 W\right) + \left[1 - \Omega^2(1+\mu)\right]\left[\omega_0^2 W - \Omega^2 W + \frac{3}{4}\gamma W^3\right]\right)\sin\varphi$$
$$= \left(-2\zeta_s\Omega\left[\omega_0^2 W - \Omega^2 W + \frac{3}{4}\gamma W^3\right] - 2\zeta\Omega\omega_0 W\left[1 - \Omega^2(1+\mu)\right]\right)\cos\varphi$$

(2.19a,b)

Squaring and adding equations (2.19a,b), and after some algebraic manipulation one obtains the following equation for W, the amplitude of the nondimensionalized relative displacement

$$aW^6 + bW^4 + cW^2 + d = 0 \qquad (2.20)$$

where

$$a = \frac{9}{16}\gamma^2,\ b = \frac{3}{2}\gamma(\omega_0^2 - \Omega^2) + \Omega^4\frac{g}{e},\ c = (\omega_0^2 - \Omega^2)^2 + 4\zeta^2\omega_0^2\Omega^2 + \Omega^4\frac{h}{e},\ d = -\frac{\Omega^4}{e},$$

$$e = \left(1 - \Omega^2(1+\mu)\right)^2 + 4\zeta_s^2\Omega^2,\ g = -\frac{3}{2}\gamma\mu(1 - \Omega^2(1+\mu)),$$

$$h = \Omega^4\mu^2 - 2\mu(1 - \Omega^2(1+\mu))(\omega_0^2 - \Omega^2) + 8\zeta_s\zeta\mu\omega_0\Omega^2$$

The phase of the relative displacement can be obtained from equation (2.19b)

$$\tan\varphi = \frac{-2\zeta_s\Omega\left[\omega_0^2 W - \Omega^2 W + \frac{3}{4}\gamma W^3\right] - 2\zeta\Omega\omega_0 W\left[1 - \Omega^2(1+\mu)\right]}{-\Omega^4\mu W - 2\zeta_s\Omega\left(2\zeta\Omega\omega_0 W\right) + \left[1 - \Omega^2(1+\mu)\right]\left[\omega_0^2 W - \Omega^2 W + \frac{3}{4}\gamma W^3\right]} \qquad (2.21)$$

In addition, equation (2.15d) is divided by (2.15c) to yield the phase of the primary system

$$\tan\varphi_s = \frac{-2\zeta\Omega\omega_0 W\cos\varphi - \left[\omega_0^2 W - \Omega^2 W + \frac{3}{4}\gamma W^3\right]\sin\varphi}{2\zeta\Omega\omega_0 W\sin\varphi - \left[\omega_0^2 \mathrm{W} - \Omega^2 \mathrm{W} + \frac{3}{4}\gamma \mathrm{W}^3\right]\cos\varphi} \tag{2.22}$$

Once the parameters for the system and the excitation frequency have been specified, then the solutions of equation (2.20) in W^2 give the three solutions, which should be checked for their physical interpretation and existence. It is noted that only real solutions for W^2 are physical responses.

The three steady-state solutions of equation (2.20) are obtained [70]

$$W_1^2 = s + t - \frac{b}{3a},$$
$$W_{2,3}^2 = -\frac{1}{2}(s+t) - \frac{b}{3a} \pm j\frac{\sqrt{3}}{2}(s-t), \tag{2.23a-c}$$

where the additional terms are given by

$$s = \sqrt[3]{r + \sqrt{\frac{-\Delta}{108a^4}}},\ t = \sqrt[3]{r - \sqrt{\frac{-\Delta}{108a^4}}},\ r = \frac{9abc - 27a^2d - 2b^3}{54a^3}$$

where the discriminant Δ of a polynomial is a function of its coefficients which gives information about the nature of its roots. This discriminant is also a polynomial in powers of the nonlinear stiffness parameter γ.

When the normalised relative displacement W has been determined, then one can substitute back into equations (2.18) and (2.21) to obtain the nondimensional amplitude of the primary system Y_s and the phase of the relative displacement φ separately. Then, substitute φ and W into equations (2.22) to yield the phase of the primary system φ_s. The same expressions as those in equations (2.18) and (2.20) were also found using the method of averaging [28].

The effect of the nonlinear stiffness γ on the primary system frequency response curves of the normalized displacement Y_s versus excitation frequency ratio Ω can be evaluated for various levels of nonlinear stiffness and are given in Figures 2.3-2.4. The response $Y_s = X_s/X_0$ is set to unity, i.e. $Y_s = 1$, which is shown by a thin horizontal solid line. The vibration reduction bandwidth is to be then determined such that $Y_s \le 1$ in that frequency range which is described

in detail in chapter 1. The vibration reduction bandwidth can be seen in Figures 2.3-2.4, i.e., the bandwidth where $Y_s = X_s / X_0 \leq 1$.

The frequency response curves in the $\Omega - Y_s$ plane was also checked by numerical integration of the equations of motion. The differential equation can be solved using the MATLAB ode45 function due to the equations not being stiff. A stiff equation is a differential equation for which certain numerical methods for solving the equation are numerically unstable, unless the step size is taken to be extremely small. It has proved difficult to formulate a precise definition of stiffness, but the main idea is that the equation includes some terms that can lead to rapid variation in the solution [71]. Equations (2.7a,b) were solved numerically and the Fourier coefficients extracted from the steady state periodic time histories. The amplitude of the first of these coefficients is depicted by circles in the frequency response curves shown in this chapter. In addition, it was verified that, for the parameters used in this work, the amplitudes of the other harmonics never exceeded 5% to be compared to the amplitude at the fundamental excitation frequency. It is noted that in order to find the stable multivalued responses the initial conditions for the displacement and velocity need to be adjusted.

For small values of nonlinearity, i.e. $\gamma \leq 1\times10^{-6}$, the amplitudes of the other harmonics never exceeded 5% of the amplitude at the fundamental frequency for all frequencies in Figure 2.3. If the nonlinearity increases to exceed γ_{NH}, i.e. $\gamma > \gamma_{\mathrm{NH}} = 1\times10^{-6}$, the approximate analytical expression for the frequency response curves fails to predict the response, which is not harmonic (NH) in a frequency range. In Figure 2.4 the absence of a numerical harmonic solution confirms the presence of the NH labelled frequency range. The amplitudes of the other harmonics never exceeded 5% of the amplitude at the fundamental frequency outside the NH frequency range. Examples of these cases are illustrated in section 2.3. The effect of the nonlinear parameter in the absorber on the harmonic response is summarised in Table 2.1.

γ	μ	ω_0	ζ	ζ_s	Numerical results
$\leq 1\times10^{-6}$	0.02	1	0.002	0.001	The solution is stable and produces a harmonic response at all frequencies.
$> 1\times10^{-6}$	0.02	1	0.002	0.001	A non-harmonic solution exists at some frequencies. The harmonic solution at other frequencies is stable.

Table 2.1 The effect of the nonlinear absorber stiffness parameter on the harmonic response.

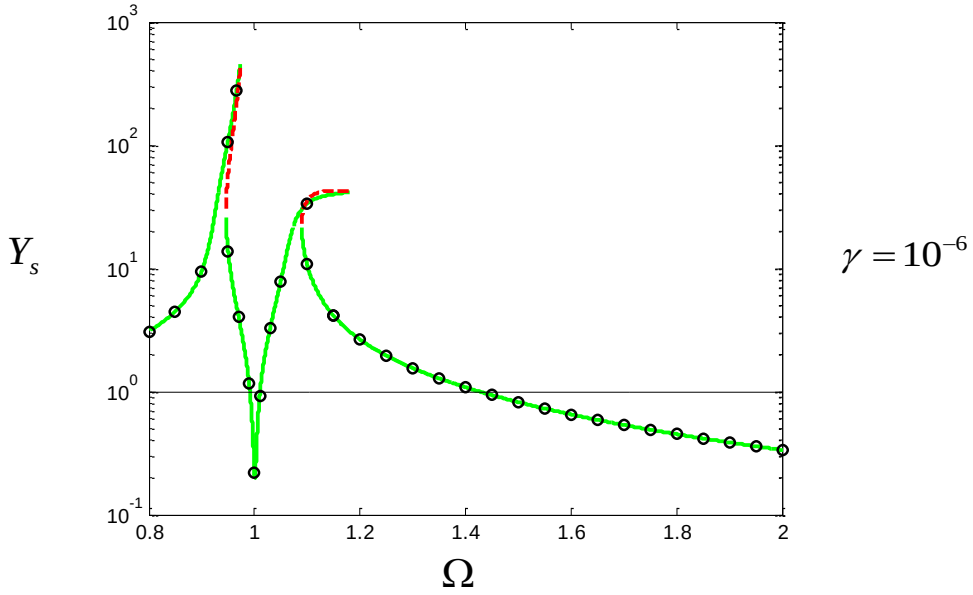

Figure 2.3 The effect of the nonlinear absorber stiffness on the primary system frequency response curves Y_s as a function of Ω. ($\gamma = 10^{-6}$, $\omega_0 = 1$, $\mu = 0.02$, $\zeta_s = 0.001$, $\zeta = 0.002$). The solid line is the stable solution and the dashed line gives the unstable solution. Direct numerical solutions are shown by the symbol ('o').

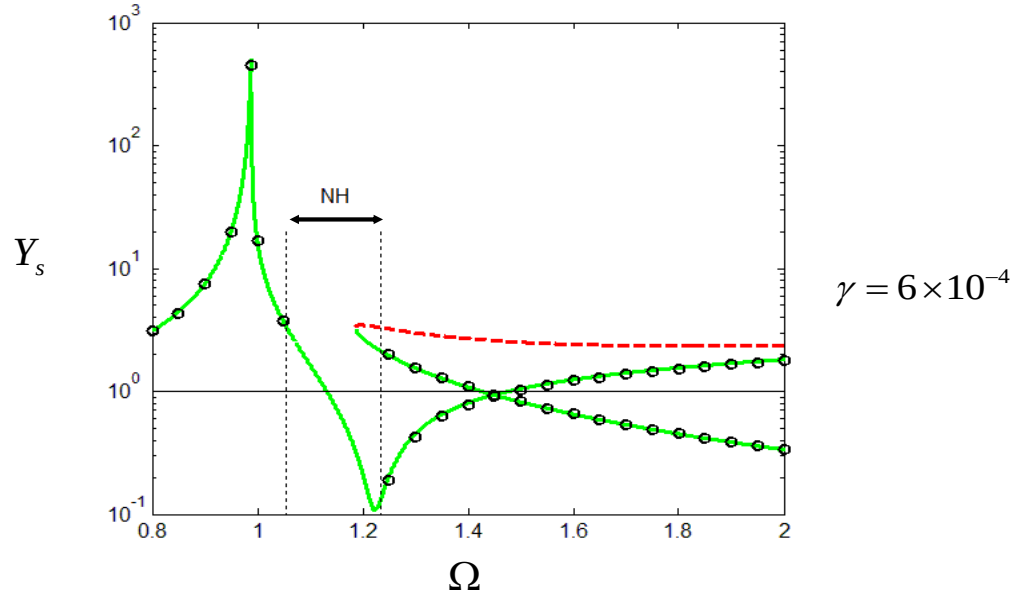

Figure 2.4 The effect of the nonlinear absorber stiffness on the primary system frequency response curves Y_s as a function of Ω. ($\gamma = 6\times10^{-4}$, $\omega_0 = 1$, $\mu = 0.02$, $\zeta_s = 0.001$, $\zeta = 0.002$). The solid line is the stable solution and the dashed line gives the unstable solution. Direct numerical solutions are shown by the symbol ('o'). The approximate analytical expression for the frequency response curves fails to predict the response, which is not harmonic (NH) in the frequency range identified.

2.3. Stability and bifurcation analysis

The stability characteristics refer to the system undergoing smooth amplitude changes in the harmonic response. Depending on the degree of nonlinearity in the NDVA system, there are combinations of the parameters which produce a multivalued response. To find the conditions for such a response, Δ, the discriminant [39, 62, 70] obtained for the cubic polynomial in W^2 in Equation (2.20) can be examined

$$\Delta = 18abcd - 27a^2d^2 - 4b^3d + b^2c^2 - 4c^3a \tag{2.24}$$

If $\Delta > 0$ there are three distinct real roots for γ, which correspond to three steady-state values for the system response (two stable and one unstable). If $\Delta < 0$ there is one real root for γ and a pair of complex conjugate roots which corresponds to a single valued response solution. Lastly, if $\Delta = 0$ then there are at least two real coincident roots for γ, which occur at the jump-up and jump-down frequencies in the system frequency response, respectively. The jump-up and jump-down phenomenon is a sudden (discontinuous) change of the amplitude of the system response when the frequency is varied very slowly and the rest of the system parameters are kept constant [23].

The bifurcation points occur when the equilibrium of the system changes qualitatively (i.e. transition from stable to unstable behaviour) or quantitatively, (e.g. from one to three solutions) [72]. To determine the bifurcation curves from one to three real solutions in Y_s and W, Equation (2.24) is set to zero i.e. $\Delta = 0$ and a polynomial equation for γ is

$$A\gamma^2 + B\gamma + C = 0 \tag{2.25}$$

That can be solved for γ to give

$$\gamma_{1,2} = \frac{-B \pm \sqrt{B^2 - 4AC}}{2A} = \frac{-B \pm \Lambda}{2A} \tag{2.26}$$

where

$$A = \frac{-27a^2d^2}{\gamma^2},\ B = \frac{-4b^3d + 18abcd}{\gamma},\ C = b^2c^2 - 4ac^3,\ \Lambda = \frac{4}{\gamma} d \left(b^2 - 3ac\right)^{\frac{3}{2}}$$

The curves corresponding to γ_1 and γ_2 obtained by Equation (2.26) in the $\Omega-\gamma$ plane are plotted in Figure 2.5. Any combination of the parameters γ and Ω from the area between the two curves yields a multivalued response, with three distinct real solutions for the steady-state amplitude Y_s and Y . The points identified C_1, C_2 and T_1 show where the two curves intersect. The values for γ_{C_1}, γ_{C_2} and γ_{T_1} could be obtained numerically from equation (2.26). It can be seen that there are minimum values for the nonlinearity γ_{C_1} and γ_{C_2} that result in multi-valued solutions.

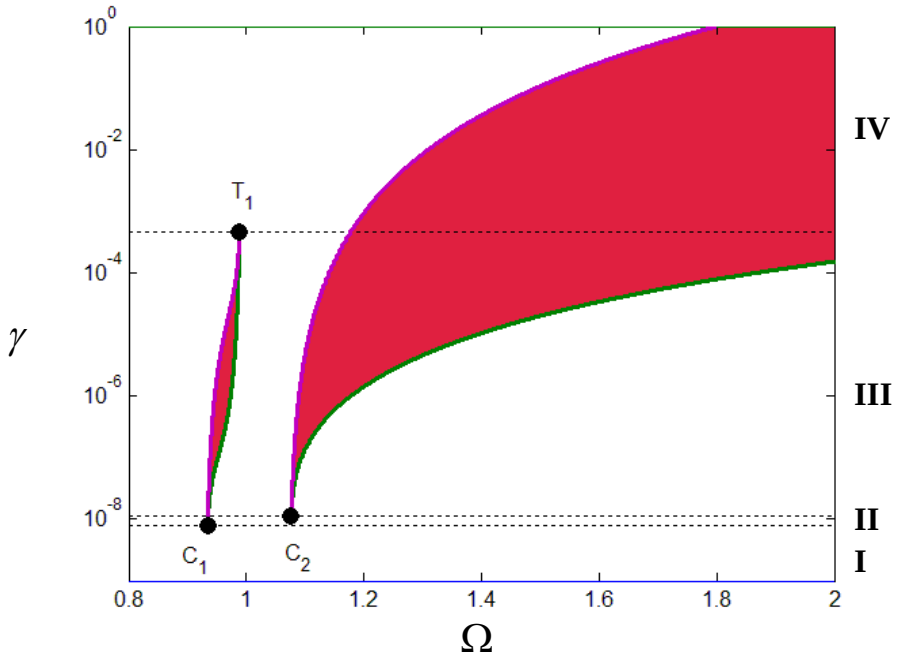

Figure 2.5 The bifurcation curves defined by equation (2.26) showing the transition and characteristic regions I, II, III and IV in the $\Omega-\gamma$ plane for the frequency amplitude response of Y_s and Y ($\omega_0=1$, $\mu=0.02$, $\zeta_s=0.001$, $\zeta=0.002$). Red shading denotes the unstable solution for the system frequency response.

In order to emphasize the relationship between the bifurcation curves in the frequency response curves in the $\Omega-Y_s$, $\Omega-Y$ and the $\Omega-\gamma$ planes, the three graphs involving the four variables Ω, γ, Y_s and Y are plotted in Figures 2.6-10. It can be seen that a thin horizontal solid line, drawn for a particular value of γ, may be interpreted as the projection of the corresponding frequency response curves on the $\Omega-\gamma$ plane. Moreover, the intersections

between the dotted line and the bifurcation curves give the value of the jump frequencies. The solid line bifurcation curve corresponding to jumps at the points P_1, P_2, Q_1 and Q_2 shown in Figures 2.7-10. The stable and unstable solutions of the frequency response curves are shown as solid and dashed lines, respectively. The determination of the unstable region for these steady-state HBM solutions is calculated by applying Floquet theory as described by Malatkar and Nayfeh [46, 47, 73] and the expressions are shown in appendix A. Thus, the characteristic regions are presented as regions I, II, III and IV in Figure 2.5. In Figure 2.7, it is noted that the unstable solutions for the dashed lines are not shown clearly due to the lower value of the nonlinear parameter.

In Figure 2.6, which corresponds to parameter values for region I, where the nonlinear parameter is very small, the frequency response curve is single-valued and the system behaves similar to a linear system, no multivalued solution exists and there are two resonant peaks. For higher values of nonlinear stiffness γ, corresponding to Region II, the multivalued solution appears close to the first resonant peak frequency range between P_1 and P_2 as shown in Figure 2.7. In Figures 2.8-9, corresponding to region III, the multivalued solution appears in the frequency ranges between P_1 and P_2, and Q_2 and Q_1 separately. Finally, as γ is increased so that the system corresponds to region VI, the frequency response curves appear to possess multivalued unstable solutions in the frequency range from Q_1, but it is now single-valued around the first resonant peak as shown in Figure 2.10.

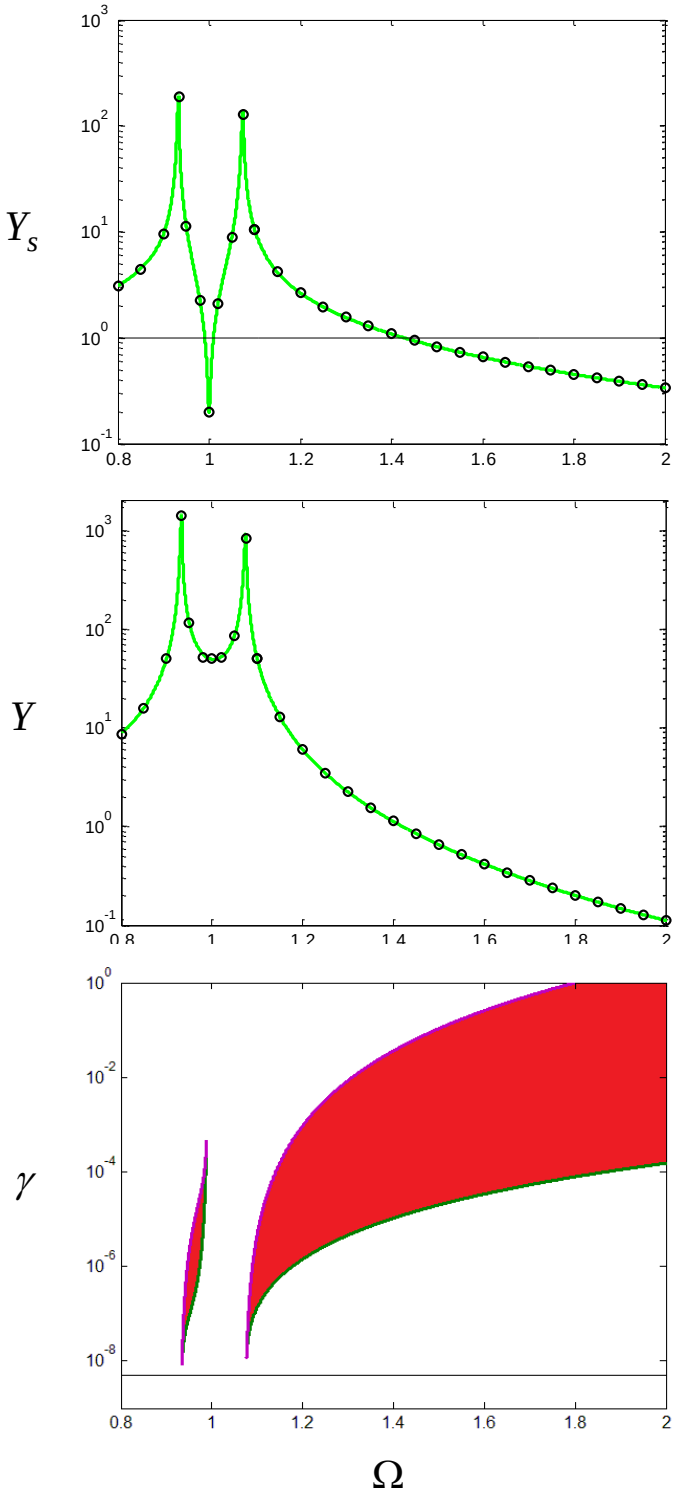

Figure 2.6 The relationship between the bifurcation curves and the frequency response curves. **(** $\gamma = 5\times10^{-9}$, $\omega_0 = 1$, $\mu = 0.02$, $\zeta_s = 0.001$, $\zeta = 0.002$). On the $\Omega - Y_s$ and $\Omega - Y$ plane, the solid line is the stable solution. Direct numerical solutions are shown by the symbol ('○'). Red shading denotes the unstable solution of the system frequency response.

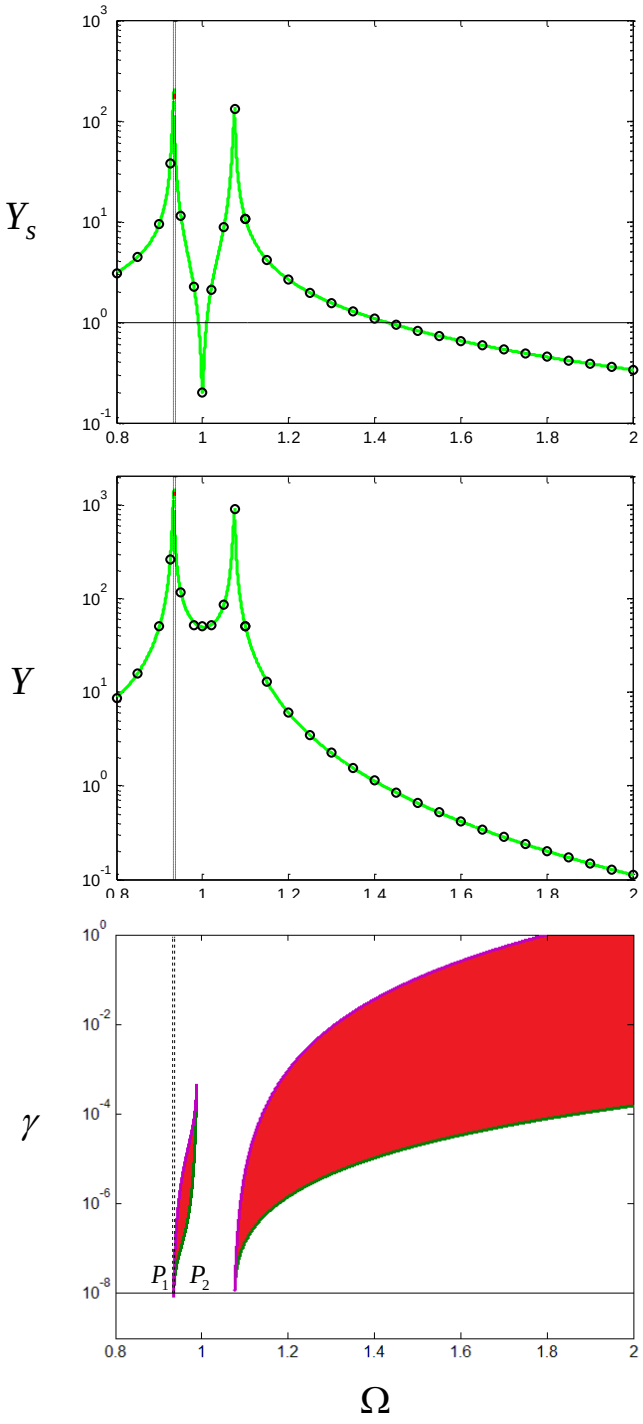

Figure 2.7 The relationship between the bifurcation curves and the frequency response curves. **(** $\gamma = 10^{-8}$, $\omega_0 = 1$, $\mu = 0.02$, $\zeta_s = 0.001$, $\zeta = 0.002$). On the $\Omega - Y_s$ and $\Omega - Y$ plane, the solid line is the stable solution and the dashed line gives the unstable solution. Direct numerical solutions are shown by the symbol ($'\circ'$). The intersections between the plane containing the frequency response curve and the bifurcation curves on the plane indicate the expected values for the jump frequencies. Red shading denotes the unstable solution of the system frequency response.

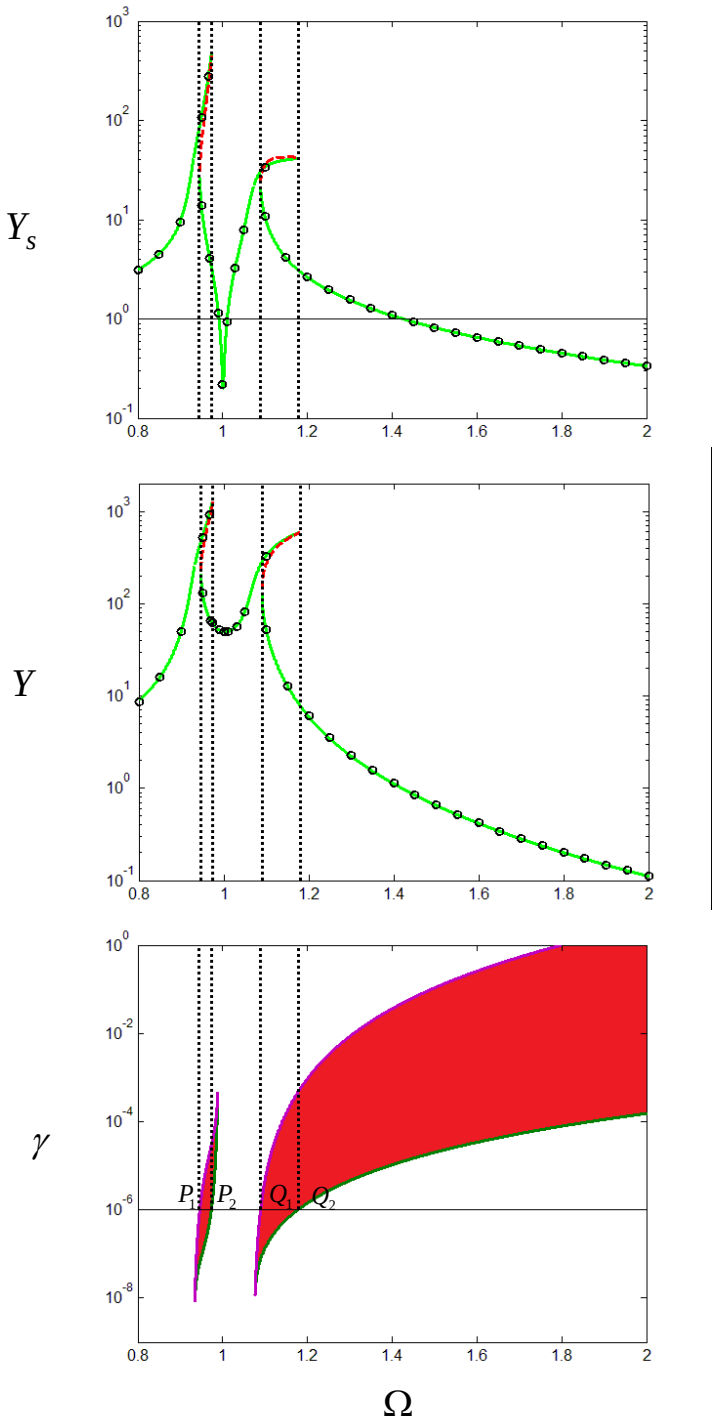

Figure 2.8 The relationship between the bifurcation curves and the frequency response curves. **(** $\gamma = 10^{-6}$, $\omega_0 = 1$, $\mu = 0.02$, $\zeta_s = 0.001$, $\zeta = 0.002$). On the $\Omega - Y_s$ and $\Omega - Y$ plane, the solid line is the stable solution and the dashed line gives the unstable solution. Direct numerical solutions are shown by the symbol ('o'). The intersections between the plane containing the frequency response curve and the bifurcation curves on the plane indicate the expected values for the jump frequencies. Red shading denotes the unstable solution of the system frequency response.

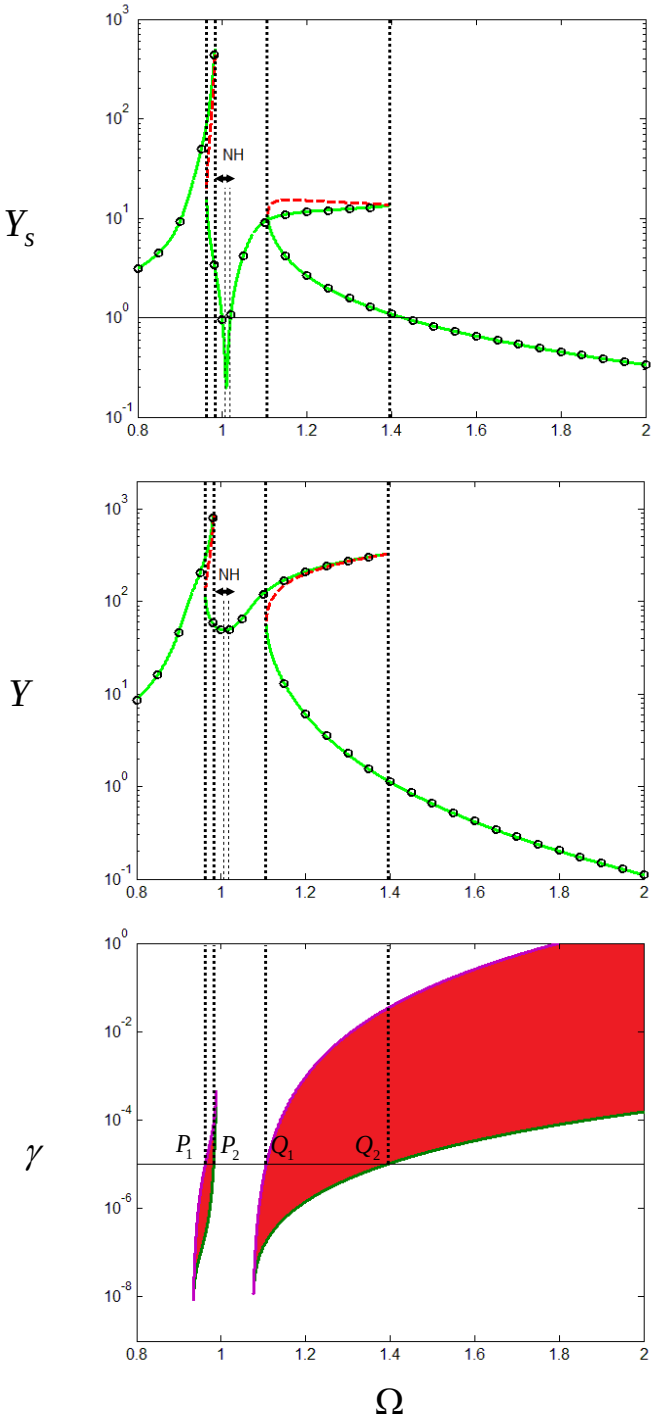

Figure 2.9 The relationship between the bifurcation curves and the frequency response curves. **(** $\gamma = 10^{-5}$, $\omega_0 = 1$, $\mu = 0.02$, $\zeta_s = 0.001$, $\zeta = 0.002$). On the $\Omega - Y_s$ and $\Omega - Y$ plane, the solid line is the stable solution and the dashed line gives the unstable solution. Direct numerical solutions are shown by the symbol ('○'). The intersections between the plane containing the frequency response curve and the bifurcation curves on the plane indicate the expected values for the jump frequencies. Red shading denotes the unstable solution of system frequency response. The approximate analytical expression for the frequency response curve fails to predict the response which is not harmonic (NH) in a frequency range.

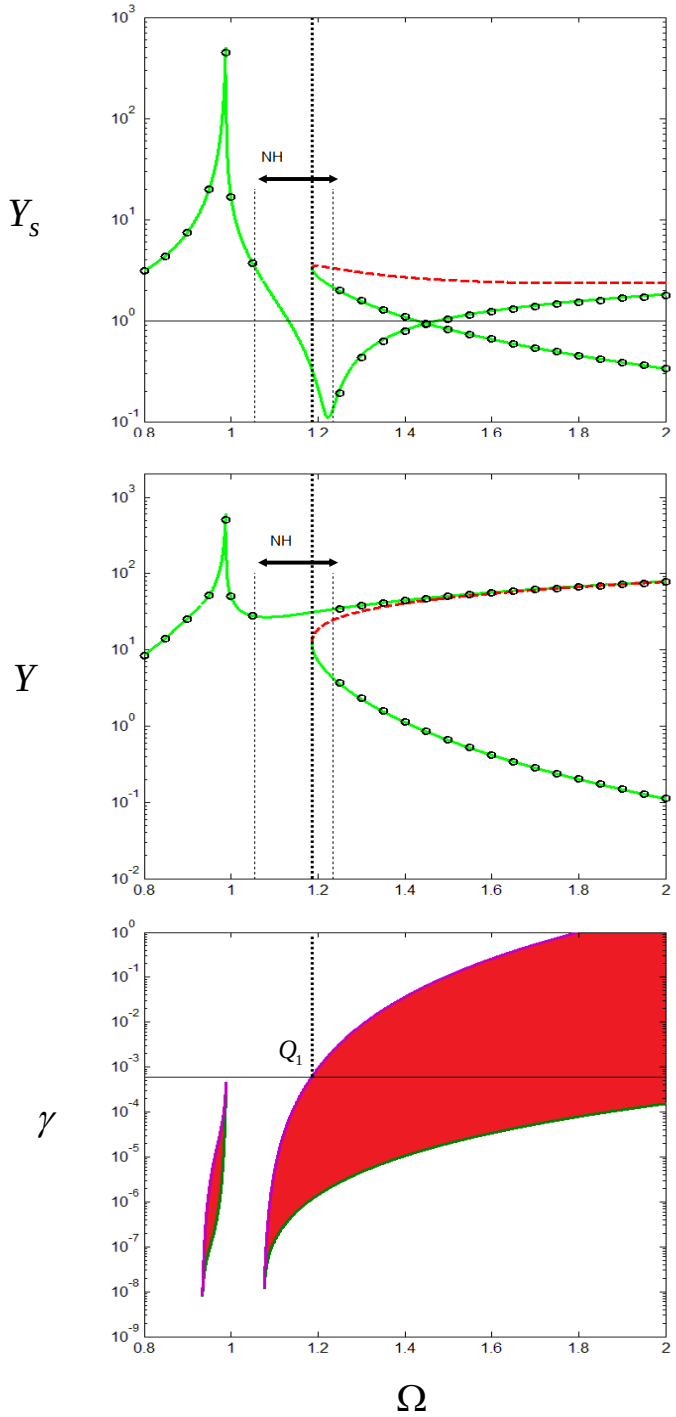

Figure 2.10 The relationship between the bifurcation curves and the frequency response curves. ($\gamma = 6\times10^{-4}$, $\omega_0 = 1$, $\mu = 0.02$, $\zeta_s = 0.001$, $\zeta = 0.002$). On the $\Omega - Y_s$ and $\Omega - Y$ plane, the solid line is the stable solution and the dashed line gives the unstable solution. Direct numerical solutions are shown by the symbol ('○'). The intersections between the plane containing the frequency response curve and the bifurcation curves on the plane indicate the expected values for the jump frequencies. Red shading denotes the unstable solution for the system frequency response. The approximate analytical expression for the frequency response curves fails to predict the response which is not harmonic (NH) in a frequency range.

The primary system response curves were presented in Figures 2.8-10, and then the corresponding time response and Fourier series coefficients are plotted in Figures 2.11-13. For small values of nonlinearity, i.e. $\gamma \leq 1\times10^{-6}$, the amplitudes of the harmonic orders of the excitation frequency do not exceeded 5% compared to the amplitude of the response at the fundamental excitation frequency. The amplitudes of the harmonic response are depicted by a Fourier series and Fourier Transform. This situation is illustrated in Figures 2.11(a)-(b). In Figures 2.12(a)-(b), the nonlinearity increases further and exceeds γ_{NH}, i.e. $\gamma>\gamma_{NH}=1\times10^{-6}$, the harmonic response at the excitation frequency did not exist at $\Omega=1.01$. The second harmonic appears in the response using the Fourier series analysis, so that the HBM expression is not sufficiently accurate in representing the actual solution around this excitation frequency. Examining this situation by Fourier Transform, other harmonics appear in the response around excitation frequency. Away from the range where non harmonic (NH) response occurs, the amplitudes of the harmonic response reduce to again less than 5% compared to the amplitude at the excitation frequency. For even higher values of γ, i.e. $\gamma=6\times10^{-4}$, a harmonic response was not be obtained and a way to chaotic motion seems to occur at $\Omega=1.15$. Examining this response using the Fourier Transform analysis, the other harmonics produce the response, so that the HBM expressions are no longer valid. However, the other harmonic responses do not appear in the response using the Fourier series analysis. But the Fourier Transform shows, for $\Omega=1.15$, the possibility of close harmonic frequency components and beating taking place. These points are illustrated in Figures 2.13(a)-(b).

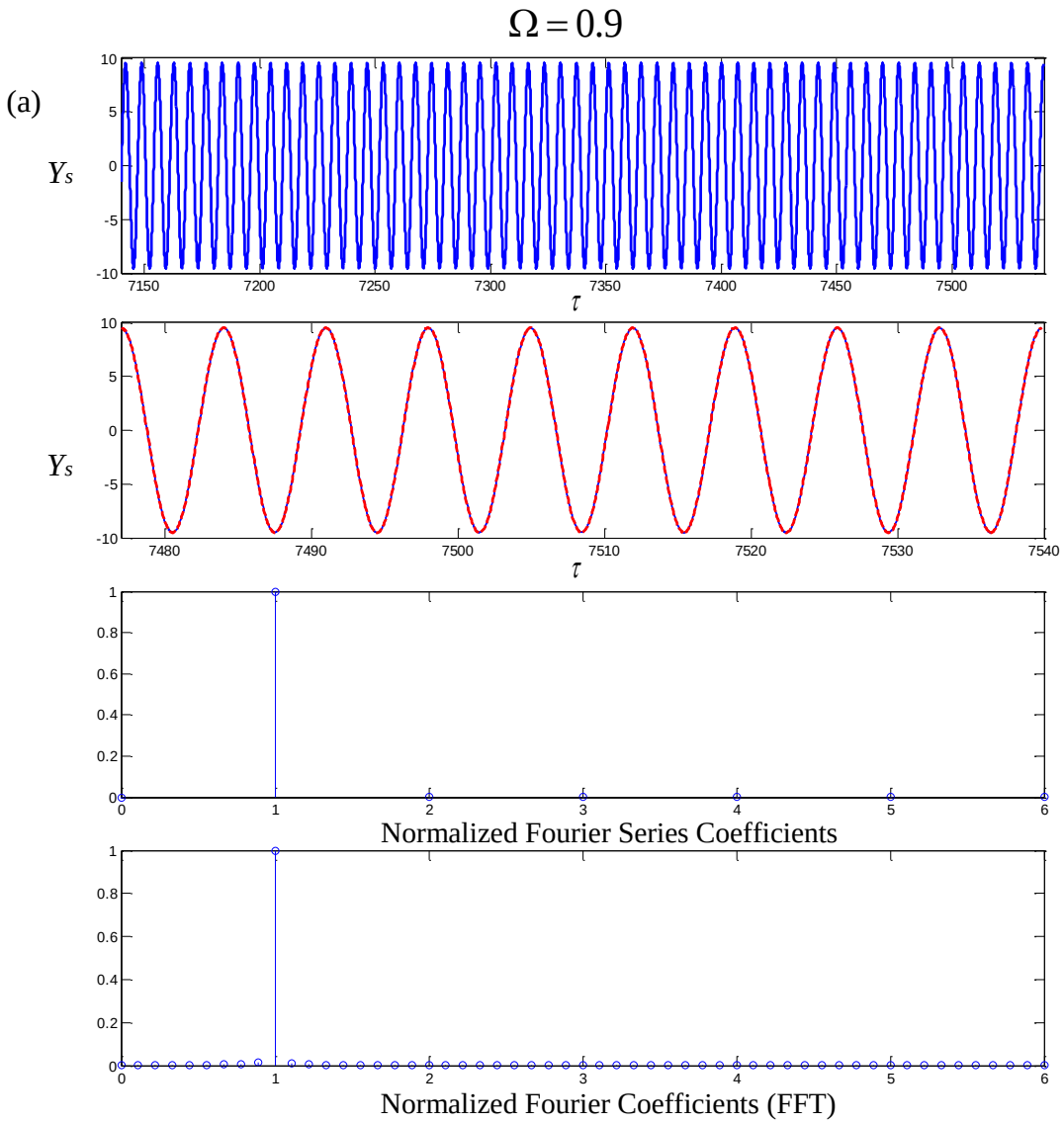

Figure 2.11(a) Time response and corresponding Fourier series coefficients of the primary system frequency response curves for the normalized displacement Y_s. (linear tuned frequency $\omega_0 = 1$, nonlinear absorber stiffness $\gamma = 10^{-6}$, mass ratio $\mu = 0.02$ and damping $\zeta_s = 0.001$, $\zeta = 0.002$). The actual response from numerical integration is the solid line and the first-harmonic approximation (HBM) is the dashed line. The corresponding excitation frequency is $\Omega = 0.9$.

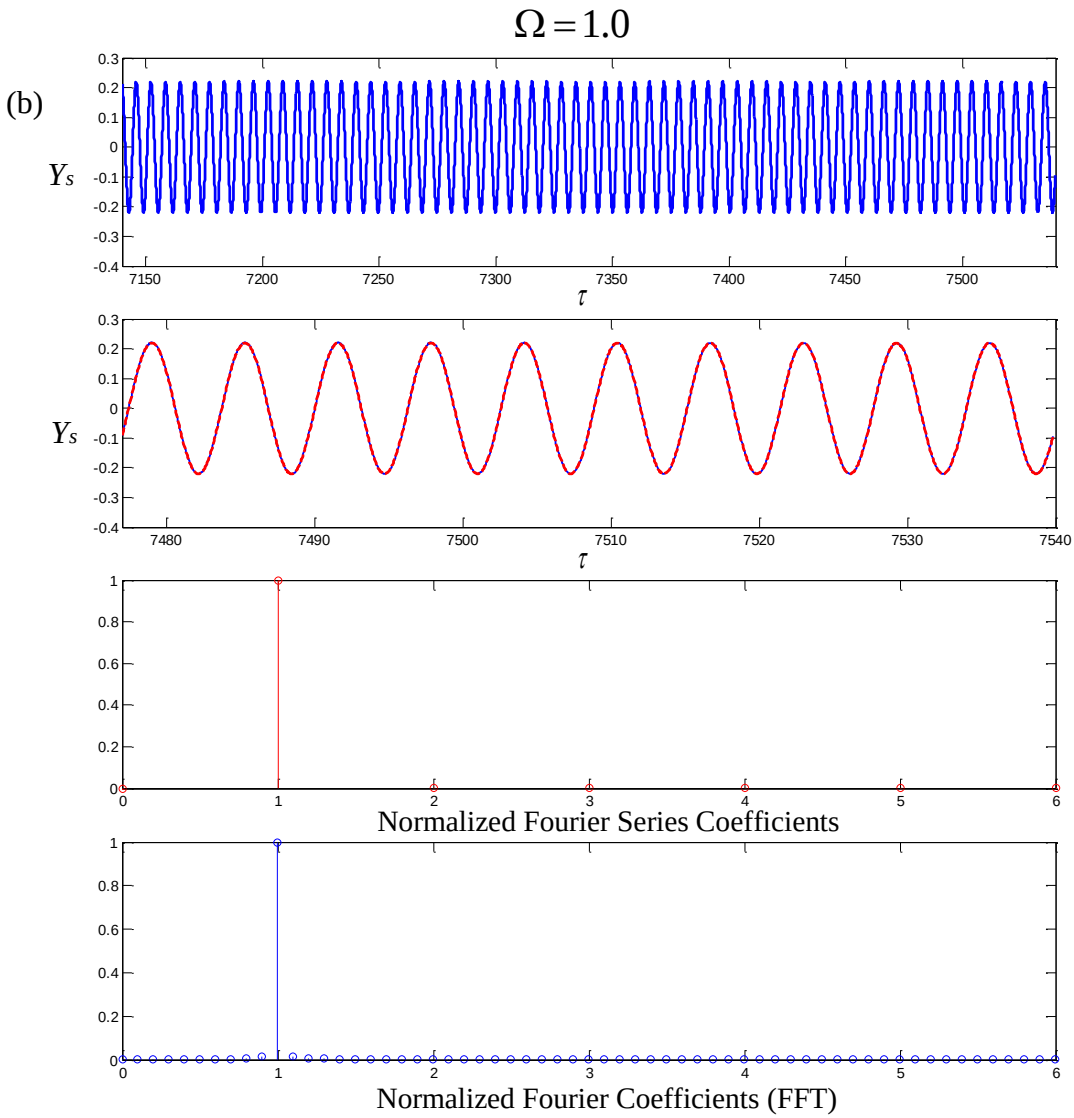

Figure 2.11(b) Time response and corresponding Fourier series coefficients of the primary system frequency response curves for the normalized displacement Y_s. (linear tuned frequency $\omega_0 = 1$, nonlinear absorber stiffness $\gamma = 10^{-6}$, mass ratio $\mu = 0.02$ and damping $\zeta_s = 0.001$, $\zeta = 0.002$). The actual response from numerical integration is the solid line and the first-harmonic approximation (HBM) is the dashed line. The corresponding excitation frequency is $\Omega = 1.0$.

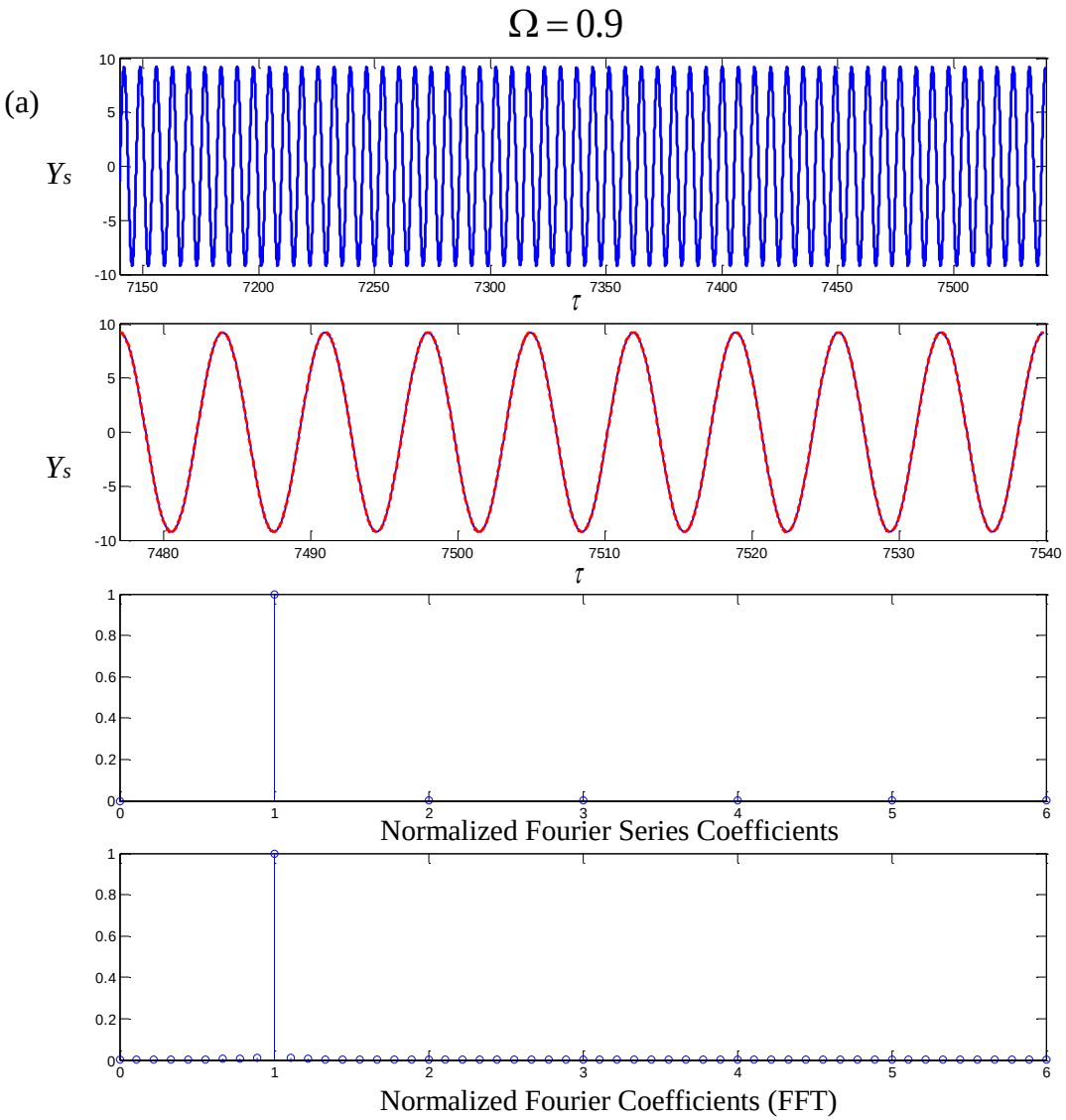

Figure 2.12(a) Time response and corresponding Fourier series coefficients of the primary system frequency response curves for the normalized displacement Y_s. (linear tuned frequency $\omega_0 = 1$, nonlinear absorber stiffness $\gamma = 10^{-5}$, mass ratio $\mu = 0.02$ and damping $\zeta_s = 0.001$, $\zeta = 0.002$). The actual response from numerical integration is the solid line and the first-harmonic approximation (HBM) is the dashed line. The corresponding excitation frequency is $\Omega = 0.9$.

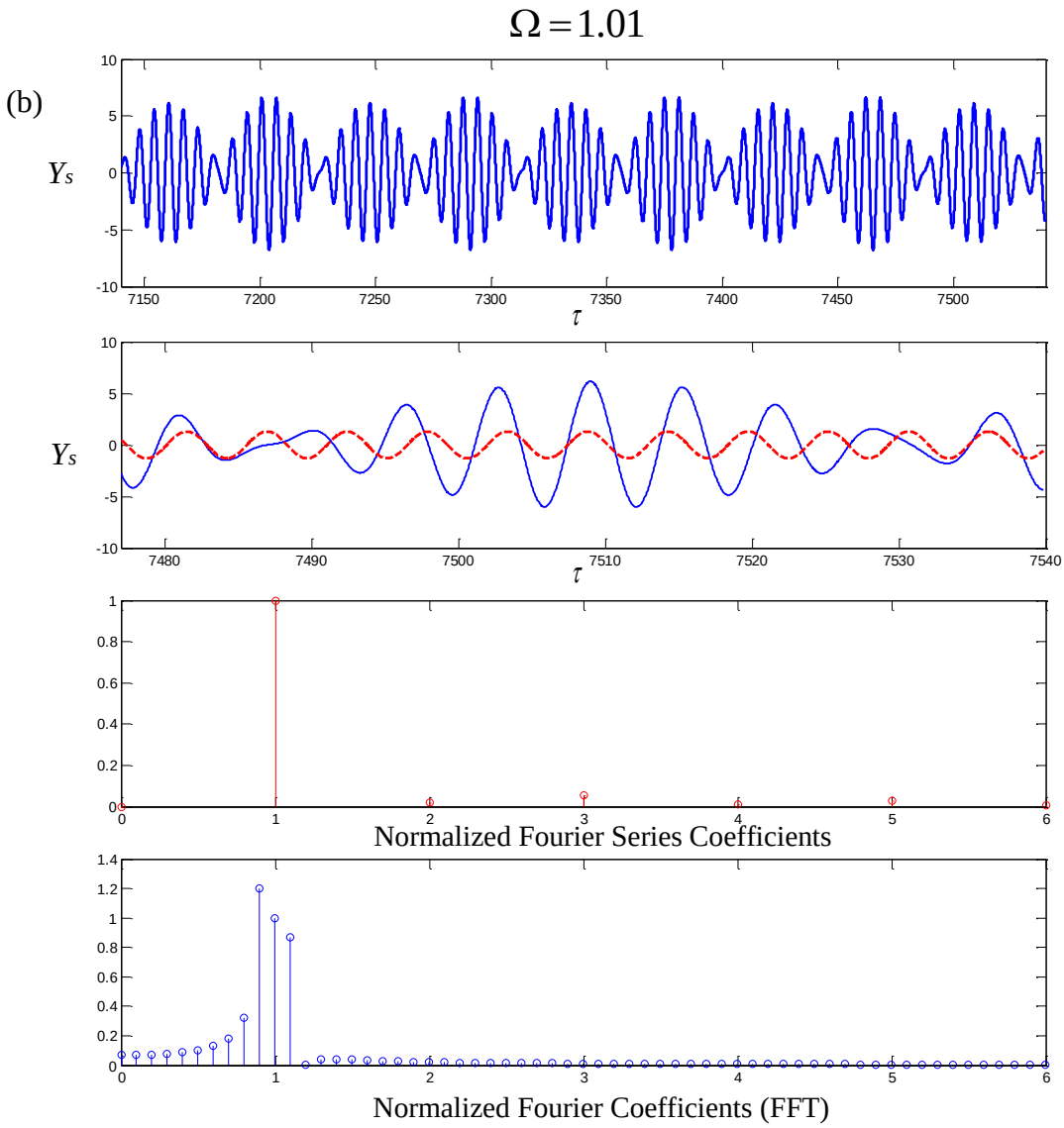

Figure 2.12(b) Time response and corresponding Fourier series coefficients of the primary system frequency response curves for the normalized displacement Y_s. (linear tuned frequency $\omega_0 = 1$, nonlinear absorber stiffness $\gamma = 10^{-5}$, mass ratio $\mu = 0.02$ and damping $\zeta_s = 0.001$, $\zeta = 0.002$). The actual response from numerical integration is the solid line and the first-harmonic approximation (HBM) is the dashed line. The corresponding excitation frequency is $\Omega = 1.01$.

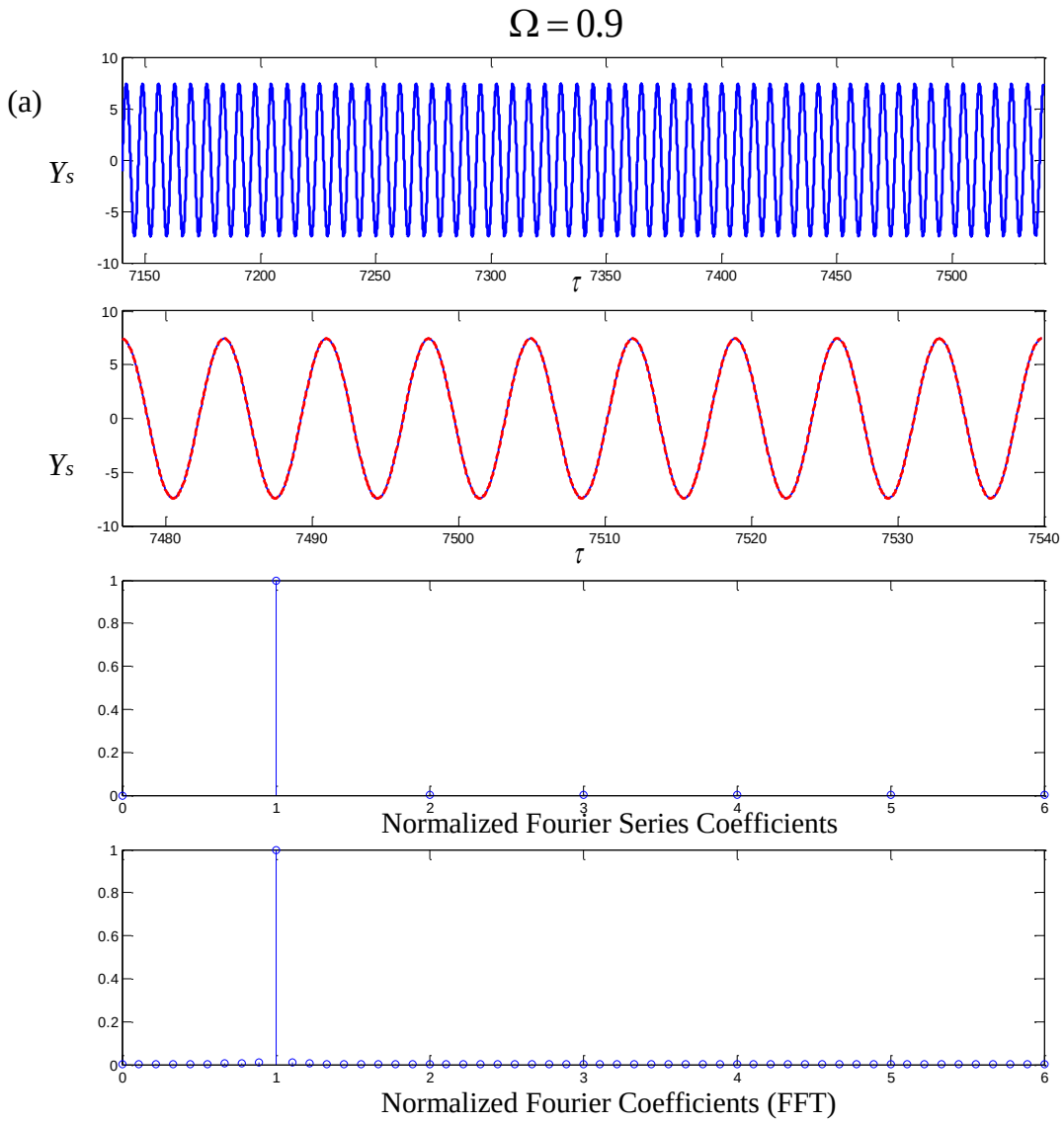

Figure 2.13(a) Time response and corresponding Fourier series coefficients of the primary system frequency response curves for the normalized displacement Y_s. (linear tuned frequency $\omega_0 = 1$, nonlinear absorber stiffness $\gamma = 6\times10^{-4}$, mass ratio $\mu = 0.02$ and damping $\zeta_s = 0.001$, $\zeta = 0.002$). The actual response from numerical integration is the solid line and the first-harmonic approximation (HBM) is the dashed line. The corresponding excitation frequency is $\Omega = 0.9$.

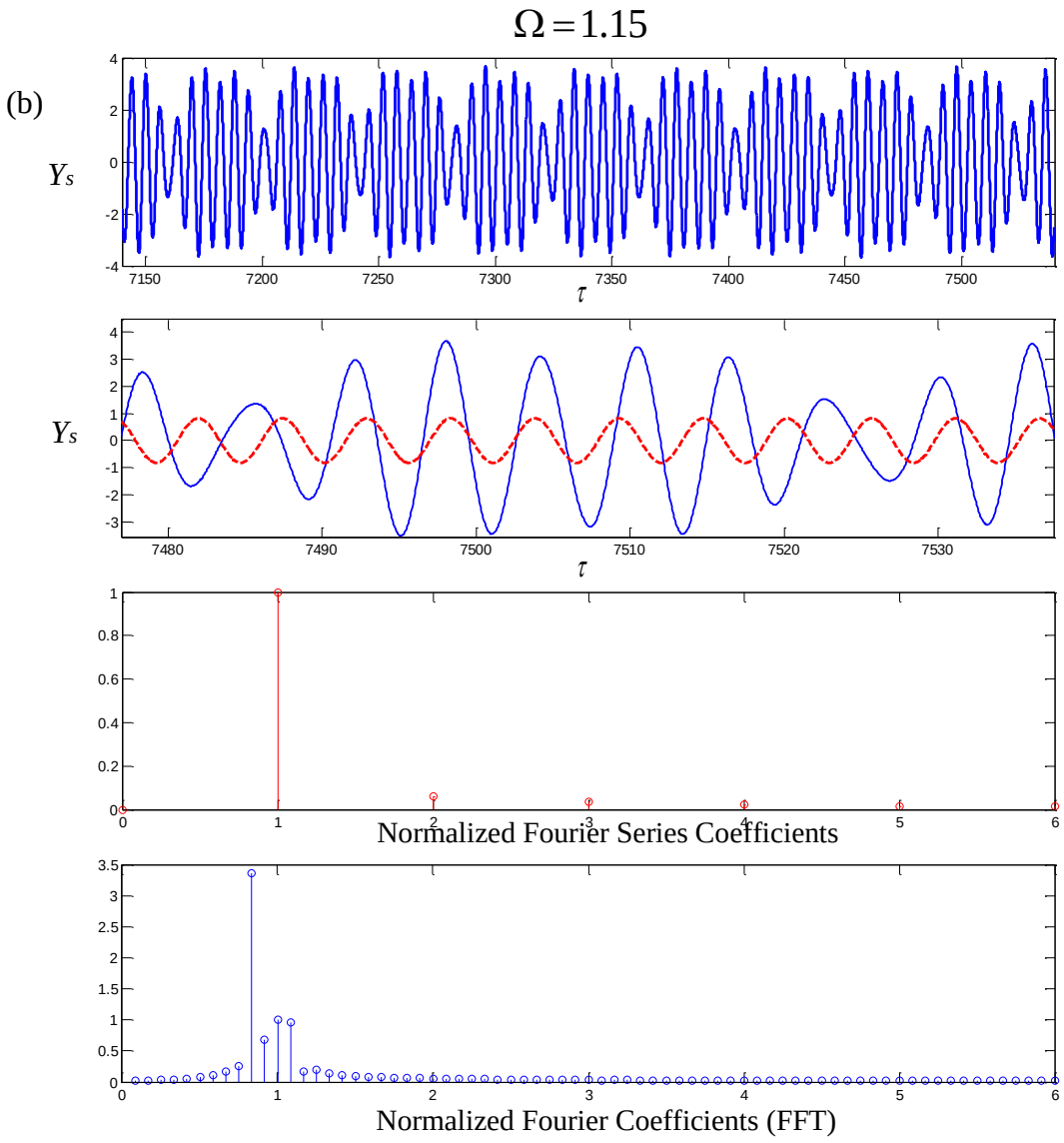

Figure 2.13(b) Time response and corresponding Fourier series coefficients of the primary system frequency response curves for the normalized displacement Y_s. (linear tuned frequency $\omega_0 = 1$, nonlinear absorber stiffness $\gamma = 6\times10^{-4}$, mass ratio $\mu = 0.02$ and damping $\zeta_s = 0.001$, $\zeta = 0.002$). The actual response from numerical integration is the solid line and the first-harmonic approximation (HBM) is the dashed line. The corresponding excitation frequency is $\Omega = 1.15$.

The bifurcation two curves plotted in Figure 2.14 are for different values of damping and for a particular value of the mass ratio. The curve for the light damping case is given as a solid line for reference. The different values of damping for the system appear to produce similar responses. From inspection of Figure 2.14 there is a level of nonlinear stiffness for the NDVA such that at this level and below the system has only one response at all frequencies. When the level of damping is increased, the level of the stiffness nonlinearity can increase such that still only one response solution occurs. In addition, the domain of the parameter values for which multi-valued solutions are present is significantly narrower for $\Omega > 1$. For $\Omega < 1$ this change is not apparent. In Table 2.2, the effect of the damping in the absorber is summarised by showing the limitation on the value of the nonlinear parameter γ_{NH} which produces a harmonic response. As the damping is increased, the value of the limiting nonlinear stiffness γ_{NH} can be slightly increased.

The bifurcation curves are also plotted for different values of the mass ratio and a fixed value of the damping ratio in Figure 2.15. It can be seen that as mass ratio increases, the level of nonlinearity can slightly increase and still only one harmonic response solution occurs. In addition, the frequency range for which multi-valued solutions exist is significantly broader for $\Omega < 1$. However, the bifurcation frequency range is smaller for higher frequencies corresponding to $\Omega > 1$. Given in Table 2.3 are the limiting values for the nonlinear stiffness parameter γ for which the single harmonic solution occurs. As the mass ratio is increased, the limiting value γ_{NH} will be slightly increased.

μ	ω_0	ζ	ζ_s	γ_{NH}	Numerical results
0.02	1	0.002	0.001	1×10^{-6}	The stable solution is harmonic at all frequencies if $\gamma < \gamma_{\mathrm{NH}}$.
0.02	1	0.005	0.001	4×10^{-6}	
0.02	1	0.008	0.001	8×10^{-6}	
0.02	1	0.01	0.001	1×10^{-5}	

Table 2.2 The effect of the damping in the absorber on the limitation of the nonlinear parameter γ which will produce a harmonic response.

μ	ω_0	ζ	ζ_s	γ_{NH}	Numerical results
0.02	1	0.002	0.001	1×10^{-6}	The stable solution is harmonic at all frequencies if $\gamma < \gamma_{\mathrm{NH}}$.
0.05	1	0.002	0.001	9×10^{-6}	
0.08	1	0.002	0.001	5×10^{-5}	
0.1	1	0.002	0.001	5×10^{-5}	

Table 2.3 The effect of the mass ratio on the limitation of the nonlinear parameter γ which will produce a harmonic response.

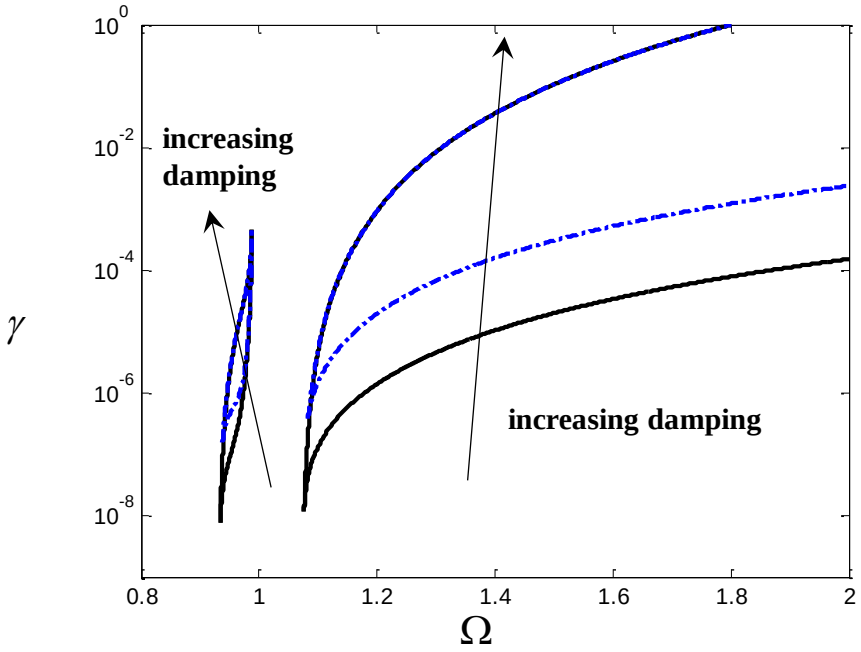

Figure 2.14 The effect of the damping ratio ζ on the bifurcation curves for the frequency amplitude response of Y_s and Y ($\omega_0 = 1$, $\mu = 0.02$, $\zeta_s = 0.001$). For $\zeta = 0.002$ (solid curve), $\zeta = 0.008$ (dash-dot curve).

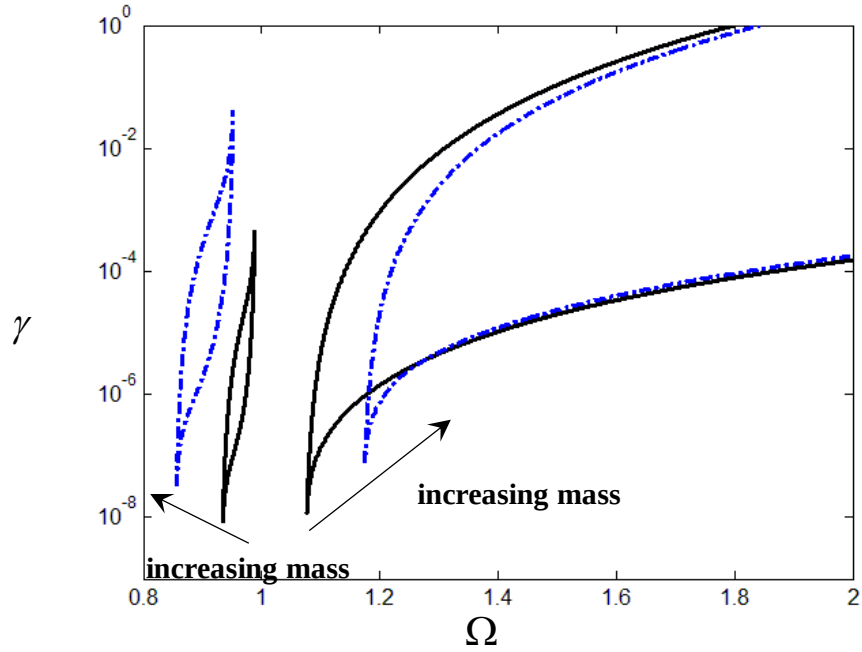

Figure 2.15 The effect of the mass ratio μ on the bifurcation curves for the frequency amplitude response of Y_s and Y ($\omega_0 = 1$, $\zeta_s = 0.001$, $\zeta = 0.002$). For $\mu = 0.02$ (solid curve), $\mu = 0.1$ (dash-dot curve).

Consider a particular numerical example with mass ratio $\mu = 0.02$, linear tuned frequency $\omega_0 = 1$ and the damping ratios of the primary system and the absorber are $\zeta_s = 0.001$ and $\zeta = 0.002$, respectively. For values of the nonlinearity $\gamma \leq 10^{-6}$, the amplitudes of the harmonic orders of the excitation frequency do not exceeded 5% compared to the amplitude of the response at the fundamental excitation frequency.

It is also useful to consider the response sensitivity on the level of the nonlinearity given by the value of the parameter γ. The effect of the linear (i.e. $\gamma = 0$) and nonlinear vibration absorber (i.e. γ=10^{-6}) on the primary system displacement versus excitation frequency ratio Ω are shown in Figure 2.8. By observation though, the nonlinear absorber produces an almost identical vibration reduction bandwidth compared to the linear absorber and tabulated in Table 2.4. It was found that some range of the parameters did not produce a wider vibration bandwidth compared to the linear absorber. An in-depth analysis of the parameters which affect the vibration response and control the vibration reduction bandwidth will be detailed and discussed in the chapter 3.

γ	Reduction Bandwidth	Bandwidth improvement compared to the linear absorber (%)
0 (Linear case)	0.019	
10^{-8}	0.019	0
5×10^{-8}	0.019	0
10^{-7}	0.019	0
5×10^{-7}	0.019	0
10^{-6}	0.019	0

Table 2.4 The frequency bandwidth for the vibration reduction produced by the nonlinear absorber on the primary system frequency response curves of the normalized displacement Y_s. ($\omega_0 = 1$, mass ratio $\mu = 0.02$ and damping $\zeta_s = 0.001$, $\zeta = 0.002$).

2.4. Conclusions

This chapter presented the nonlinear differential equation for a vibration absorber possessing a linear plus cubic restoring force, the latter with a hardening characteristic. The HBM approach has been applied to solve the equation of motion under harmonic excitation. Simple algebraic expressions which describe the behaviour, in terms of different nondimensional parameters of the nonlinear absorber, have been derived.

The stability characteristics of the periodic steady state solution have been analyzed using Floquet theory. The relationship between the frequency response curves and the bifurcation curves are presented. At low nonlinear absorber stiffness levels the solutions are stable, similar to a linear absorber with no bifurcation. For a medium nonlinear stiffness the solutions can be either stable or unstable, unstable solutions appears around the first and second resonance frequencies with bifurcation occurring. At higher levels for the nonlinear stiffness, unstable solutions appear around the second resonance frequency, but now only stable solutions appear around the first resonance frequency. It should be noted that when the stiffness nonlinearity exceeded at certain values, the HBM expressions are inaccurate in producing the actual solution at some frequencies. The numerical solutions, using direct numerical integration, show the presence of multiple frequencies in the response is not at the harmonic excitation frequency. In addition, the limitations on the nonlinear absorber parameters were also presented. The effect of the magnitude of the nonlinear absorber parameters on the vibration reduction effectiveness and frequency bandwidth, under harmonic excitation over a wide frequency range, will be examined in detail and discussed in the following chapter.

Chapter 3

Vibration reduction of a nonlinear vibration absorber: harmonic excitation

As described in Chapter 2, the equations of motion were derived for the primary system installed with an NDVA under harmonic excitation force and solved using the approximate analytical solutions (HBM). Mathematical expressions for the frequency response curves of the primary system were subsequently determined. A detailed analysis of the bifurcation and stability characteristics of the indentified periodic steady state solutions have been given in Section 2.3.

The aim of this chapter is to investigate the performance of an NDVA attached to a single degree-of-freedom primary system. The effect of the nonlinear stiffness parameter (γ), the damping ratio (ζ), the mass ratio (μ) and the linear tuned frequency (ω_0) on the vibration reduction will be investigated using the approximate analytical solutions (HBM).

In order to produce a harmonic response at all frequencies, a limited value for the nonlinear stiffness parameter was obtained. These were checked by direct numerical integration of the equations of motion. The vibration control dependent upon the nonlinear stiffness parameter can

be considered in terms of the vibration bandwidth effectiveness of the absorber. The effect of the nonlinear stiffness is also discussed for higher values of the linear tuned frequency. These characteristics and behaviour are both presented and discussed.

Following this, the other absorber parameters (damping ratio, mass ratio and linear tuned frequency) that affect the vibration bandwidth effectiveness and the sensitivity of it to these parameters is examined using separate variations in just one parameter at a time. In addition, the vibration reduction bandwidth for a linear and nonlinear absorber at the same linear absorber tuned frequency is presented for comparsion.

3.1 The effect of the nonlinear stiffness parameter (γ)

3.1.1 The effect of the nonlinear stiffness parameter at the 'tuned' frequency ($\omega_0 = \omega_1/\omega_s = 1$)

The mass ratio for the nonlinear vibration absorber to the primary system is set to $\mu = 0.06$, the linear tuned frequency is set to $\omega_0 = 1$, i.e. the absorber linear natural frequency is equal to the natural frequency of the primary system and the damping ratio of the primary system is $\zeta_s = 0.001$ and two values of the damping ratios for the absorber are considered, namely $\zeta = 0.002$ and $\zeta = 0.02$, respectively. Various values of nonlinearity are selected, i.e. for $\gamma \le 10^{-5}$ and $\gamma \le 2\times10^{-4}$, respectively, in order to produce a harmonic response at all frequencies. The amplitude of the other harmonics never exceeded 5% of the harmonic amplitude at the excitation frequency. It is useful to consider the response sensitivity to the level of nonlinearity given by the value of the parameter γ. The effect of the linear (i.e. $\gamma = 0$) and nonlinear vibration absorber on the primary system and the secondary system displacement versus excitation frequency ratio Ω are shown in Figures 3.1-4(a)-(c).

When the damping is relatively low, it can be observed in Figures 3.1(a)-(c) that the effect of the nonlinear absorber on the normalized primary system displacement Y_s is to shift the first resonance peak Ω_{r1}, the effective tuned frequency Ω_t and bend the second resonance peak Ω_{r2} to the right. An unstable branch appears in between the two stable branches of the response level of the first resonance peak Ω_{r1}. In addition, the unstable branch may appear between the

two stable branches or partially above the response level of the second resonance peak Ω_{r2}. In Figures 3.2(a)-(c) the effect of the nonlinearity on the secondary system displacement Y is also to shift the first resonance peak Ω_{r1} and bend the second resonance peak Ω_{r2} to the right. A corresponding unstable branch appears in between the two stable branches of the response level of the first resonance peak for the displacement of the absorber mass Y. In addition, the unstable branch presents between the two stable branches of the response level of the second resonance peak. The corresponding phase curves for the primary and the secondary system are given in Figures 3.5-6(a)-(c). An unstable branch appears in between the two stable branches of the first resonance peak as observed in the plots of the response amplitudes. The unstable branch presents between the two stable branches of the response level of the second resonance peak.

When the damping is higher than in the previous case, it can be observed in Figures 3.3(a)-(c). An unstable branch appears in between the two stable branches of the response level of the first resonance peak Ω_{r1}. The response effect is slightly different for the second resonance peak Ω_{r2}. For low values of the nonlinearity, the unstable branch may appear between the two stable branches or partially above the response level of the second resonance peak Ω_{r2}. For higher values of the nonlinearity, the unstable branch may appear at a response level above the stable branches of the second resonance peak Ω_{r2}. In Figures 3.4(a)-(c) the corresponding unstable branch also appears in between the two stable branches of the response level of the first resonance peak for the displacement of the absorber mass Y. In addition, the unstable branch is present between the two stable branches of the response level of the second resonance peak. The corresponding phase curves for the primary and the secondary system are given in Figures 3.5-8(a)-(c).

By observation though, a difference is apparent between the vibration reduction of the linear and the nonlinear absorbers; the nonlinear device has a wider effective bandwidth. In Table 3.1-2, using numerical values based on the HBM expressions, the effective bandwidth is increased by about 2% compared to the linear case when the damping is low. When the damping is higher, the effective bandwidth is increased from 4% to 17% compared to the linear absorber. These were also checked by numerical integration of the equations of motion.

The vibration attenuation amplitude could also be examined as a measure of the nonlinear absorber effectiveness. The nonlinear absorber parameters (e.g., nonlinear stiffness, damping ratio, mass ratio) will affect the vibration reduction. However, no analytical expression for the vibration attenuation derived due to the complexity of the mathematical algebraic relationships.

Figures 3.1(a)-(b) also show that the first resonance frequency Ω_{r1} moves to a slightly higher frequency as it is affected by the nonlinearity. The peak response of the primary mass at the first resonance frequency is also higher than that for a linear absorber. Compared to the linear absorber, with a nonlinear absorber it can be seen that the nonlinearity has the effect of shifting the second resonant peak Ω_{r2} moving to higher frequency away from the effective tuned frequency Ω_t thus improving the robustness of the device to mistuning. Above the vibration reduction bandwidth, i.e. $\Omega > \Omega_{r1}$, but not too far above this frequency, the primary mass response is lower with the nonlinear absorber attached. The frequency limit for this behaviour appears in the second frequency region where an unstable solution is possible and corresponds to the extreme bending of the second resonance peak. This 'peak' is almost at a constant value over a wide range of frequencies. Subsequently, above $\Omega = \Omega_{r2}$, this solution could not occur and the only real solution is the one valid at much higher frequencies. The primary system response with the attached linear and nonlinear absorber are almost identical in behaviour at very high frequencies, i.e. $\Omega >> 1$.

γ	Ω_{r1}	Ω_{r2}	Ω_t	Bandwidth for NDVA	Bandwidth improvement compared to a linear absorber (%)
0 (Linear case)	0.885	1.130	1	0.056	
5×10^{-7}	0.916	1.163	1	0.056	0
10^{-6}	0.927	1.189	1	0.057	2
5×10^{-6}	0.945	1.303	1	0.057	2
10^{-5}	0.951	1.382	1.001	0.057	2

Table 3.1 The frequency bandwidth for the vibration reduction produced by the nonlinear absorber on the primary system frequency response curves of the normalized displacement Y_s. ($\omega_0 = 1$, mass ratio $\mu = 0.06$ and damping $\zeta_s = 0.001$, $\zeta = 0.002$).

γ	Ω_{r1}	Ω_{r2}	Ω_t	Bandwidth for NDVA	Bandwidth improvement compared to a linear absorber (%)
0 (Linear case)	0.885	1.130	1	0.042	
10^{-5}	0.919	1.143	1.001	0.042	0
5×10^{-5}	0.957	1.178	1.005	0.044	4
10^{-4}	0.961	1.207	1.010	0.046	10
2×10^{-4}	0.963	1.248	1.019	0.049	17

Table 3.2 The frequency bandwidth for the vibration reduction produced by the nonlinear absorber on the primary system frequency response curves of the normalized displacement Y_s. ($\omega_0 = 1$, mass ratio $\mu = 0.06$ and damping $\zeta_s = 0.001$, $\zeta = 0.02$).

(a)

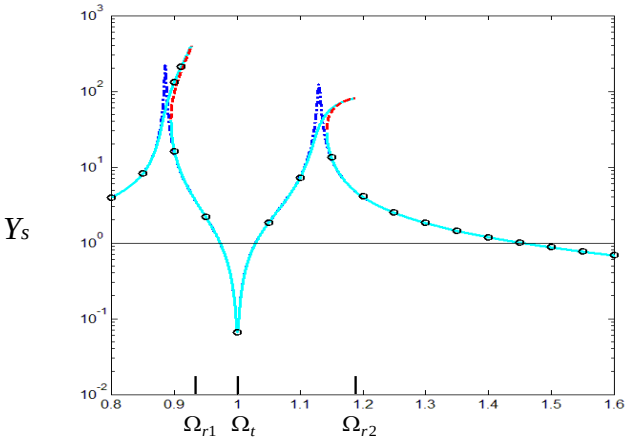

$\gamma = 10^{-6}$

(b)

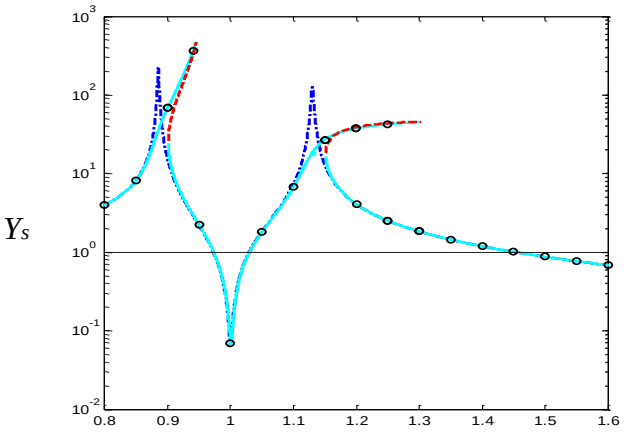

$\gamma = 5\times10^{-6}$

(c)

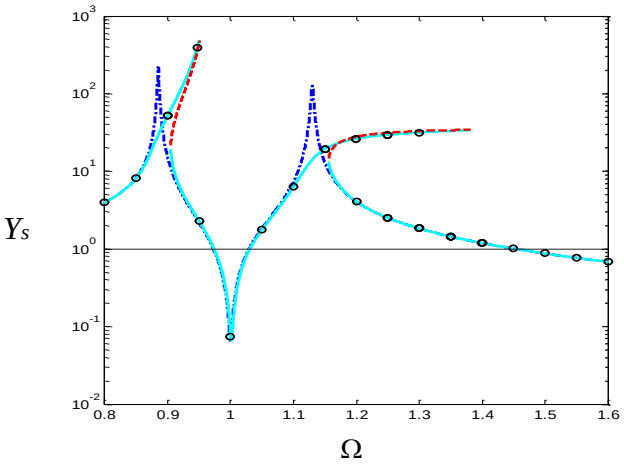

$\gamma = 10^{-5}$

Figure 3.1 The effect of the nonlinear absorber stiffness on the primary system frequency response curves Y_s as a function of Ω. (The 'tuned' frequency $\omega_0 = \omega_1/\omega_s = 1$, mass ratio $\mu = 0.06$ and damping $\zeta_s = 0.001$, $\zeta = 0.002$). The response for the system with the linear absorber is given by the dashed-dotted line. For the NDVA, the solid line is the stable solution and the dashed line gives the unstable solution. Direct numerical solutions are shown by the symbol ('○'). (a) $\gamma = 10^{-6}$, (b) $\gamma = 5\times10^{-6}$ and (b) $\gamma = 10^{-5}$.

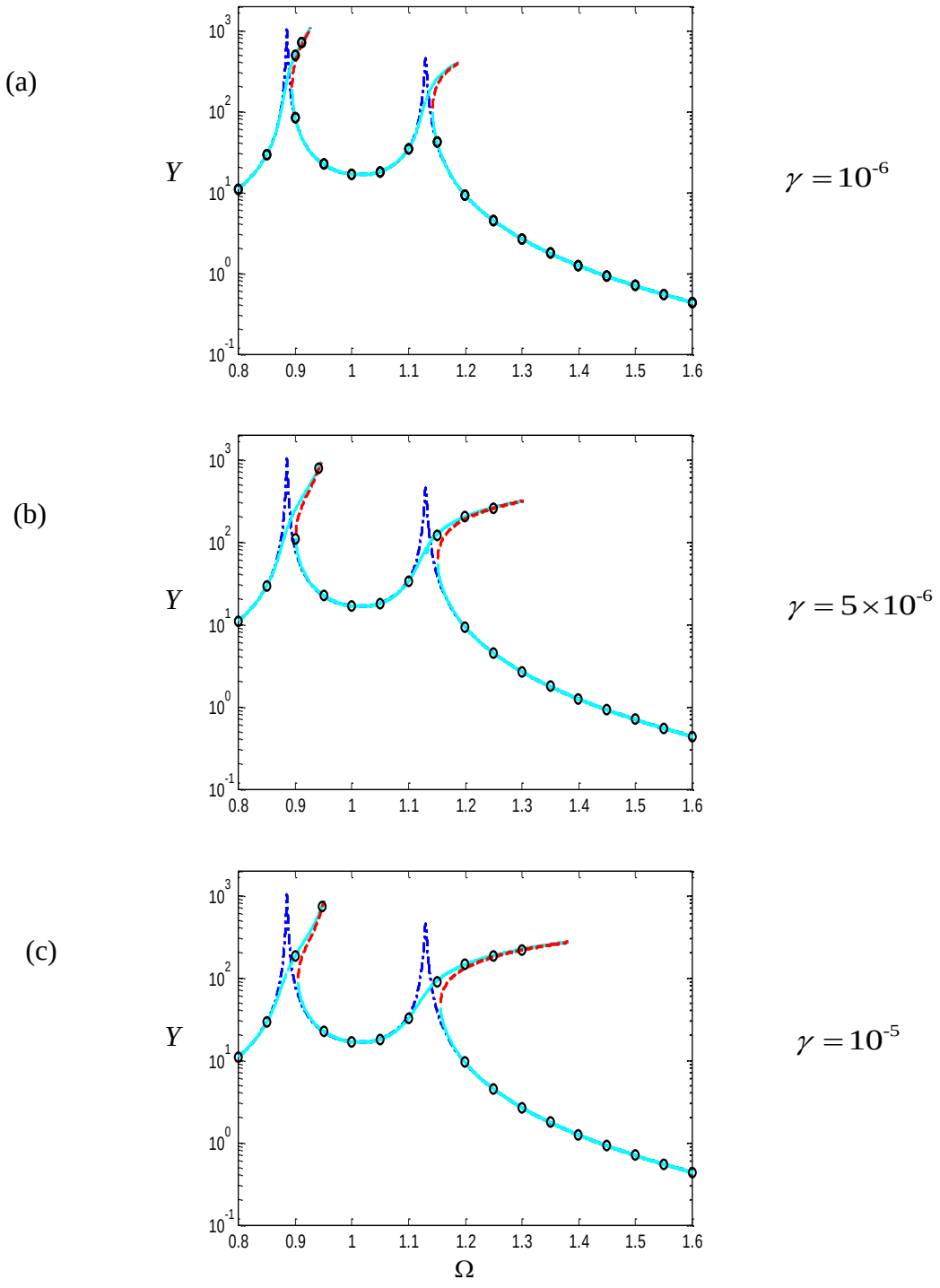

Figure 3.2 The effect of the nonlinear absorber stiffness on the secondary system frequency response curves Y as a function of Ω. (The 'tuned' frequency $\omega_0 = \omega_1/\omega_s = 1$, mass ratio $\mu = 0.06$ and damping $\zeta_s = 0.001$, $\zeta = 0.002$). The response for the system with the linear absorber is given by the dashed-dotted line. For the NDVA, the solid line is the stable solution and the dashed line gives the unstable solution. Direct numerical solutions are shown by the symbol ('○'). (a) $\gamma = 10^{-6}$, (b) $\gamma = 5\times10^{-6}$ and (b) $\gamma = 10^{-5}$.

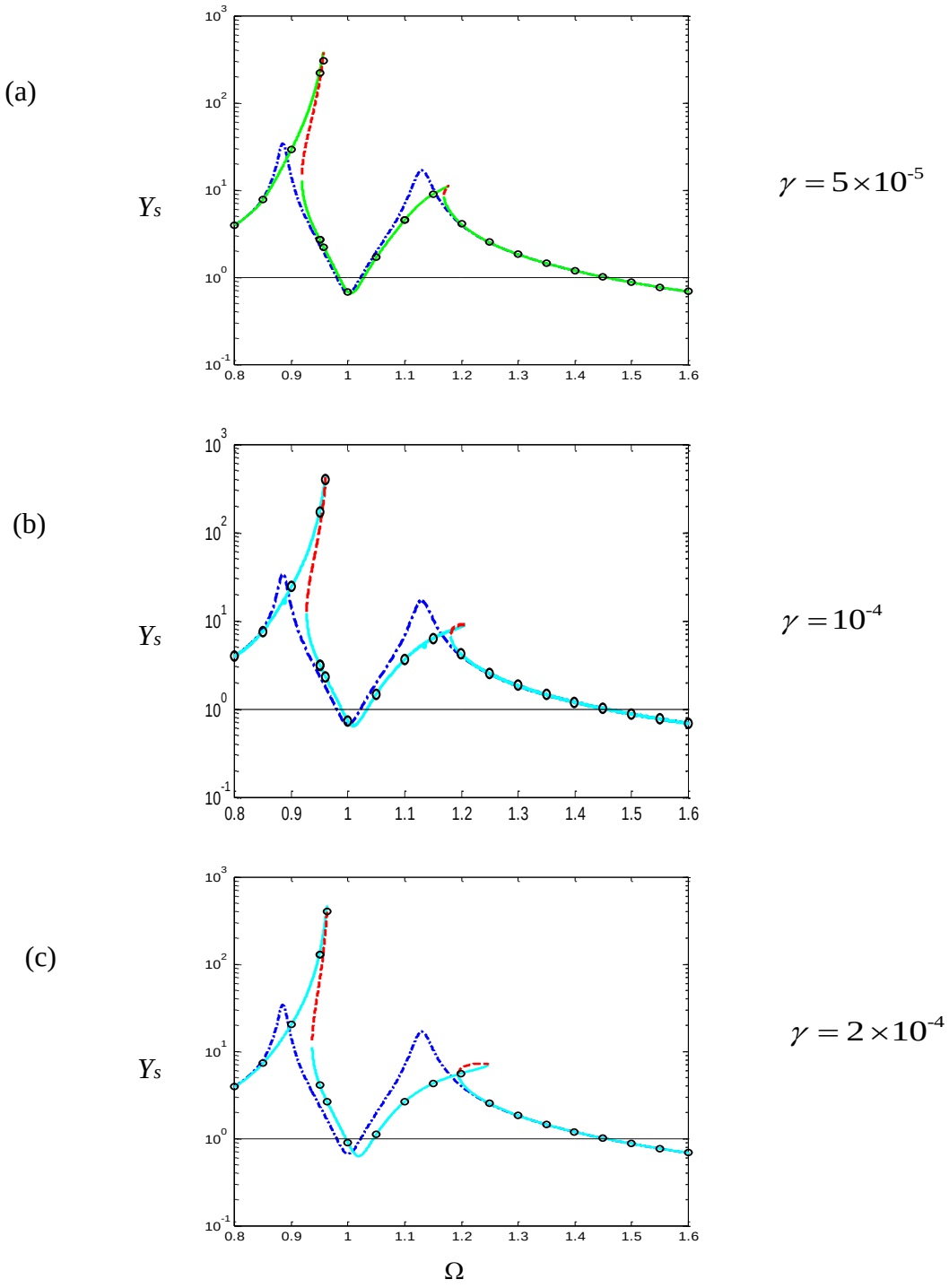

Figure 3.3 The effect of the nonlinear absorber stiffness on the primary system frequency response curves Y_s as a function of Ω. (The 'tuned' frequency $\omega_0 = \omega_1/\omega_s = 1$, mass ratio $\mu = 0.06$ and damping $\zeta_s = 0.001$, $\zeta = 0.02$). The response for the system with the linear absorber is given by the dashed-dotted line. For the NDVA, the solid line is the stable solution and the dashed line gives the unstable solution. Direct numerical solutions are shown by the symbol ('○'). (a) $\gamma = 5\times10^{-5}$, (b) $\gamma = 10^{-4}$ and (b) $\gamma = 2\times10^{-4}$.

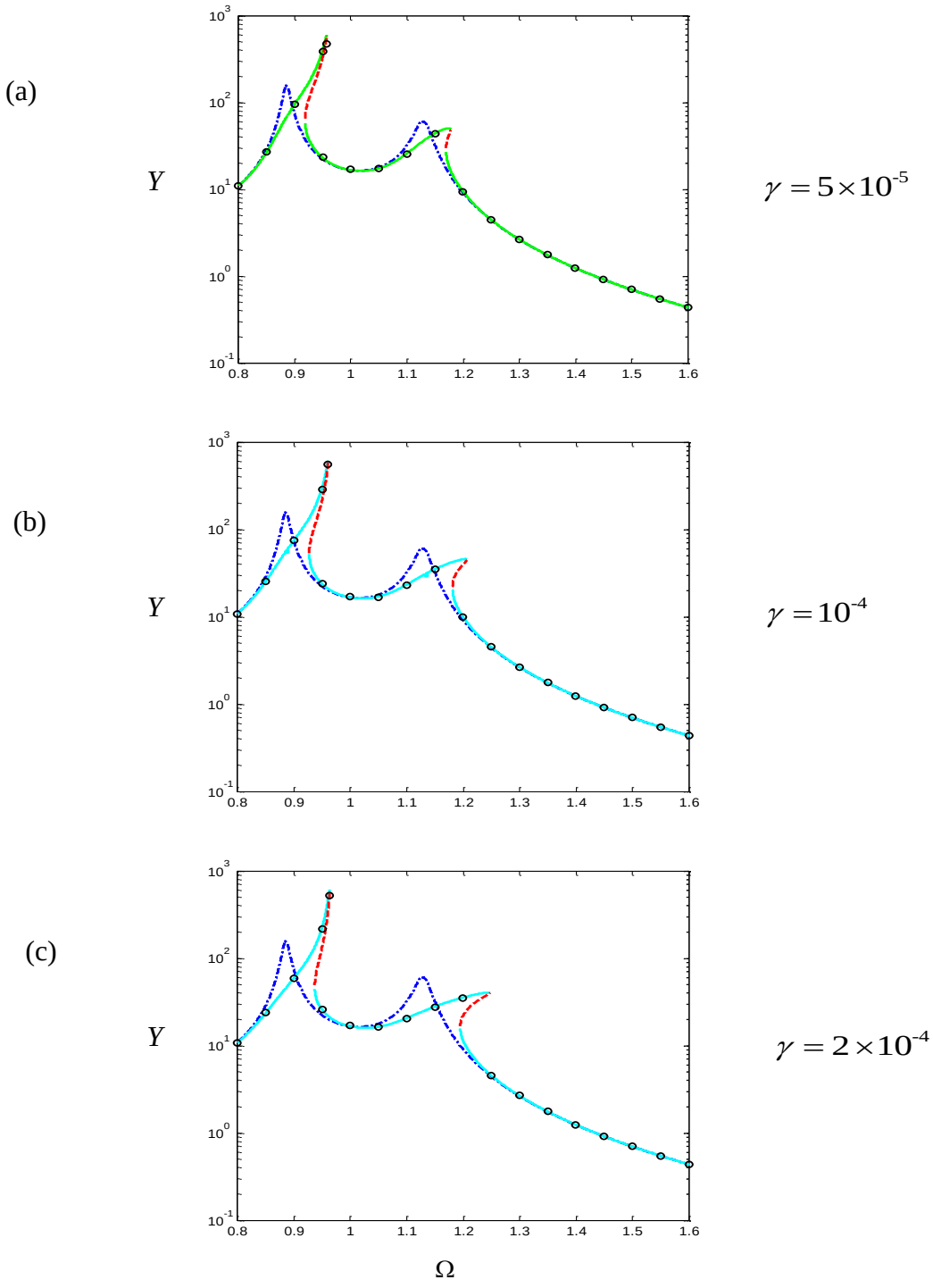

Figure 3.4 The effect of the nonlinear absorber stiffness on the secondary system frequency response curves Y as a function of Ω. (The 'tuned' frequency $\omega_0 = \omega_1/\omega_s = 1$, mass ratio $\mu = 0.06$ and damping $\zeta_s = 0.001$, $\zeta = 0.02$). The response for the system with the linear absorber is given by the dashed-dotted line. For the NDVA, the solid line is the stable solution and the dashed line gives the unstable solution. Direct numerical solutions are shown by the symbol ('o'). (a) $\gamma = 5\times10^{-5}$, (b) $\gamma = 10^{-4}$ and (b) $\gamma = 2\times10^{-4}$.

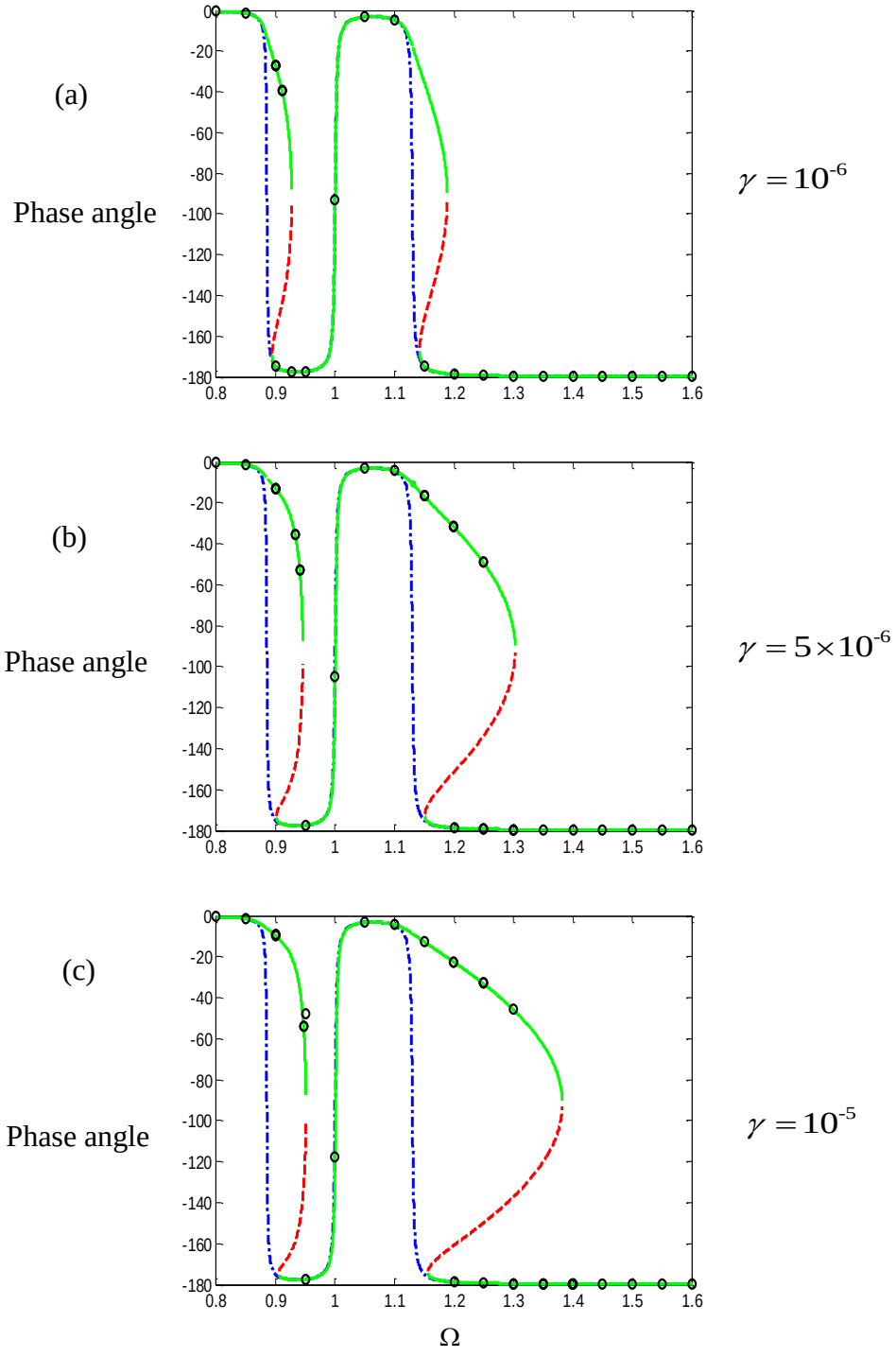

Figure 3.5 The effect of the nonlinear absorber stiffness on the phase of primary system frequency response curves Y_s as a function of Ω. (The 'tuned' frequency $\omega_0 = \omega_1/\omega_s = 1$, mass ratio $\mu = 0.06$ and damping $\zeta_s = 0.001$, $\zeta = 0.002$). The response for the system with the linear absorber is given by the dashed-dotted line. For the NDVA, the solid line is the stable solution and the dashed line gives the unstable solution. Direct numerical solutions are shown by the symbol ('○'). (a) $\gamma = 10^{-6}$, (b) $\gamma = 5\times10^{-6}$ and (b) $\gamma = 10^{-5}$.

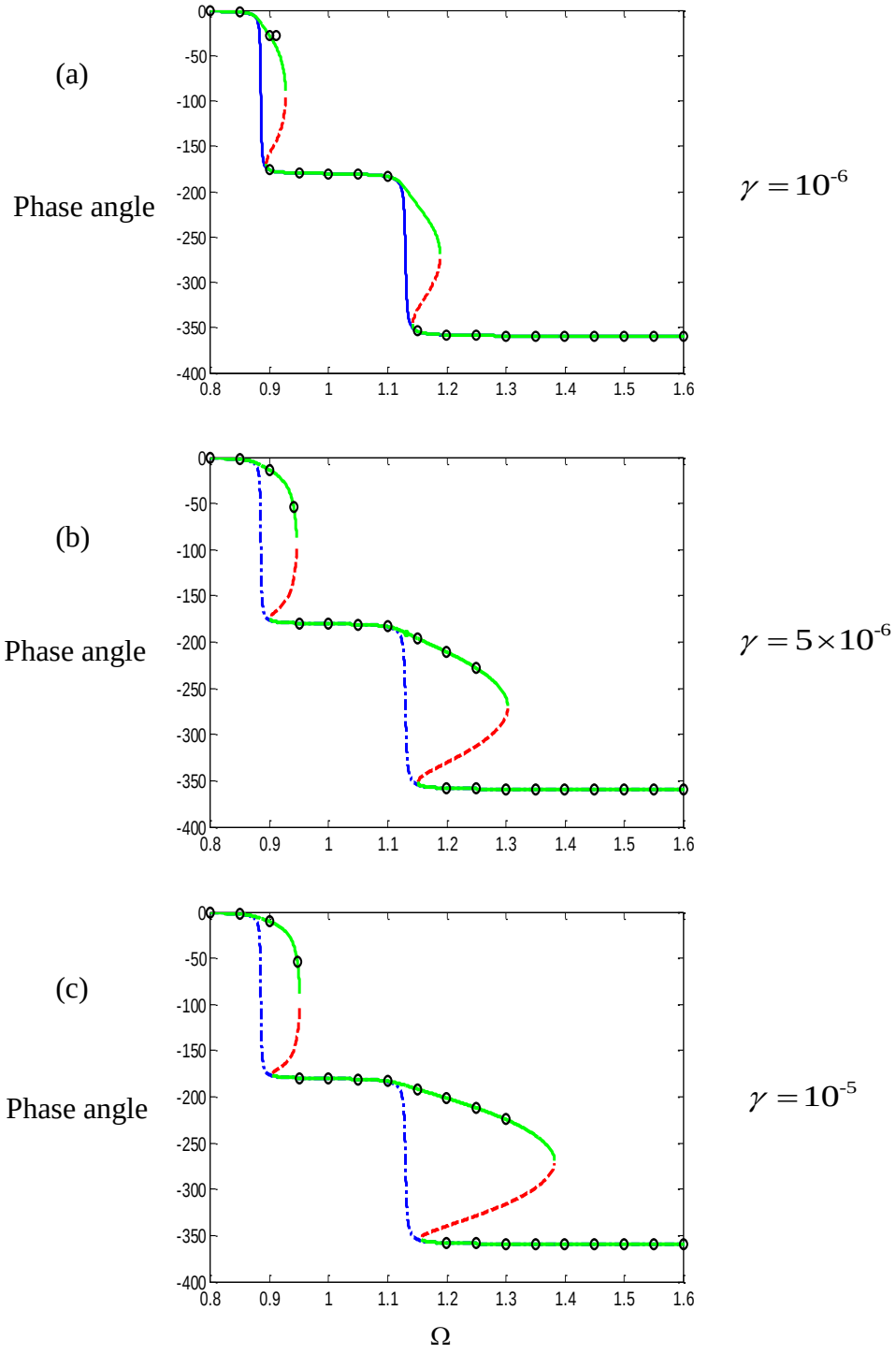

Figure 3.6 The effect of the nonlinear absorber stiffness on the phase of secondary system frequency response curves *Y* as a function of Ω. (The 'tuned' frequency $\omega_0 = \omega_1/\omega_s = 1$, mass ratio $\mu = 0.06$ and damping $\zeta_s = 0.001$, $\zeta = 0.02$). The response for the system with the linear absorber is given by the dashed-dotted line. For the NDVA, the solid line is the stable solution and the dashed line gives the unstable solution. Direct numerical solutions are shown by the symbol ('○').(a) $\gamma = 10^{-6}$, (b) $\gamma = 5\times10^{-6}$ and (b) $\gamma = 10^{-5}$.

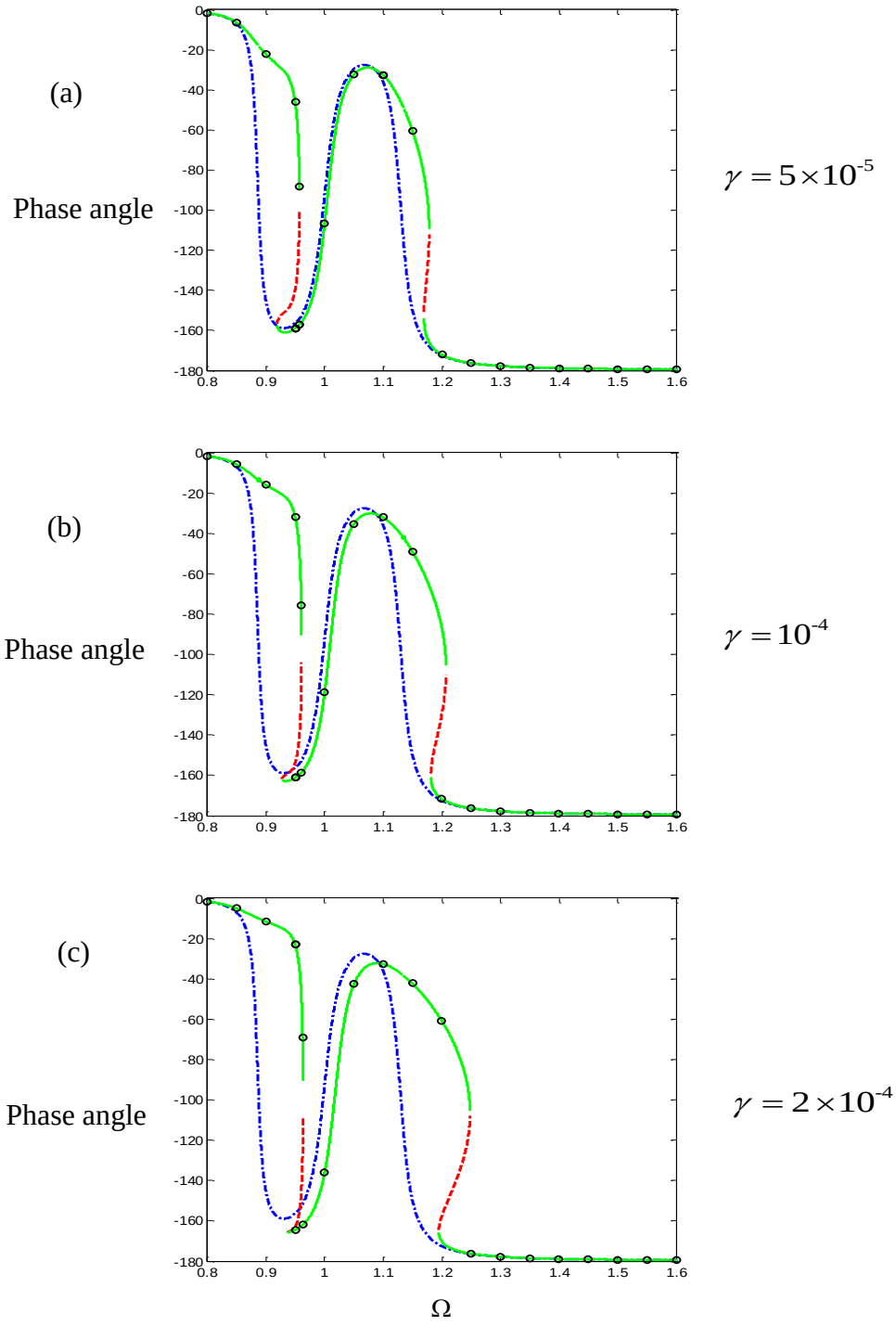

Figure 3.7 The effect of the nonlinear absorber stiffness on the phase of primary system frequency response curves Y_s as a function of Ω. (The 'tuned' frequency $\omega_0 = \omega_1/\omega_s = 1$, mass ratio $\mu = 0.06$ and damping $\zeta_s = 0.001$, $\zeta = 0.02$). The response for the system with the linear absorber is given by the dashed-dotted line. For the NDVA, the solid line is the stable solution and the dashed line gives the unstable solution. Direct numerical solutions are shown by the symbol ('○'). (a) $\gamma = 5\times10^{-5}$, (b) $\gamma = 10^{-4}$ and (b) $\gamma = 2\times10^{-4}$.

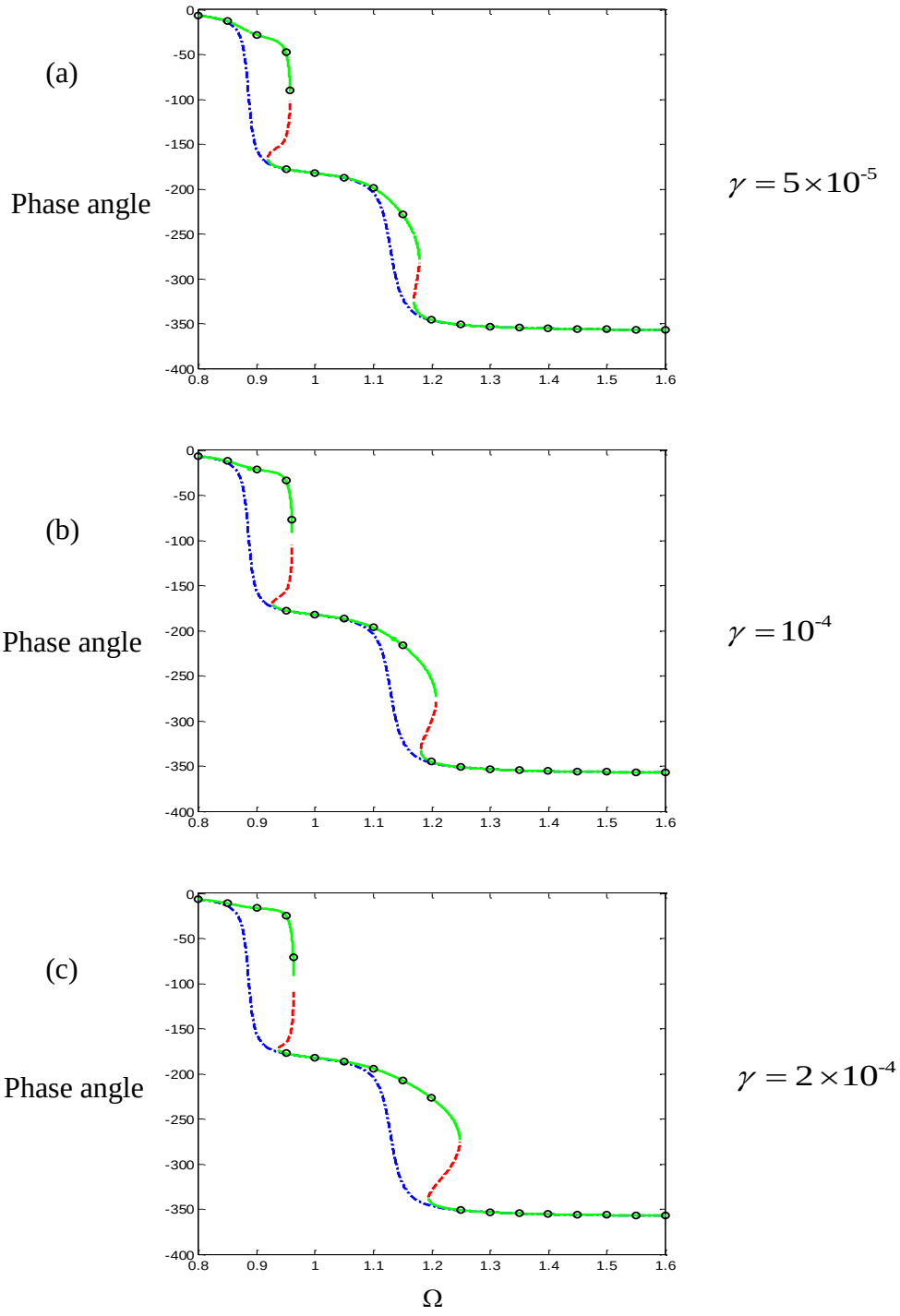

Figure 3.8 The effect of the nonlinear absorber stiffness on the phase of secondary system frequency response curves *Y* as a function of Ω. (The 'tuned' frequency $\omega_0 = \omega_1/\omega_s = 1$, mass ratio $\mu = 0.06$ and damping $\zeta_s = 0.001$, $\zeta = 0.02$). The response for the system with the linear absorber is given by the dashed-dotted line. For the NDVA, the solid line is the stable solution and the dashed line gives the unstable solution. Direct numerical solutions are shown by the symbol ('○'). (a) $\gamma = 5\times10^{-5}$, (b) $\gamma = 10^{-4}$ and (b) $\gamma = 2\times10^{-4}$.

3.1.2 The effect of the nonlinear stiffness parameter when the tuned absorber frequency ω_0 is much higher ($\omega_0 = \omega_1/\omega_s = 3$)

Consider an absorber tuned to a high frequency by changing the linear tuned frequency ω_1 of the absorber, but keeping the mass ratio μ and damping values ζ_s and ζ constant. In a practical case, an absorber can be tuned to a high frequency by changing only the linear stiffness of the absorber but keeping the mass constant, but then the damping ζ will be changed. The corresponding vibration responses of the primary system due to a linear and the nonlinear absorber are shown in Figures 3.9 and 3.11(a)-(b). For a high tuned absorber frequency, the unstable response disappears. In this scenario the linear and the nonlinear absorber have approximately equal vibration reduction bandwidths. The corresponding displacement amplitude at the tuned frequency ω_0 for a nonlinear absorber attached is approximately equal to the response with a linear absorber. The reason for this is that the linear stiffness effect becomes larger in comparison to the stiffness nonlinearity and it reduces the influence of the nonlinear contribution. In Figures 3.9 and 3.11(a)-(b) the tuned frequency ratio is $\omega_0 = 3$ ($\omega_1 \equiv 3 \times \omega_s$) and the minimum in the response is at the effective tuned frequency. Hence, there appears to be little benefit in having a nonlinear stiffness in the absorber if the tuned frequency, dependent upon the linear absorber stiffness, is too high compared to the primary system resonance; the effect is then minimal for reasonable values of the nonlinearity. In addition, the corresponding absorber response displacement is given in Figures 3.10 and 3.12(a)-(b). For the latter the effect of the nonlinear stiffness is neither apparent nor noticeable.

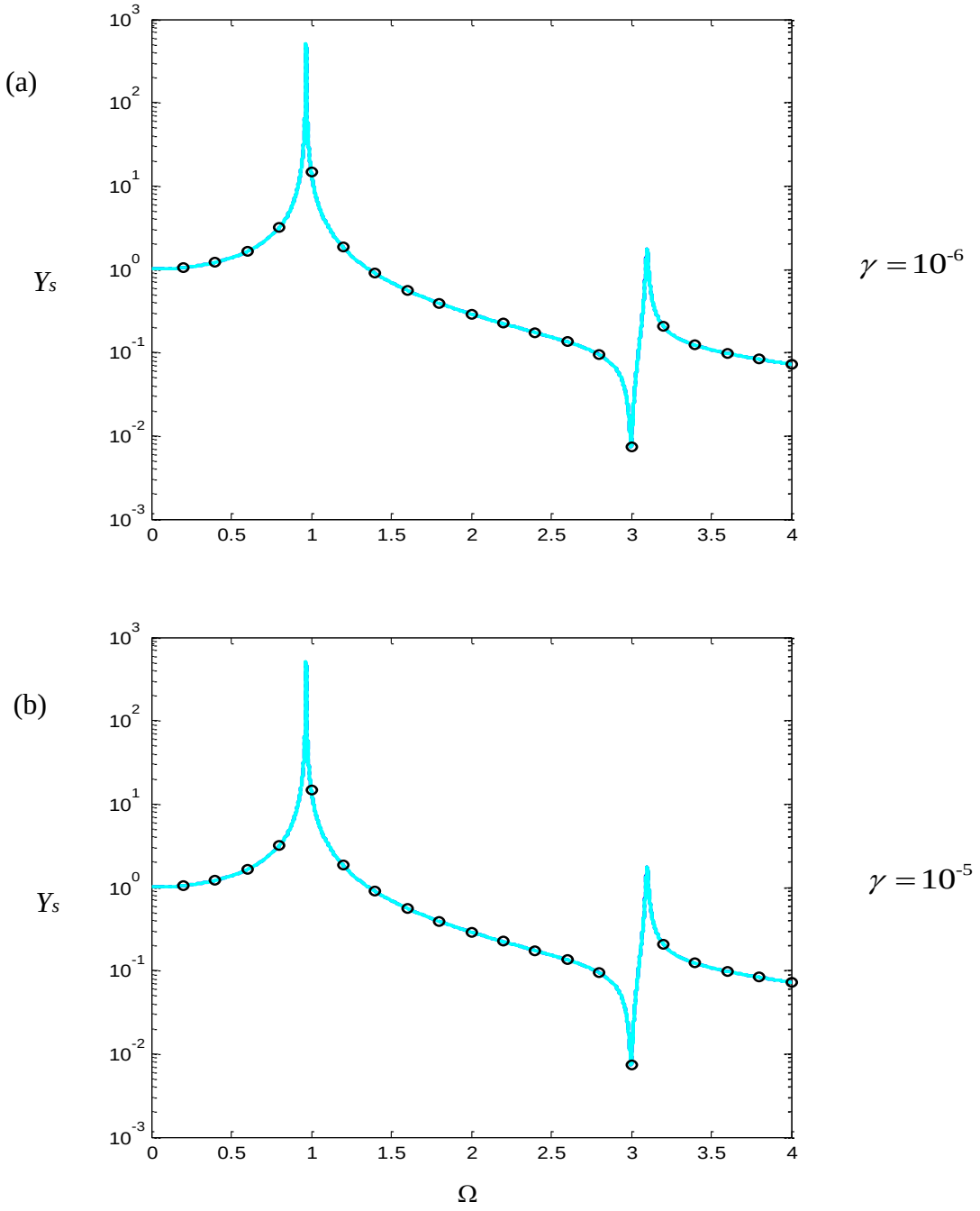

Figure 3.9 The effect of the nonlinear absorber stiffness on the primary system frequency response curves Y_s as a function of Ω. The tuned frequency ω_0 is much higher than ω_s. ($\omega_0 = 3$, mass ratio $\mu = 0.06$ and damping $\zeta_s = 0.001$, $\zeta = 0.002$). The response for the system with the linear absorber is given by the dashed-dotted line, the solid line is the stable solution using the NDVA. Direct numerical solutions are shown by the symbol ('○'). (a) $\gamma = 10^{-6}$ low absorber stiffness and (b) $\gamma = 10^{-5}$ high absorber stiffness.

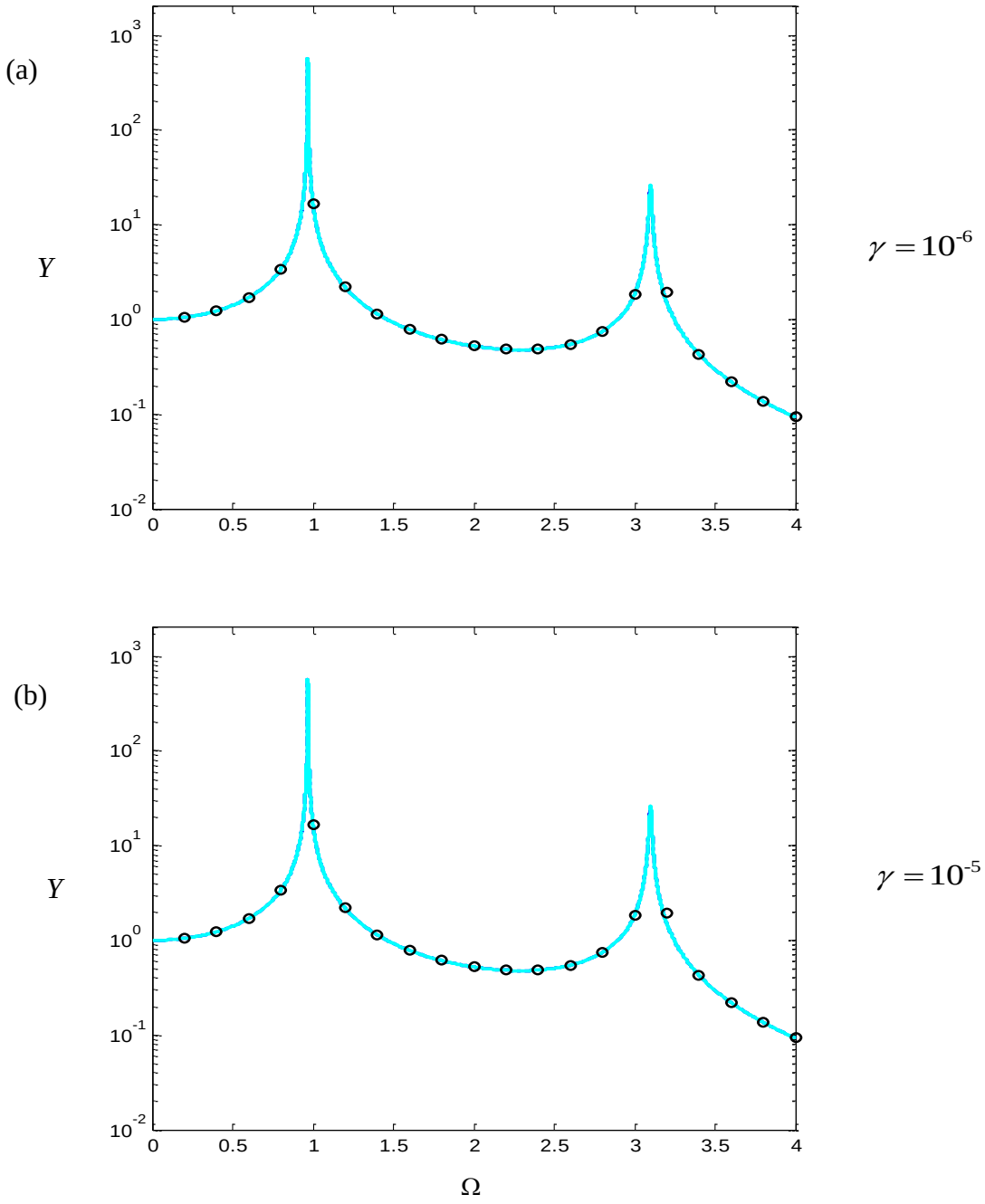

Figure 3.10 The effect of the nonlinear absorber stiffness on the secondary system frequency response curves Y as a function of Ω. The tuned frequency ω_0 is much higher than ω_s. ($\omega_0 = 3$, mass ratio $\mu = 0.06$ and damping $\zeta_s = 0.001$, $\zeta = 0.002$). The response for the system with the linear absorber is given by the dashed-dotted line, the solid line is the stable solution using the NDVA. Direct numerical solutions are shown by the symbol ('○'). (a) $\gamma = 10^{-6}$ low absorber stiffness and (b) $\gamma = 10^{-5}$ high absorber stiffness.

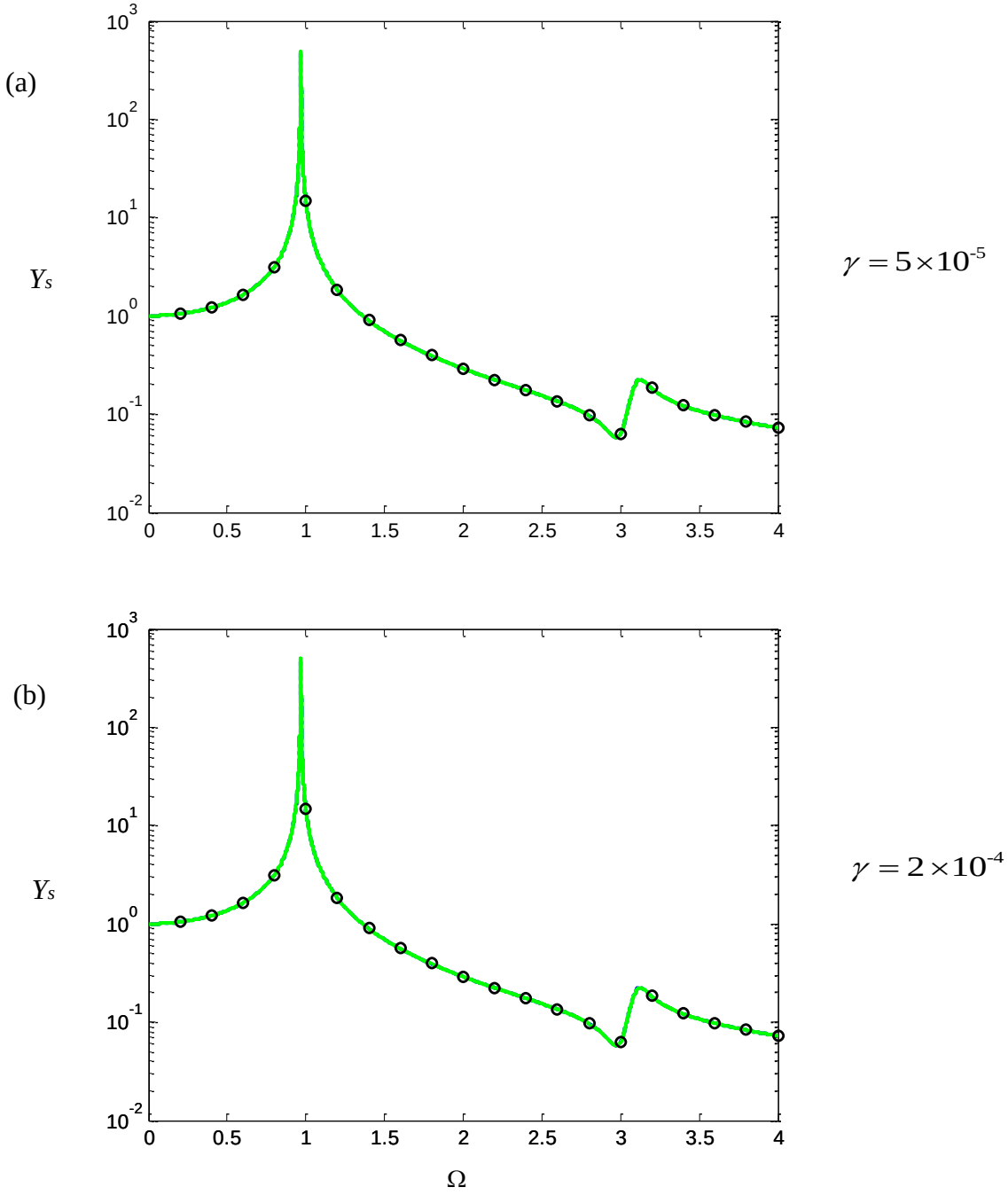

Figure 3.11 The effect of the nonlinear absorber stiffness on the primary system frequency response curves Y_s as a function of Ω. The tuned frequency ω_0 is much higher than ω_s. ($\omega_0 = 3$, mass ratio $\mu = 0.06$ and damping $\zeta_s = 0.001$, $\zeta = 0.02$). The response for the system with the linear absorber is given by the dashed-dotted line, the solid line is the stable solution using the NDVA. Direct numerical solutions are shown by the symbol ('o'). (a) $\gamma = 5\times10^{-5}$ low absorber stiffness and (b) $\gamma = 2\times10^{-4}$ high absorber stiffness.

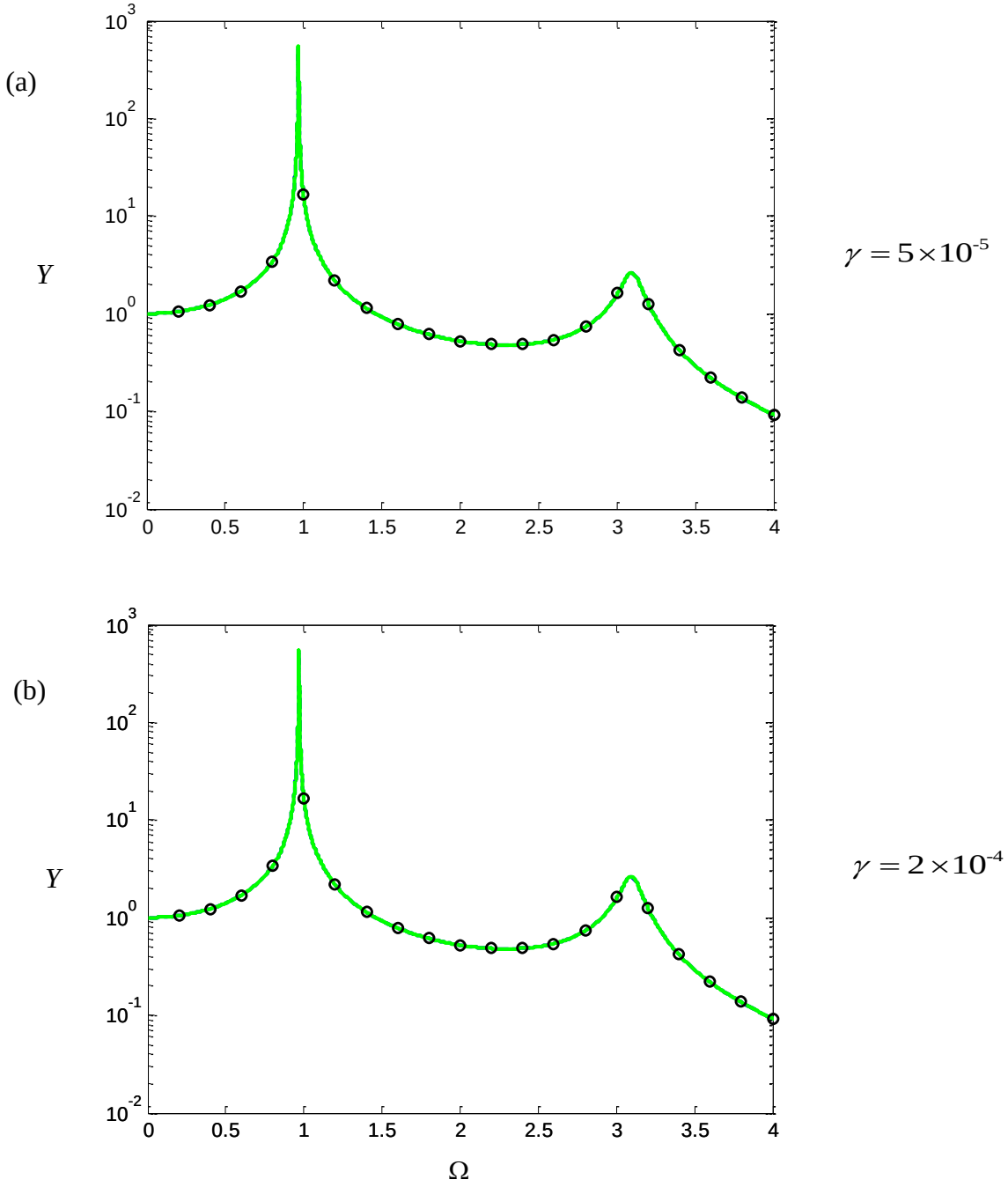

Figure 3.12 The effect of the nonlinear absorber stiffness on the secondary system frequency response curves Y as a function of Ω. The tuned frequency ω_0 is much higher than ω_s. ($\omega_0 = 3$, mass ratio $\mu = 0.06$ and damping $\zeta_s = 0.001$, $\zeta = 0.02$). The response for the system with the linear absorber is given by the dashed-dotted line, the solid line is the stable solution using the NDVA. Direct numerical solutions are shown by the symbol ('○'). (a) $\gamma = 5\times10^{-5}$ low absorber stiffness and (b) $\gamma = 2\times10^{-4}$ high absorber stiffness.

3.1.3 The effect of the nonlinear stiffness parameter on the effective tuned frequency and resonance frequencies

From inspection of the previous results, the effective tuned frequency Ω_t and the two resonance frequencies Ω_{r1} and Ω_{r2} have been identified. From various numerical simulations, using the HBM solution, these values have been presented as the nonlinear stiffness γ has been increased. Figures 3.13 and 3.15(a)-(c) show the change in these resonance frequencies Ω_{r1}, Ω_{r2} and effective tuned frequency Ω_t as the amount of nonlinearity γ increases. Inspecting Figures 3.13 and 3.15(a), it appears that the nonlinearity has a much greater effect on the second resonance frequency Ω_{r2} than on the effective tuned frequency Ω_t and on the first resonance frequency Ω_{r1} for a low tuned frequency ω_0. This is because the nonlinearity has a much greater effect when the relative displacement across the nonlinear spring in the absorber is large. The effective bandwidth range for the nonlinear absorber are shown in Figures 3.13 and 3.15(a). The range shaded indicates the range of the nonlinear stiffness γ when there is an improvement in using the nonlinear absorber compared to the linear absorber. The frequency range for the nonlinear absorber is $\Omega_L \le \Omega \le \Omega_R$, where Ω_L and Ω_R are the lower and upper frequency edges for the vibration reduction bandwidth range respectively. This effective vibration bandwidth was determined as $\Omega = \Omega_R - \Omega_L$ in Tables 3.1 and 3.2, separately.

Figures 3.14(a) and 3.16(a) show that the value for the first resonance frequency Ω_{r1} appears to be slightly shifted to both the amount of nonlinear stiffness γ and also the tuned frequency ω_0. The change in ω_0=1 produce a variation in Ω_{r1} of 6% and 9%, respectively. Figure 3.14(b) and 3.16(b) show that the effective tuned frequency in the normalized primary system displacement Y_s is affected more by the level of the stiffness nonlinearity when the tuned frequency ω_0 is low, e.g. $\omega_0 = 1$. However, it is only slightly affected by the nonlinearity when the tuned frequency is high, e.g. $\omega_0 = 3$, which was previously examined for light damping [66]. In Figures 3.14 and 3.16(c), the second resonance frequency is dependent on ω_0 and on the nonlinearity γ, the latter having a much greater effect when the relative displacement across the nonlinear spring in the nonlinear absorber is large, corresponding to the response at Ω_{r2}.

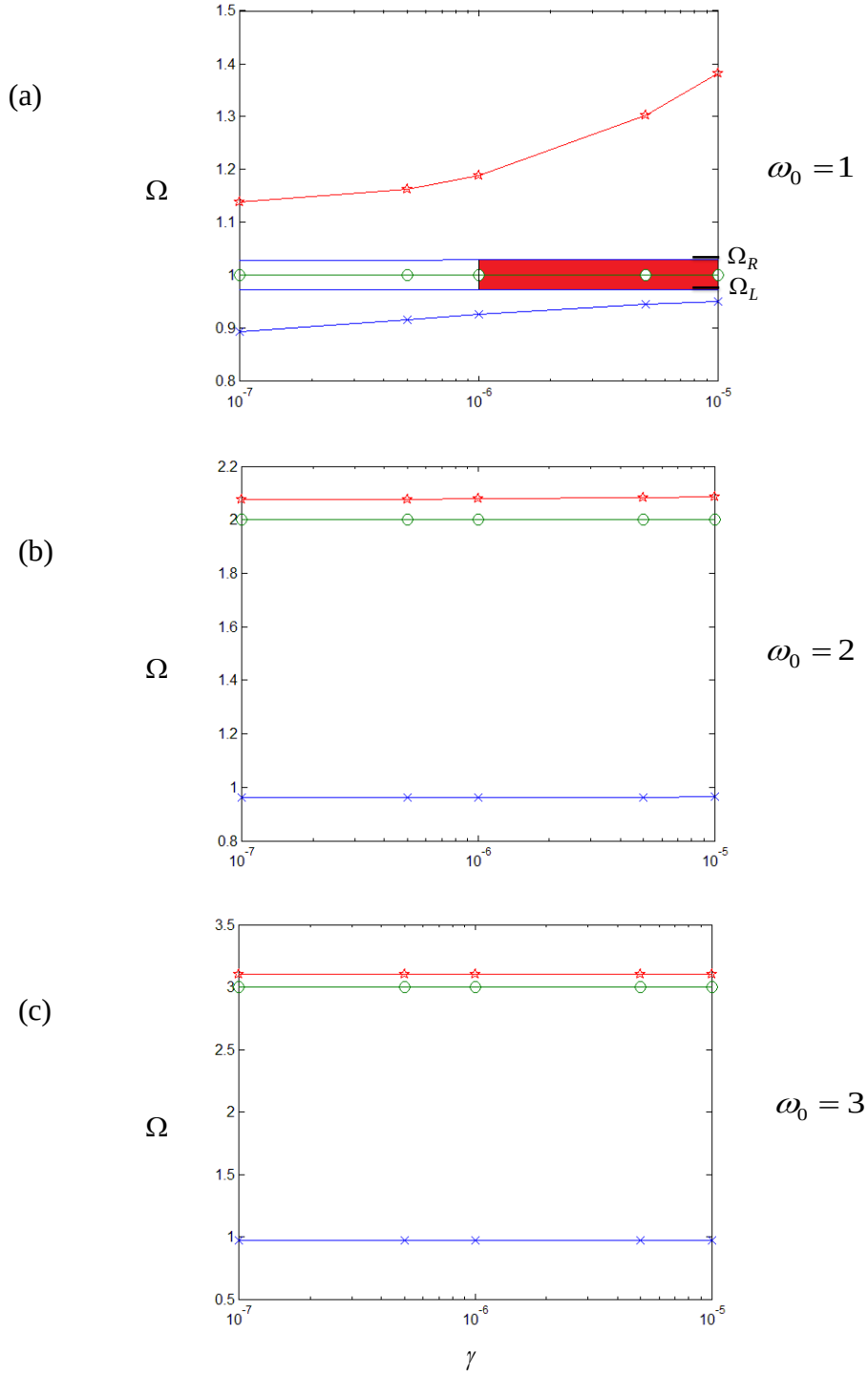

Figure 3.13 The effect of the nonlinear absorber stiffness γ for different linear tuned absorber frequencies ((a) $\omega_0 = 1$ (b) $\omega_0 = 2$ (c) $\omega_0 = 3$) on the primary system: first resonance frequency Ω_{r1} ('×'), effective tuned frequency Ω_t ('o') and second resonance frequency Ω_{r2} ('☆'). (mass ratio $\mu = 0.06$ and damping $\zeta_s = 0.001$, $\zeta = 0.002$). The solid lines around Ω_t are the lower and upper frequency ranges for the vibration reduction bandwidth range respectively. Red shading denotes a bandwidth improvement compared to a linear absorber.

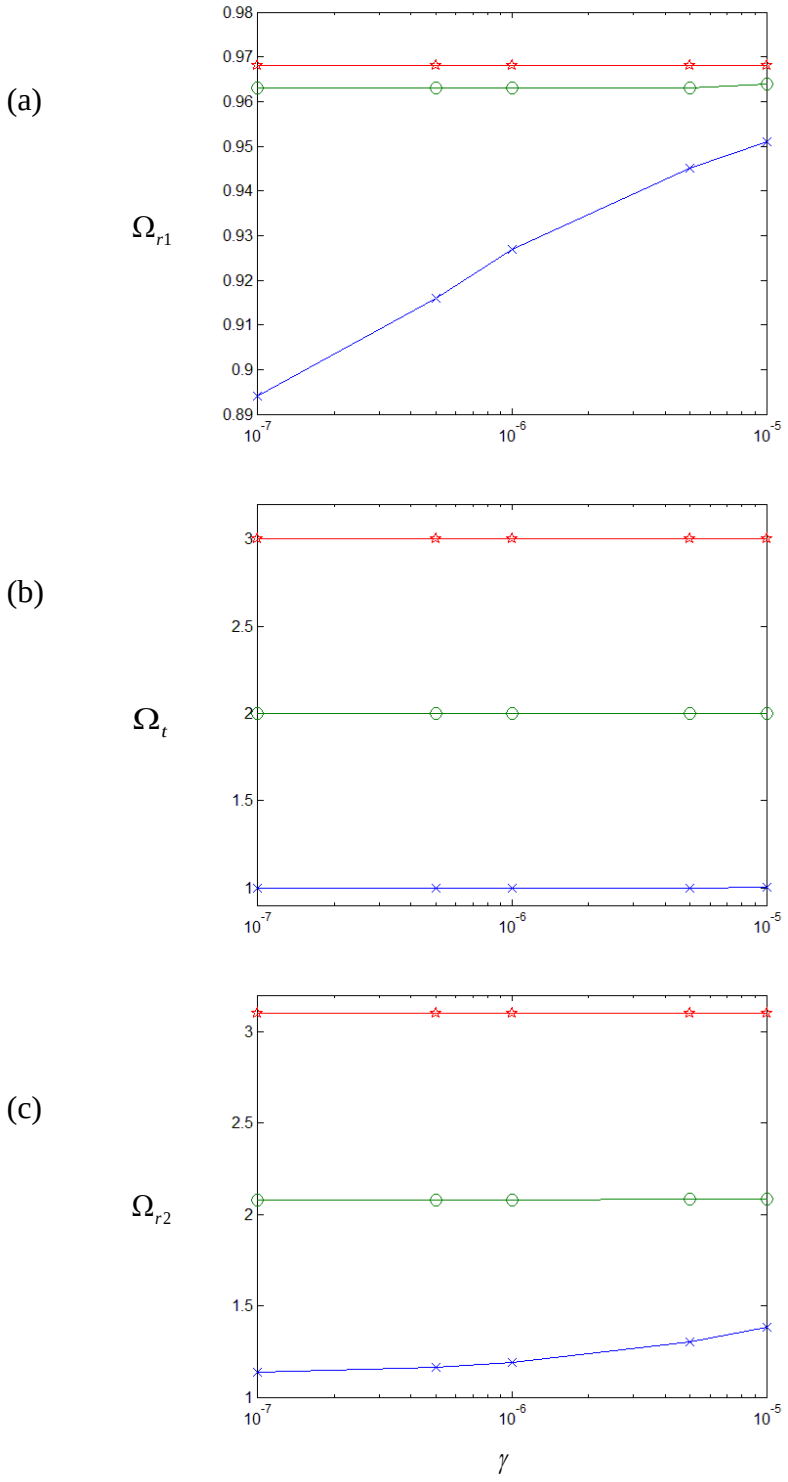

Figure 3.14 The effect of the nonlinear absorber stiffness γ for different linear tuned absorber frequencies ($\omega_0 = 1$ ('×'), $\omega_0 = 2$ ('o'), $\omega_0 = 5$ ('☆')) on the primary system: (a) first resonance frequency Ω_{r1} , (b) effective tuned frequency Ω_t and (c) second resonance frequency Ω_{r2}. (mass ratio $\mu = 0.06$ and damping $\zeta_s = 0.001$, $\zeta = 0.002$).

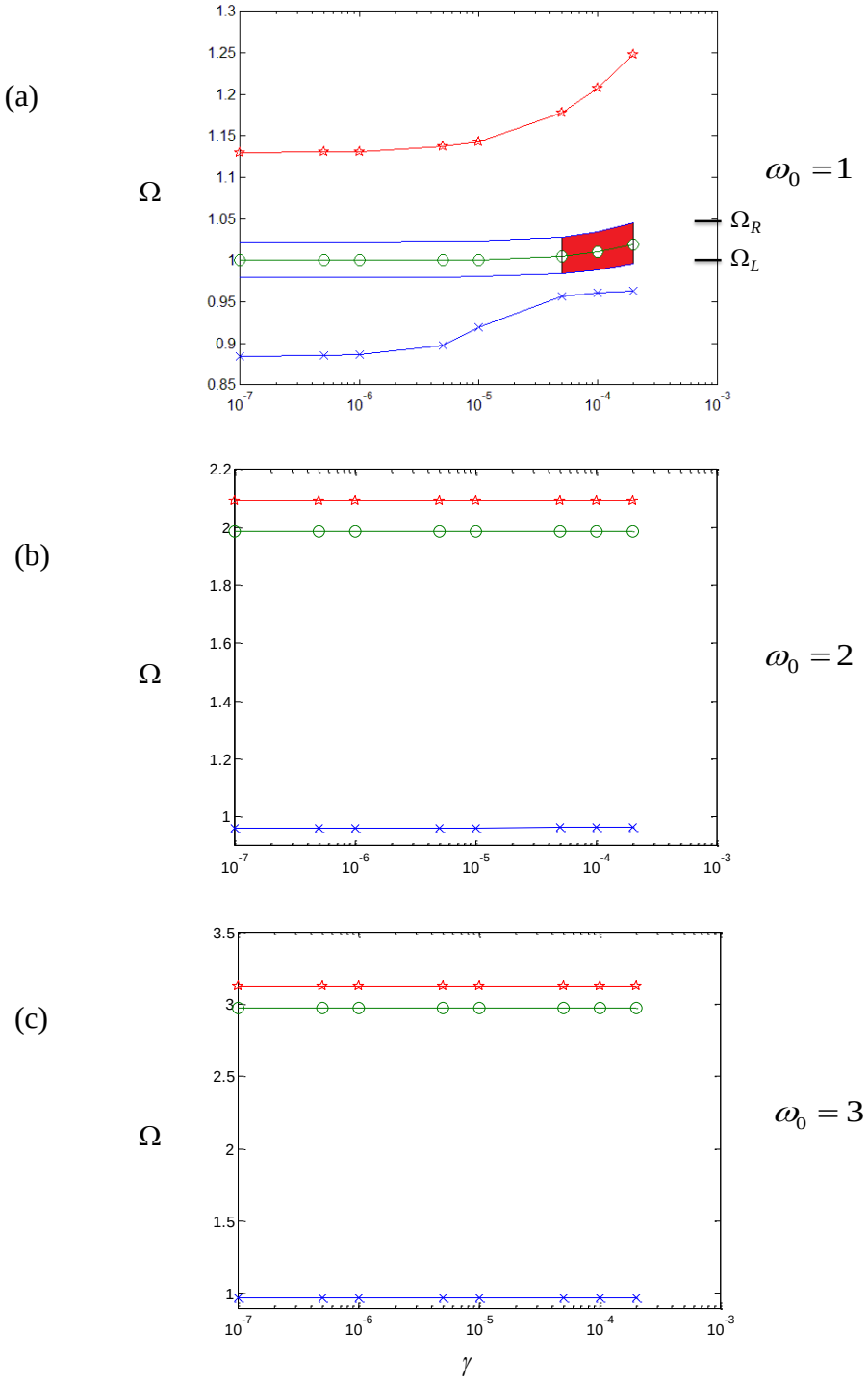

Figure 3.15 The effect of the nonlinear absorber stiffness γ for different linear tuned absorber frequencies ((a) $\omega_0 = 1$ (b) $\omega_0 = 2$ (c) $\omega_0 = 3$) on the primary system: first resonance frequency Ω_{r1} ('×'), effective tuned frequency Ω_t ('o') and second resonance frequency Ω_{r2} ('☆'). (mass ratio $\mu = 0.06$ and damping $\zeta_s = 0.001$, $\zeta = 0.02$). The solid lines around Ω_t are the lower and upper frequency ranges for the vibration reduction bandwidth range respectively. Red shading denotes a bandwidth improvement compared to a linear absorber.

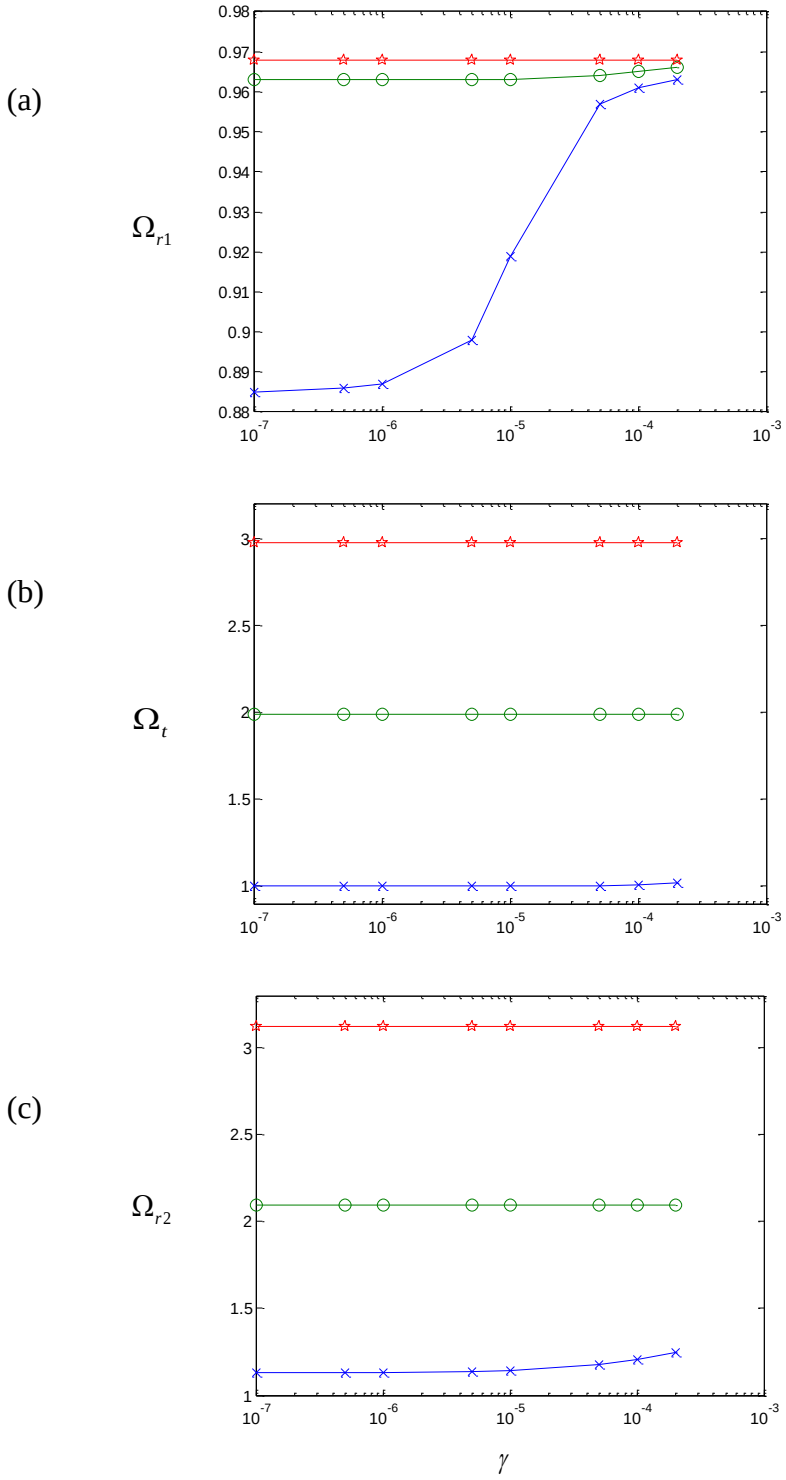

Figure 3.16 The effect of the nonlinear absorber stiffness γ for different linear tuned absorber frequencies ($\omega_0 = 1$ ('×'), $\omega_0 = 2$ ('o'), $\omega_0 = 3$ ('☆')) on the primary system: (a) first resonance frequency Ω_{r1} , (b) effective tuned frequency Ω_t and (c) second resonance frequency Ω_{r2}. (mass ratio $\mu = 0.06$ and damping $\zeta_s = 0.001$, $\zeta = 0.02$).

3.2 The effect of damping in the attached nonlinear absorber (ζ)

The mass ratio for the nonlinear absorber mass to the primary system mass is set to $\mu = 0.06$, the nonlinear stiffness parameter is $\gamma = 10^{-4}$, the linear tuned frequency is $\omega_0 = 1$ and the damping ratio for the primary system is $\zeta_s = 0.001$. The value of damping is $\zeta \geq 0.012$, in order to produce a harmonic response at all frequencies, the amplitude of the other harmonics never exceeded 5% of the harmonic amplitude at the excitation frequency. The effect of the absorber damping ζ on the primary system frequency response curves of the normalized displacement Y_s versus excitation frequency ratio Ω has been evaluated for various levels of damping and are given in Figures 3.17(a)-(c). An unstable branch appears in between the two stable branches of the response level of the first resonance peak. In addition, an unstable branch may appear between the two stable branches or partially above the response level of second resonance peak. In Figures 3.18(a)-(c), the effect of the absorber damping on the secondary system displacement Y can also be observed. A corresponding unstable branch appears in between the two stable branches of the response level of the first resonance peak for the displacement of the absorber mass Y. In addition, the unstable branch presents between the two stable branches of the response level of the second resonance peak.

In Figures 3.17(a)-(c) the linear damping ratio for the attached system is increased from $\zeta = 1.25 \times 10^{-2}$ to $\zeta = 2.5 \times 10^{-2}$. The difference between the vibration response due to the linear and the nonlinear absorber is again that the nonlinear absorber has a much wider bandwidth. In Table 3.3, it is increased by about 6%, 10% and 9% compared to the linear case for values of $\zeta = 1.25 \times 10^{-2}$, $\zeta = 2 \times 10^{-2}$ and $\zeta = 2.5 \times 10^{-2}$ respectively. It is noted that for a larger damping ratio ζ, the vibration reduction bandwidth is wider for the nonlinear absorber compared to the linear absorber case. In addition, in the response curves of the system, the larger damping has a much greater effect on the second resonance frequency Ω_{r2} than on the effective tuned frequency Ω_t shifting to a lower frequency. The unstable branch occurs over a frequency which will significantly reduce around the second resonance frequency Ω_{r2}.

In general by adding damping for both the linear and nonlinear absorber, the disadvantage is to produce a smaller vibration reduction bandwidth compared to lower absorber damping. When damping in the nonlinear absorber is greater than about 0.031, there appears to be no reduction, i.e. Y_s = normalised primary mass response is greater than 1 at all frequencies i.e. $Y_s > F/k_s$. This is observed in Figure 3.19. In many practical applications it is desirable to have a large vibration reduction bandwidth, so that the damping in the absorber needs to be quite low [26]. In addition, for higher absorber damping, the reduction of vibration at the effective tuned frequency Ω_t will be less.

For the case of high damping, one might expect that the nonlinear absorber will dissipate more vibrational energy at some frequencies when the relative velocity is high. Thus, the 'resonance' peaks might be expected to be significantly reduced with increased damping. This is apparent in the reduction in the peak response amplitude at the resonance frequencies Ω_{r1} and Ω_{r2} for the linear absorber. However, for the nonlinear absorber the amplitude of the peaks at the resonance frequencies Ω_{r1} and Ω_{r2} appear only to be slightly affected. The first peak occurs near to a frequency where the solution is unstable and the second resonance occurs where the frequency response curve has bent to the right.

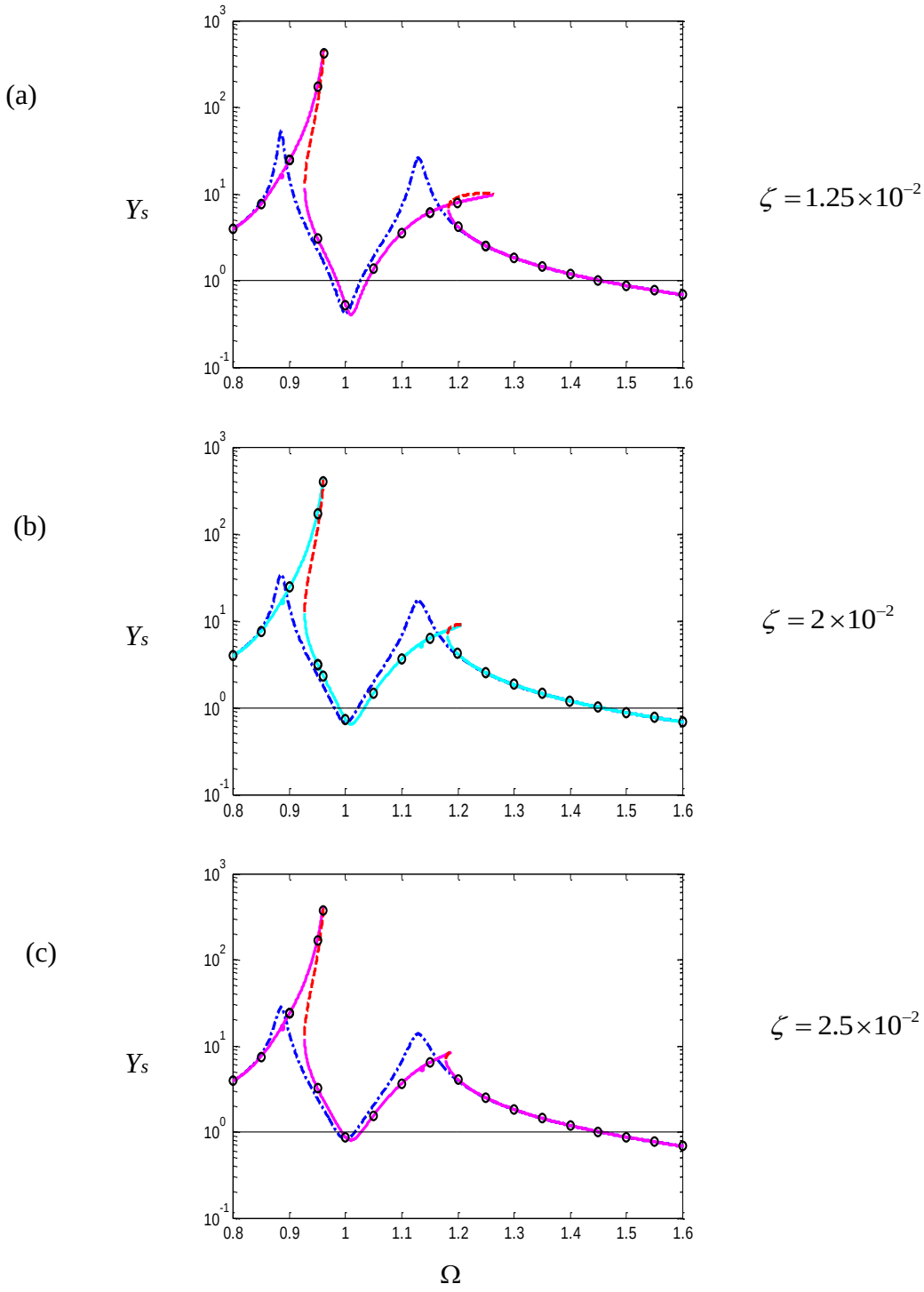

Figure 3.17 The effect of the damping in the nonlinear absorber on the primary system frequency response curves Y_s as a function of Ω. (The 'tuned' frequency $\omega_0 = \omega_1/\omega_s = 1$, nonlinear absorber stiffness $\gamma = 10^{-4}$, mass ratio $\mu = 0.06$ and damping $\zeta_s = 0.001$). The response for the system with the linear absorber is given by the dashed-dotted line. For the NDVA, the solid line is the stable solution and the dashed line gives the unstable solution. Direct numerical solutions are shown by the symbol ('o'). (a) $\zeta = 1.25\times10^{-2}$, (b) $\zeta = 2\times10^{-2}$ and (c) $\zeta = 2.5\times10^{-3}$.

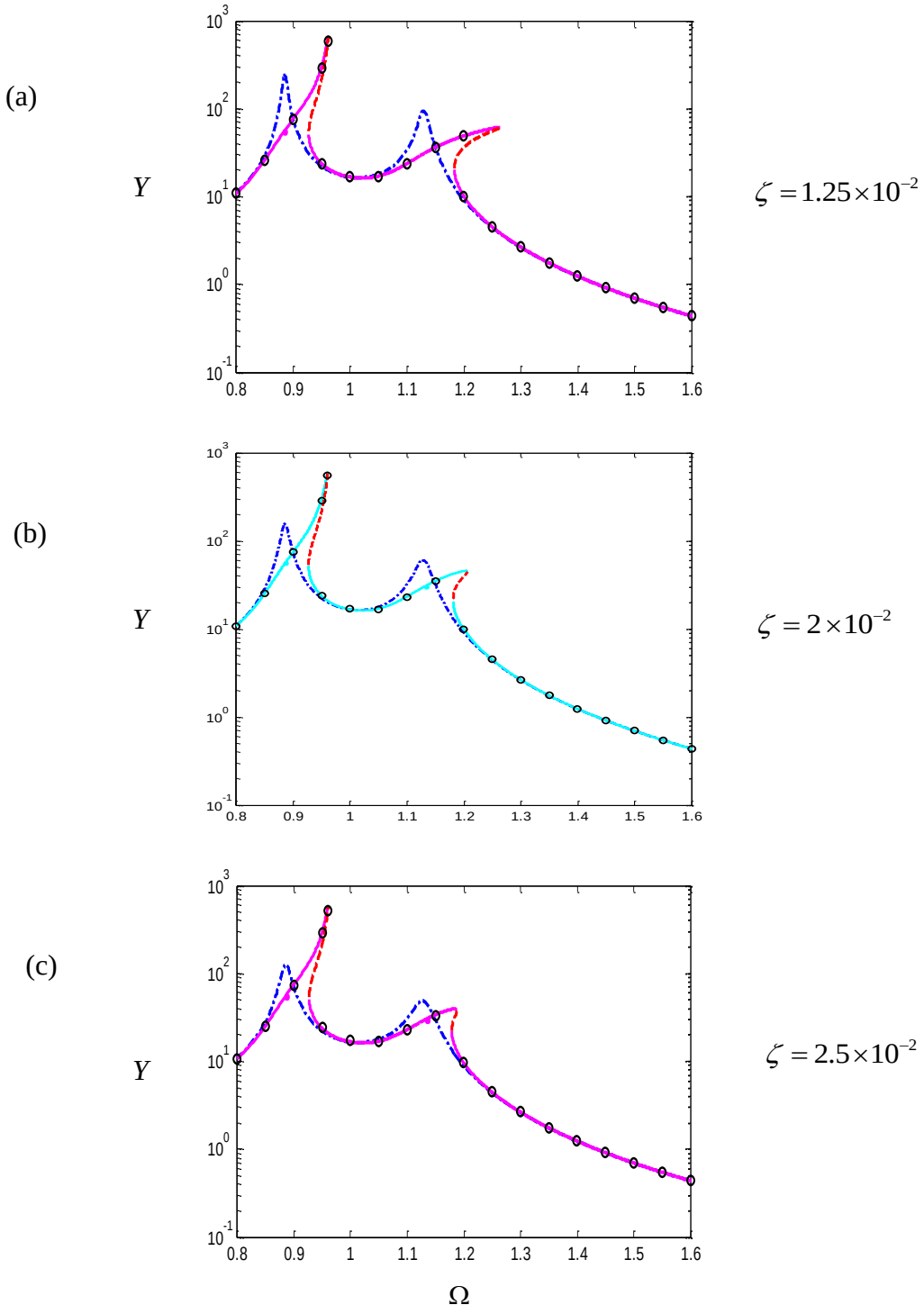

Figure 3.18 The effect of the nonlinear absorber stiffness on the secondary system frequency response curves Y as a function of Ω. (The 'tuned' frequency $\omega_0 = \omega_1/\omega_s = 1$, nonlinear absorber stiffness $\gamma = 10^{-4}$, mass ratio $\mu = 0.06$ and damping $\zeta_s = 0.001$). The response for the system with the linear absorber is given by the dashed-dotted line. For the NDVA, the solid line is the stable solution and the dashed line gives the unstable solution. Direct numerical solutions are shown by the symbol ('o').(a) $\zeta = 1.25\times10^{-2}$, (b) $\zeta = 2\times10^{-2}$ and (c) $\zeta = 2.5\times10^{-3}$.

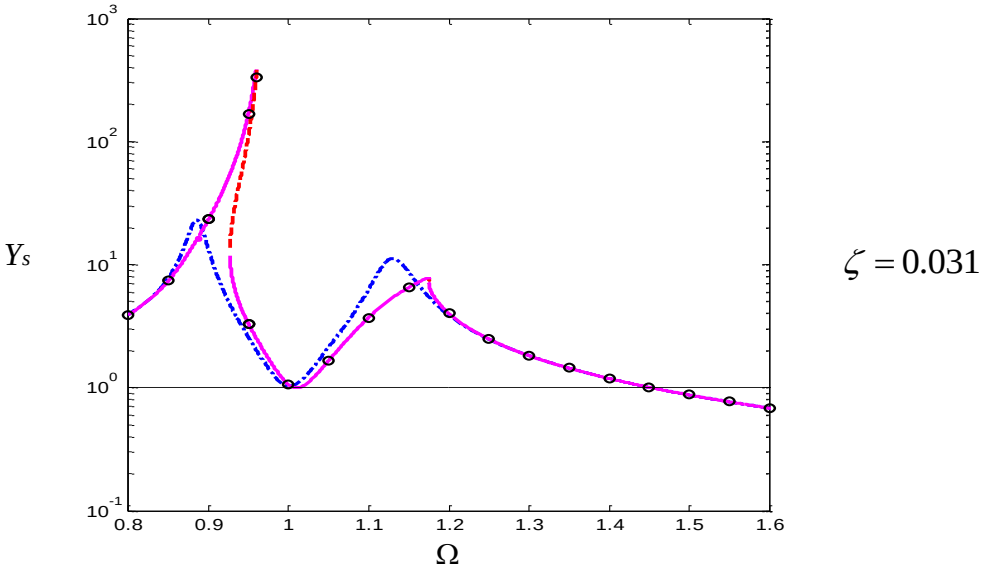

Figure 3.19 The effect for damping in the nonlinear absorber equal to $\zeta = 0.031$ on the primary system frequency response curves Y_s as a function of Ω. (The 'tuned' frequency $\omega_0 = \omega_1/\omega_s = 1$, nonlinear absorber stiffness $\gamma = 10^{-4}$, mass ratio $\mu = 0.06$ and damping $\zeta_s = 0.001$). The response for the system with the linear absorber is given by the dashed-dotted line. For the NDVA, the solid line is the stable solution and the dashed line gives the unstable solution.

ζ	Ω_{r1}	Ω_{r2}	Ω_t	Bandwidth for NDVA	Bandwidth for linear absorber	Bandwidth improvement compared to a linear absorber (%)
1.2×10^{-2}	0.961	1.271	1.010	0.055	0.052	6
1.25×10^{-2}	0.961	1.265	1.010	0.055	0.052	6
1.5×10^{-2}	0.961	1.239	1.010	0.052	0.050	4
1.75×10^{-2}	0.961	1.221	1.010	0.049	0.046	7
2×10^{-2}	0.961	1.207	1.010	0.046	0.042	10
2.25×10^{-2}	0.960	1.196	1.010	0.041	0.038	7
2.5×10^{-2}	0.960	1.188	1.010	0.035	0.032	9
2.75×10^{-2}	0.960	1.182	1.010	0.027	0.024	14
3×10^{-2}	0.960	1.176	1.010	0.015	0.006	150

Table 3.3 The frequency bandwidth for the vibration reduction produced by the nonlinear absorber on the primary system frequency response curves of the normalized displacement Y_s. ($\omega_0 = 1$, mass ratio $\mu = 0.06$, nonlinear parameter $\gamma = 10^{-4}$ and damping $\zeta_s = 0.001$).

3.2.1 The effect of the damping ratio in the nonlinear absorber on the effective and resonance frequencies

Figure 3.20 shows the effect of the damping ratio ζ in the attached nonlinear absorber on the effective tuned frequency Ω_t and the first and second resonance frequencies Ω_{r1}, Ω_{r2}. One can observe the change in these frequencies Ω_{r1}, Ω_{r2} and Ω_t as the damping ratio ζ increases. The effective tuned frequency Ω_{r1} is only slightly affected by the damping ratio ζ, Ω_{r1} moving to a lower frequency. The effective tuned frequency Ω_t is essentially constant. The second resonance frequency Ω_{r2} moves to lower frequencies as the damping ratio ζ increases. So, the damping ratio has a much greater effect on the second resonance frequency Ω_{r2} than on the first resonance frequency Ω_{r1} and on the effective tuned frequency Ω_t.

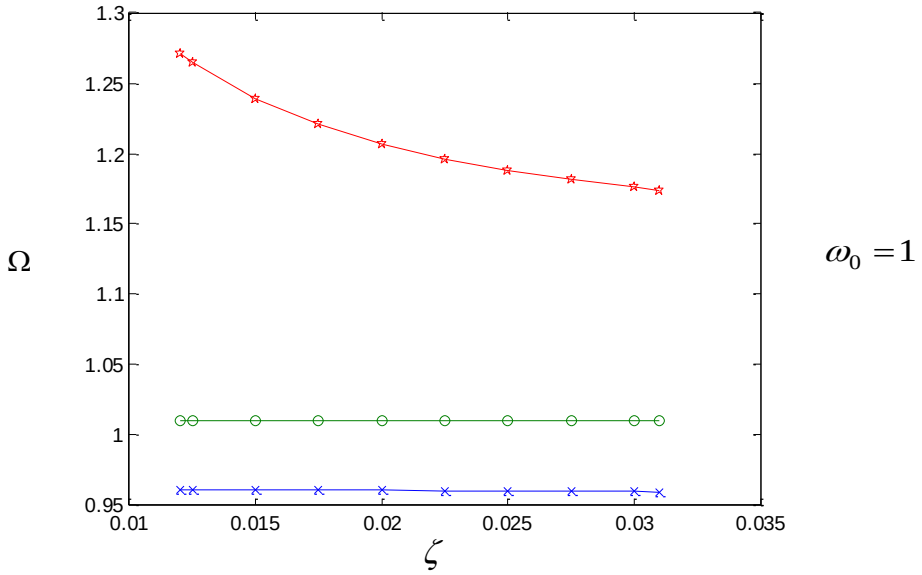

Figure 3.20 The effect of the nonlinear absorber damping ratio ζ on the primary system response effective tuned frequency Ω_t ('o'), first resonance frequency Ω_{r1} ('×') and second resonance frequency Ω_{r2} ('☆'). ($\omega_0 = 1$, nonlinear absorber stiffness $\gamma = 10^{-4}$, mass ratio $\mu = 0.06$ and damping $\zeta_s = 0.001$).

3.3 The effect of the nonlinear absorber mass ratio (μ)

Consider a nonlinear absorber with a reasonably high nonlinearity, i.e. the nonlinear stiffness parameter is $\gamma = 10^{-4}$, the linear tuned frequency is $\omega_0 = 1$ and the damping ratios for the primary system and the absorber are $\zeta_s = 0.001$ and $\zeta = 0.02$ respectively. For this case variations of the mass ratio μ have been investigated. The value of mass ratio is chosen, i.e. $0.05 \le \mu$, in order to produce a harmonic response at all frequencies, the amplitude of the other harmonics never exceeded 5% of the harmonic amplitude at the excitation frequency. The primary system frequency response curves of the normalized displacement Y_s versus excitation frequency ratio Ω are shown in Figures 3.21(a)-(c), where the mass ratio is increased from $\mu = 0.05$ to $\mu = 0.1$. An unstable branch appears in between the two stable branches of the first resonance peak. For low values of the mass ratio, the unstable branch may be between the two stable branches or partially above the level of the second resonance peak. For higher values of the mass ratio, the unstable branch appears in between the two stable branches of the response level of the second resonance peak. In Figures 3.22(a)-(c), the effect of the mass ratio on the secondary system displacement Y can also be observed. A corresponding unstable branch appears in between the two stable branches of the response level of the first resonance peak for the displacement of the absorber mass Y. In addition, the unstable branch is present between the two stable branches of the response level of the second resonance peak.

In Figures 3.21(a)-(c), the vibration reduction bandwidth for the nonlinear absorber generally has a wider bandwidth compared to the linear absorber. Given in Table 3.4, the bandwidth is increased by about 14%, 10% and 1% compared to the linear absorber case for a mass ratio value of $\mu = 0.05$, $\mu = 0.06$ and $\mu = 0.1$, respectively. From these values it can be seen that for a larger mass ratio μ, a smaller increase occurs in the vibration reduction bandwidth of the nonlinear absorber compared to the linear case; it is known that the linear absorber becomes more effective when its mass is higher [2]. For a linear absorber, a broader vibration reduction bandwidth can be achieved by adding mass to the absorber.

In addition, the nonlinear behaviour will be affected, the first resonance frequency Ω_{r1} and second resonance frequency Ω_{r2} move to slightly lower frequencies, but the effective tuned

frequency Ω_t shifts to the linear tuned frequency, i.e. $\Omega = 1$. In practical cases, it is not reasonable for the mass of the absorber to be too large because additional static loading of the primary system will occur. As a result, the mass ratio of absorber is typically restricted to a factor equivalent of about 10% or less of the original primary system mass.

μ	Ω_{r1}	Ω_{r2}	Ω_t	Bandwidth for NDVA	Bandwidth for linear absorber	Bandwidth improvement compared to a linear absorber (%)
0.05	0.967	1.203	1.014	0.033	0.029	14
0.06	0.961	1.207	1.010	0.046	0.042	10
0.07	0.954	1.212	1.007	0.056	0.055	2
0.08	0.948	1.217	1.006	0.066	0.064	3
0.09	0.942	1.222	1.005	0.076	0.075	1
0.1	0.936	1.227	1.004	0.086	0.085	1

Table 3.4 The frequency bandwidth for the vibration reduction produced by the nonlinear absorber on the primary system frequency response curves of the normalized displacement Y_s ($\omega_0 = 1$, nonlinear parameter $\gamma = 10^{-4}$ and damping $\zeta_s = 0.001$, $\zeta = 0.02$).

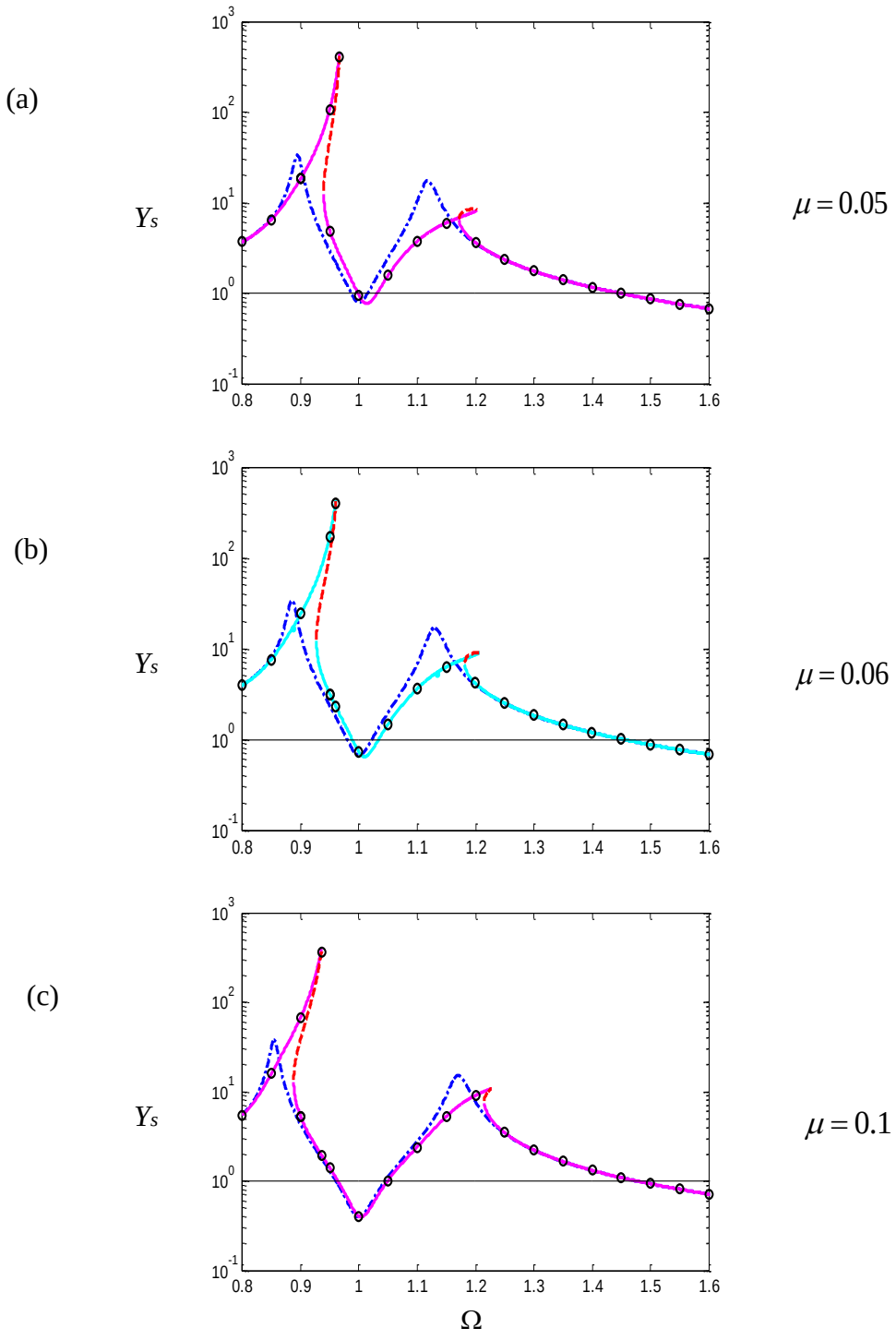

Figure 3.21 The effect of the mass in the nonlinear absorber on the primary system frequency response curves Y_s as a function of Ω. (The 'tuned' frequency $\omega_0 = \omega_1/\omega_s = 1$, nonlinear absorber stiffness $\gamma = 10^{-4}$ and damping $\zeta_s = 0.001$, $\zeta = 0.02$). The response for the system with the linear absorber is given by the dashed-dotted line. For the NDVA, the solid line is the stable solution and the dashed line gives the unstable solution. Direct numerical solutions are shown by the symbol ('○'). (a) $\mu = 0.05$, (b) $\mu = 0.06$ and (c) $\mu = 0.1$.

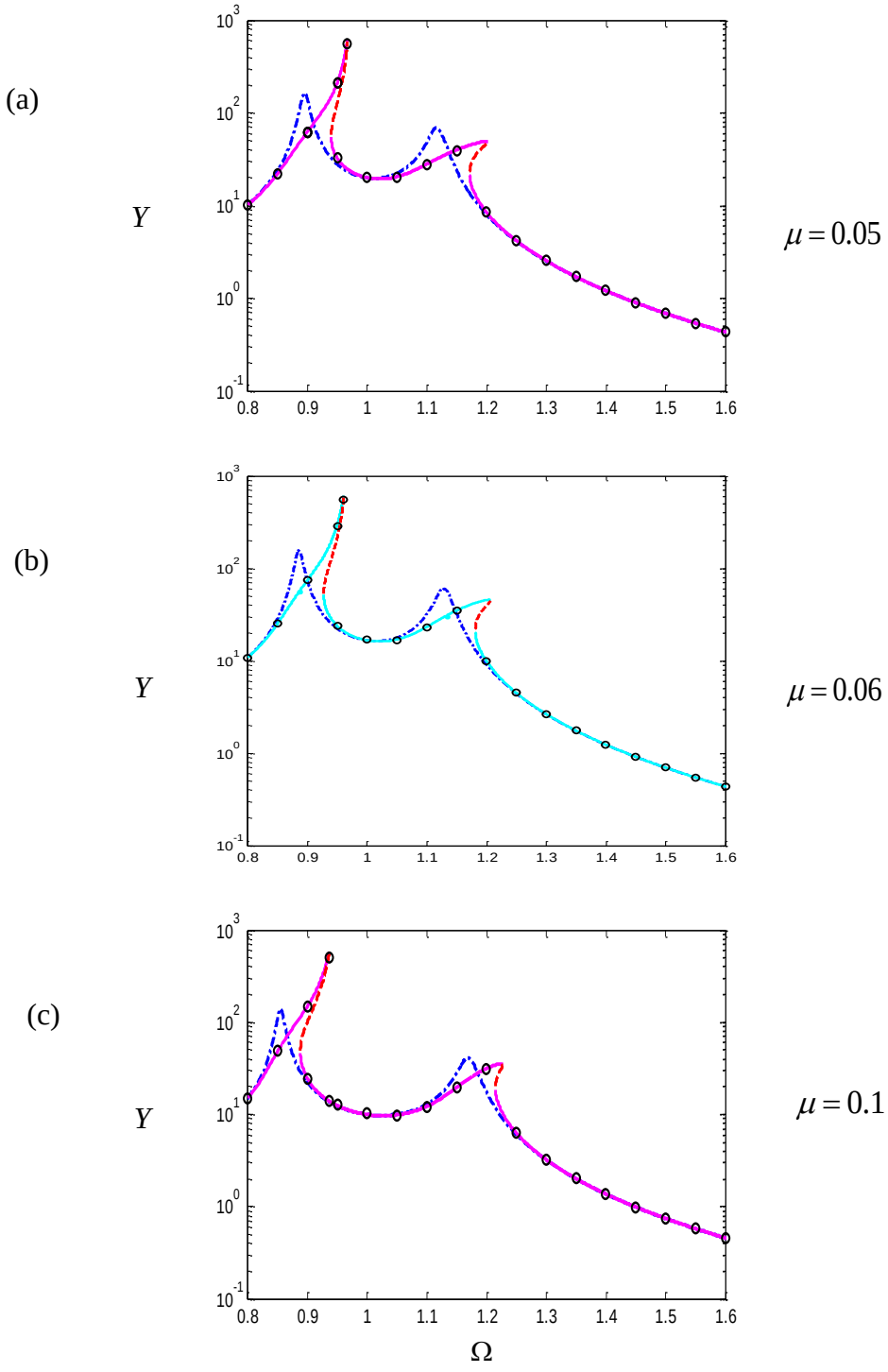

Figure 3.22 The effect of the mass in the nonlinear absorber on the second system frequency response curves Y as a function of Ω. (The 'tuned' frequency $\omega_0 = \omega_1/\omega_s = 1$, nonlinear absorber stiffness $\gamma = 10^{-4}$ and damping $\zeta_s = 0.001$, $\zeta = 0.02$). The response for the system with the linear absorber is given by the dashed-dotted line. For the NDVA, the solid line is the stable solution and the dashed line gives the unstable solution. Direct numerical solutions are shown by the symbol ('○'). (a) $\mu = 0.05$, (b) $\mu = 0.06$ and (c) $\mu = 0.1$.

3.3.1 The effect of the mass ratio in the nonlinear absorber on the effective and resonance frequencies

Figure 3.23 shows the change in these frequencies Ω_{r1}, Ω_{r2} and Ω_t as the mass ratio μ increases. The first resonance frequency Ω_{r1} moves to lower frequencies as the mass ratio μ increases. The effective tuned frequency Ω_t is slightly affected by the mass ratio μ, moving to lower frequencies. However, the second resonance frequency Ω_{r2} is affected most by the mass ratio μ, moving to higher frequencies.

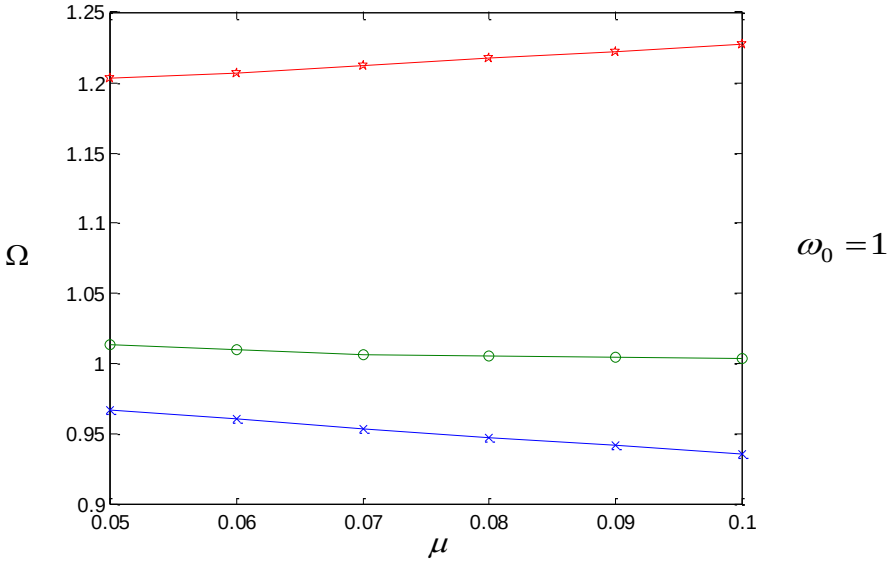

Figure 3.23 The effect of the nonlinear absorber mass ratio μ on the primary system response effective tuned frequency Ω_t ('o'), first resonance frequency Ω_{r1} ('×') and second resonance frequency Ω_{r2} ('☆'). ($\omega_0 = 1$, nonlinear parameter $\gamma = 10^{-4}$ and damping $\zeta_s = 0.001$, $\zeta = 0.02$).

3.4 The effect of the linear tuned frequency of the nonlinear absorber (ω_0)

In this section, the mass ratio for the nonlinear absorber to the primary system is set to be constant with μ=0.06, the nonlinear stiffness parameter is $\gamma = 10^{-4}$ and the damping ratios for the primary system and the nonlinear absorber are $\zeta_s = 0.001$ and $\zeta = 0.02$ respectively. The value of linear tuned frequency is chosen such that $\omega_0 \geq 0.97$, in order to produce a harmonic response at all frequencies, the amplitude of the other harmonics never exceeded 5% of the harmonic amplitude at the excitation frequency. The effect of the linear tuned frequency of the nonlinear absorber ($\omega_0 = \omega_1/\omega_s$, where $\omega_1 = \sqrt{k_1/m}$) on the primary system frequency response curves of the normalized displacement Y_s versus excitation frequency ratio Ω is shown in Figures 3.24(a)-(c). An unstable branch appears in between the two stable branches of the response level of the first resonance peak Ω_{r1}. The unstable branch is between the two stable branches or partially above the level of the response level of the second resonance peak. The effect of the linear tuned frequency of the nonlinear absorber on the secondary system displacement Y can also be observed in Figures 3.25(a)-(c). A corresponding unstable branch appears in between the two stable branches of the response level of the first resonance peak for the displacement of the absorber mass Y. In addition, the unstable branch presents between the two stable branches of the response level of the second resonance peak.

The linear tuned frequency is increased from $\omega_0 = 0.97$ to $\omega_0 = 1.1$, effectively by changing the value of the linear stiffness term k_1 in the absorber, producing the responses plotted shown in Figures 3.24(a)-(c). As shown in Table 3.5, the linear tuned frequency chosen for the nonlinear absorber produced a vibration reduction bandwidth which is increased by about 5%, 10% and 8% compared to the linear absorber case for a linear tuned frequency of $\omega_0 = 0.97$, $\omega_0 = 1.0$ and $\omega_0 = 1.1$, respectively. The vibration reduction bandwidth of the nonlinear absorber is not significantly wider than the linear absorber for a value of $\omega_0 = 0.97$. However, if the linear tuned frequency of the nonlinear absorber is higher, i.e. $\omega_0 > 0.99$, the effective tuned frequency Ω_t will occur at frequencies above the linear tuned frequency, i.e. $\Omega_t > 1$. This is in contrast to the linear absorber whose maximum benefit is at or very close to $\Omega = \omega_0$,

the linear absorber tuned frequency. It is noted that for a higher value of the linear tuned frequency ω_0, i.e. $\omega_0 > 1$, the effective bandwidth of the nonlinear absorber will be smaller compared to the nonlinear absorber whose linear tuned frequency is set to ω_0. An optimal choice for the linear tuned frequency might be possible if the objective is to maximize the size of the vibration reduction bandwidth.

ω_0	Ω_{r1}	Ω_{r2}	Ω_t	Bandwidth for NDVA	Bandwidth for linear absorber	Bandwidth improvement compared to a linear absorber (%)
0.97	0.961	1.120	0.982	0.039	0.037	5
1	0.961	1.207	1.010	0.046	0.042	10
1.05	0.961	1.228	1.057	0.057	0.053	8
1.1	0.961	1.254	1.104	0.069	0.064	8
1.15	0.961	1.285	1.152	0.084	0.079	6
1.2	0.961	1.321	1.200	0.101	0.095	6

Table 3.5 The frequency bandwidth for the vibration reduction produced by the nonlinear absorber on the primary system frequency response curves of the normalized displacement Y_s (nonlinear parameter $\gamma = 10^{-4}$, mass ratio $\mu = 0.06$ and damping $\zeta_s = 0.001$, $\zeta = 0.02$). The results are compared to a linear absorber with the same tuned frequency, mass ratio and damping parameters.

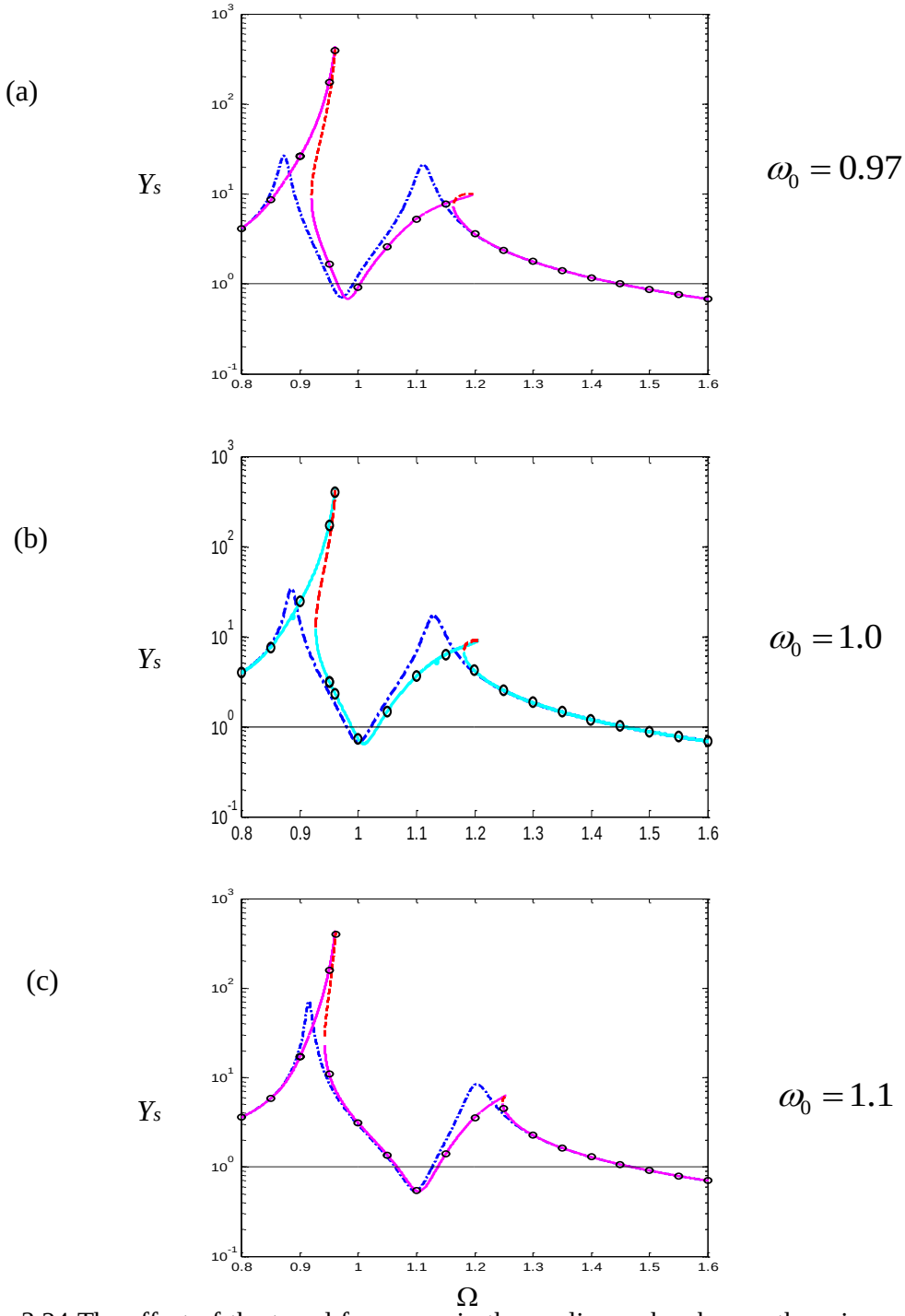

Figure 3.24 The effect of the tuned frequency in the nonlinear absorber on the primary system frequency response curves Y_s as a function of Ω. (nonlinear absorber stiffness $\gamma = 10^{-4}$, mass ratio $\mu = 0.06$ and damping $\zeta_s = 0.001$, $\zeta = 0.02$). The response for the system with the linear absorber is given by the dashed-dotted line. For the NDVA, the solid line is the stable solution and the dashed line gives the unstable solution. Direct numerical solutions are shown by the symbol ('○'). The corresponding tuned frequencies are (a) $\omega_0 = 0.97$, (b) $\omega_0 = 1.0$ and (c) $\omega_0 = 1.2$.

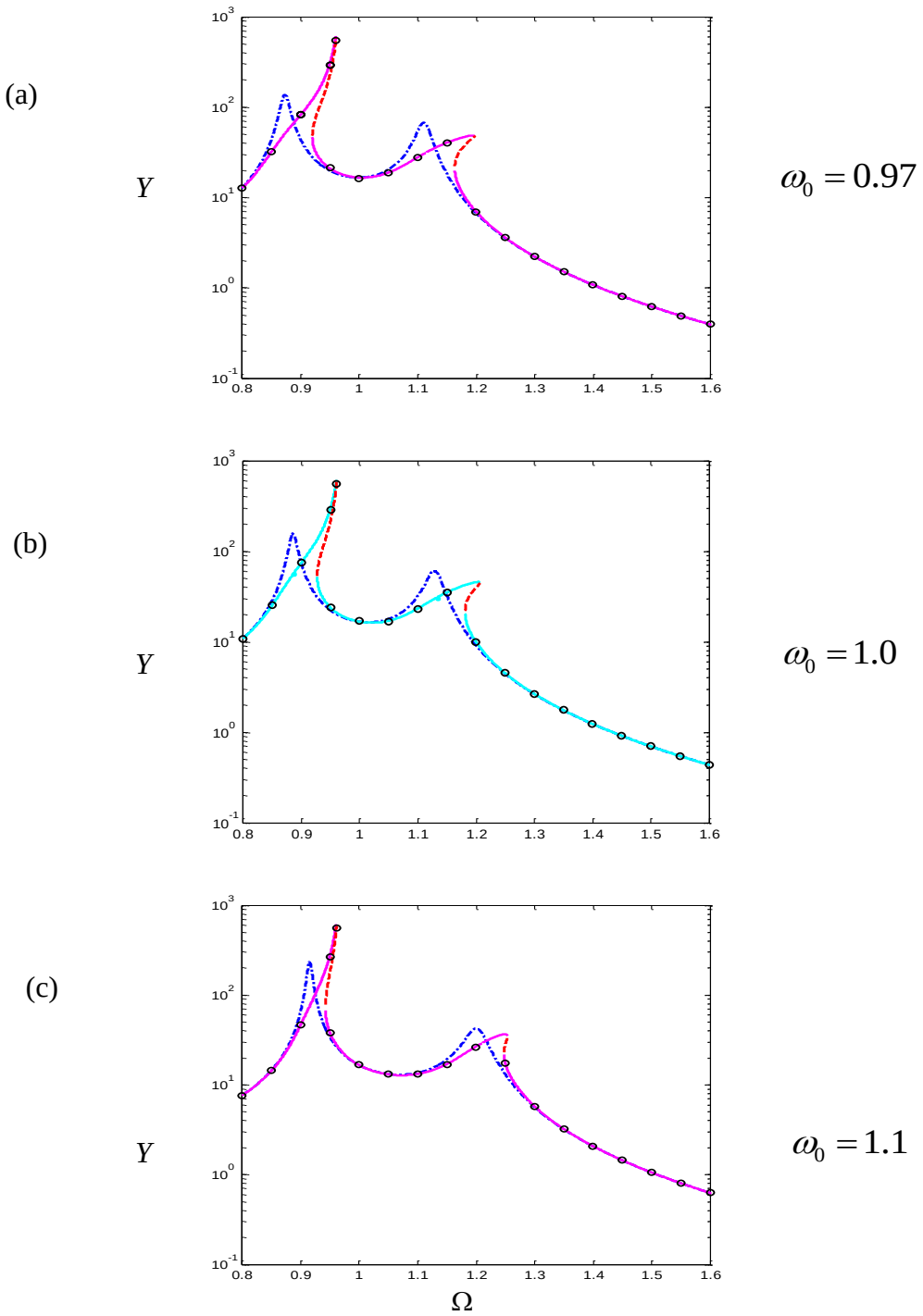

Figure 3.25 The effect of the tuned frequency in the nonlinear absorber on the secondary system frequency response curves Y as a function of Ω. (nonlinear absorber stiffness $\gamma = 10^{-4}$, mass ratio $\mu = 0.06$ and damping $\zeta_s = 0.001$, $\zeta = 0.02$). The response for the system with the linear absorber is given by the dashed-dotted line. For the NDVA, the solid line is the stable solution and the dashed line gives the unstable solution. Direct numerical solutions are shown by the symbol ('o').The corresponding tuned frequencies are (a) $\omega_0 = 0.97$, (b) $\omega_0 = 1.0$ and (c) $\omega_0 = 1.2$.

3.4.1 Comparison of the vibration reduction bandwidth for a linear and nonlinear absorber at the same effective tuned frequency

Let a nonlinear absorber be chosen with the parameters so that the reduction due to it occurs at $\Omega = 1$, the vibration reduction bandwidth is then compared to the linear absorber. Consider a nonlinear absorber with mass ratio μ=0.06, the nonlinear stiffness parameter is $\gamma = 10^{-4}$ and the damping ratios for the primary system and the absorber are $\zeta_s = 0.001$ and $\zeta = 0.02$, respectively. The linear tuned frequency for the NDVA is set to $\omega_0 = 0.99$, in order to compare the vibration reduction bandwidth of the linear and nonlinear absorber at the same effective tuned frequency. The primary and secondary system frequency response curves of the normalized displacement versus excitation frequency ratio Ω are shown in Figures 3.26(a)-(b). The nonlinear absorber produces a wider vibration reduction bandwidth around an effective tuned frequency equal to $\Omega_t = 1$ compared to the linear absorber case. Given in Table 3.6, the bandwidth is increased by about 3% compared to the linear absorber.

μ	Bandwidth for NDVA	Bandwidth for linear absorber	Bandwidth improvement compared to a linear absorber (%)
0.06	0.044	0.042	3

Table 3.6 The frequency bandwidth for the vibration reduction produced by the nonlinear absorber with linear tuned frequency $\omega_0 = 0.99$ on the primary system frequency response curves of the normalized displacement Y_s compared to the linear absorber at the same tuned frequency $\Omega = 1$ (nonlinear parameter $\gamma = 10^{-4}$ and damping $\zeta_s = 0.001$, $\zeta = 0.02$).

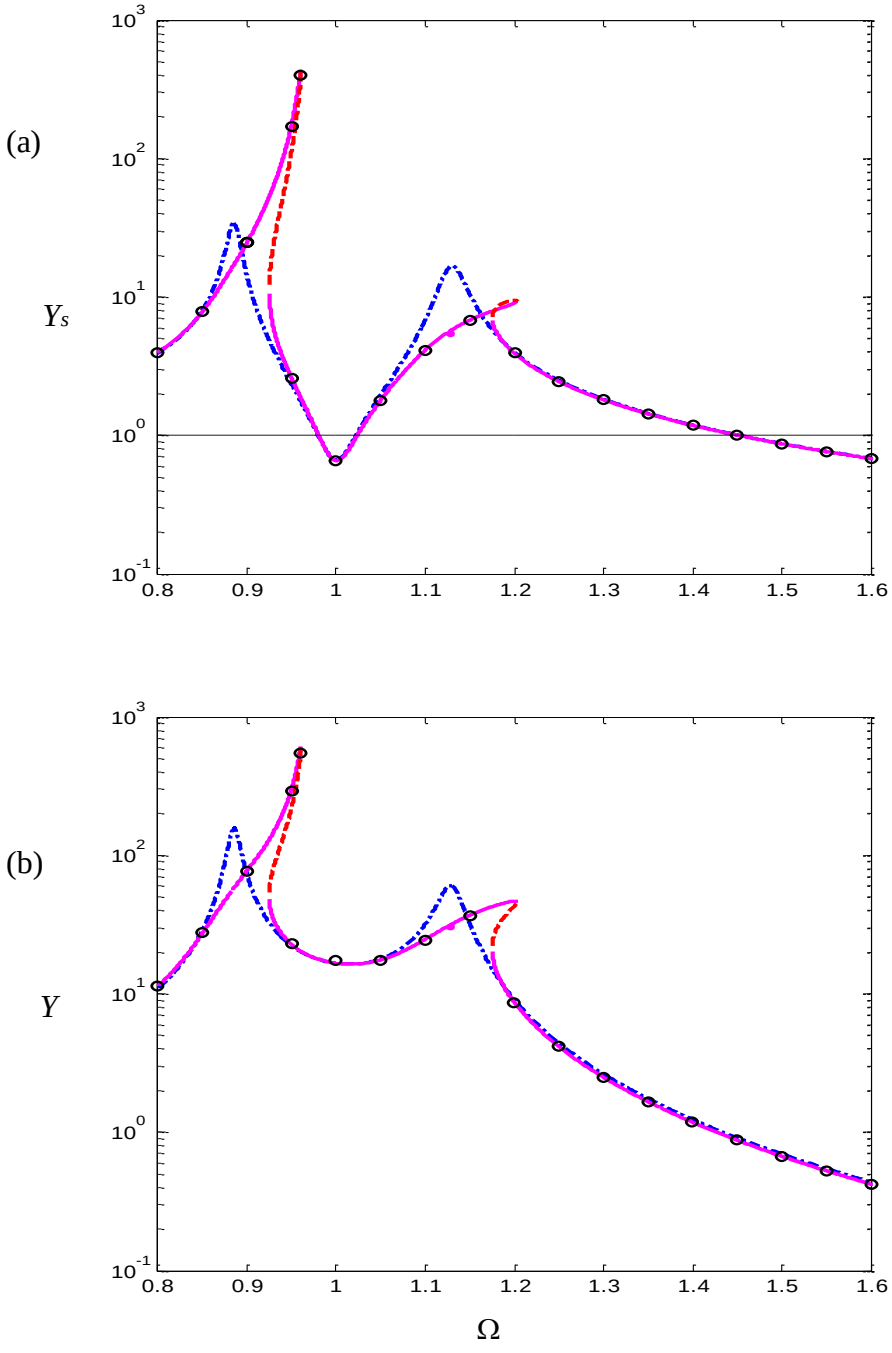

Figure 3.26 Comparison of the linear and nonlinear absorber at the same effective tuned frequency on (a) the primary system frequency response curves Y_s and (b) the secondary system frequency response curves Y as a function of Ω. (nonlinear absorber stiffness $\gamma = 10^{-4}$, mass ratio $\mu = 0.06$ and damping $\zeta_s = 0.001$, $\zeta = 0.02$). The response for the system with the linear absorber is given by the dashed-dotted line. For the NDVA, the solid line is the stable solution and the dashed line gives the unstable solution. Direct numerical solutions are shown by the symbol ('o').

3.5 Conclusions

This chapter presented numerical results based on the HBM solutions and direct numerical integration. The cases shown consider the effect of the nonlinear stiffness parameter (γ), the damping ratio (ζ), the mass ratio (μ) and linear tuned frequency (ω_0) on the vibration reduction. In order to produce a harmonic response at all frequencies, a limited range of values for the above parameters was determined. From the results, it is seen that the above-mentioned parameters have significant effects on the resonances, the effective tuned frequency and the vibration reduction bandwidth. The key results are summarized again below:

The nonlinear absorber can possess a much wider effective vibration bandwidth compared to a conventional linear absorber. The use of the stiffness nonlinearity will greatly increase the attractiveness of using a passive absorber to reduce excessive vibration amplitudes to acceptable levels in applications where the excitation bandwidth is restricted to match the vibration reduction bandwidths. Compared to the linear absorber, the nonlinearity has the effect of shifting the second resonant peak Ω_{r2} to a higher frequency away from the effective tuned frequency Ω_t, improving the robustness of the device to mistune. For the linear absorber this can be achieved by adding mass to the absorber, so in some way the nonlinearity has the same beneficial effect as adding to the absorber mass.

Damping could increase the stability of the harmonic response for the system in the neighbourhood of the vibration reduction bandwidth. In general, by adding damping for both the linear and nonlinear absorber, a disadvantage is that a smaller vibration reduction bandwidth is produced compared to lower damping. However, for lower damping in the nonlinear absorber ζ, the effective bandwidth is slightly increased compared to the linear absorber with the same level of damping. Large damping in the nonlinear absorber generally produces a wider frequency vibration reduction bandwidth compared to the linear absorber. When damping in the nonlinear absorber is further increased above a certain value though, there appears to be no effective vibration bandwidth. In addition, the second resonance frequency moves to lower frequencies as the damping ratio increases. The damping ratio has a much greater effect on the second resonance frequency than on the first resonance frequency and on the effective tuned frequency.

For larger mass ratios the vibration reduction bandwidth for the nonlinear absorber is not significantly larger than that for a linear absorber. That is because the linear absorber can also produce a broader vibration reduction bandwidth by adding mass to the absorber. As the mass ratio increases, the effective tuned frequency is slightly affected by the mass ratio, moving to lower frequencies. For larger mass ratios the first resonance frequency moves to lower frequencies and the second resonance frequency moves to higher frequencies, respectively.

For the nonlinear absorber, an optimal choice for the linear tuned frequency might be possible if the objective is to maximize the size of the vibration reduction bandwidth. In addition, the linear tuned frequency of the nonlinear absorber can be adjusted to compare the linear absorber at the same effective tuned frequency. In this case, the nonlinear absorber has a slightly wider vibration reduction bandwidth compared to the linear case.

For a hardening stiffness nonlinear absorber design, the limitation on the value of the nonlinear stiffness parameter should be identified first. In order to produce an effective vibration bandwidth, the limitation on the value of the damping and the mass were determined. The larger the damping and the heavier the mass in the nonlinear absorber, a much wider effective vibration bandwidth will be produced compared to using a linear absorber with the same damping and mass levels.

Following a similar pattern, the next chapter will focus on the dynamic characteristics of a system with an attached nonlinear absorber system under random excitation.

Chapter 4

Dynamic behaviour of a nonlinear vibration absorber: random excitation

For harmonic excitation in chapter 2, the mathematical expressions for the frequency response curves of the structural system were determined using the Harmonic Balance Method. The effect of the nonlinear vibration absorber parameters on the vibration reduction was presented in chapter 3. The objective of this chapter is to investigate the vibration response of a system with an attached nonlinear vibration absorber under random excitation. This chapter will briefly introduce the statistical techniques for random linear and nonlinear signal analysis. Time and frequency domain techniques are used to investigate the dynamic behaviour of the nonlinear vibration absorber. The effect of the random input amplitude, nonlinear stiffness, damping ratio and mass ratio on the vibration response will be discussed.

The predictions given represent the vibration response due to Gaussian broadband force input. The Gaussian broadband input can investigate the vibration response of multiple degree-of-freedom systems over a wide excitation range. The time domain analysis concentrates on determining the basic response statistics (mean, mean square, skew and kurtosis). The time series are often studied by observing the system mean square response and its behaviour for a range of excitation bandwidths and levels.

The power spectral density (PSD) is also referred to as the mean square spectral density. It is a measure of the frequency content of the total process. The linear frequency response functions can be considered as estimates of the variance for the linear part of the random response. The majority of the nonlinear aspects of the system response can be more easily shown and determined in the frequency domain. Numerical simulations of the nonlinear coherence functions are given and provide a keen insight into a model that could present the response of such systems.

4.1 Analysis approaches for the simulated responses

This section briefly introduces the numerical techniques for random linear and nonlinear signal analysis. To investigate the performance of the nonlinear vibration absorber one can use a statistical analysis technique on the time domain data. The frequency domain techniques present an insight into the response of such systems. In order to obtain good estimates of the spectrum of a signal the procedure adopted uses the smoothing spectral density method [19].

4.1.1Time domain analysis

The mean value (first moment) of a continuous function *x* is given by

$$\mu_x = E[x] = \int_{-\infty}^{\infty} xp(x)dx \tag{4.1}$$

where $p(x)$ is the probability density function (PDF) of *x*.

For a discrete sampled signal, the estimated mean value is given by

$$\hat{\mu}_x = \left(\frac{1}{N}\right)\sum_{j=1}^{N} x_j \tag{4.2}$$

where x_j are discrete values and N is the number of data points.

The mean square value (second moment) of *x* is defined by

$$\psi_x^2 = E\left[x^2\right] = \int_{-\infty}^{\infty} x^2 p(x)dx \tag{4.3}$$

For a discrete signal the equivalent estimation is the mean square value

$$\hat{\psi}_x^2 = \left(\frac{1}{N}\right)\sum_{j=1}^{N} x_j^2 \tag{4.4}$$

The second central moment (variance) about the mean is defined by

$$\sigma_x^2 = E\left[\left(x-\mu_x\right)^2\right] = \int_{-\infty}^{\infty}\left(x-\mu_x\right)^2 p(x)dx \tag{4.5}$$

For a discrete signal this is

$$\hat{\sigma}_x^2 = \left(\frac{1}{N}\right)\sum_{j=1}^{N}\left(x_j-\hat{\mu}_x\right)^2 \tag{4.6}$$

The variance can be expanded to obtain a relationship with the mean values namely

$$\sigma_x^2 = \psi_x^2 - \mu_x^2 \tag{4.7}$$

where ψ_x^2 is the mean square value.

The standard deviation σ (equivalent to the root mean square (rms) response for a signal with a zero mean) is

$$\sigma_x = \sqrt{\sigma_x^2} = \psi_x \tag{4.8}$$

The third central moment (skew) is defined as

$$\iota = E\left[\left(\frac{x-\mu_x}{\sigma_x}\right)^3\right] = \int_{-\infty}^{\infty}\left(\frac{x-\mu_x}{\sigma_x}\right)^3 p(x)dx \tag{4.9}$$

For a discrete signal this is

$$\hat{\iota} = \left(\frac{1}{N}\right)\sum_{j=1}^{N}\left(\frac{x_j-\mu_x}{\sigma_x}\right)^3 \tag{4.10}$$

The skew is equal to zero for a Gaussian distribution, since it has a symmetric PDF. A non-symmetric PDF can have positive or negative skew.

The fourth central moment (kurtosis) is defined as

$$\kappa = E\left[\left(\frac{x-\mu_x}{\sigma_x}\right)^4\right] = \int_{-\infty}^{\infty}\left(\frac{x-\mu_x}{\sigma_x}\right)^4 p(x)dx \tag{4.11}$$

For a discrete signal this is

$$\hat{\kappa} = \left(\frac{1}{N}\right)\sum_{j=1}^{N}\left(\frac{x_j-\mu_x}{\sigma_x}\right)^4 \tag{4.12}$$

For Gaussian random signals, the kurtosis is equal to three. For non-Gaussian systems the kurtosis presents positive values less or greater than three. Values higher than three corresponds to more peaks in the time domain of the response, whilst values lower than three corresponds to fewer peaks. Such systems are called leptokurtic and platykurtic respectively.

The third and fourth central moments are widely used for detecting non-Gaussianity. These may be used to check nonlinearity, since nonlinear systems typically exhibit non-Gaussian response

[74]. It should be noted though that linear multi-modal systems also have a non-Gaussian response when excited by a broadband Gaussian input.

4.1.2Frequency domain analysis and definitions

4.1.2.1 Time-frequency relationships

The Fourier transform of a signal $x(t)$ is defined as [74]

$$X(f) = \int_{-\infty}^{\infty} x(t)e^{-j2\pi ft}dt = F\left(x(t)\right) \tag{4.13}$$

and the inverse Fourier transform is

$$x(t) = \int_{-\infty}^{\infty} X(f)e^{j2\pi ft}df = F^{-1}\left(X(f)\right) \tag{4.14}$$

The autocorrelation function with a time separation τ is

$$R_{xx}(\tau) = \int_{-\infty}^{\infty} x(t)x(t+\tau)dt = E\left[x(t)x(t+\tau)\right] \tag{4.15}$$

The auto power spectral density (PSD) and autocorrelation functions are related by the Fourier transform pair

$$S_{xx}(f) = \int_{-\infty}^{\infty} R_{xx}(\tau)e^{-j2\pi f\tau}d\tau \tag{4.16}$$

$$R_{xx}(\tau) = \int_{-\infty}^{\infty} S_{xx}(f)e^{j2\pi f\tau}df \tag{4.17}$$

4.1.2.2 Random time history from PSD using IFT

For analysis conditions it is useful to generate random time histories with a prescribed PSD. The system responses, which are produced from the random inputs, are then presented as a set of response PSDs. The input random time histories were obtained from an inverse Fourier transform (IFT) of the complex Fourier spectrum possessing frequency domain amplitudes and uniformly distributed random phase angles from 0 to 2π [75].

The finite Fourier transform is defined from $-f_{nyq} \le f \le f_{nyq}$ and the Nyquist frequency is determined by $f_{nyq} = 1/(2\Delta t)$, where Δt is a time spacing. The magnitude of the Fourier transform based on the prescribed PSD is determined by

$$|F(f)| = \sqrt{TS_{FF}(f)} \tag{4.18}$$

where $S_{FF}(f)$ is the two-sided prescribed PSD of the white noise excitation, $T = 1/\Delta f$ is the total time period and Δf is a chosen frequency spacing.

The complex form of the force spectrum is given by [74]

$$F(f) = |F(f)|e^{j\theta} \tag{4.19}$$

where $F(f)$ is the spectrum of the input signal F, which is a constant for a white noise random excitation signal. θ is the phase with uniform probability of a value in the range 0 to 2π.

The time domain input signal is subsequently determined using the inverse Fourier transform

$$F(t) = \int_{-f_{nyq}}^{f_{nyq}} F(f)e^{j2\pi ft}df \tag{4.20}$$

4.1.2.3 Frequency response and coherence functions

The estimation process for the nonlinear frequency response function (FRF) is based on the estimation method used for linear systems [74]. The FRF is estimated by averaging the appropriate auto-spectral and cross-spectral density. The FRF estimators are defined as

$$H_0(f) = \sqrt{\frac{S_{yy}(f)}{S_{xx}(f)}},\ H_1(f) = \frac{S_{xy}(f)}{S_{xx}(f)} \text{ and } H_2(f) = \frac{S_{yy}(f)}{S_{yx}(f)} \tag{4.21a,b,c}$$

where $S_{xx}(f)$ is the auto-spectral density of input, $S_{yy}(f)$ is the auto-spectral density of output and $S_{xy}(f)$ and $S_{yx}(f)$ are the cross-spectral densities between the input and the output.

Equation (4.21a) can only provide the result for the transfer function amplitude, whilst equation (4.21b,c) provide the magnitude and phase. For a linear system, the $H_1(f)$ estimate usually underestimates the FRF at resonances of the structure, but gives better estimates at the anti-resonance frequencies than $H_2(f)$. On the other hand, $H_2(f)$ is relatively unbiased at resonances but significantly overestimates near the anti-resonance frequencies [74].

For a nonlinear system, it is known that in general a harmonic input will produce a non-harmonic response. The latter could contain sub and super harmonics or even frequency content which is not related to rational orders of one excitation frequency, e.g. in systems with impacts a harmonic input might produce a broadband response. Thus it is likely that the nonlinear absorber system will display frequency spectra which are not linearly related to the input. Thus when using a transfer function approach, these nonlinear responses will not contribute in any of the linear H_1 or H_2 estimators, as potentially the responses at certain frequencies will not be coherent with the input at these frequencies. The H_0 estimator, that uses the spectra of the outputs and inputs, takes a ratio of them at each frequency. So it is an estimator of the transfer function, but it cannot separate out what in the frequency content of the input produces a particular frequency content in the output [74-76]. In some cases the inspection of the input and output PSDs is more insightful.

The coherence function between the ideal single input and output is a real valued function that ranges between 0 and 1 and is defined by

$$\gamma_{xy}^2(f) = \frac{\left|S_{xy}(f)\right|^2}{S_{xx}(f)S_{yy}(f)} \tag{4.22}$$

When the output is completely determined by a linear function of the input the coherence value is 1. Coherence values less than 1 can be exhibited when noise is present, in either of both signals, or when nonlinear contributions exist in the output (e.g., nonlinear response terms) [75].

4.1.3 Smoothing spectral density estimates

The accuracy of a spectral estimation is dependent on the effective bandwidth of the estimated spectrum and the record length of the time history data. Normally a suitable record length and sampling interval for digital spectral analysis of a continuous time series is chosen with a Nyquist frequency f_{nyq}. The time spacing can be determined by $\Delta t = 1/(2 f_{nyq})$. For good estimates of the spectrum of a signal it is necessary to achieve a resolution frequency $f_r = 1/T_{\text{block}}$ in the frequency range [19, 77]

$$\frac{\text{Var}(\hat{S}_{xx}(f))}{S_{xx}^2(f)} = \frac{1}{B_e T} \tag{4.23}$$

where B_e is the effective bandwidth of the estimated spectrum and $T = NT_{\text{block}}$ is the total

record length of the time history data $x(t)$ used for the estimation.

To achieve really reliable results with small variance $\mathrm{Var}(\hat{S}_{xx}(f))$ on the predicted levels of the spectrum, the value of B_eT must be greater than 9 [19]. In order to resolve a frequency difference of f_r, the effective bandwidth B_e should certainly not exceed f_r and preferably should be less.

Suppose that one puts $B_e = f_r/2$, then the required record length is at least

$$T = \frac{9}{B_e} = \frac{9}{(f_r/2)} = \frac{18}{f_r}$$

Then, good estimates of the spectrum of a signal can be produced.

4.2 Time domain simulation of the governing differential equation

The equations of motion for the system studied in chapter 2, namely the nonlinear absorber attached to a single degree-of-freedom primary system are given by

$$m_s\ddot{x}_s + c_s\dot{x}_s + k_s x_s + c(\dot{x}_s - \dot{x}) + k_1(x_s - x) + k_3(x_s - x)^3 = F(t) \qquad (4.24a,b)$$

$$m\ddot{x} - c(\dot{x}_s - \dot{x}) - k_1(x_s - x) - k_3(x_s - x)^3 = 0$$

It is convenient to write equations (4.24a,b) in non-dimensional form as given by

$$y_s'' + 2\zeta_s y_s' + y_s + 2\mu\zeta\omega_0 w' + \mu\omega_0^2 w + \mu\alpha w^3 = B(\frac{\tau}{\omega_s}) \qquad (4.25a,b)$$

$$w'' + 2\zeta\omega_0 w' + \omega_0^2 w + \alpha w^3 = y_s''$$

where the substitutions for the non-dimensional parameters are given below.

$$y_s'' = \frac{\ddot{x}_s}{\omega_s^2 x_0},\ y_s' = \frac{\dot{x}_s}{\omega_s x_0},\ y_s = \frac{x_s}{x_0};\ y'' = \frac{\ddot{x}}{\omega_s^2 x_0},\ y' = \frac{\dot{x}}{\omega_s x_0},\ y = \frac{x}{x_0}$$

$w'' = \frac{\ddot{z}}{\omega_s^2 x_0}$, $w' = \frac{\dot{z}}{\omega_s x_0}$, $w = \frac{z}{x_0}$; $\omega_s^2 = \frac{k_s}{m_s}$, $\omega_1^2 = \frac{k_1}{m}$, $z = x_s - x$, $\tau = \omega_s t$ and $B(\frac{\tau}{\omega_s}) = \frac{F(\tau/\omega_s)}{k_s x_0}$.

x_0 is a reference displacement which is taken as the root mean square (rms) displacement of the primary system in the absence of the absorber, obtained analytically for a linear system [19] as $x_0 = \sqrt{\pi S_0/k_s c_s}$, where S_0 is the stationary Gaussian process with a constant power spectral

density for the force input around the natural frequency ω_s . $(\bullet)' = \frac{\mathrm{d}}{d\tau}(\bullet)$ is the derivative with respect to non-dimensional time $\tau = \omega_s t$.

In equations (4.25a,b), the non-dimensional terms μ , α , ζ_s , ζ , ω_0 and $B(\frac{\tau}{\omega_s})$ are, respectively, the mass ratio, a nonlinear stiffness parameter used for the random vibration case, the linear damping ratio of the main system, the linear damping ratio of the NDVA, the linear tuned frequency ratio and the non-dimensional excitation force given by the following algebraic expressions:

$$\mu = \frac{m}{m_s},\ \alpha = \frac{k_3 x_0^2}{k_s \mu},\ \zeta_s = \frac{c_s}{2 m_s \omega_s},\ \zeta = \frac{c}{2 m \omega_1},\ \omega_0 = \frac{\omega_1}{\omega_s},\ B(\frac{\tau}{\omega_s}) = \frac{F(\tau/\omega_s)}{k_s x_0}$$

The non-dimensional terms μ , ζ_s , ζ and ω_0 are actually the same as those used for the harmonic excitation case in Chapter 3. However, the non-dimensional terms α and B are different from those used previously, because of the change in the reference displacement x_0 .

The responses in the time domain presented later were determined using direct numerical integration (using the MATLAB ode45 function) of the non-dimensional equations of motion. As some of the non-dimensional terms are identical. Then some limited comparsion with the response to harmonic excitation might be possible.

4.3 The effect of the random input amplitude

The non-dimensional system parameters used for predictions with the model consider a mass ratio for the system as μ=0.02, a linear tuned frequency set to $\omega_0 = 1$ and damping ratios for the primary system and the absorber are $\zeta_s = 0.01$ and $\zeta = 0.008$ respectively. The primary and secondary system physical parameter values are set to m_s=1.26×10^{-1} (kg) , c_s=2.12 $(\mathrm{N\cdot s/m})$, k_s=8.93×10^{4} $(\mathrm{N/m})$, m=2.52×10^{-3} (kg) , c=3.4×10^{-2} $(\mathrm{N\cdot s/m})$ k_1=1.79×10^{3} $(\mathrm{N/m})$ and k_3=8.93×10^{9} $(\mathrm{N/m^3})$, respectively. For this case variations of the input amplitude have been investigated. It is noted that the non-dimensional parameter α will be affected by input amplitude

The data record length was 40.96 s with a sample rate of 800 Hz (with a Nyquist frequency of 400 Hz). The system was excited using a flat white noise random input from 50 to 250 Hz. The input data was obtained using an equivalent Fourier Transform of the PSD spectrum magnitude $|F(f)|$ with random phase angles for each frequency point (see section 4.1.2). The spectrum was zero padded above the maximum input frequency to 400 Hz to ensure a smooth time history that could be linearly interpolated while running the ODE solver. A 1.28s time record with a corresponding 0.78 Hz frequency spacing was used. The Inverse Fourier Transform of this spectrum can be calculated to yield time domain records for the random input.

For the time domain analysis, the basic response statistics (mean, variance, mean square, skew and kurtosis) have been determined. The dynamic response for the system is described by Equations (4.26a,b). The vibration response of a typical input force and corresponding system are presented in Figures 4.1(a)-(c).

Consider the sample data from Figures 4.1(b)-(c), which is used to estimate the mean, variance, mean square, skew and kurtosis using the formulae in section 4.1.1. In Table 4.1-2 the displacement response statistics of the primary and secondary system show that the behaviour of the nonlinear system is different compared to the linear absorber case, exhibiting a kurtosis value less than 3. In Table 4.3, the mean square displacement of the primary system without an absorber $\psi_{x_0}^2$ is produced by numerical simulation for variations of the input amplitude. The mean square displacement of the primary system without an absorber $\psi_{x_0}^2$ is taken as the value for evaluating the nondimensional mean square displacement of the primary and absorber

system for the linear and nonlinear systems, i.e. $\psi_{y_s}^2 = \psi_{x_s}^2 / \psi_{x_0}^2$ and $\psi_y^2 = \psi_x^2 / \psi_{x_0}^2$, respectively. The linear and nonlinear absorbers produce a lower mean square primary system displacement compared to the primary system without an absorber, i.e. $\psi_{y_s}^2 < 1$. In Table 4.3 and Figure 4.2(a), the difference between the vibration response using the linear and nonlinear absorber is observed in that the mean square primary system displacement for the nonlinear absorber is not the same as the linear absorber case. The mean square primary system displacement for the nonlinear absorber is higher compared to the linear absorber case for a force amplitude $\sigma_F \geq 0.1$. It can also be observed that the displacement primary system PSD of the nonlinear absorber is much higher than the linear absorber at the first mode shown in Figure 4.4. This is in agreement in that the displacement PSD of the primary system for the first mode is the main contribution in the mean square response. The cumulative mean square displacement of primary system for the nonlinear absorber is also higher when using the linear absorber in Figure 4.6. In Figure 4.2(b), the mean square secondary system displacement response using the nonlinear absorber is lower compared to the linear absorber case.

In Figure 4.3(a), the standard deviation of the primary system displacement with an attached nonlinear absorber does not present a linear increase for a linear increase in the input rms force. The displacement response exhibits a nonlinear behaviour due to the nonlinear absorber. In addition, for the nonlinear absorber there is a higher standard deviation for the primary system displacement compared to the linear absorber case for a force amplitude $\sigma_F \geq 0.1$. In Figure 4.3(b), the standard deviation for the absorber system displacement for the nonlinear absorber is lower compared to the linear absorber case i.e. the response of the absorber mass is reduced relative to the linear absorber case.

For some range of non-dimensional parameters for the nonlinear absorber under random excitation, when increasing the force input magnitude there is a higher increase in the primary system response with a corresponding smaller than the input increase in the absorber system response, i.e. a negative effect when considering vibration control.

Input force	Linear absorber				Nonlinear absorber			
σ_F (N)	$\mu_{x_s}(m)$	$\psi^2_{x_s}(m^2)$	ι_{x_s}	κ_{x_s}	$\mu_{x_s}(m)$	$\psi^2_{x_s}(m^2)$	ι_{x_s}	κ_{x_s}
0.1	1.0×10^{-10}	3.0×10^{-11}	-1.1×10^{-3}	3	8.5×10^{-11}	3.1×10^{-11}	-2.1×10^{-3}	3.1
0.3	4.1×10^{-10}	2.9×10^{-10}	-1.1×10^{-3}	3	-4.8×10^{-10}	3.6×10^{-10}	-6.9×10^{-4}	3.1
0.5	5.1×10^{-10}	8.0×10^{-10}	-1.2×10^{-3}	3	-1.5×10^{-10}	1.1×10^{-9}	4.4×10^{-4}	3.1
0.7	3.3×10^{-10}	1.6×10^{-9}	-1.1×10^{-3}	3	7.8×10^{-10}	2.4×10^{-9}	1.6×10^{-4}	3.3
0.9	5.5×10^{-10}	2.6×10^{-9}	-1.1×10^{-3}	3	1.2×10^{-10}	4.0×10^{-9}	4.0×10^{-5}	3.4
1	1.0×10^{-10}	3.2×10^{-9}	-1.2×10^{-3}	3	-5.2×10^{-10}	5.0×10^{-9}	2.7×10^{-5}	3.4
1.1	1.2×10^{-9}	3.8×10^{-9}	-1.2×10^{-3}	3	-1.0×10^{-9}	6.2×10^{-9}	-1.8×10^{-5}	3.3
1.3	8.6×10^{-10}	5.4×10^{-9}	-1.1×10^{-3}	3	-3.4×10^{-10}	8.6×10^{-9}	6.1×10^{-5}	3.1
1.5	1.2×10^{-9}	7.2×10^{-9}	-1.1×10^{-3}	3	-9.7×10^{-10}	1.2×10^{-8}	2.3×10^{-4}	3.1
1.7	2.3×10^{-9}	9.2×10^{-9}	-1.2×10^{-3}	3	-1.6×10^{-9}	1.6×10^{-8}	-4.5×10^{-4}	3.1
1.9	1.9×10^{-9}	1.1×10^{-8}	-1.1×10^{-3}	3	-1.4×10^{-9}	1.9×10^{-8}	3.1×10^{-4}	3.1

Table 4.1 The effect of the random input force amplitude on the mean, mean square, skewness and kurtosis of the displacement response of the primary system. ($m_s=1.26\times10^{-1}$ (kg), $c_s=2.12$ ($\mathrm{N\cdot s/m}$), $k_s=8.93\times10^{4}$ $\left(\mathrm{N/m}\right)$, $m=2.52\times10^{-3}$ (kg), $c=3.4\times10^{-2}$ ($\mathrm{N\cdot s/m}$) $k_1=1.79\times10^{3}$ $\left(\mathrm{N/m}\right)$ and $k_3=8.93\times10^{9}$ $\left(\mathrm{N/m^3}\right)$)

Input force	Linear absorber				Nonlinear absorber			
σ_F (N)	$\mu_x(m)$	$\psi^2_x(m^2)$	ι_x	κ_x	$\mu_x(m)$	$\psi^2_x(m^2)$	ι_x	κ_x
0.1	-1.2×10^{-10}	1.5×10^{-9}	3.6×10^{-5}	3	-3.6×10^{-10}	1.5×10^{-9}	-2.0×10^{-5}	3.1
0.3	-6.2×10^{-10}	1.4×10^{-8}	2.4×10^{-5}	3	5.9×10^{-9}	1.2×10^{-8}	1.8×10^{-4}	2.7
0.5	-6.1×10^{-10}	4.0×10^{-8}	2.3×10^{-5}	3	7.2×10^{-9}	2.6×10^{-8}	9.0×10^{-5}	2.5
0.7	-1.3×10^{-9}	7.9×10^{-8}	2.7×10^{-5}	3	-2.5×10^{-9}	4.1×10^{-8}	-3.4×10^{-4}	2.5
0.9	-1.9×10^{-9}	1.3×10^{-7}	2.5×10^{-5}	3	-2.5×10^{-9}	5.4×10^{-8}	6.8×10^{-4}	2.5
1	-2.5×10^{-9}	1.6×10^{-7}	3.4×10^{-5}	3	9.6×10^{-9}	6.0×10^{-8}	-4.3×10^{-4}	2.5
1.1	-2.7×10^{-9}	1.9×10^{-7}	2.4×10^{-5}	3	-1.5×10^{-8}	6.8×10^{-8}	1.7×10^{-4}	2.5
1.3	-3.3×10^{-9}	2.7×10^{-7}	2.5×10^{-5}	3	3.2×10^{-8}	8.2×10^{-8}	-5.9×10^{-4}	2.4
1.5	-4.1×10^{-9}	3.6×10^{-7}	3.0×10^{-5}	3	-2.6×10^{-8}	9.8×10^{-8}	-5.3×10^{-4}	2.4
1.7	-2.3×10^{-9}	4.7×10^{-7}	2.8×10^{-5}	3	5.2×10^{-9}	1.1×10^{-7}	7.9×10^{-4}	2.4
1.9	-3.5×10^{-9}	5.8×10^{-7}	3.4×10^{-5}	3	3.9×10^{-8}	1.3×10^{-7}	6.6×10^{-4}	2.4

Table 4.2 The effect of the random input force amplitude on the mean, mean square, skewness and kurtosis of the displacement response of the secondary system (absorber mass). ($m_s=1.26\times10^{-1}$ (kg), $c_s=2.12$ ($\mathrm{N\cdot s/m}$), $k_s=8.93\times10^{4}$ $\left(\mathrm{N/m}\right)$, $m=2.52\times10^{-3}$ (kg), $c=3.4\times10^{-2}$ ($\mathrm{N\cdot s/m}$) $k_1=1.79\times10^{3}$ $\left(\mathrm{N/m}\right)$ and $k_3=8.93\times10^{9}$ $\left(\mathrm{N/m^3}\right)$

Input force	Input force	Nonlinear stiffness	The primary system without absorber	Nondimensional response			
				Linear absorber		Nonlinear absorber	
σ_F (N)	B	α	$\psi^2_{x_0}\ (m^2)$	$\psi^2_{y_s}$	ψ^2_y	$\psi^2_{y_s}$	ψ^2_y
0.1	0.14	2.9×10^{-4}	5.37×10^{-11}	0.56	27.9	0.58	27.9
0.3	0.14	2.8×10^{-3}	5.11×10^{-10}	0.57	27.4	0.71	23.5
0.5	0.14	7.8×10^{-3}	1.42×10^{-9}	0.56	28.2	0.78	18.3
0.7	0.14	1.5×10^{-2}	2.79×10^{-9}	0.57	28.3	0.86	14.7
0.9	0.14	2.5×10^{-2}	4.59×10^{-9}	0.57	28.3	0.87	11.8
1	0.14	3.1×10^{-2}	5.64×10^{-9}	0.57	28.4	0.89	10.6
1.1	0.14	3.8×10^{-2}	6.84×10^{-9}	0.56	27.8	0.91	9.9
1.3	0.14	5.2×10^{-2}	9.61×10^{-9}	0.56	28.1	0.90	8.5
1.5	0.14	7.0×10^{-2}	1.28×10^{-8}	0.56	28.1	0.94	7.7
1.7	0.14	9.0×10^{-2}	1.64×10^{-8}	0.56	28.7	0.98	6.7
1.9	0.14	1.1×10^{-2}	2.04×10^{-8}	0.54	28.4	0.93	6.4

Table 4.3 The effect of the random input force amplitude on the response of the primary system. $\psi^2_{x_0}$ is mean square displacement of the primary system without absorber. ($\omega_0 = 1$, mass ratio $\mu = 0.02$ and damping $\zeta_s = 0.01$ and $\zeta = 0.008$), where $B = \sigma_F / k_s x_0$, $x_0 = \sqrt{\psi^2_{x_0}}$.

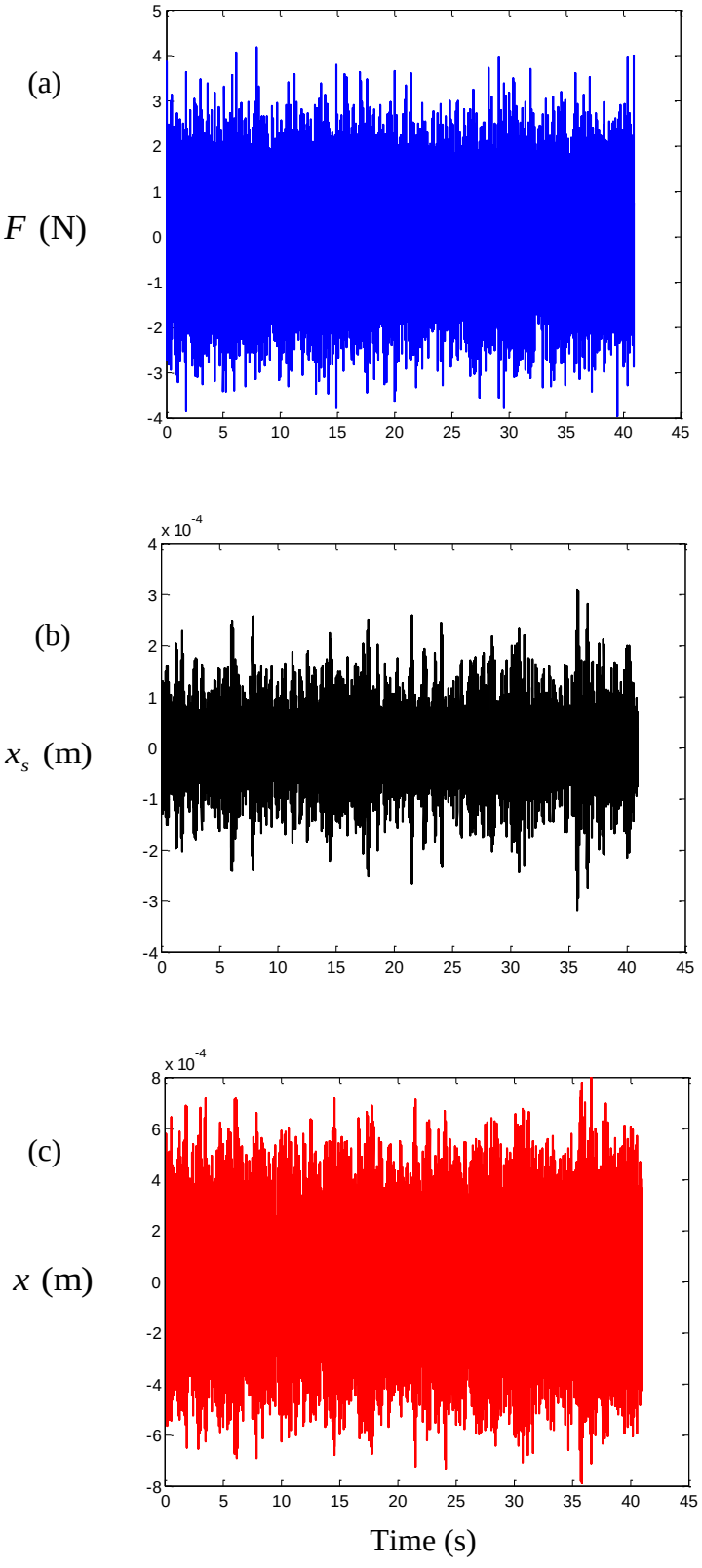

Figure 4.1 The vibration response of time history for signals whose rms force amplitude are 1 N . (a) input random excitation (b) primary system (c) secondary system

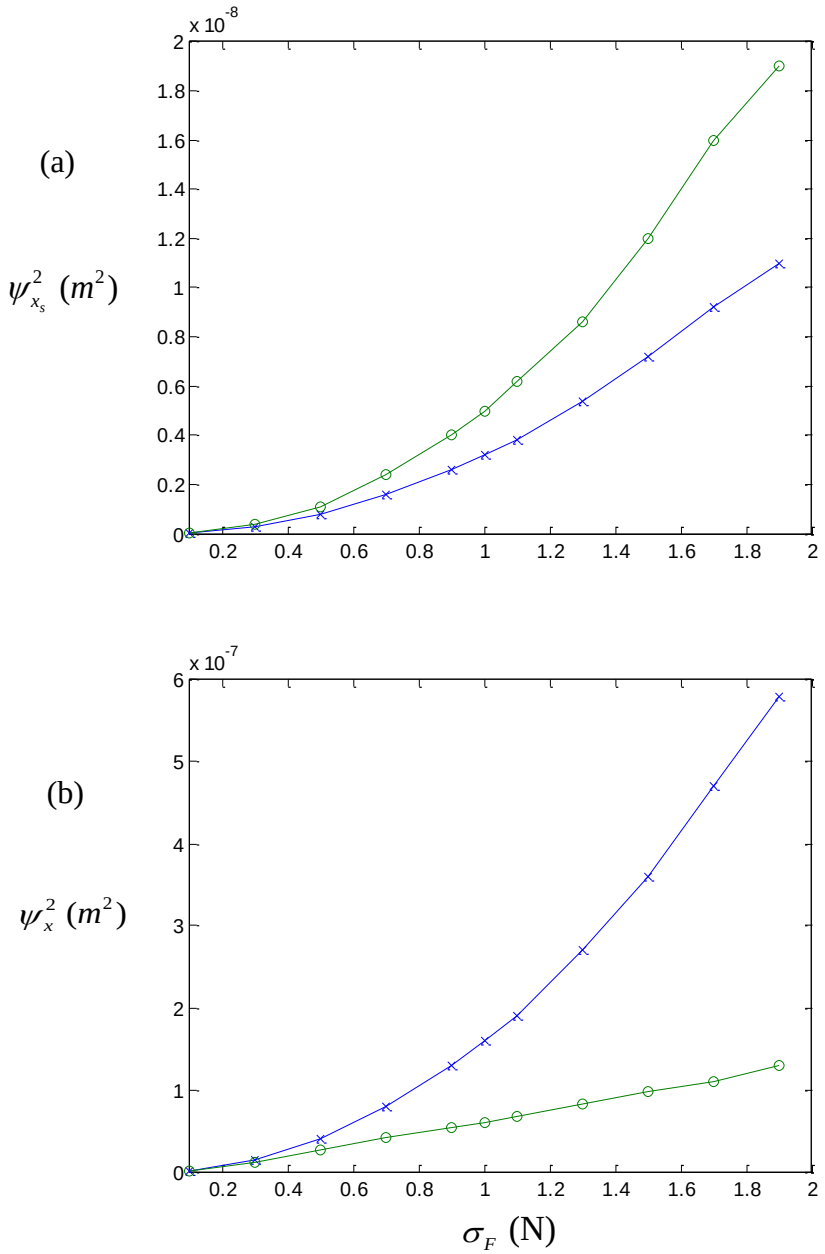

Figure 4.2 The effect of the input rms force amplitude σ_F on the (a) primary and (b) absorber system mean square displacement response. Nonlinear absorber ($'o'$) and linear absorber ($'\times'$). ($\omega_0 = 1$,mass ratio $\mu = 0.02$ and damping $\zeta_s = 0.01$ and $\zeta = 0.008$).

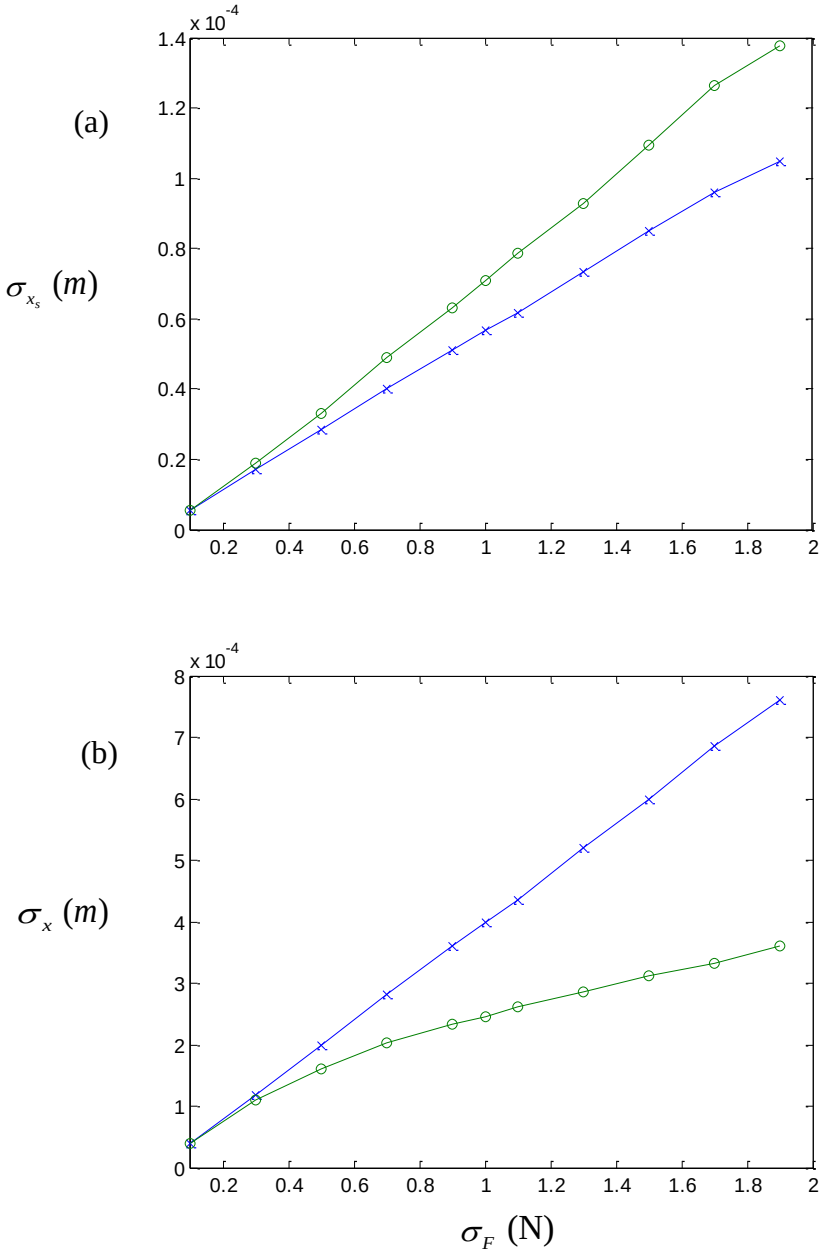

Figure 4.3 The effect of the input rms force amplitude σ_F on the (a) primary and (b) absorber system displacement standard deviation. Nonlinear absorber ($'o'$) and linear absorber ($'\times'$). ($\omega_0 = 1$,mass ratio $\mu = 0.02$ and damping $\zeta_s = 0.01$ and $\zeta = 0.008$).

The nonlinear aspects of the system response are readily shown and considered in the frequency domain. The PSD, frequency response function (FRF) and coherence will help to identify the response of the nonlinear system. The methods used to estimate the FRFs are the standard estimated methods [74], which as stated previously are strictly only applicable to linear system behaviour.

The displacement spectral density functions (PSD) for the primary and secondary system are presented in Figures 4.4-5. The sample size chosen for the PSD estimates was 1.28 s, which resulted in a frequency resolution Δf of 0.78 Hz. The PSD estimates were made using a Hanning window, 67% overlap of the windowed data [78] and a sample rate of 800 Hz resulting in 1024 points for the FFT and 512 frequency domain points. A frequency resolution of 0.78 Hz was chosen as a compromise between the number of averages and frequency resolution (see Section 4.1.3). In this case, the number of averages was chosen to be 32.

The dynamic performance of the primary system employing the nonlinear absorbers is evaluated through the PSD characteristics of the system response. The effect of the input force amplitude on the primary and secondary system PSD response versus excitation frequency can be evaluated for various levels of input force as shown in Figures 4.4-5. A difference between the vibration response due to the linear and the nonlinear absorber is that the nonlinear absorber has a higher response at the first mode. The cumulative displacement for primary system, by integrating the PSD, with a nonlinear absorber also shows a final higher response than when a linear absorber is used, see Figure 4.6. For the nonlinear absorber the high force amplitude applied to the primary system produced a much broader PSD for the primary and secondary response at the second mode and produces a larger vibration response at higher frequencies. The reason for this could be possibly due to the nonlinear stiffness effect. It shows a nonlinear effect as the amplitude of the force input is changed compared to the linear absorber case.

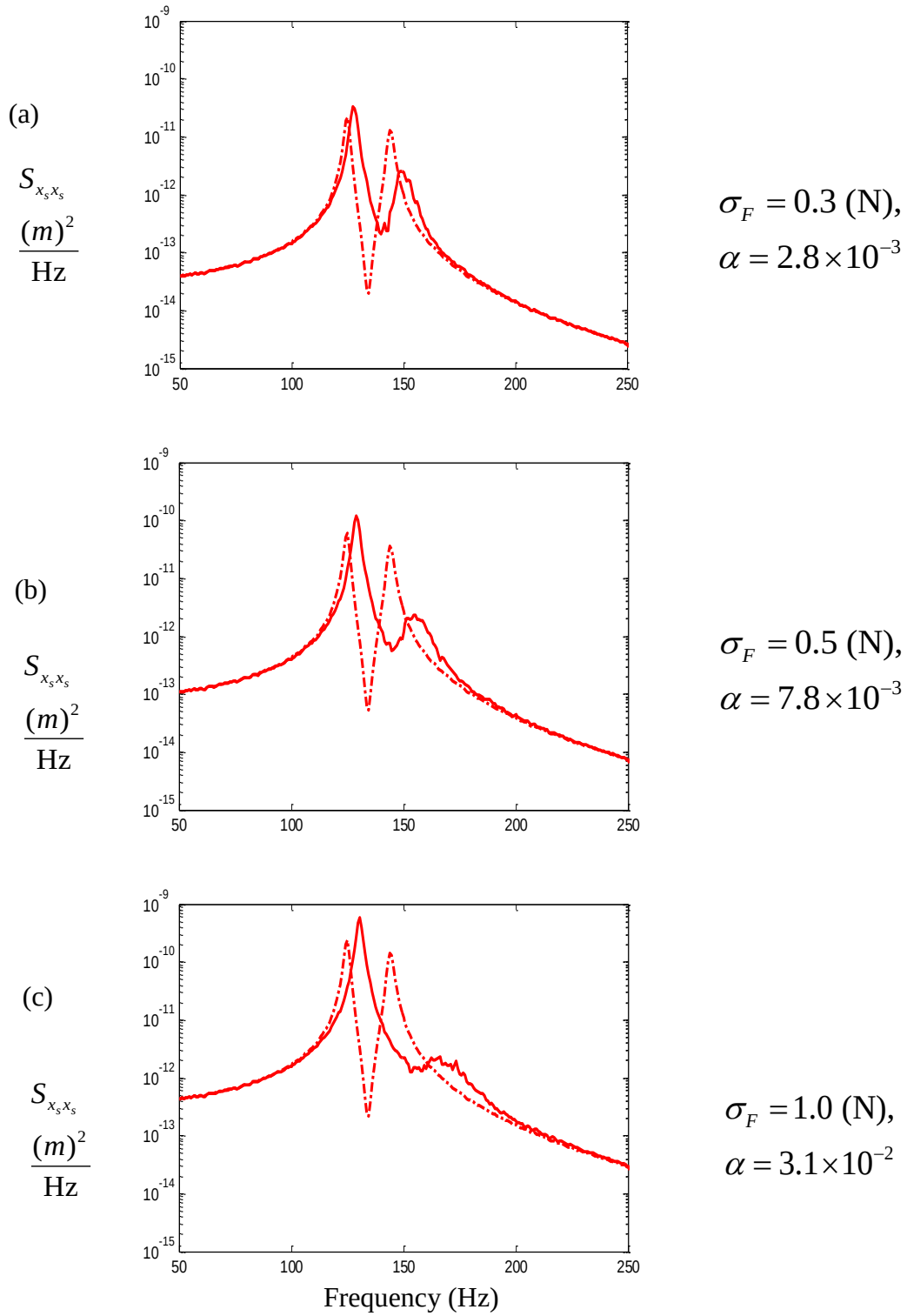

Figure 4.4 The effect of the input force amplitude on the primary system displacement PSD. (The 'tuned' frequency $\omega_1/\omega_s = 1$, mass ratio $\mu = 0.02$ and damping $\zeta_s = 0.01$, $\zeta = 0.008$). The response for the system with the linear absorber is given by the dashed-dotted line, the solid line is the nonlinear absorber. (a) $\sigma_F = 0.3$ (N), (b) $\sigma_F = 0.5$ (N) and (c) $\sigma_F = 1.0$ (N).

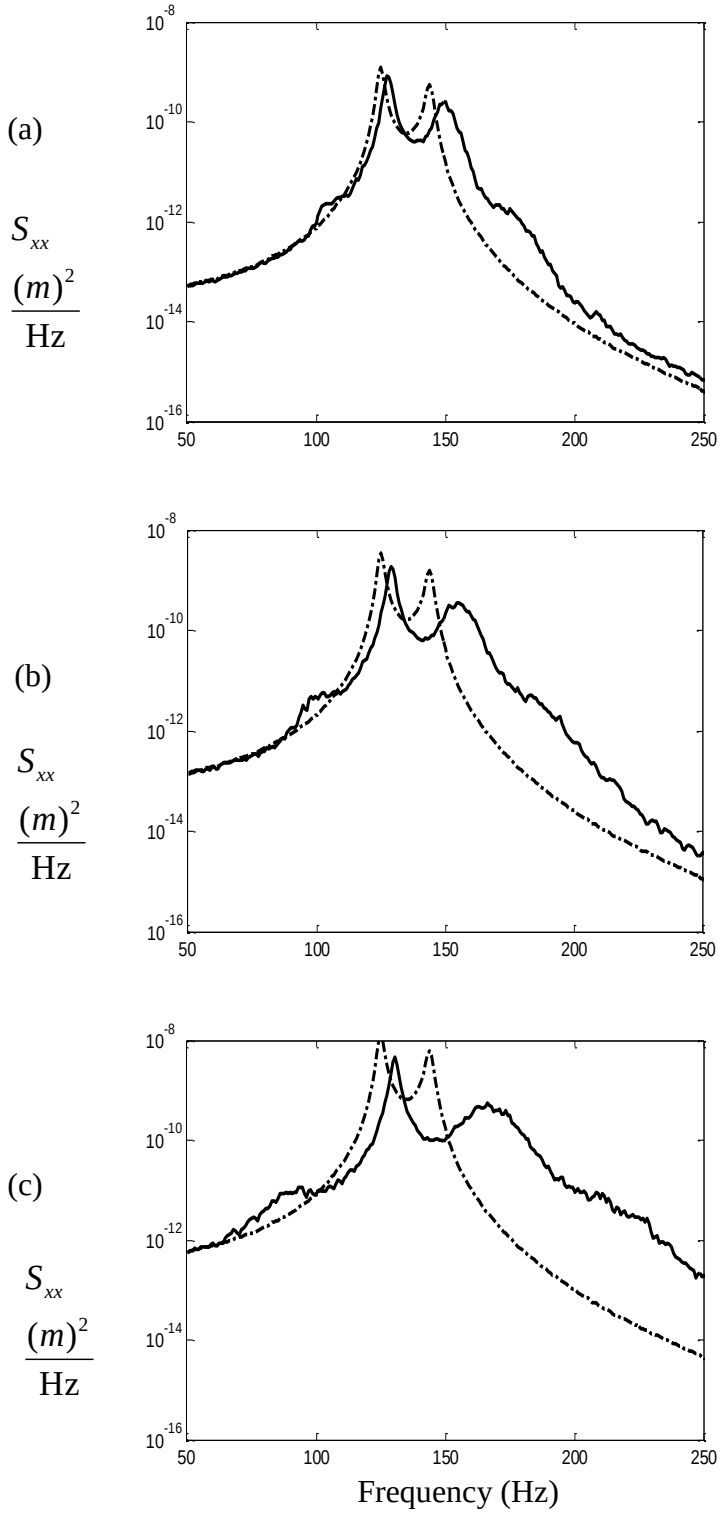

Figure 4.5 The effect of the input force amplitude on the secondary system (absorber) displacement PSD. (The 'tuned' frequency $\omega_1/\omega_s = 1$, mass ratio $\mu = 0.02$ and damping $\zeta_s = 0.01$, $\zeta = 0.008$). The response for the system with the linear absorber is given by the dashed-dotted line, the solid line is the nonlinear absorber. (a) $\sigma_F = 0.3$ (N) , (b) $\sigma_F = 0.5$ (N) and (c) $\sigma_F = 1.0$ (N).

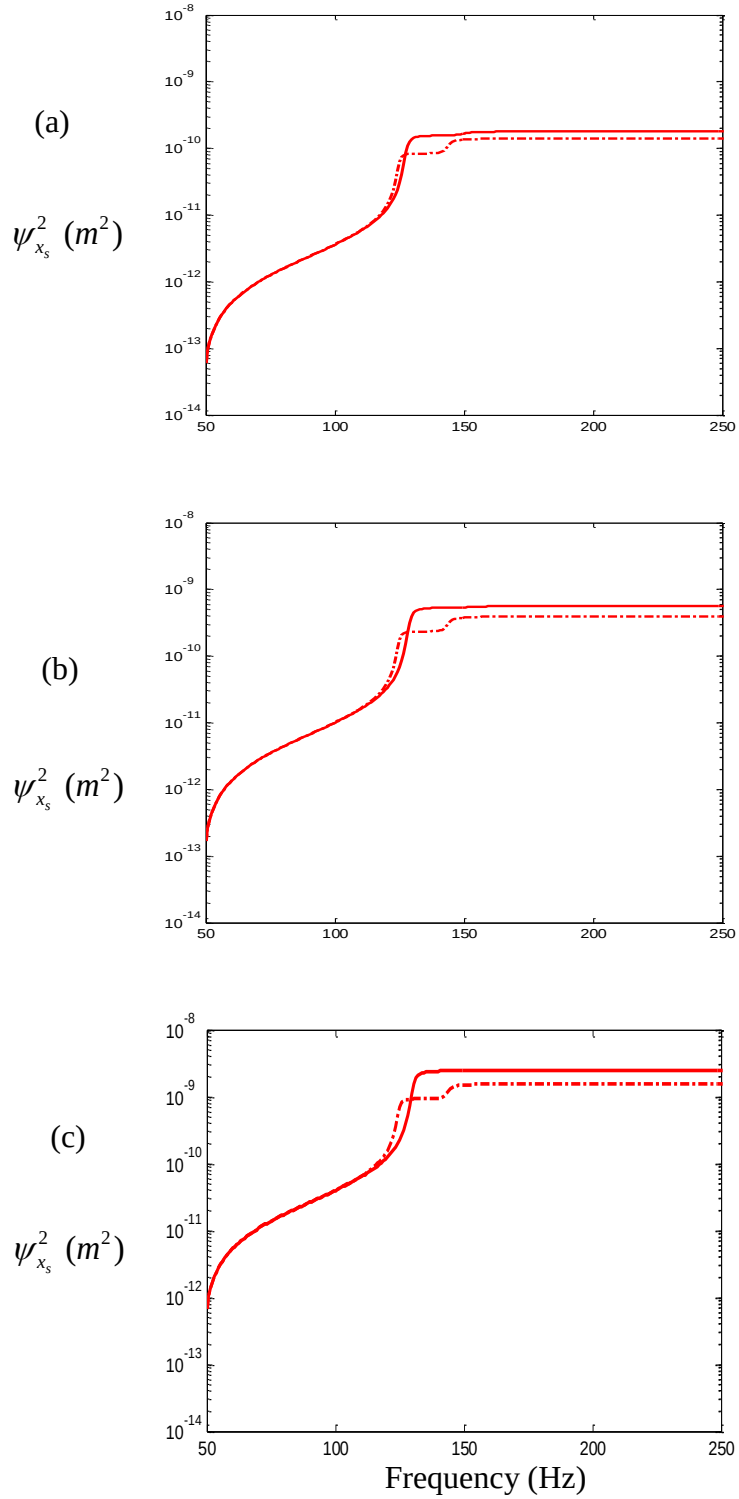

Figure 4.6 The effect of the input force amplitude on the primary system cumulative mean square displacement. (The 'tuned' frequency $\omega_1/\omega_s = 1$, mass ratio $\mu = 0.02$ and damping $\zeta_s = 0.01$, $\zeta = 0.008$). The response for the system with the linear absorber is given by the dashed-dotted line, the solid line is the nonlinear absorber. (a) $\sigma_F = 0.3$ (N), (b) $\sigma_F = 0.5$ (N) and (c) $\sigma_F = 1.0$ (N).

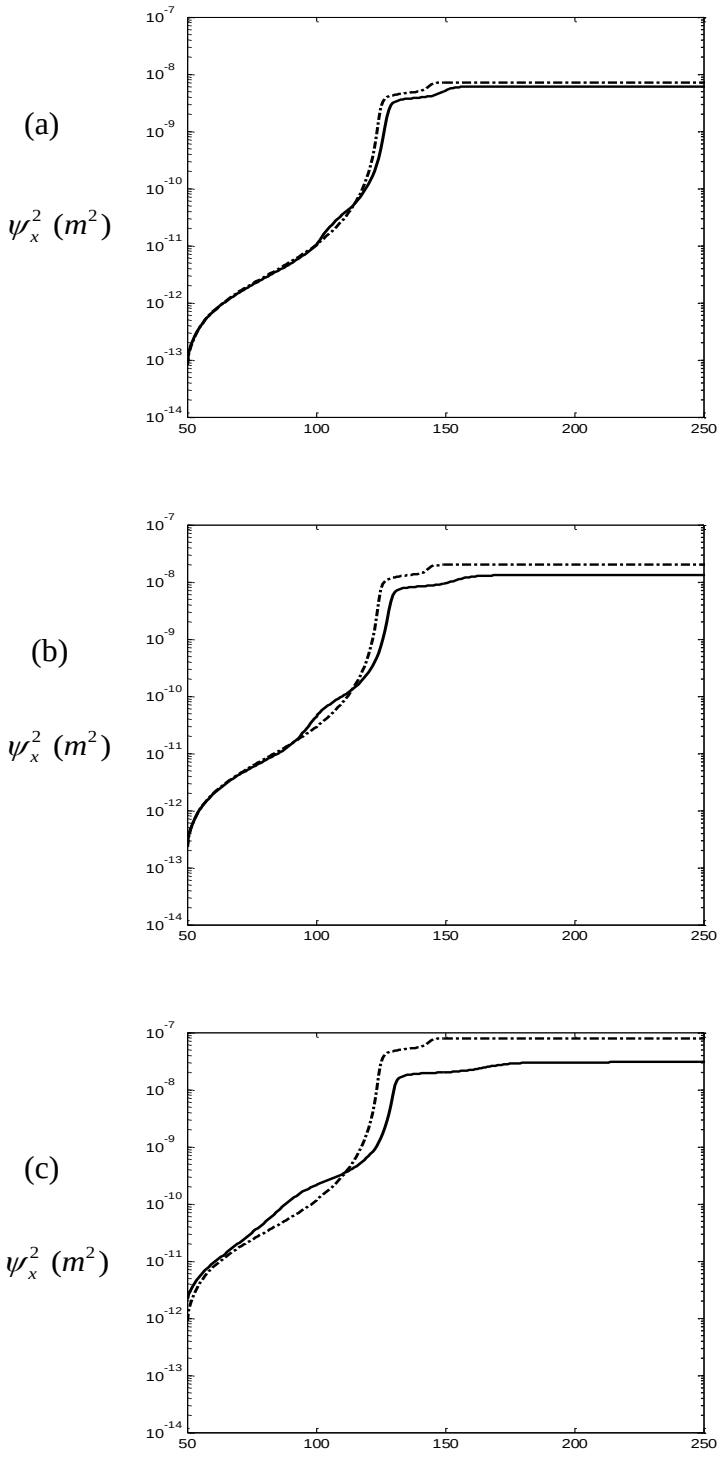

Figure 4.7 The effect of the input force amplitude on the secondary system (absorber) cumulative mean square displacement. (The 'tuned' frequency $\omega_1/\omega_s = 1$, mass ratio $\mu = 0.02$ and damping $\zeta_s = 0.01$, $\zeta = 0.008$). The response for the system with the linear absorber is given by the dashed-dotted line, the solid line is the nonlinear absorber. (a) $\sigma_F = 0.3$ (N), (b) $\sigma_F = 0.5$ (N) and (c) $\sigma_F = 1.0$ (N).

In Figures 4.8-9, the estimated displacement FRF of the primary and secondary system (H_0) is given for an applied input force amplitude. The H_0 estimator, that uses the spectra of the outputs and inputs, takes a ratio of them at each frequency to determine the effect of nonlinearity. However, a limitation of the H_0 estimator is that it cannot separate out what in the frequency content of the input process produces a particular frequency content in the output. The effect on the displacement response of the primary system is to shift the first resonance peak Ω_{r1}, the effective tuned frequency Ω_t and the second resonance peak Ω_{r2} to higher frequencies. The effect of the nonlinearity on the secondary displacement response is also to shift the first resonance peak Ω_{r1} and the second resonance peak Ω_{r2} to the right. The nonlinear absorber has a higher vibration response at the first mode compared to using a linear absorber. The primary system responded over a much broader frequency response. The response at the second mode produces a vibration response across a wider and higher frequency range. It shows a nonlinear effect compared to the linear absorber case. For higher input levels of the force, the second peak at Ω_{r2} of the primary system does not obviously exhibit a resonance or peak response compared to a lower input force.

The estimated displacement FRFs of the system (H_1 and H_2) are given in Figures 4.10-11 and 4.12-13. The definitions of $H_1 = S_{xy}/S_{xx}$ and $H_2 = S_{yy}/S_{yx}$ were described in section 4.1.2. However, the nonlinear absorber system will display frequency spectra which are not linearly related to the input. The nonlinear responses will not contribute in any of the H_1 or H_2 estimators, as potentially the response at certain frequencies will not be coherent with the input at these frequencies. It shows a nonlinear effect compared to the linear absorber case. In addition, the corresponding phase information for the transfer function (H_1) are shown in Figures 4.14-15. The effect of the primary and secondary system is to shift the first resonance, the effective tuned frequency and the second resonance peak to higher frequencies. For higher input force levels, the second resonance peak of the primary system will be reduced in amplitude compared to lower input force, but a broadening of the frequency content also occurs.

The coherence functions in Figures 4.16-17 show that the transfer functions calculated are able to account for almost of the response for the linear absorber. However, the response with a nonlinear absorber does not fair as well, which results from significant nonlinear response

behaviour as expected in the simulated output data. The coherence for the responses with a linear absorber for a lightly damped system do not produce good values at the resonances and effective tuned frequencies due to bias errors. The bias error can be reduced by improving the resolution of the FRF estimates, i.e. the frequency resolution bandwidth should be reduced which requires more time history data [74].

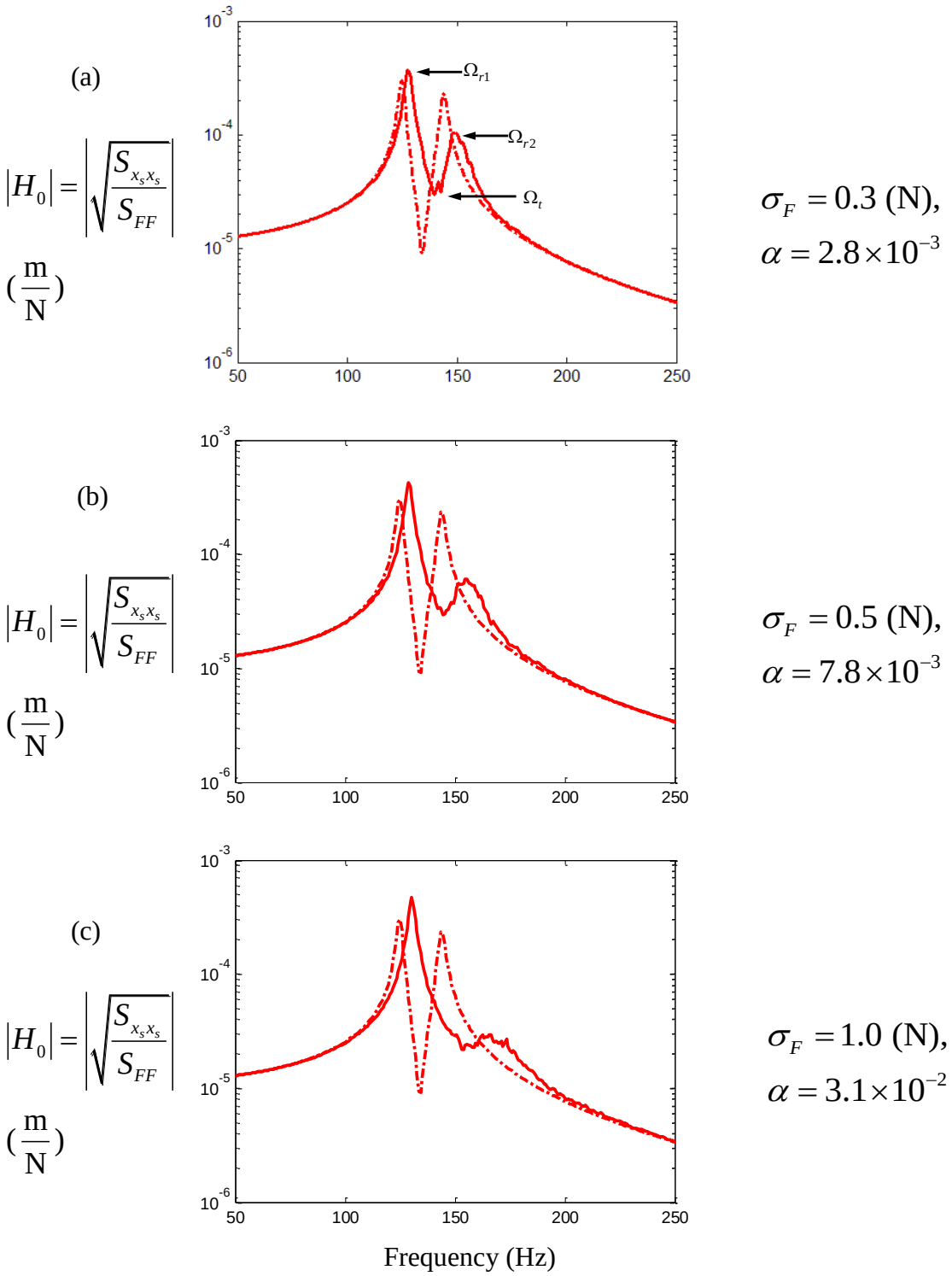

Figure 4.8 The effect of the input force amplitude on the primary system frequency response (H_0 estimator). (The 'tuned' frequency $\omega_1/\omega_s = 1$, mass ratio $\mu = 0.02$ and damping $\zeta_s = 0.01$, $\zeta = 0.008$). The response for the system with the linear absorber is given by the dashed-dotted line, the solid line is the nonlinear absorber. (a) $\sigma_F = 0.3$ (N) , (b) $\sigma_F = 0.5$ (N) and (c) $\sigma_F = 1.0$ (N).

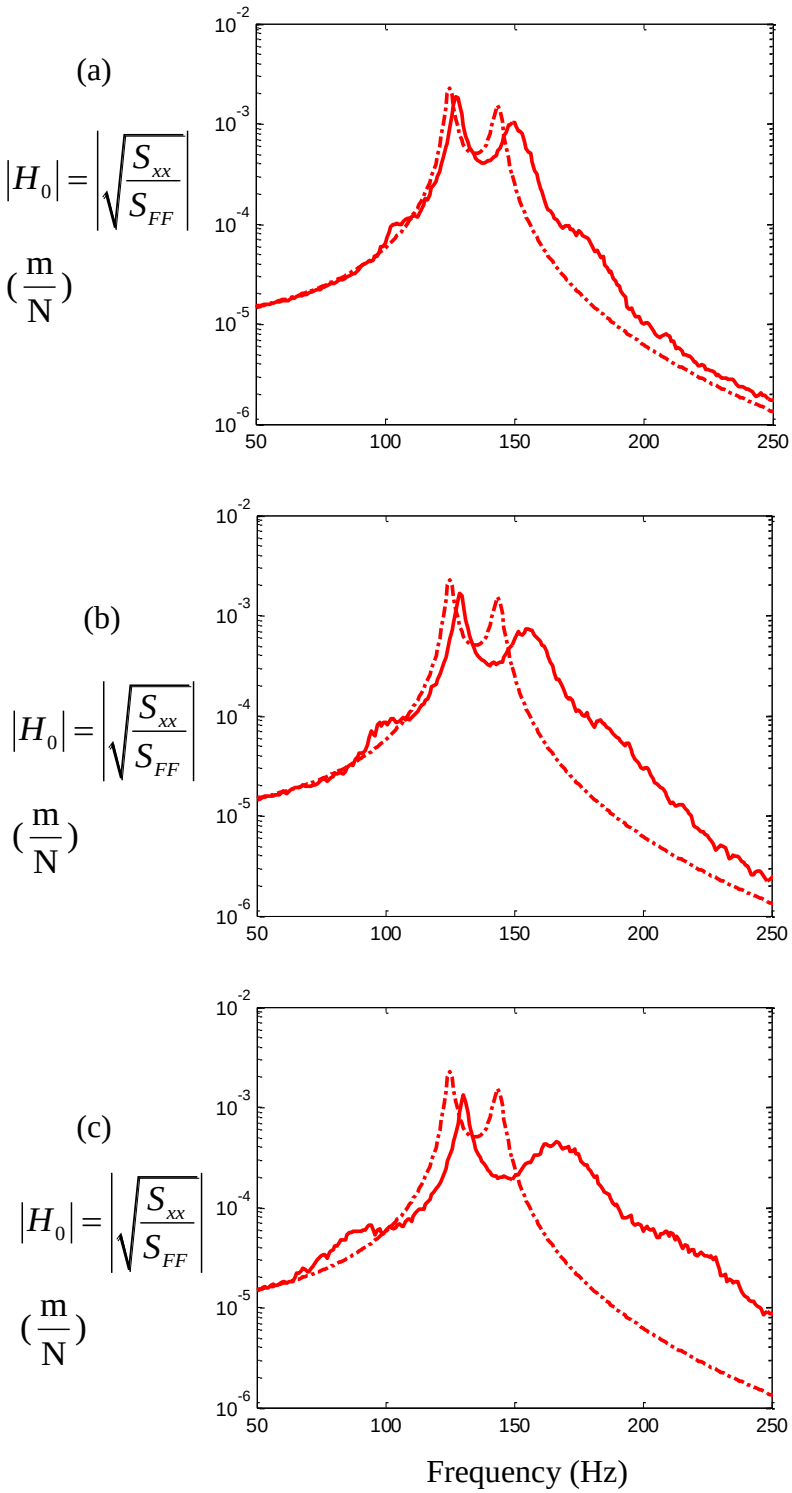

Figure 4.9 The effect of the input force amplitude on the secondary system (absorber) frequency response (H_0 estimator). (The 'tuned' frequency $\omega_1/\omega_s = 1$, mass ratio $\mu = 0.02$ and damping $\zeta_s = 0.01$, $\zeta = 0.008$). The response for the system with the linear absorber is given by the dashed-dotted line, the solid line is the nonlinear absorber. (a) $\sigma_F = 0.3$ (N) , (b) $\sigma_F = 0.5$ (N) and (c) $\sigma_F = 1.0$ (N).

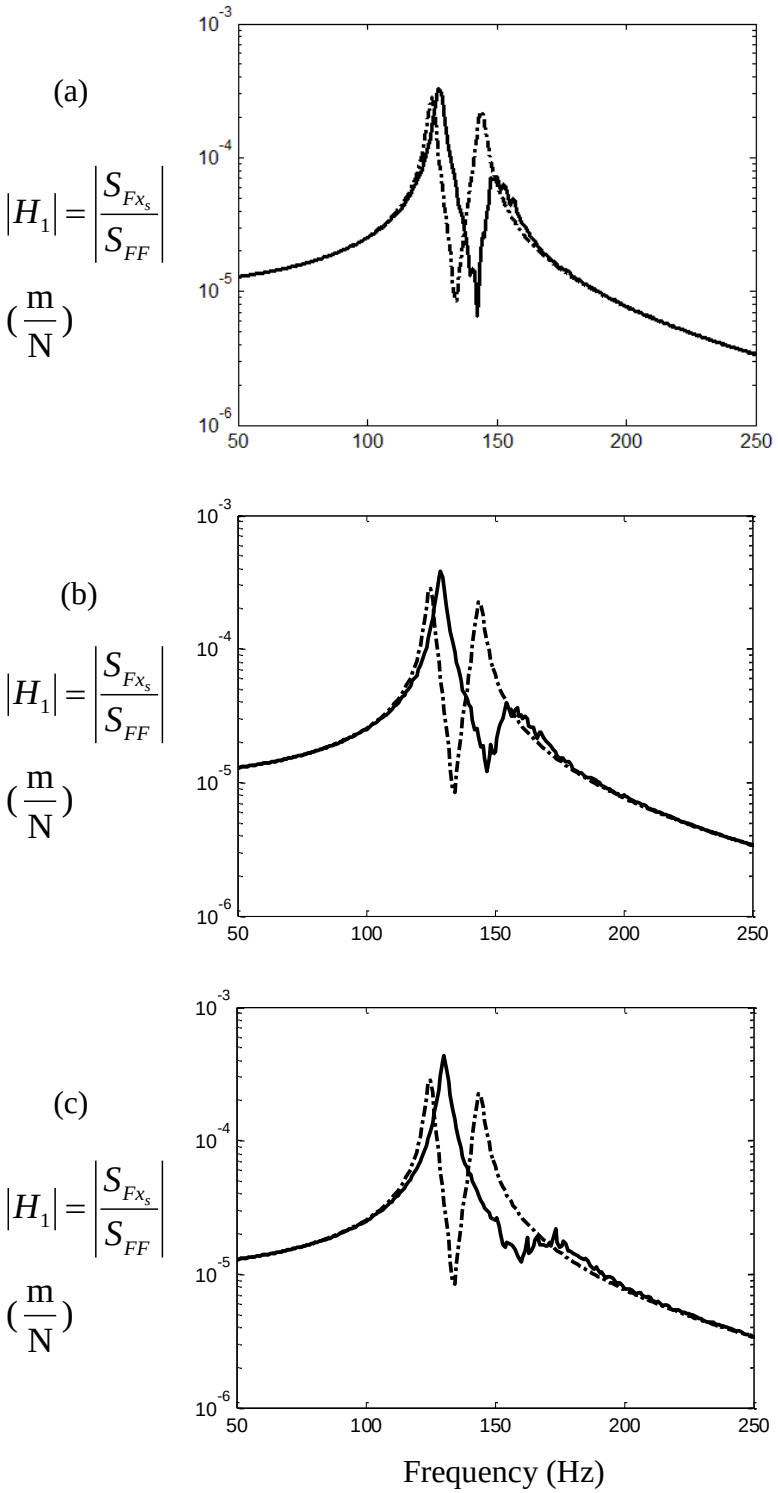

Figure 4.10 The effect of the input force amplitude on the primary system frequency response (H_1 estimator). (The 'tuned' frequency $\omega_1/\omega_s = 1$, mass ratio $\mu = 0.02$ and damping $\zeta_s = 0.01$, $\zeta = 0.008$). The response for the system with the linear absorber is given by the dashed-dotted line, the solid line is the nonlinear absorber. (a) $\sigma_F = 0.3$ (N) , (b) $\sigma_F = 0.5$ (N) and (c) $\sigma_F = 1.0$ (N).

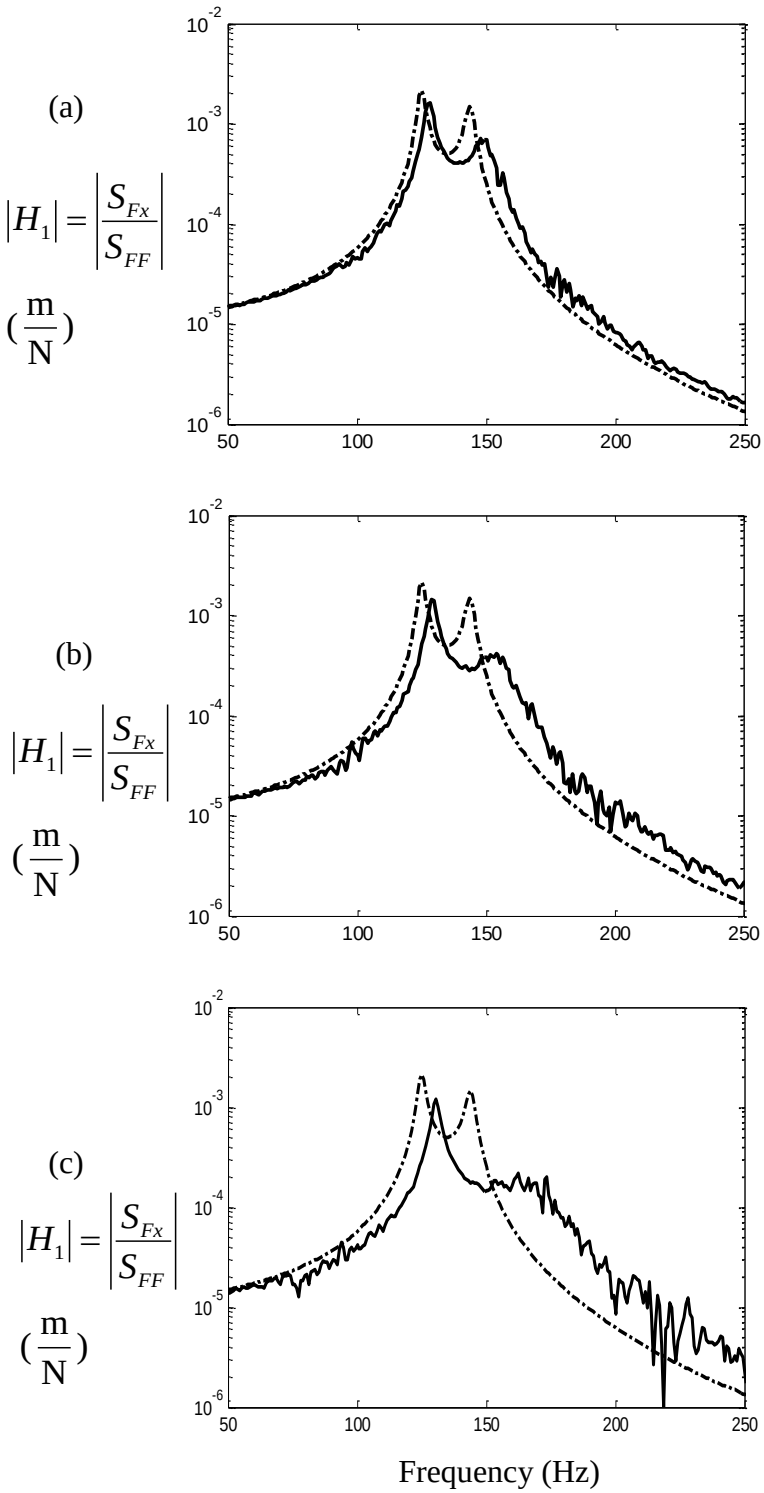

Figure 4.11 The effect of the input force amplitude on the secondary system (absorber) frequency response (H_1 estimator). (The 'tuned' frequency $\omega_1/\omega_s = 1$, mass ratio $\mu = 0.02$ and damping $\zeta_s = 0.01$, $\zeta = 0.008$). The response for the system with the linear absorber is given by the dashed-dotted line, the solid line is the nonlinear absorber. (a) $\sigma_F = 0.3$ (N), (b) $\sigma_F = 0.5$ (N) and (c) $\sigma_F = 1.0$ (N).

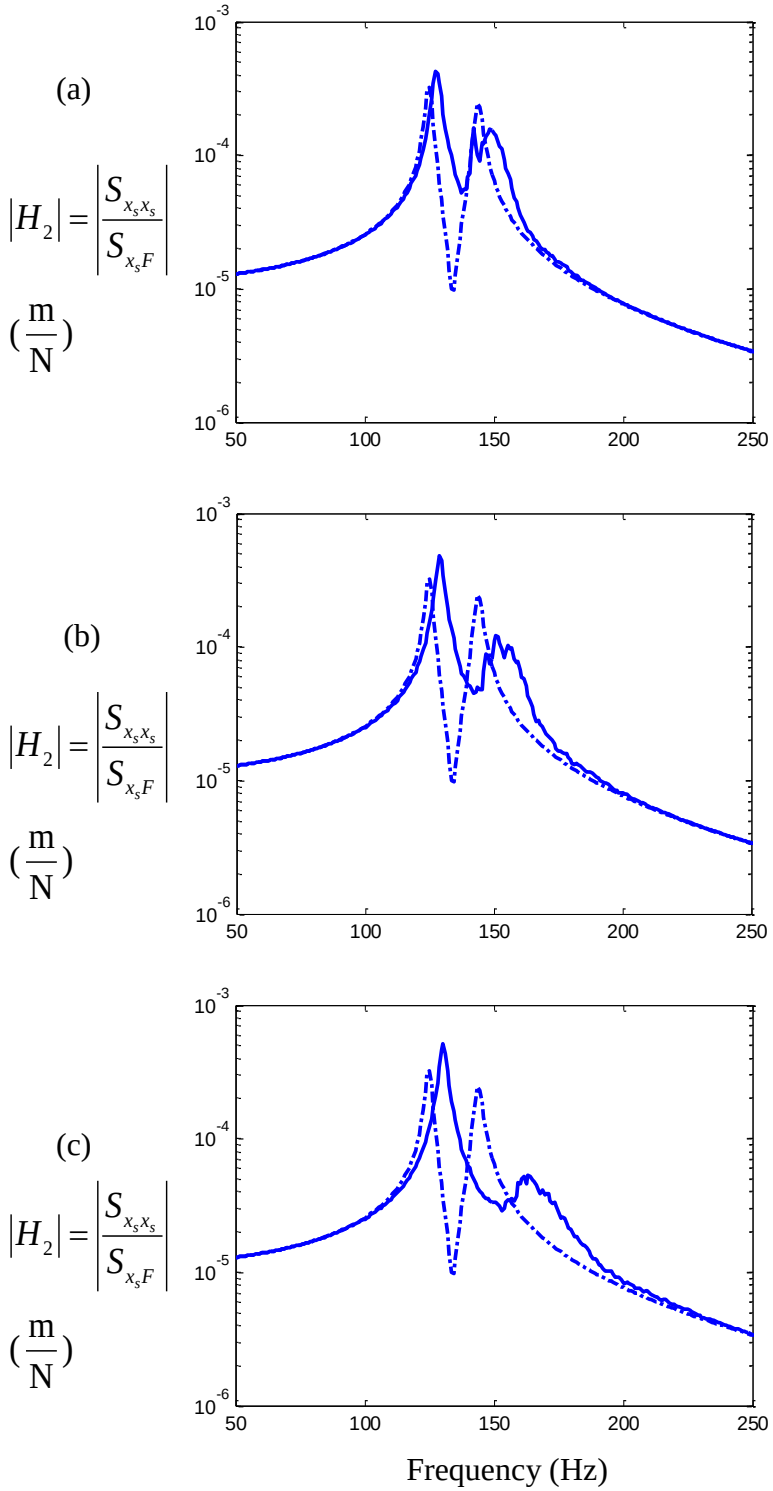

Figure 4.12 The effect of the input force amplitude on the primary system frequency response (H_2 estimator). (The 'tuned' frequency $\omega_1/\omega_s = 1$, mass ratio $\mu = 0.02$ and damping $\zeta_s = 0.01$, $\zeta = 0.008$). The response for the system with the linear absorber is given by the dashed-dotted line, the solid line is the nonlinear absorber. (a) $\sigma_F = 0.3$ (N) , (b) $\sigma_F = 0.5$ (N) and (c) $\sigma_F = 1.0$ (N) .

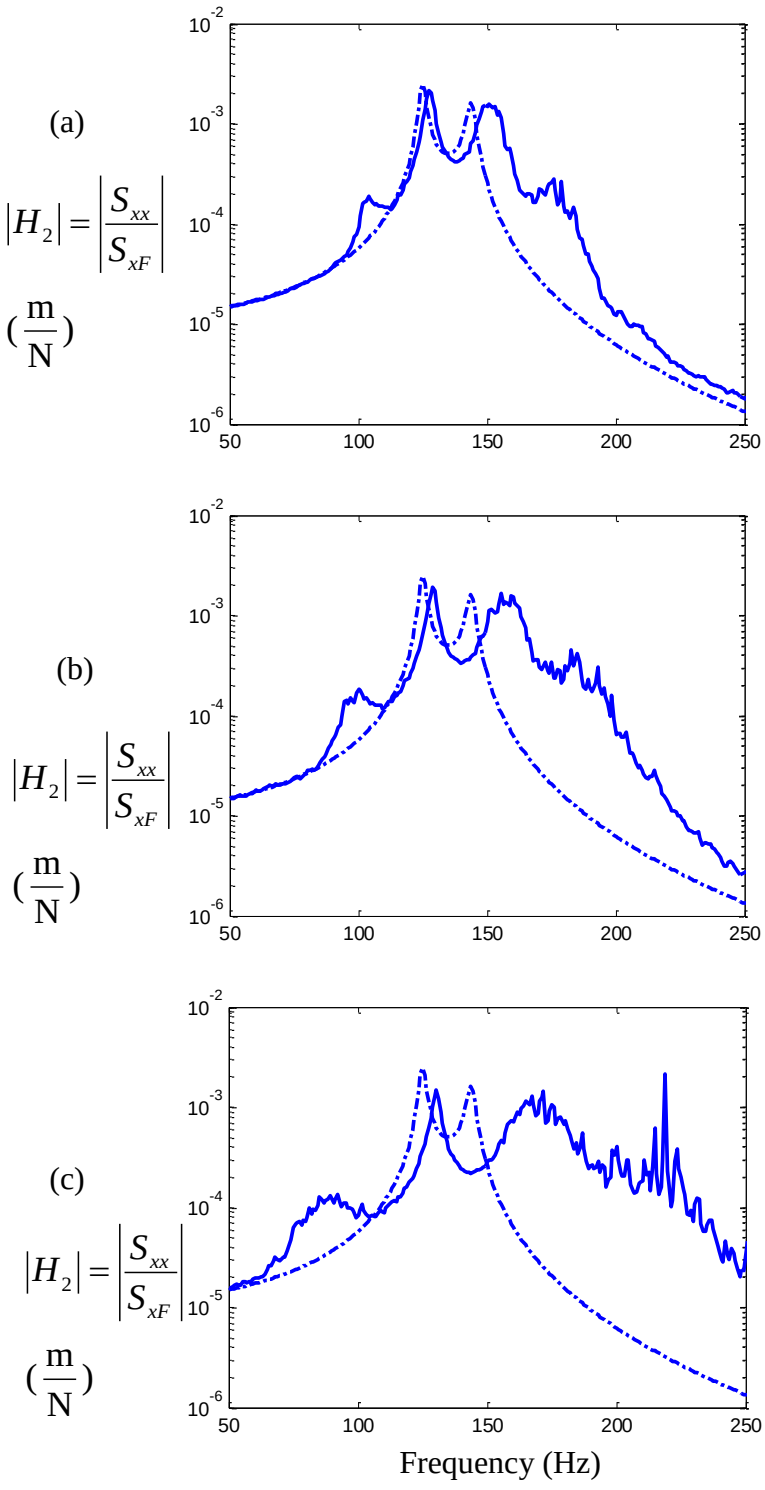

Figure 4.13 The effect of the input force amplitude on the secondary system (absorber) frequency response (H_2 estimator). (The 'tuned' frequency $\omega_1/\omega_s = 1$, mass ratio $\mu = 0.02$ and damping $\zeta_s = 0.01$, $\zeta = 0.008$). The response for the system with the linear absorber is given by the dashed-dotted line, the solid line is the nonlinear absorber. (a) $\sigma_F = 0.3$ (N), (b) $\sigma_F = 0.5$ (N) and (c) $\sigma_F = 1.0$ (N).

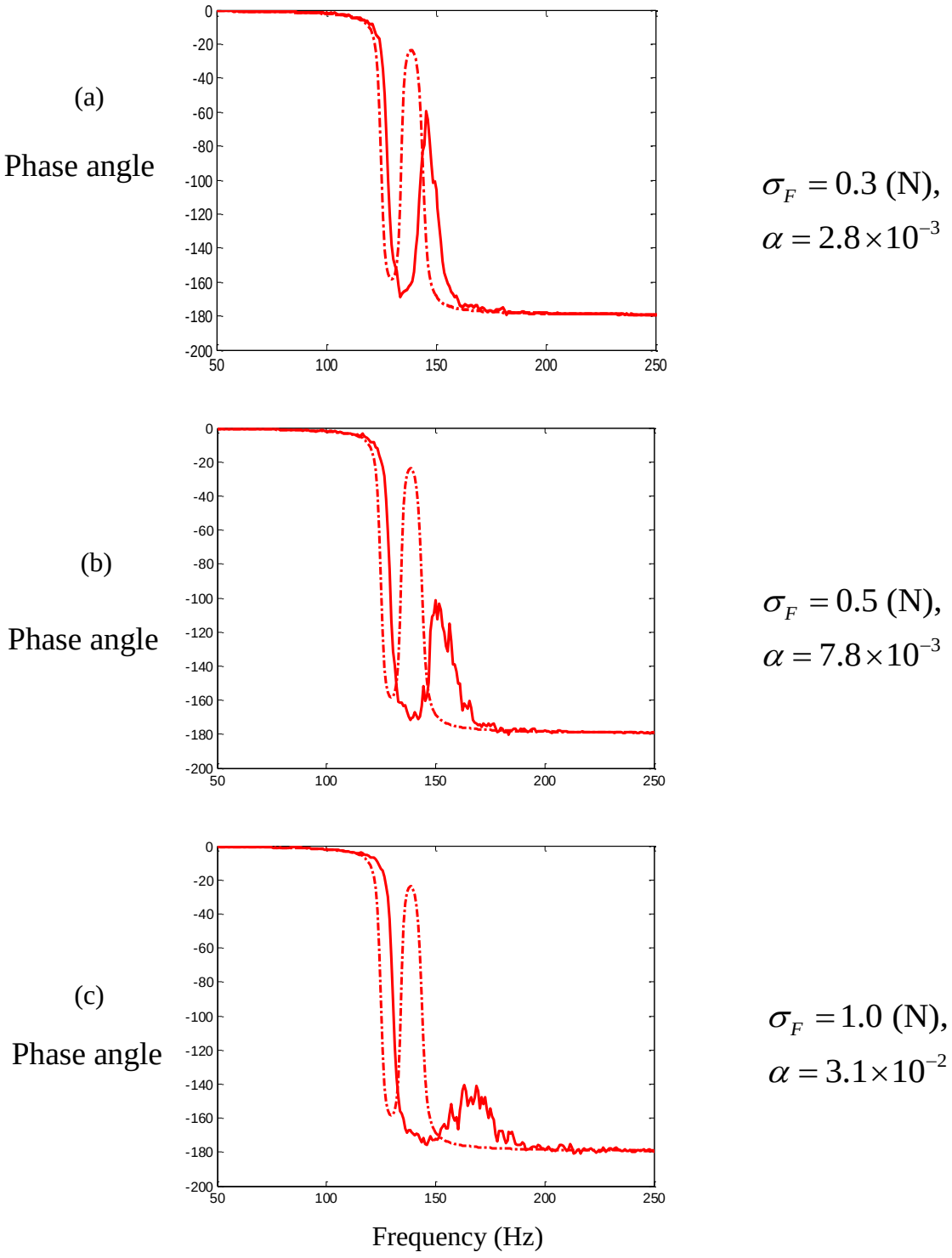

Figure 4.14 The effect of the input force amplitude on the primary system showing the phase of the frequency response (H_1 estimator). (The 'tuned' frequency $\omega_1/\omega_s = 1$, mass ratio $\mu = 0.02$ and damping $\zeta_s = 0.01$, $\zeta = 0.008$). The response for the system with the linear absorber is given by the dashed-dotted line, the solid line is the nonlinear absorber. (a) $\sigma_F = 0.3$ (N), (b) $\sigma_F = 0.5$ (N) and (c) $\sigma_F = 1.0$ (N).

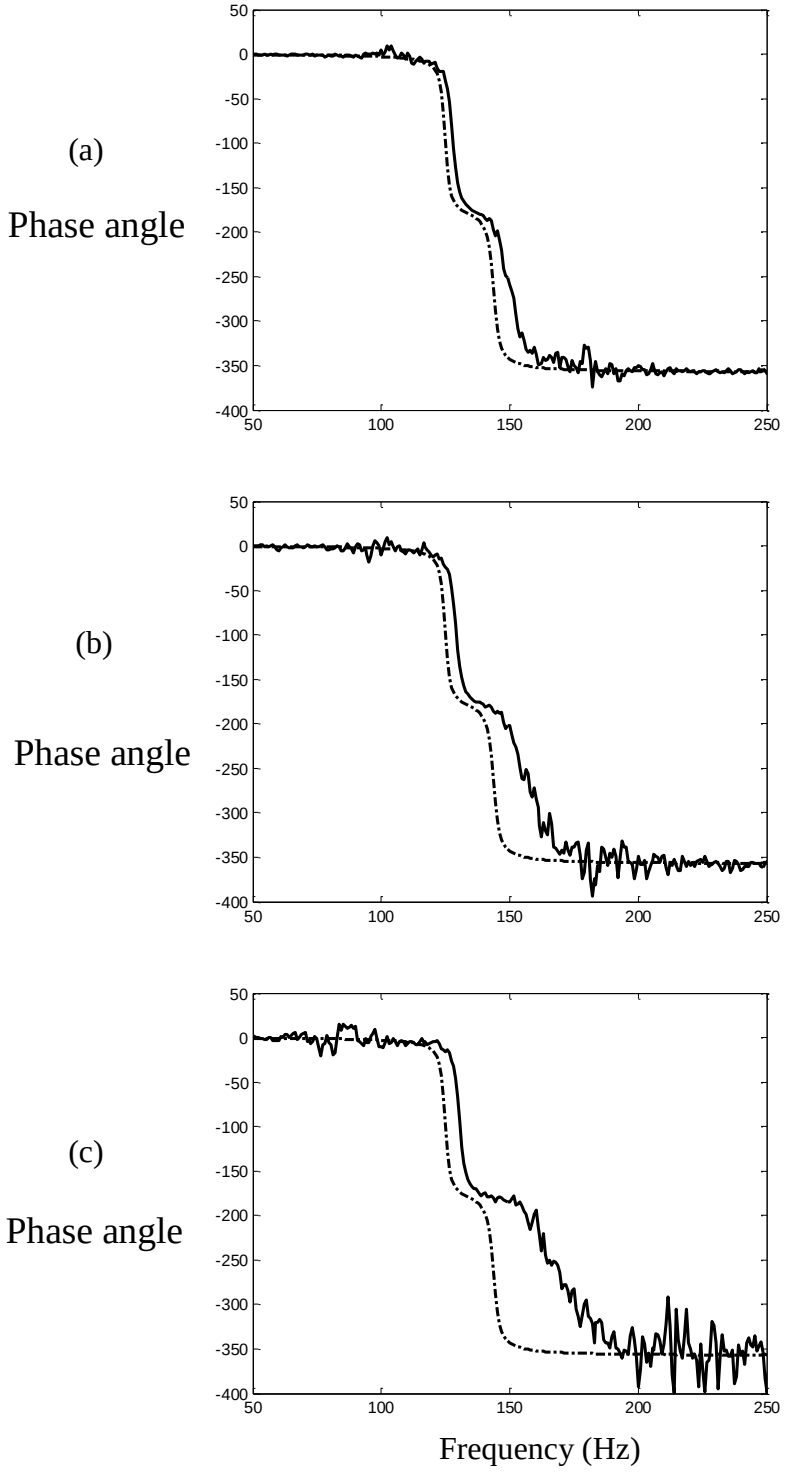

Figure 4.15 The effect of the input force amplitude on the secondary system (absorber) showing the phase of the frequency response (H_1 estimator). (The 'tuned' frequency $\omega_1/\omega_s = 1$, mass ratio $\mu = 0.02$ and damping $\zeta_s = 0.01$, $\zeta = 0.008$). The response for the system with the linear absorber is given by the dashed-dotted line, the solid line is the nonlinear absorber. (a) $\sigma_F = 0.3$ (N), (b) $\sigma_F = 0.5$ (N) and (c) $\sigma_F = 1.0$ (N).

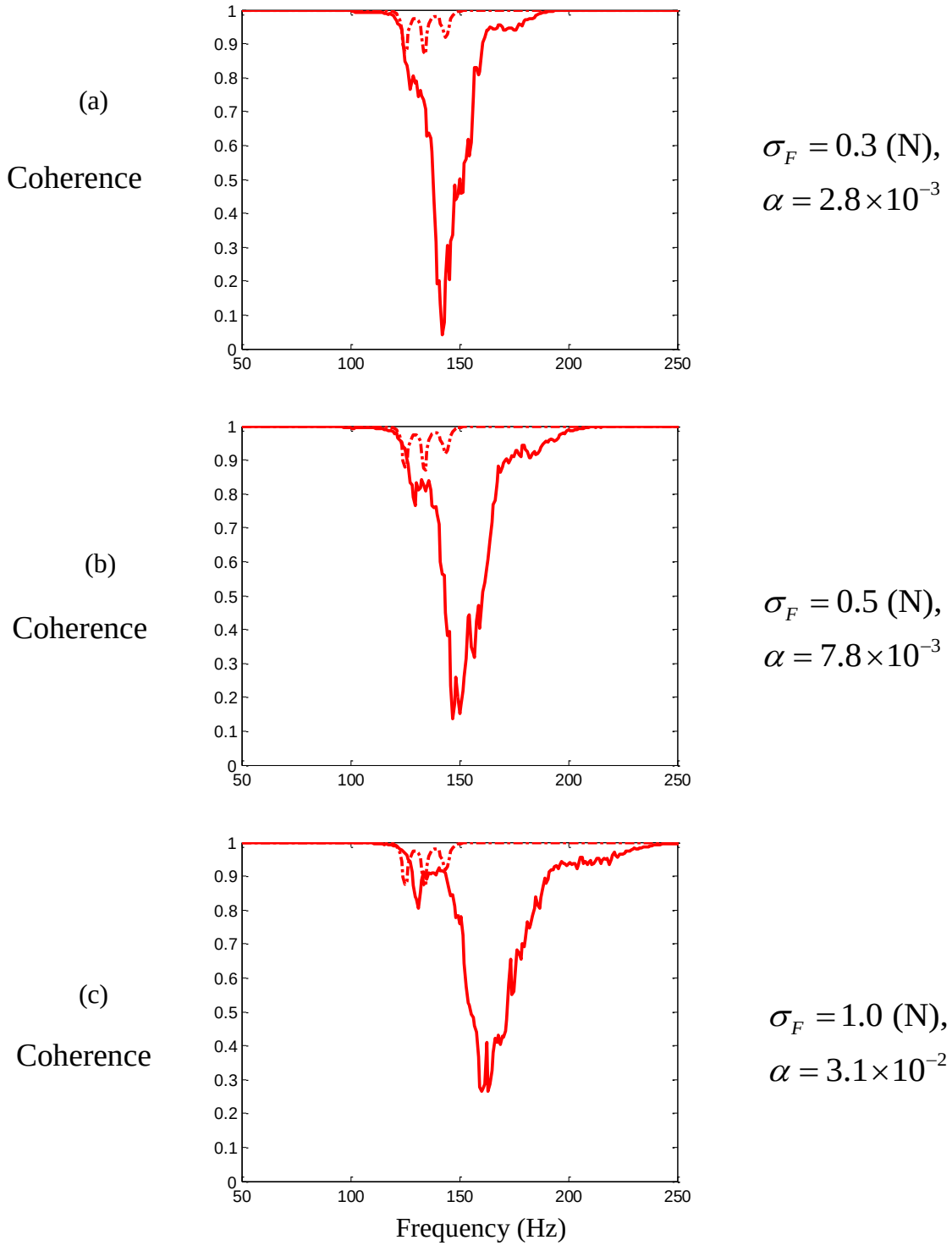

Figure 4.16 The effect of the input force amplitude on the primary system displacement and the coherence of the frequency response. (The 'tuned' frequency $\omega_1/\omega_s = 1$, mass ratio $\mu = 0.02$ and damping $\zeta_s = 0.01$, $\zeta = 0.008$). The response for the system with the linear absorber is given by the dashed-dotted line, the solid line is the nonlinear absorber. (a) $\sigma_F = 0.3$ (N), (b) $\sigma_F = 0.5$ (N) and (c) $\sigma_F = 1.0$ (N).

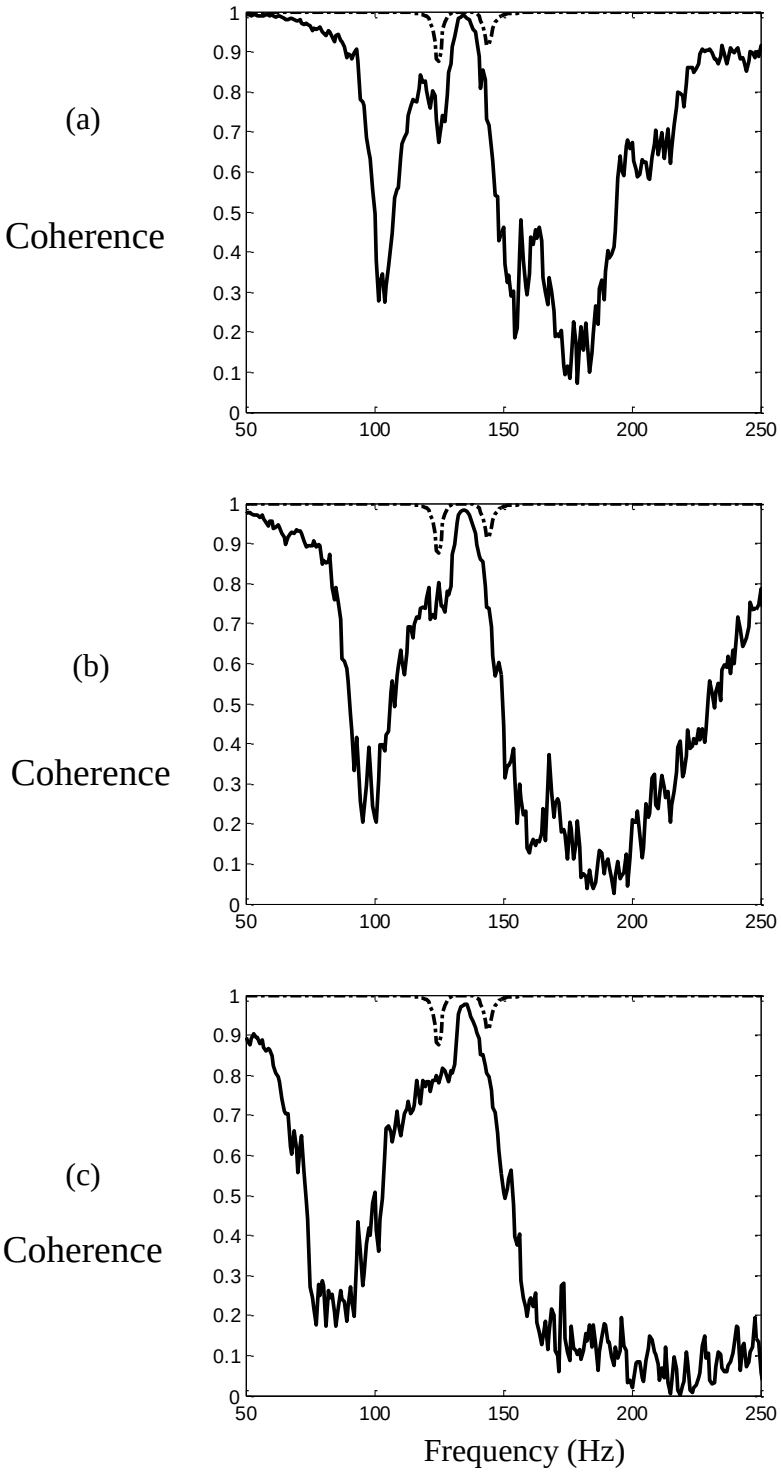

Figure 4.17 The effect of the input force amplitude on the secondary system (absorber) displacement and the coherence of the frequency response. (The 'tuned' frequency $\omega_1/\omega_s = 1$, mass ratio $\mu = 0.02$ and damping $\zeta_s = 0.01$, $\zeta = 0.008$). The response for the system with the linear absorber is given by the dashed-dotted line, the solid line is the nonlinear absorber. (a) $\sigma_F = 0.3$ (N), (b) $\sigma_F = 0.5$ (N) and (c) $\sigma_F = 1.0$ (N).

4.4 The effect of the nonlinear stiffness parameter (α)

In this section the mass ratio for the nonlinear absorber to the primary system is μ=0.02, the linear tuned frequency is $\omega_0 = 1$ and the damping ratios for the primary system and the nonlinear absorber are $\zeta_s = 0.01$ and $\zeta = 0.008$, respectively. The primary and secondary system parameters are set to m_s=1.26×10^{-1} (kg), c_s=2.12 ($\mathrm{N\cdot s/m}$), k_s=8.93×10^{4} $(\mathrm{N/m})$, m=2.52×10^{-3} (kg), c=3.4×10^{-2} ($\mathrm{N\cdot s/m}$) and k_1=1.79×10^{3} $(\mathrm{N/m})$, respectively. Variations of the nonlinear stiffness parameter (α) have been investigated and a summary of the response statistics presented in Tables 4.4-5. The displacement response of the primary and secondary system show the nonlinear behaviour of the system resulted in a kurtosis value less than 3. The mean square displacement of the primary system without absorber $\psi_{x_0}^2$ is evaluated by numerical simulation as 1.42×10^{-9} (m^2). In Table 4.4 and Figure 4.18(a), for a low nonlinear stiffness parameter $\alpha \le 7.8\times10^{-5}$, the nonlinear absorber produces the same mean square primary system displacement compared to the linear absorber. For high nonlinear absorber stiffness, the nonlinear absorber produces a higher mean square primary system displacement compared to the linear absorber case. In addition, for high nonlinear absorber stiffness, the primary system displacement PSD of the nonlinear absorber is much higher compared to the linear case at the first mode, as shown in Figure 4.19. The cumulative mean square displacement of the primary system when using the nonlinear absorber also shows much higher responses compared to using a linear absorber in Figure 4.21. In Table 4.5 and Figure 4.18(b), the mean square secondary system (absorber mass) displacement for the nonlinear absorber mass is lower than in the case of the linear absorber. This again appears to be a detrimental effect for increased values for the nonlinear stiffness in the absorber.

nonlinear parameter		Nonlinear absorber				
α	$k_3\ \left(\mathrm{N/m^3}\right)$	$\mu_{x_s}\ (m)$	$\psi^2_{x_s}\ (m^2)$	ι_{x_s}	κ_{x_s}	Nondimensional response $\psi^2_{y_s}$
0 (linear case)	0	5.1×10^{-10}	8.0×10^{-10}	-1.2×10^{-3}	3	0.56
7.8×10^{-5}	8.93×10^{7}	4.3×10^{-10}	8.0×10^{-10}	-1.5×10^{-3}	3	0.57
3.9×10^{-4}	4.47×10^{8}	1.7×10^{-10}	8.2×10^{-10}	-2.1×10^{-3}	3.1	0.58
7.8×10^{-4}	8.93×10^{8}	-2.2×10^{-10}	8.4×10^{-10}	-2.4×10^{-3}	3.1	0.59
3.9×10^{-3}	4.47×10^{9}	-3.5×10^{-10}	1.0×10^{-9}	-5.4×10^{-4}	3.1	0.73
7.8×10^{-3}	8.93×10^{9}	-1.5×10^{-10}	1.1×10^{-9}	4.4×10^{-4}	3.1	0.80
3.9×10^{-2}	4.47×10^{10}	1.8×10^{-10}	1.3×10^{-9}	-2.5×10^{-4}	3.2	0.91
7.8×10^{-2}	8.93×10^{10}	7.9×10^{-11}	1.3×10^{-9}	2.1×10^{-4}	3.1	0.94
3.9×10^{-1}	4.47×10^{11}	-4.8×10^{-10}	1.4×10^{-9}	5.6×10^{-4}	3	0.98
7.8×10^{-1}	8.93×10^{11}	-6.0×10^{-10}	1.4×10^{-9}	5.2×10^{-5}	3	0.98

Table 4.4 The effect of the nonlinear stiffness parameter on the mean, mean square, skewness and kurtosis of the displacement response of the primary system. The random input rms force amplitude is 0.5 N. The mean square displacement of the primary system without absorber is $1.42\times10^{-9}\ m^2$. ($\omega_0 = 1$, mass ratio $\mu = 0.02$ and damping $\zeta_s = 0.01$ and $\zeta = 0.008$), where $\alpha = k_3 x_0^2 / k_s \mu$.

nonlinear parameter		Nonlinear absorber				
α	$k_3\ \left(\mathrm{N/m^3}\right)$	$\mu_x\ (m)$	$\psi^2_x\ (m^2)$	ι_{x_s}	κ_{x_s}	Nondimensional response ψ^2_y
0 (linear case)	0	-6.1×10^{-10}	4.0×10^{-8}	2.3×10^{-5}	3	28.5
7.8×10^{-5}	8.93×10^{7}	-1.3×10^{-9}	4.0×10^{-8}	4.9×10^{-5}	3	28.5
3.9×10^{-4}	4.47×10^{8}	9×10^{-11}	4.0×10^{-8}	4.6×10^{-5}	3	27.9
7.8×10^{-4}	8.93×10^{8}	5.3×10^{-9}	3.9×10^{-8}	5.1×10^{-5}	2.9	27.0
3.9×10^{-3}	4.47×10^{9}	2.9×10^{-9}	3.2×10^{-8}	2.9×10^{-4}	2.6	22.3
7.8×10^{-3}	8.93×10^{9}	7.2×10^{-9}	2.6×10^{-8}	9.0×10^{-5}	2.5	18.5
3.9×10^{-2}	4.47×10^{10}	6.3×10^{-9}	1.4×10^{-8}	-5.3×10^{-4}	2.4	9.93
7.8×10^{-2}	8.93×10^{10}	-3.4×10^{-9}	1.1×10^{-8}	1.8×10^{-4}	2.4	7.39
3.9×10^{-1}	4.47×10^{11}	1.6×10^{-8}	5.5×10^{-9}	-3.2×10^{-3}	2.5	3.87
7.8×10^{-1}	8.93×10^{11}	3.9×10^{-8}	4.4×10^{-9}	-2.6×10^{-3}	2.6	3.11

Table 4.5 The effect of the nonlinear stiffness parameter on the mean, mean square, skewness and kurtosis of the displacement response of the secondary system (absorber mass). The random input rms force amplitude is 0.5 N. The mean square displacement of the primary system without absorber is $1.42\times10^{-9}\ m^2$. ($\omega_0 = 1$, mass ratio $\mu = 0.02$ and damping $\zeta_s = 0.01$ and $\zeta = 0.008$), where $\alpha = k_3 x_0^2 / k_s \mu$.

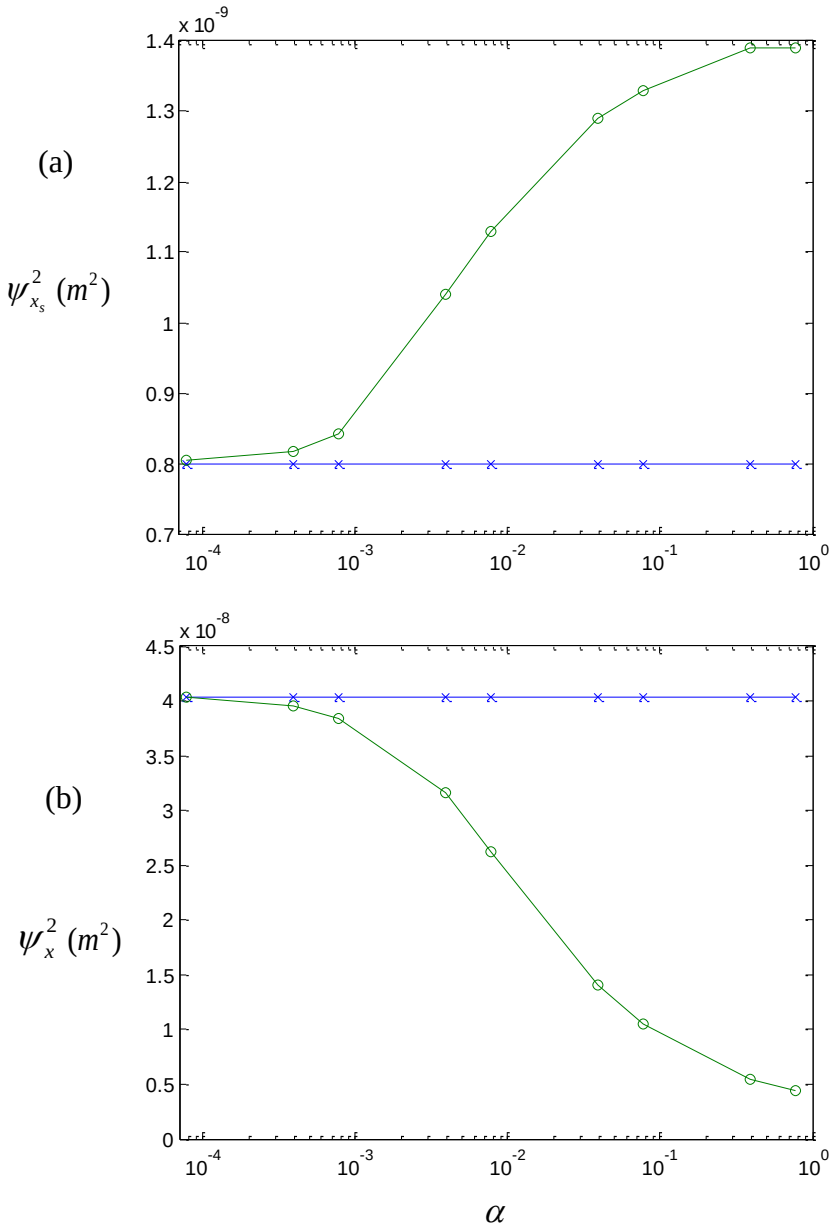

Figure 4.18 The effect of the nonlinear stiffness α on the (a) primary and (b) absorber system mean square displacement response. The random input rms force amplitude is 0.5 N. Nonlinear absorber ('o') and linear absorber ('×'). ($\omega_0 = 1$, mass ratio $\mu = 0.02$ and damping $\zeta_s = 0.01$ and $\zeta = 0.008$), where $\alpha = k_3 x_0^2 / k_s \mu$.

The effect of the nonlinear stiffness parameter on the primary and secondary system displacement response PSD versus excitation frequency is illustrated in Figures 4.19-20, where the nonlinear absorber stiffness parameter is increased from $\alpha = 7.8 \times 10^{-4}$ to $\alpha = 7.8 \times 10^{-2}$. For high nonlinear absorber stiffness, the nonlinear absorber produces a higher displacement response PSD in the primary system in the first mode compared to the linear absorber case seen in Figure 4.19. The cumulative displacement of the primary system using the nonlinear absorber is higher than the linear absorber, see Figure 4.21. The nonlinear absorber also produces a broader PSD for the primary and secondary system responses at the second mode and produces a vibration response at higher frequencies. It shows the nonlinear effect compared to the linear absorber case. For higher nonlinear stiffness, the second mode of the primary system does not obviously exhibit a resonance or peak response compared to the lower nonlinear stiffness case. These findings are similar to the vibration response for different input force amplitudes. In Figure 4.20 the effect on the increased nonlinearity on the absorber system mass displacement response PSD is to reduce it in the frequency region around the first mode. The cumulative displacement secondary system using the nonlinear absorber is lower than using the linear absorber in Figure 4.22.

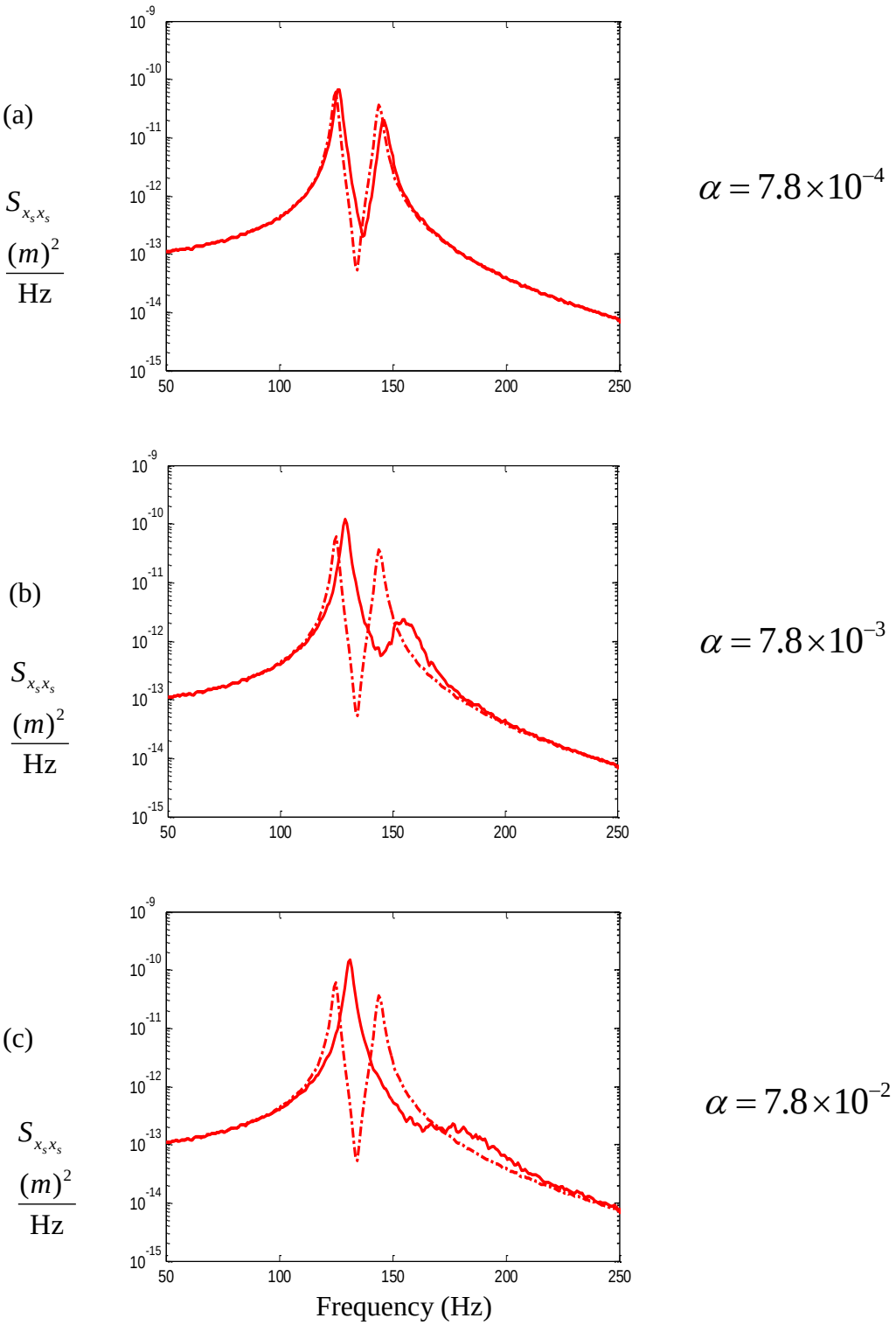

Figure 4.19 The effect of the nonlinear absorber stiffness on the primary system displacement PSD. The random input rms force amplitude is 0.5 N. (The 'tuned' frequency $\omega_1/\omega_s = 1$, mass ratio $\mu = 0.02$ and damping $\zeta_s = 0.01$, $\zeta = 0.008$). The response for the system with the linear absorber is given by the dashed-dotted line, the solid line is the nonlinear absorber. (a) $\alpha = 7.8\times10^{-4}$, (b) $\alpha = 7.8\times10^{-3}$ and (c) $\alpha = 7.8\times10^{-2}$, where $\alpha = k_3 x_0^2/k_s\mu$.

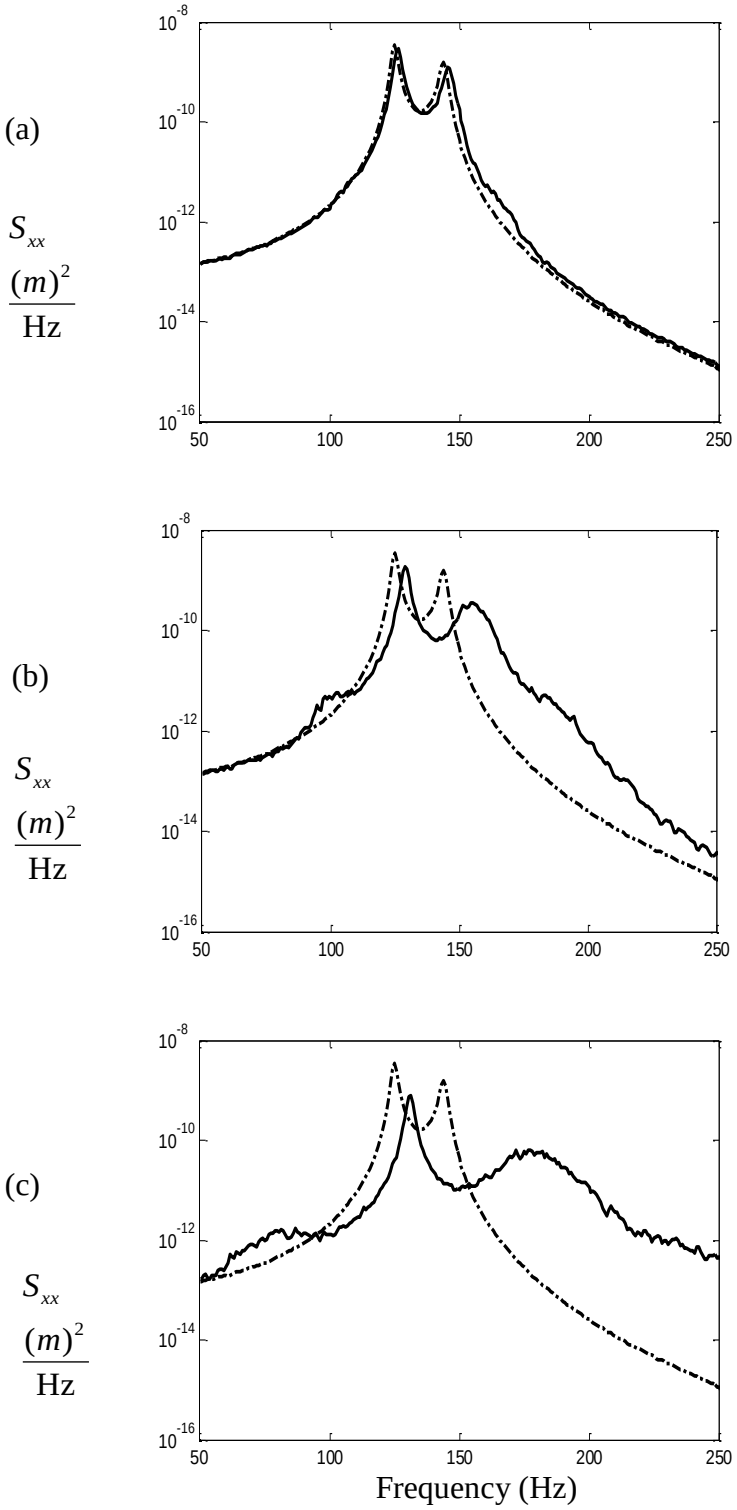

Figure 4.20 The effect of the nonlinear absorber stiffness on the secondary system displacement PSD. The random input rms force amplitude is 0.5 N. (The 'tuned' frequency $\omega_1/\omega_s = 1$, mass ratio $\mu = 0.02$ and damping $\zeta_s = 0.01$, $\zeta = 0.008$). The response for the system with the linear absorber is given by the dashed-dotted line, the solid line is the nonlinear absorber. (a) $\alpha = 7.8\times10^{-4}$, (b) $\alpha = 7.8\times10^{-3}$ and (c) $\alpha = 7.8\times10^{-2}$, where $\alpha = k_3 x_0^2/k_s\mu$.

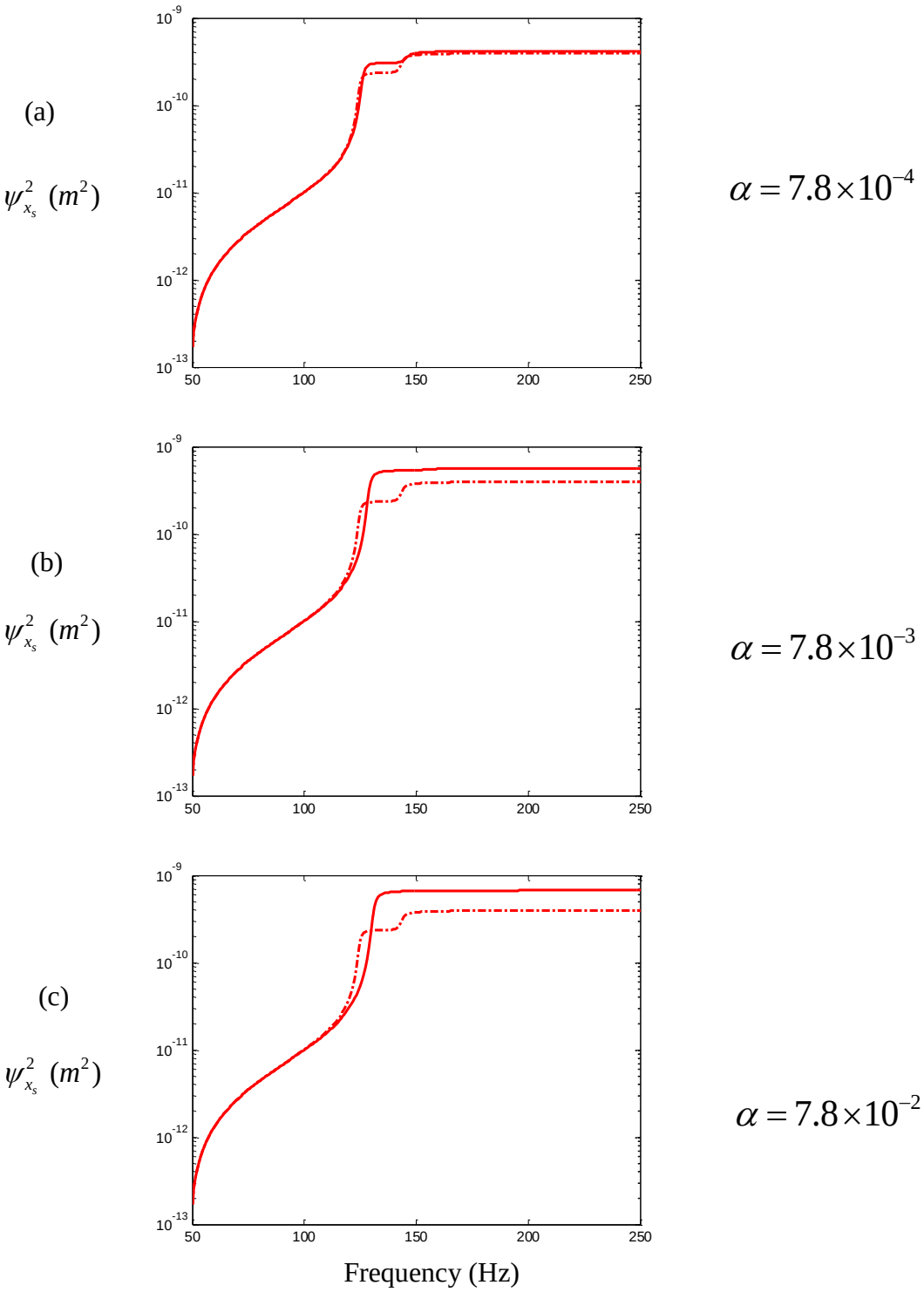

Figure 4.21 The effect of the nonlinear absorber stiffness on the primary system cumulative mean square displacement. The random input rms force amplitude is 0.5 N. (The 'tuned' frequency $\omega_1/\omega_s = 1$, mass ratio $\mu = 0.02$ and damping $\zeta_s = 0.01$, $\zeta = 0.008$). The response for the system with the linear absorber is given by the dashed-dotted line, the solid line is the nonlinear absorber. (a) $\alpha = 7.8\times10^{-4}$, (b) $\alpha = 7.8\times10^{-3}$ and (c) $\alpha = 7.8\times10^{-2}$, where $\alpha = k_3 x_0^2/k_s\mu$.

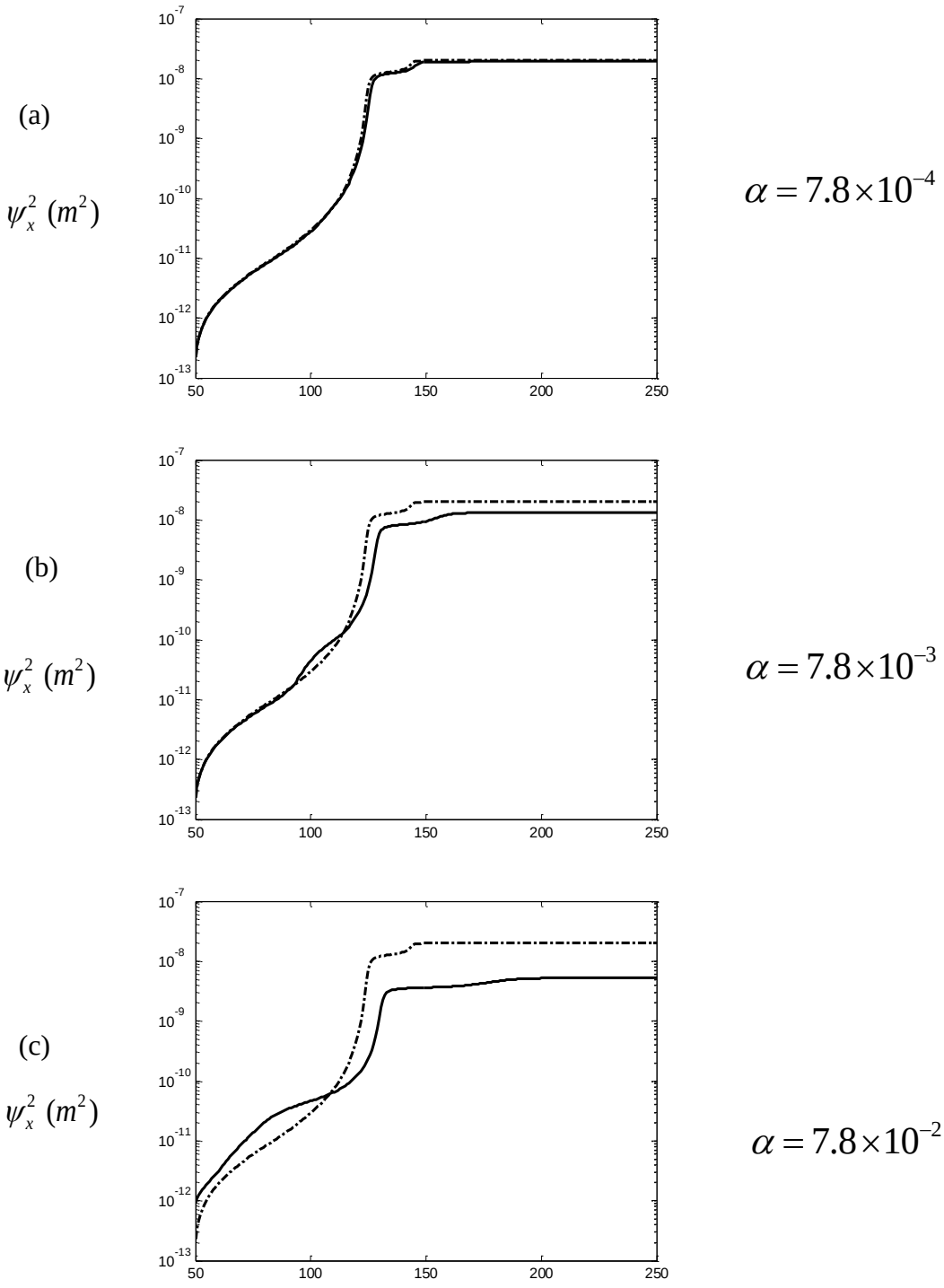

Figure 4.22 The effect of the nonlinear absorber stiffness on the secondary system cumulative mean square displacement. The random input rms force amplitude is 0.5 N. (The 'tuned' frequency $\omega_1/\omega_s = 1$, mass ratio $\mu = 0.02$ and damping $\zeta_s = 0.01$, $\zeta = 0.008$). The response for the system with the linear absorber is given by the dashed-dotted line, the solid line is the nonlinear absorber. (a) $\alpha = 7.8\times10^{-4}$, (b) $\alpha = 7.8\times10^{-3}$ and (c) $\alpha = 7.8\times10^{-2}$, where $\alpha = k_3 x_0^2/k_s\mu$.

4.5 The effect of the level of damping (ζ) in the nonlinear absorber

The non-dimensional system parameters where chosen with the mass ratio for the nonlinear vibration absorber to the primary system low, e.g. μ=0.02, the nonlinear stiffness parameter $\alpha = 7.8\times10^{-3}$, the linear tuned frequency $\omega_0 = 1$ and a damping ratio for the primary system $\zeta_s = 0.01$. The corresponding physical parameters of the primary and secondary system are set to m_s=1.26×10^{-1} (kg), c_s=2.12 ($\mathrm{N\cdot s/m}$), k_s=8.93×10^{4} ($\mathrm{N/m}$), m=2.52×10^{-3} (kg), k_1=1.79×10^{3} ($\mathrm{N/m}$) and k_3=8.93×10^{9} ($\mathrm{N/m^3}$), respectively. It is useful to consider the response sensitivity to the level of absorber damping given by the value of the parameter ζ.

In Table 4.6, the difference seen between the vibration response due to the linear and the nonlinear absorber is that the nonlinear absorber produces a higher mean square primary system displacement. On increasing the absorber damping, the primary system has a higher mean square displacement with a nonlinear absorber attached compared to the linear absorber case, as plotted in Figure 4.23(a). In Table 4.7 and Figure 4.23(b), the mean square displacement of the secondary system for the nonlinear absorber remains lower for all damping values considered in the nonlinear absorber compared to the linear absorber case.

Damping		Linear absorber				
ζ	c (N·s/m)	μ_{x_s} (m)	$\psi^2_{x_s}$ (m^2)	ι_{x_s}	κ_{x_s}	Nondimensional response $\psi^2_{y_s}$
0.002	8.49×10^{-3}	1.5×10^{-10}	1.2×10^{-9}	-9.0×10^{-4}	3	0.85
0.004	1.70×10^{-2}	5.9×10^{-10}	1.0×10^{-9}	-9.0×10^{-4}	3	0.70
0.005	2.12×10^{-2}	5.5×10^{-10}	9.5×10^{-10}	-1.0×10^{-3}	3	0.67
0.008	3.40×10^{-2}	5.1×10^{-10}	8.0×10^{-10}	-1.2×10^{-3}	3	0.56
0.012	5.09×10^{-2}	7.6×10^{-10}	6.6×10^{-10}	-1.4×10^{-3}	3	0.47
0.016	6.79×10^{-2}	5.9×10^{-10}	5.7×10^{-10}	-1.6×10^{-3}	3	0.40
0.020	8.49×10^{-2}	1.2×10^{-10}	5.1×10^{-10}	-1.7×10^{-3}	3	0.36
0.024	1.02×10^{-1}	-1.1×10^{-10}	4.6×10^{-10}	-2.1×10^{-3}	3	0.32
0.028	1.19×10^{-1}	7.4×10^{-11}	4.3×10^{-10}	-2.1×10^{-3}	3	0.30
0.032	1.36×10^{-1}	-1.2×10^{-10}	4.0×10^{-10}	-2.4×10^{-3}	3	0.28
Damping		Nonlinear absorber				
ζ	c (N·s/m)	μ_{x_s} (m)	$\psi^2_{x_s}$ (m^2)	ι_{x_s}	κ_{x_s}	Nondimensional response $\psi^2_{y_s}$
0.002	8.49×10^{-3}	3.2×10^{-10}	1.4×10^{-9}	1.6×10^{-4}	3.1	0.99
0.004	1.70×10^{-2}	-9.0×10^{-12}	1.3×10^{-9}	3.6×10^{-4}	3.1	0.92
0.005	2.12×10^{-2}	-2.4×10^{-10}	1.2×10^{-9}	4.3×10^{-4}	3.2	0.85
0.008	3.40×10^{-2}	-1.5×10^{-10}	1.1×10^{-9}	4.4×10^{-4}	3.1	0.78
0.012	5.09×10^{-2}	-1.8×10^{-10}	1.0×10^{-9}	3.5×10^{-4}	3.2	0.70
0.016	6.79×10^{-2}	2.6×10^{-10}	9.2×10^{-10}	1.9×10^{-5}	3.3	0.65
0.020	8.49×10^{-2}	1.6×10^{-10}	8.3×10^{-10}	-4.2×10^{-4}	3.4	0.59
0.024	1.02×10^{-1}	-5.3×10^{-10}	7.6×10^{-10}	-7.0×10^{-4}	3.4	0.54
0.028	1.19×10^{-1}	-4.6×10^{-10}	7.0×10^{-10}	-9.1×10^{-4}	3.4	0.49
0.032	1.36×10^{-1}	-1.3×10^{-10}	6.5×10^{-10}	-1.1×10^{-3}	3.4	0.46

Table 4.6 The effect of the damping on the mean, mean square, skewness and kurtosis of the displacement response of the primary system. The random input rms force amplitude is 0.5 N. The mean square displacement of the primary system without absorber is $1.56\times10^{-9}\ m^2$. ($\omega_0 = 1$, nonlinear absorber stiffness $\alpha = 7.8\times10^{-3}$, mass ratio $\mu = 0.02$ and damping $\zeta_s = 0.01$).

Damping		Linear absorber				
ζ	c (N·s/m)	$\mu_x\ (m)$	$\psi_x^2\ (m^2)$	ι_{x_s}	κ_{x_s}	Nondimensional response ψ_y^2
0.002	8.49×10^{-3}	-3.2×10^{-9}	6.1×10^{-8}	7.5×10^{-5}	3	43.0
0.004	1.70×10^{-2}	-1.9×10^{-9}	5.2×10^{-8}	7.8×10^{-5}	3	36.6
0.005	2.12×10^{-2}	-2.2×10^{-9}	4.9×10^{-8}	7.8×10^{-5}	3	34.5
0.008	3.40×10^{-2}	-6.1×10^{-10}	4.0×10^{-8}	2.3×10^{-5}	3	28.2
0.012	5.09×10^{-2}	-1.2×10^{-10}	3.3×10^{-8}	5.2×10^{-6}	3	23.2
0.016	6.79×10^{-2}	1.6×10^{-9}	2.8×10^{-8}	8.9×10^{-6}	3.1	19.7
0.02	8.49×10^{-2}	1.5×10^{-9}	2.4×10^{-8}	-1.2×10^{-5}	3.1	16.9
0.024	1.02×10^{-1}	1.8×10^{-9}	2.1×10^{-8}	-3.1×10^{-5}	3.1	14.8
0.028	1.19×10^{-1}	1.6×10^{-9}	1.9×10^{-8}	-1.0×10^{-5}	3.1	13.4
0.032	1.36×10^{-1}	8.1×10^{-9}	1.7×10^{-8}	-1.7×10^{-5}	3.1	12.0
Damping		Nonlinear absorber				
ζ	c (N·s/m)	$\mu_x\ (m)$	$\psi_x^2\ (m^2)$	ι_x	κ_x	Nondimensional response ψ_y^2
0.002	8.49×10^{-3}	-7.1×10^{-9}	3.5×10^{-8}	-5.3×10^{-4}	2.5	24.6
0.004	1.70×10^{-2}	3.6×10^{-9}	3.1×10^{-8}	2.6×10^{-4}	2.5	21.8
0.005	2.12×10^{-2}	1.9×10^{-9}	3.0×10^{-8}	2.4×10^{-5}	2.5	21.1
0.008	3.40×10^{-2}	7.2×10^{-9}	2.6×10^{-8}	9.0×10^{-5}	2.5	18.3
0.012	5.09×10^{-2}	4.6×10^{-10}	2.4×10^{-8}	2.3×10^{-4}	2.5	16.9
0.016	6.79×10^{-2}	2.6×10^{-9}	2.2×10^{-8}	-3.5×10^{-4}	2.5	15.5
0.02	8.49×10^{-2}	2.7×10^{-9}	2.0×10^{-8}	-1.2×10^{-4}	2.6	14.1
0.024	1.02×10^{-1}	-1.2×10^{-9}	1.9×10^{-8}	-1.6×10^{-4}	2.6	13.4
0.028	1.19×10^{-1}	-8.6×10^{-10}	1.7×10^{-8}	1.9×10^{-5}	2.6	12.0
0.032	1.36×10^{-1}	1.8×10^{-9}	1.6×10^{-8}	1.4×10^{-4}	2.6	11.3

Table 4.7 The effect of the damping on the mean, mean square, skewness and kurtosis of the displacement response of the secondary system (absorber mass). The random input rms force amplitude is 0.5 N. The mean square displacement of the primary system without absorber is $1.56\times10^{-9}\ m^2$. ($\omega_0 = 1$, nonlinear absorber stiffness $\alpha = 7.8\times10^{-3}$, mass ratio $\mu = 0.02$ and damping $\zeta_s = 0.01$).

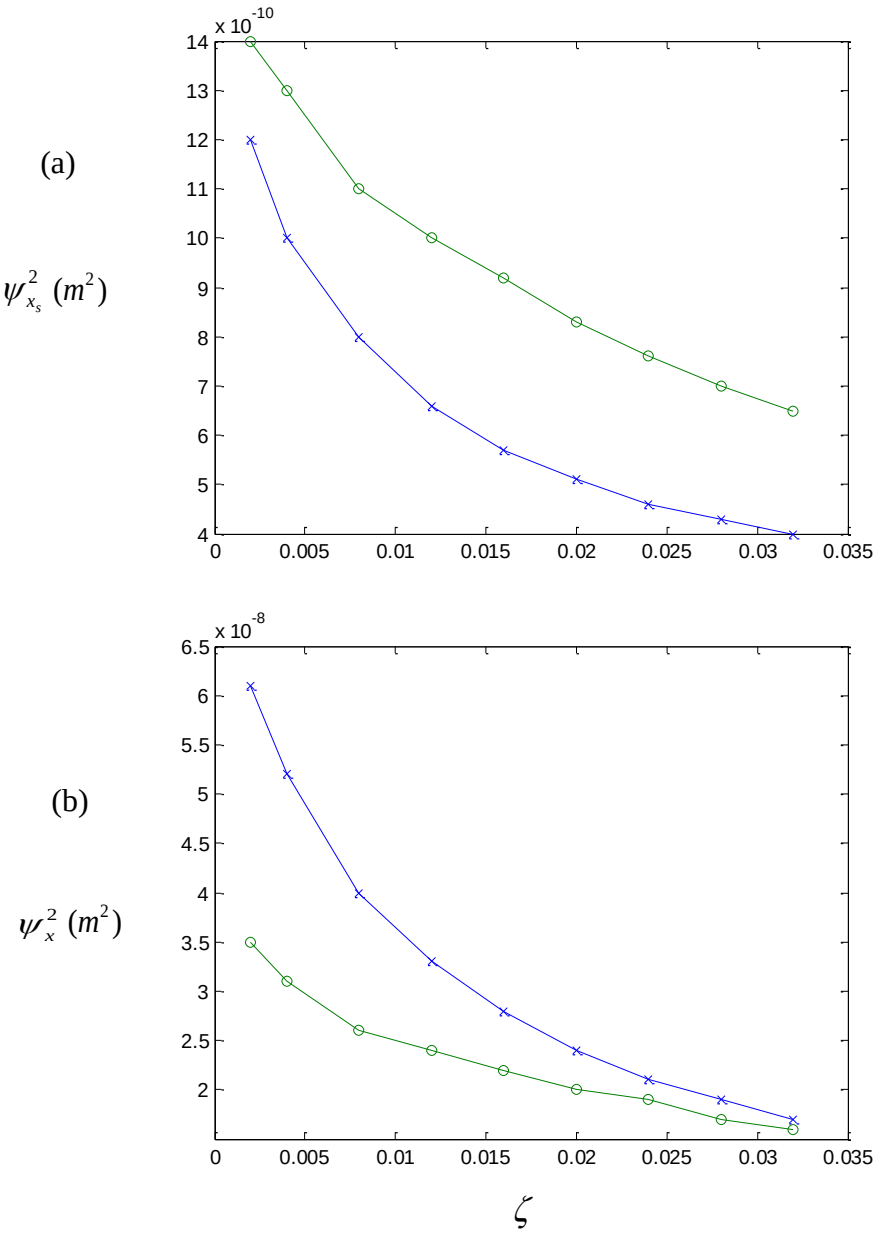

Figure 4.23 The effect of the nonlinear absorber damping ratio ζ on the (a) primary and (b) absorber system mean square displacement response. The random input rms force amplitude is 0.5 N. Nonlinear absorber ('o') and linear absorber ('×'). ($\omega_0 = 1$, nonlinear absorber stiffness $\alpha = 7.8\times10^{-3}$, mass ratio $\mu = 0.02$ and damping $\zeta_s = 0.01$).

In Figures 4.24-25, the effect of the absorber damping on the primary and secondary system displacement response PSD is considered when ζ is increased from $\zeta = 5\times10^{-3}$ to $\zeta = 2\times10^{-2}$. In Figure 4.24, the nonlinear absorber produced a higher primary system vibration response at the first mode compared to the linear absorber. The cumulative displacement of the primary system using the nonlinear absorber is also higher compared to the linear absorber case, as shown in Figure 4.26. The nonlinear absorber produces a broader PSD for both the primary and secondary system responses at the second mode and produces a vibration response at higher frequencies. It can be observed that a high value of damping in the nonlinear absorber produces a narrower PSD in the primary and secondary displacement response at the second mode and reduced vibration response at higher frequencies compared to less absorber damping. For higher damping, there is an apparent reduction in the peak response amplitude at the first and second modes for the linear absorber, but it does not appear to be the case for the nonlinear absorber at the first mode. The cumulative displacement of the absorber system mass of the nonlinear absorber is also lower than that producing using the linear absorber, as seen in Figure 4.27.

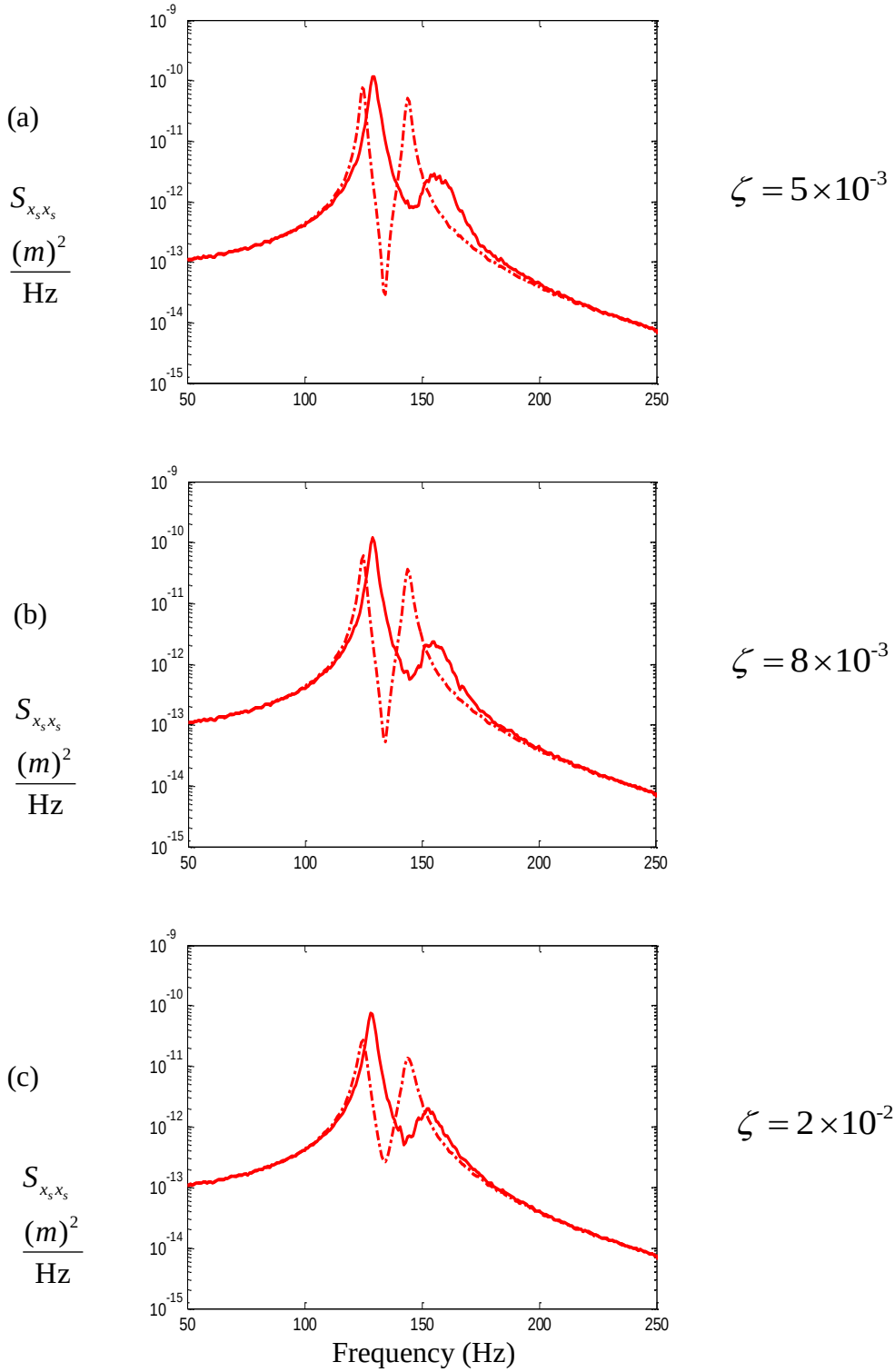

Figure 4.24 The effect of absorber damping on the primary system displacement PSD. The random input rms force amplitude is 0.5 N. (nonlinear parameter $\alpha = 7.8\times10^{-3}$, 'tuned' frequency $\omega_1/\omega_s = 1$, mass ratio $\mu = 0.02$ and damping $\zeta_s = 0.01$). The response for the system with the linear absorber is given by the dashed-dotted line, the solid line is the nonlinear absorber. (a) $\zeta = 5\times10^{-3}$, (b) $\zeta = 8\times10^{-3}$ and (c) $\zeta = 2\times10^{-2}$.

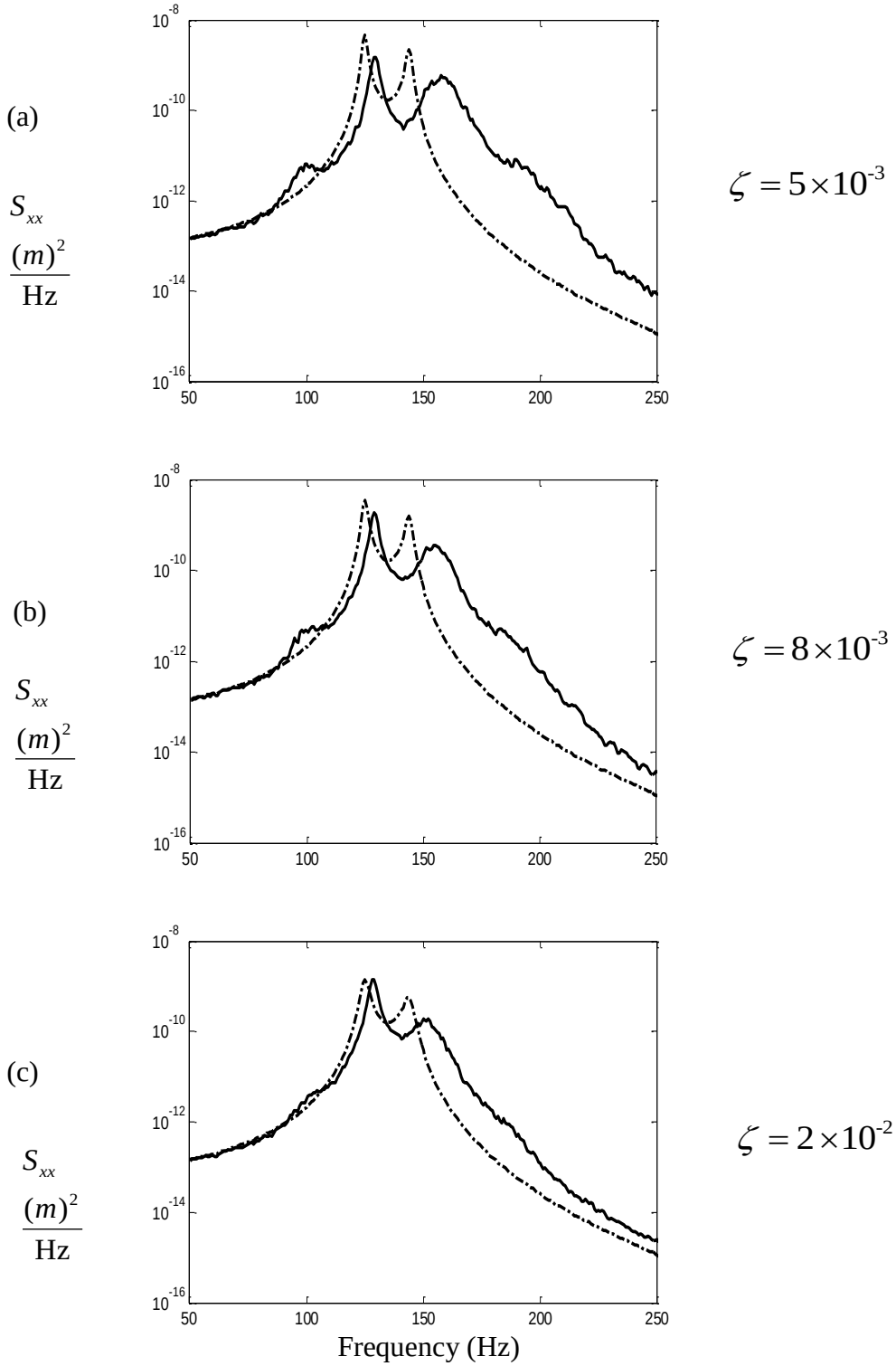

Figure 4.25 The effect of absorber damping on the secondary system displacement PSD. The random input rms force amplitude is 0.5 N. (nonlinear parameter $\alpha = 7.8\times10^{-3}$, 'tuned' frequency $\omega_1/\omega_s = 1$, mass ratio $\mu = 0.02$ and damping $\zeta_s = 0.01$). The response for the system with the linear absorber is given by the dashed-dotted line, the solid line is the nonlinear absorber. (a) $\zeta = 5\times10^{-3}$, (b) $\zeta = 8\times10^{-3}$ and (c) $\zeta = 2\times10^{-2}$.

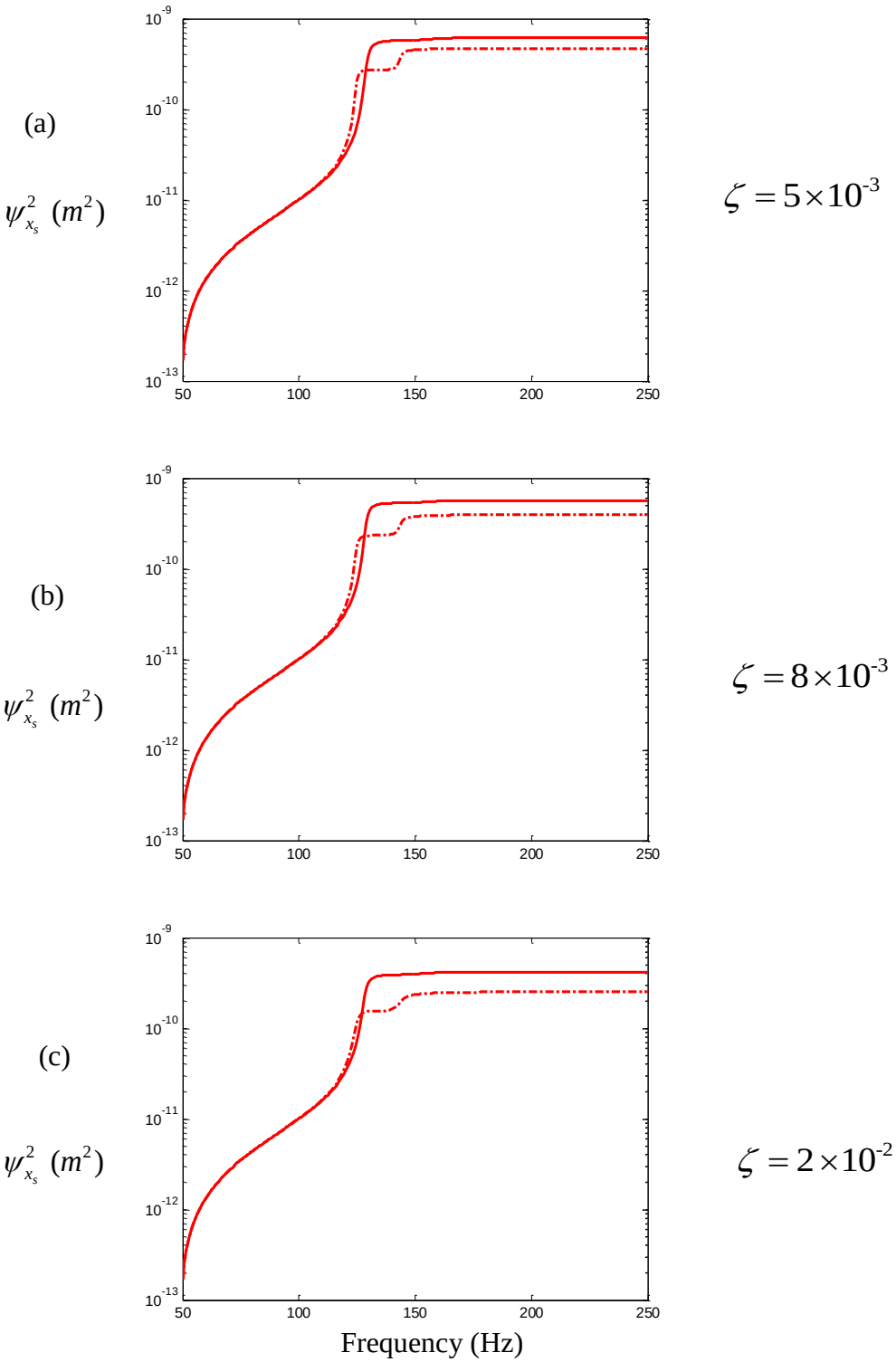

Figure 4.26 The effect of absorber damping on the primary system cumulative mean square displacement. The random input rms force amplitude is 0.5 N. (nonlinear parameter $\alpha = 7.8\times10^{-3}$, 'tuned' frequency $\omega_1/\omega_s = 1$, mass ratio $\mu = 0.02$ and damping $\zeta_s = 0.01$). The response for the system with the linear absorber is given by the dashed-dotted line, the solid line is the nonlinear absorber. (a) $\zeta = 5\times10^{-3}$, (b) $\zeta = 8\times10^{-3}$ and (c) $\zeta = 2\times10^{-2}$.

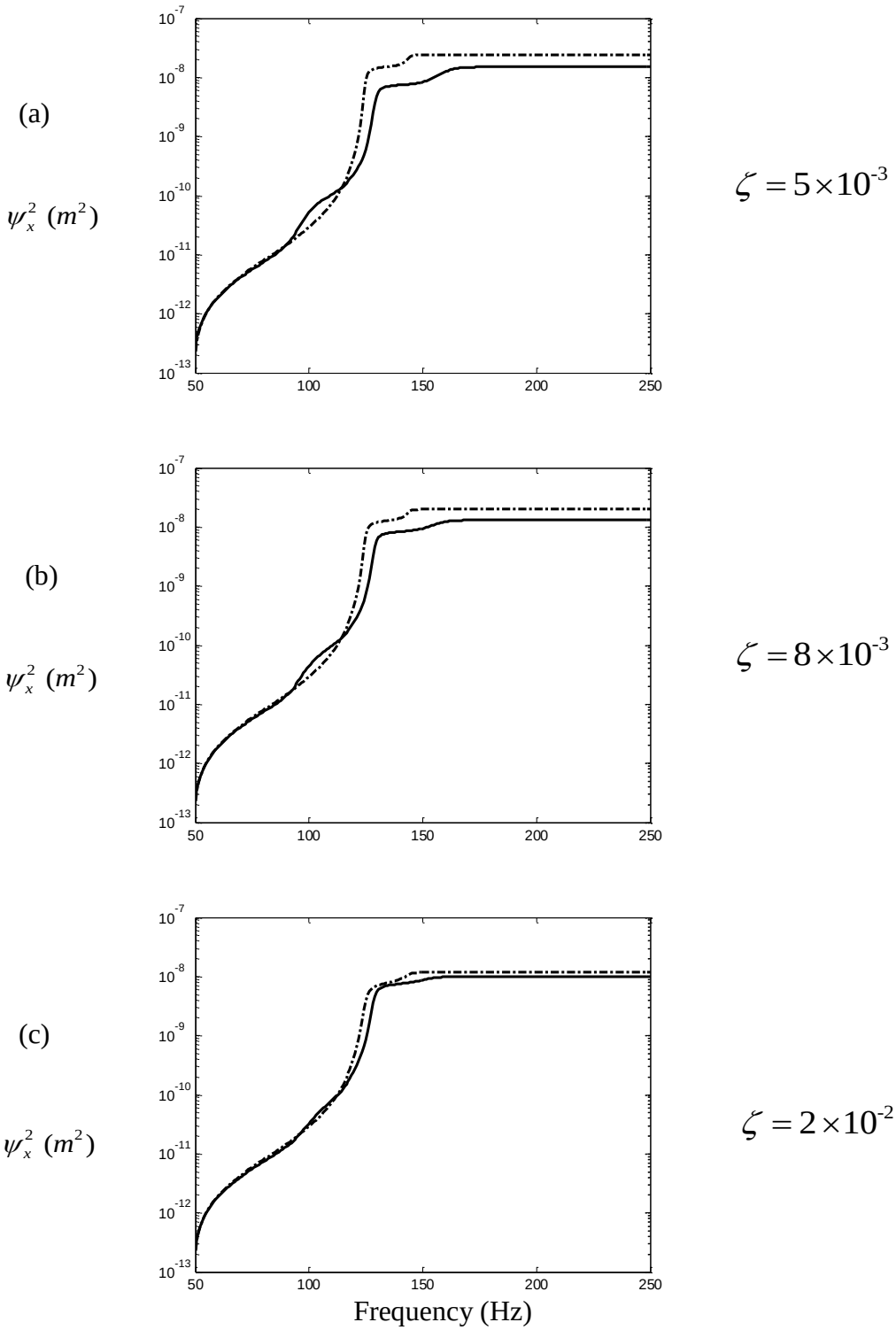

Figure 4.27 The effect of absorber damping on the secondary system cumulative mean square displacement. The random input rms force amplitude is 0.5 N. (nonlinear parameter $\alpha = 7.8\times10^{-3}$, 'tuned' frequency $\omega_1/\omega_s = 1$, mass ratio $\mu = 0.02$ and damping $\zeta_s = 0.01$). The response for the system with the linear absorber is given by the dashed-dotted line, the solid line is the nonlinear absorber. (a) $\zeta = 5\times10^{-3}$, (b) $\zeta = 8\times10^{-3}$ and (c) $\zeta = 2\times10^{-2}$.

4.6 The effect of the mass ratio (μ)

Numerical solutions have been obtained when the linear tuned frequency is set to $\omega_0 = 1$ and the damping ratios for the primary system and the absorber are $\zeta_s = 0.01$ and $\zeta = 0.008$ respectively. The primary system parameters are set to m_s=1.26×10^{-1} (kg) , c_s=2.12 $(\mathrm{N}\cdot\mathrm{s/m})$, k_s=8.93×10^{4} $(\mathrm{N/m})$, respectively. The secondary system parameter and non-dimensional parameters μ and α values are presented in Table 4.8. It is noted that the simulation results are obtained using dimensional parameters, the non-dimensional parameter μ will affect the nonlinear stiffness α which could be not kept constant. Numerical solutions have been simulated for variations in the mass ratio (μ) in Tables 4.9-10.

Consider the nonlinear absorber whose parameters are given in Table 4.8. On increasing the mass ratio, the mean square displacement of primary system using the nonlinear absorber will reduce as seen in Table 4.9 and Figure 4.28(a). A reason may be that as the absorber mass increases, the nonlinear stiffness α reduction in the level of the nonlinearity then occurs. However, the mean square primary system displacement using a linear absorber slightly increases.

In Table 4.9 and Figure 4.28(a), a difference between the vibration response using the linear and the nonlinear absorber is that the nonlinear absorber produces a higher mean square primary system displacement. On increasing the mass in the absorber, the primary system has a higher mean square displacement with a nonlinear absorber attached compared to the linear absorber. The cumulative displacement of the primary system using the nonlinear absorber is also higher than the linear absorber case, as seen in Figure 4.31. In Figure 4.28(b), as the mass ratio values between $0.01 \le \mu < 0.07$, the mean square displacement of the secondary system for the nonlinear absorber remains lower values compared to the linear absorber. For higher mass ratio values between $0.07 \le \mu \le 0.1$, the nonlinear absorber produces approximately the same mean square secondary system displacement compared to the linear absorber case.

Mass ratio	Nonlinear stiffness	absorber system			
μ	α	m (kg)	$c\ (\mathrm{N\cdot s/m})$	$k_1\ (\mathrm{N/m})$	$k_3\ (\mathrm{N/m^3})$
0.01	1.56×10^{-2}	1.26×10^{-3}	1.70×10^{-2}	8.93×10^{2}	8.93×10^{9}
0.02	7.80×10^{-3}	2.52×10^{-3}	3.40×10^{-2}	1.79×10^{3}	8.93×10^{9}
0.03	5.20×10^{-3}	3.78×10^{-3}	5.10×10^{-2}	2.68×10^{3}	8.93×10^{9}
0.04	3.90×10^{-3}	5.04×10^{-3}	6.79×10^{-2}	3.57×10^{3}	8.93×10^{9}
0.05	3.12×10^{-3}	6.30×10^{-3}	8.49×10^{-2}	4.47×10^{3}	8.93×10^{9}
0.06	2.60×10^{-3}	7.56×10^{-3}	1.02×10^{-1}	5.36×10^{3}	8.93×10^{9}
0.07	2.23×10^{-3}	8.82×10^{-3}	1.19×10^{-1}	6.25×10^{3}	8.93×10^{9}
0.08	1.95×10^{-3}	1.01×10^{-2}	1.36×10^{-1}	7.15×10^{3}	8.93×10^{9}
0.09	1.74×10^{-3}	1.13×10^{-2}	1.53×10^{-1}	8.04×10^{3}	8.93×10^{9}
0.1	1.56×10^{-3}	1.26×10^{-2}	1.70×10^{-1}	8.93×10^{3}	8.93×10^{9}

Table 4.8 The secondary system parameters are estimated for the model predictions. ($k_3 = 8.93\times10^{9}\ \left(\mathrm{N/m^3}\right)$).

Mass ratio	Linear absorber				
μ	$\mu_{x_s}\ (m)$	$\psi^2_{x_s}\ (m^2)$	ι_{x_s}	κ_{x_s}	Nondimensional response $\psi^2_{y_s}$
0.01	-1×10^{-9}	8×10^{-10}	-7×10^{-4}	3.1	0.57
0.02	5.1×10^{-10}	8×10^{-10}	-1.2×10^{-3}	3	0.56
0.03	-9.6×10^{-10}	8×10^{-10}	-1.2×10^{-4}	3.1	0.56
0.04	-2×10^{-9}	8×10^{-10}	1.5×10^{-4}	2.9	0.56
0.05	-2×10^{-10}	8×10^{-10}	1.6×10^{-3}	3	0.57
0.06	-6.1×10^{-10}	8×10^{-10}	2.2×10^{-3}	3	0.57
0.07	-1.9×10^{-10}	8.1×10^{-10}	-1×10^{-3}	3	0.57
0.08	2.2×10^{-10}	8.1×10^{-10}	-1.2×10^{-3}	3	0.57
0.09	-1.7×10^{-10}	8.1×10^{-10}	-2.9×10^{-3}	3.1	0.57
0.1	-7.7×10^{-10}	8.1×10^{-10}	-4.1×10^{-3}	3	0.57

Mass ratio	Nonlinear stiffness	Nonlinear absorber				
μ	α	$\mu_{x_s}\ (m)$	$\psi^2_{x_s}\ (m^2)$	ι_{x_s}	κ_{x_s}	Nondimensional response $\psi^2_{y_s}$
0.01	1.56×10^{-2}	-1.4×10^{-10}	1.3×10^{-9}	7.9×10^{-4}	3	0.90
0.02	7.80×10^{-3}	-1.5×10^{-10}	1.1×10^{-9}	4.4×10^{-4}	3.1	0.80
0.03	5.20×10^{-3}	3.4×10^{-9}	9.8×10^{-10}	-8.7×10^{-5}	3.3	0.69
0.04	3.90×10^{-3}	1.1×10^{-9}	8.9×10^{-10}	1.2×10^{-4}	3.1	0.63
0.05	3.12×10^{-3}	-1.7×10^{-9}	8.7×10^{-10}	3.2×10^{-4}	3.1	0.61
0.06	2.60×10^{-3}	-6.1×10^{-10}	8.4×10^{-10}	3.3×10^{-3}	3	0.60
0.07	2.23×10^{-3}	-2×10^{-10}	8.3×10^{-10}	2.4×10^{-3}	3	0.59
0.08	1.95×10^{-3}	-1.3×10^{-10}	8.2×10^{-10}	-8.2×10^{-4}	3.1	0.58
0.09	1.74×10^{-3}	-5×10^{-10}	8.2×10^{-10}	-2.2×10^{-3}	3.1	0.58
0.1	1.56×10^{-3}	-5×10^{-10}	8.3×10^{-10}	-4.9×10^{-3}	3	0.58

Table 4.9 The effect of the mass ratio on the mean, mean square, skewness and kurtosis of the displacement response of the primary system. The random input rms force amplitude is 0.5 N. The mean square displacement of the primary system without absorber is $1.42\times10^{-9}\ m^2$. ($\omega_0 = 1$ and damping $\zeta_s = 0.01$ and $\zeta = 0.008$).

Mass ratio	Linear absorber				
μ	$\mu_x\ (m)$	$\psi_x^2\ (m^2)$	ι_x	κ_x	Nondimensional response ψ_y^2
0.01	7.7×10^{-9}	7.8×10^{-8}	4.7×10^{-6}	3.1	54.9
0.02	-6.1×10^{-10}	4×10^{-8}	2.3×10^{-5}	3	28.5
0.03	2.5×10^{-9}	2.7×10^{-8}	5.9×10^{-5}	3.1	19.3
0.04	-4.3×10^{-9}	2.1×10^{-8}	3.9×10^{-5}	2.9	14.9
0.05	-2×10^{-9}	1.7×10^{-8}	-1.6×10^{-4}	2.9	12.2
0.06	-3.1×10^{-9}	1.5×10^{-8}	-2×10^{-4}	2.9	10.4
0.07	-1.5×10^{-9}	1.3×10^{-8}	1.5×10^{-4}	3	9.01
0.08	-1.9×10^{-9}	1.1×10^{-8}	2.1×10^{-4}	3	8.03
0.09	-1.4×10^{-9}	1×10^{-8}	5.6×10^{-4}	3	7.25
0.1	-1.2×10^{-9}	9.4×10^{-9}	7.7×10^{-4}	3	6.65

Mass ratio	Nonlinear stiffness	Nonlinear absorber				
μ	α	$\mu_x\ (m)$	$\psi_x^2\ (m^2)$	ι_x	κ_x	Nondimensional response ψ_y^2
0.01	1.56×10^{-2}	-7.1×10^{-9}	2.4×10^{-8}	-6.3×10^{-4}	2.4	16.5
0.02	7.80×10^{-3}	7.2×10^{-9}	2.6×10^{-8}	9×10^{-5}	2.5	18.5
0.03	5.20×10^{-3}	2.2×10^{-10}	2.3×10^{-8}	-1.5×10^{-3}	2.7	16.3
0.04	3.90×10^{-3}	3.2×10^{-9}	1.9×10^{-8}	1.8×10^{-4}	2.8	13.5
0.05	3.12×10^{-3}	-7×10^{-9}	1.7×10^{-8}	3.7×10^{-5}	2.8	11.6
0.06	2.60×10^{-3}	-1.1×10^{-9}	1.4×10^{-8}	-3.3×10^{-4}	2.9	10.1
0.07	2.23×10^{-3}	-2.9×10^{-9}	1.3×10^{-8}	-2.6×10^{-4}	2.9	8.87
0.08	1.95×10^{-3}	-3.7×10^{-10}	1.1×10^{-8}	3.6×10^{-5}	3	7.82
0.09	1.74×10^{-3}	-1.2×10^{-9}	1.0×10^{-8}	4.4×10^{-4}	3	7.18
0.1	1.56×10^{-3}	-2.4×10^{-9}	9.4×10^{-9}	8.5×10^{-4}	3	6.61

Table 4.10 The effect of the mass ratio on the mean, mean square, skewness and kurtosis of the displacement response of the secondary system (absorber mass). The random input rms force amplitude is 0.5 N. The mean square displacement of the primary system without absorber is $1.42\times10^{-9}\ m^2$. ($\omega_0 = 1$ and damping $\zeta_s = 0.01$ and $\zeta = 0.008$).

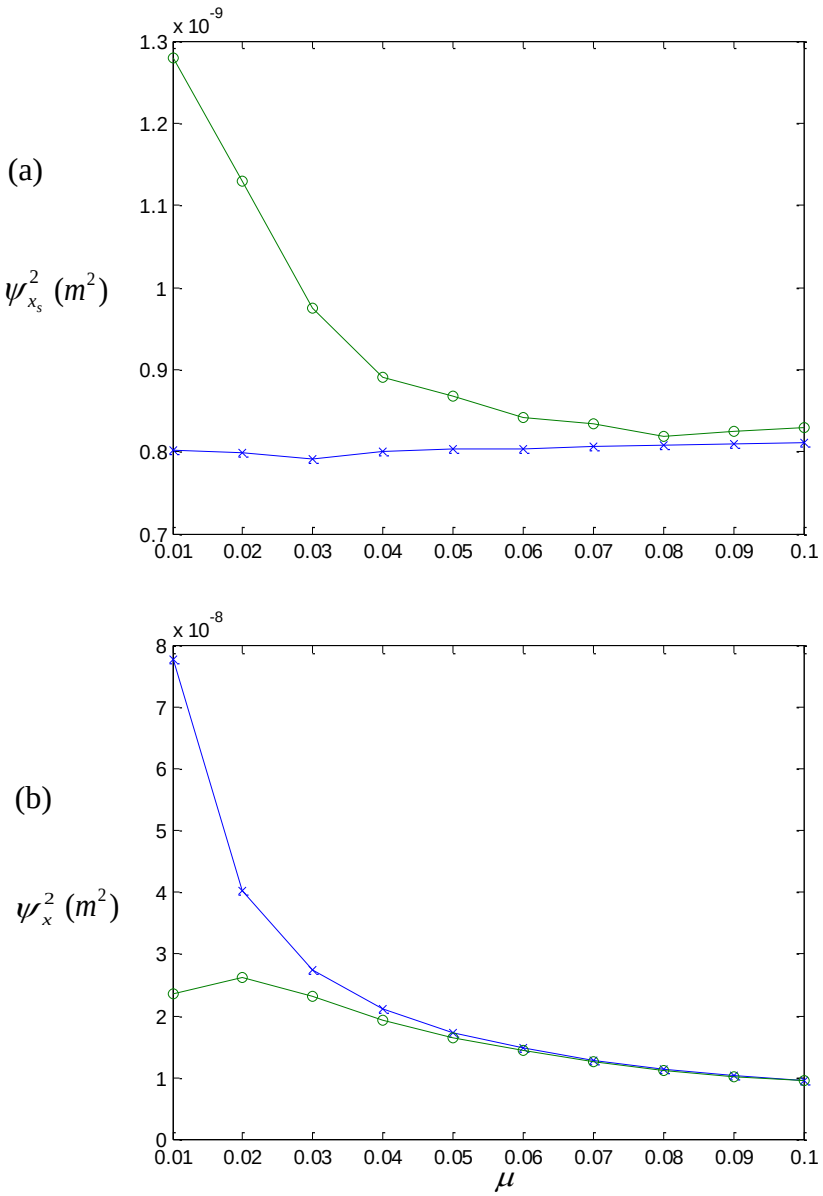

Figure 4.28 The effect of the mass ratio μ on the (a) primary and (b) absorber system mean square displacement response. The random input rms force amplitude is 0.5 N. Nonlinear absorber ('o') and linear absorber ('×'). ($\omega_0 = 1$ and damping $\zeta_s = 0.01$ and $\zeta = 0.008$).

The effect of the mass ratio on the primary and secondary system displacement PSD are presented in Figures 4.29-30, where the mass ratio is increased from $\mu = 0.02$ to $\mu = 0.1$. For higher absorber mass, the linear absorber produces a broader and well separated range for the first and second resonance peaks compared to less absorber mass. The higher mass in the absorber results in a slightly higher displacement primary system PSD compared to the less absorber mass at the second resonance peak in Figure 4.29. The cumulative displacement of the primary system for higher absorber mass is also higher as seen in Figure 4.31. This is in agreement with the mean square primary system displacement is shown in Figure 4.28(a). The nonlinear absorber produces a higher displacement PSD for the primary system at the first mode compared to a linear absorber when the mass ratios are in the range $\mu = 0.02$ to $\mu = 0.1$. The cumulative displacement of the primary system using the nonlinear absorber is also higher compared to the linear absorber case in Figure 4.31. It can be observed that higher values of the mass ratio of the nonlinear absorber produces a narrower PSD in the primary and secondary displacement response at the second mode and reduced vibration response at higher frequencies compared to less absorber mass.

In Figures 4.29(c), for high mass ratios e.g. $\mu = 0.1$, the nonlinear absorber for the given value of nonlinear stiffness starts to produce a similar response to the linear absorber. The reason for this could be possibly be because as the absorber mass m increases, then the nonlinear stiffness α as defined will reduce, i.e. less nonlinearity in the response results.

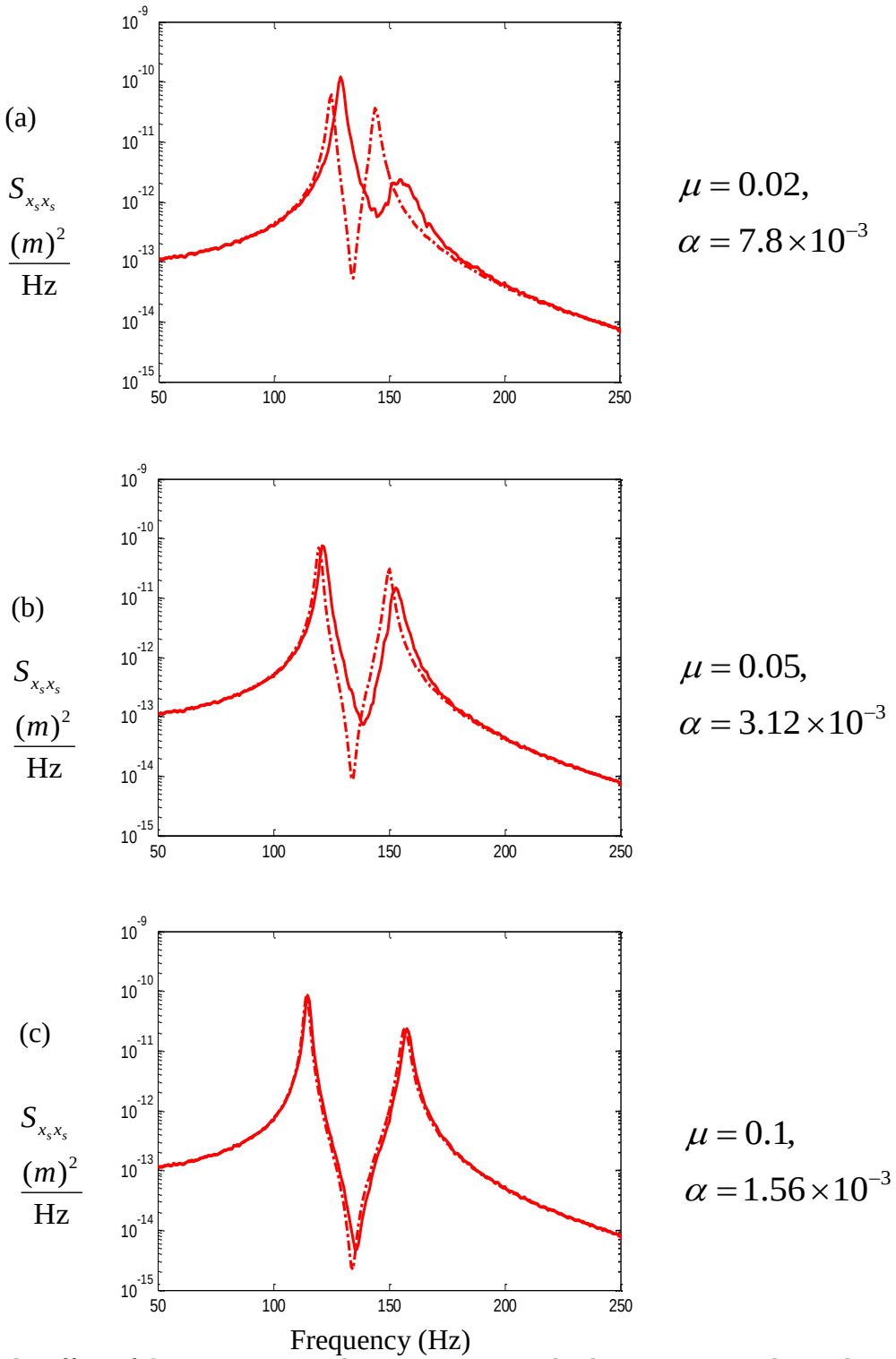

Figure 4.29 The effect of the mass ratio on the primary system displacement PSD. The random input rms force amplitude is 0.5 N. (The 'tuned' frequency $\omega_1/\omega_s = 1$ and damping $\zeta_s = 0.01$, $\zeta = 0.008$). The response for the system with the linear absorber is given by the dashed-dotted line, the solid line is the nonlinear absorber. (a) $\mu = 0.02$, (b) $\mu = 0.05$ and (c) $\mu = 0.1$.

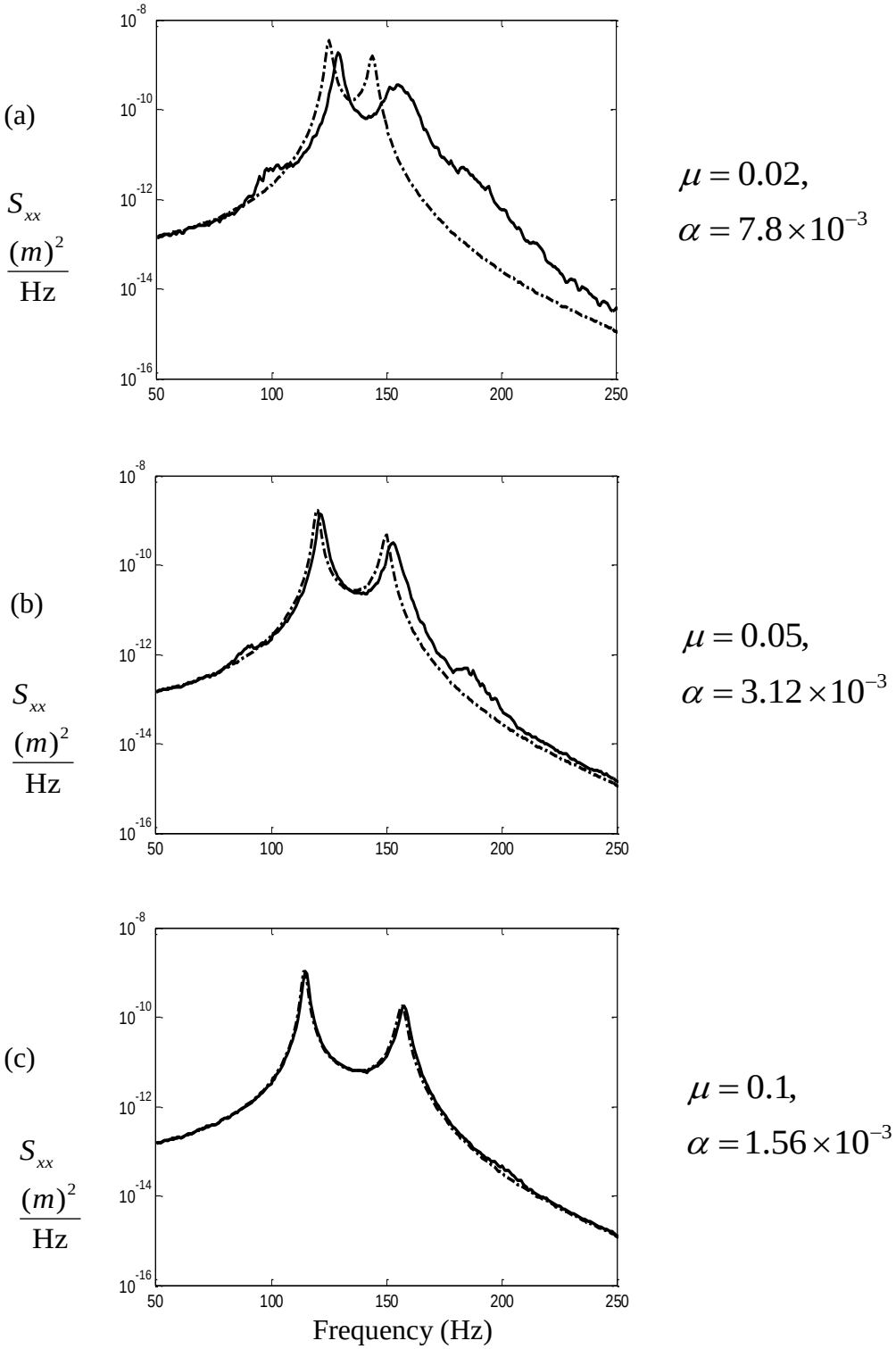

Figure 4.30 The effect of the mass ratio on the secondary system displacement PSD. The random input rms force amplitude is 0.5 N. (The 'tuned' frequency $\omega_1/\omega_s = 1$ and damping $\zeta_s = 0.01$, $\zeta = 0.008$). The response for the system with the linear absorber is given by the dashed-dotted line, the solid line is the nonlinear absorber. (a) $\mu = 0.02$, (b) $\mu = 0.05$ and (c) $\mu = 0.1$.

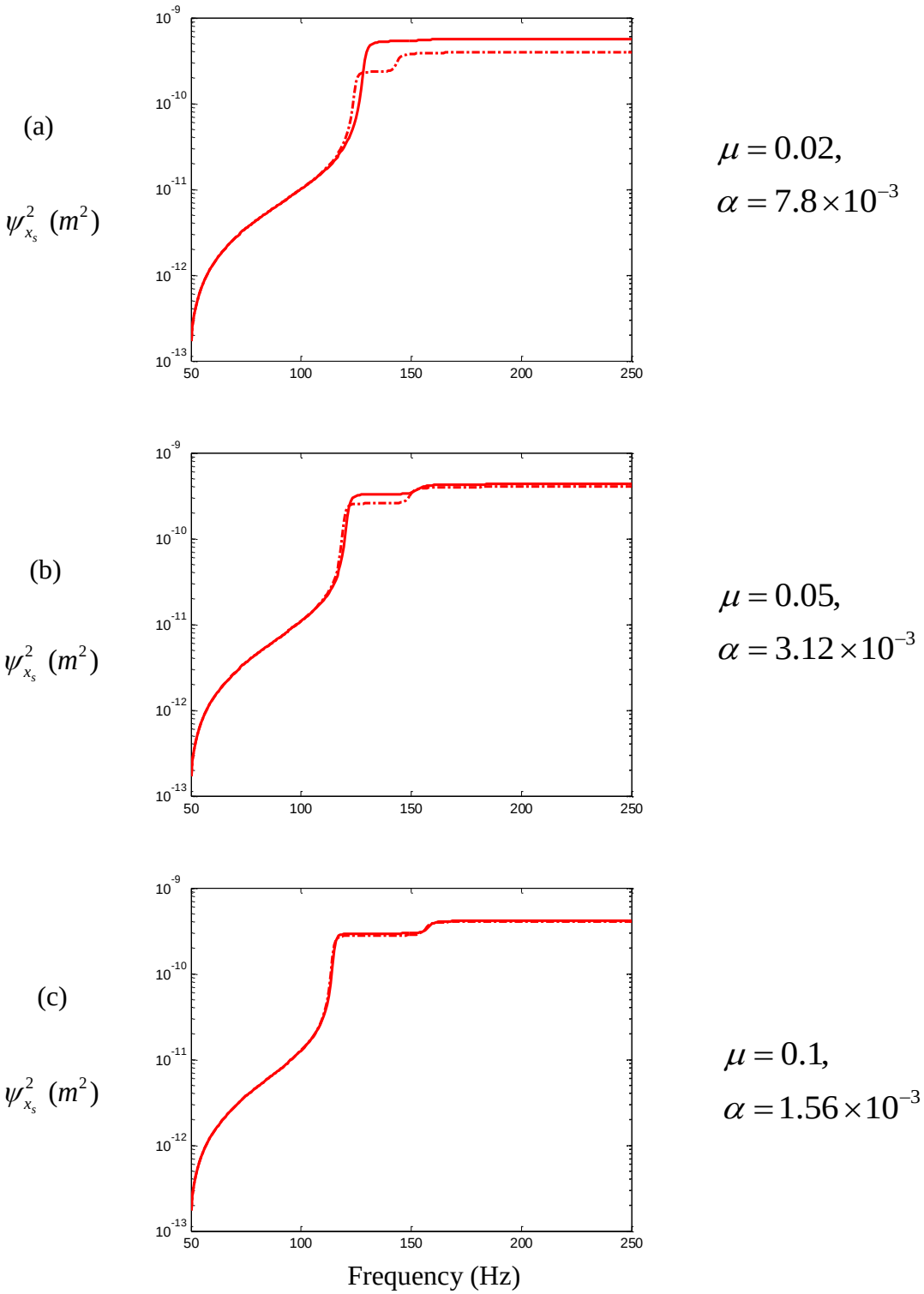

Figure 4.31 The effect of the mass ratio on the primary system cumulative mean square displacement. The random input rms force amplitude is 0.5 N. (The 'tuned' frequency $\omega_1/\omega_s = 1$ and damping $\zeta_s = 0.01$, $\zeta = 0.008$). The response for the system with the linear absorber is given by the dashed-dotted line, the solid line is the nonlinear absorber. (a) $\mu = 0.02$, (b) $\mu = 0.05$ and (c) $\mu = 0.1$.

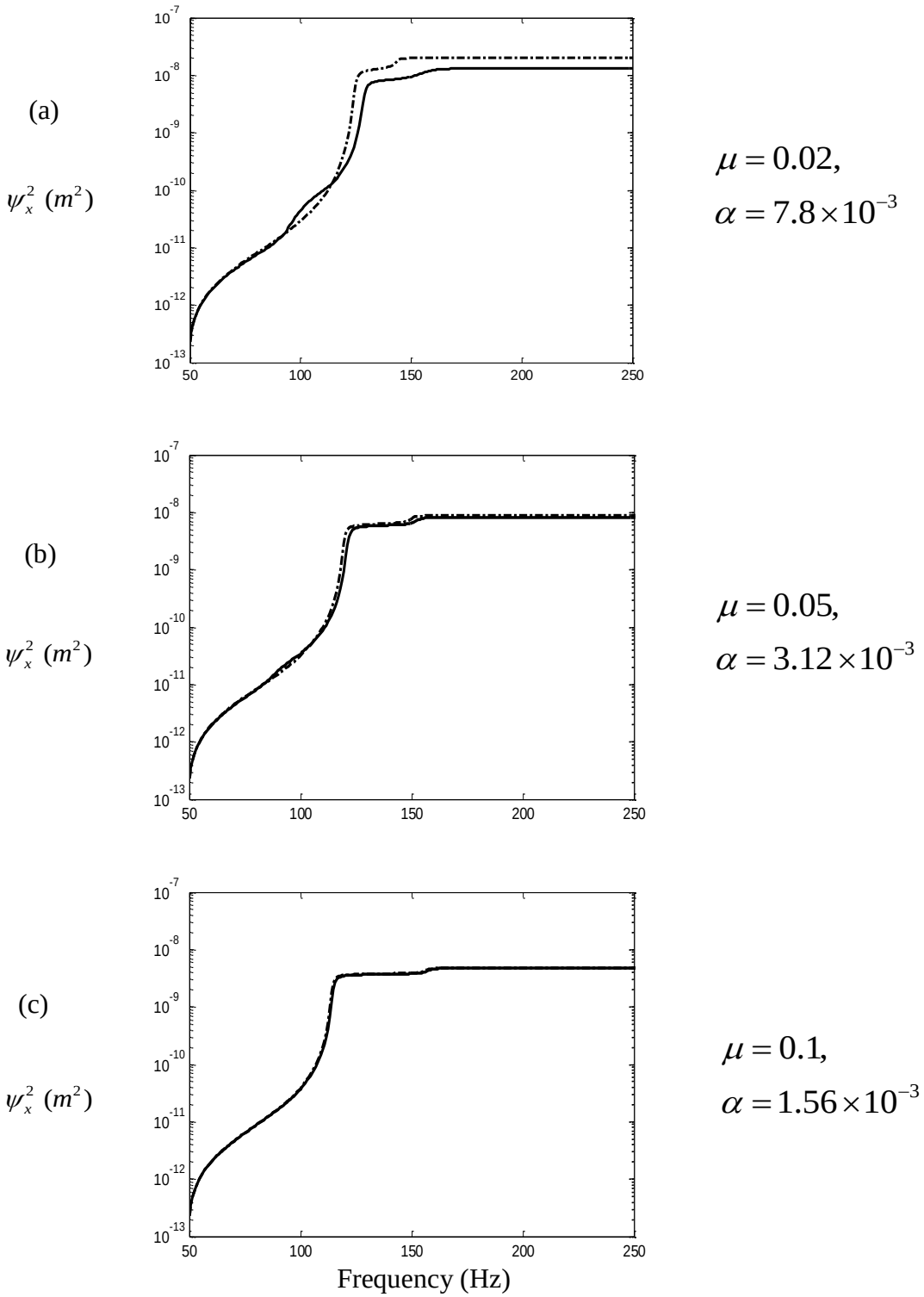

Figure 4.32 The effect of the mass ratio on the secondary system cumulative mean square displacement. The random input rms force amplitude is 0.5 N. (The 'tuned' frequency $\omega_1/\omega_s = 1$ and damping $\zeta_s = 0.01$, $\zeta = 0.008$). The response for the system with the linear absorber is given by the dashed-dotted line, the solid line is the nonlinear absorber. (a) $\mu = 0.02$, (b) $\mu = 0.05$ and (c) $\mu = 0.1$.

The primary system parameters are set to m_s=1.26×10^{-1} (kg) , c_s=$2.12\ (\mathrm{N\cdot s/m})$, k_s=$8.93\times10^{4}\ \left(\mathrm{N/m}\right)$, respectively. The secondary system parameter and nondimensional parameters μ and α values are presented in Table 4.11 and 4.12. Numerical solutions have been presented for the mean square displacement of the primary and absorber system, for values of the mass ratio and for various values of the nonlinear stiffness in Figure 4.33(a)-(b). The effect of the mass ratio on the primary and secondary system displacement PSD are presented in Figures 4.34-35 and 4.38-39. The cumulative displacement of the primary and secondary system, for values of the mass ratio and for various values of the nonlinear stiffness are given in Figure 4.36-37 and 4.40-41.

As the mass ratio increases between $0.01\le\mu<0.06$, using the nonlinear absorber has a higher mean square primary system displacement compared to the linear absorber with the same mass level in Figure 4.33(a). The cumulative displacement of the primary system using the nonlinear absorber is also higher than using the linear absorber in Figures 4.31, 4.36 and 4.40. For higher mass ratios, i.e. between $0.06\le\mu\le0.1$, for small nonlinear stiffness, i.e. k_3= $8.93\times10^{8}\ \left(\mathrm{N/m^3}\right)$, it gives the same mean square primary system displacement compared to using the linear absorber. When the nonlinear stiffness is higher, the nonlinear absorber produces a higher mean square primary system displacement compared to the linear absorber with the same linear stiffness and mass levels in Figure 4.38. The displacement PSD of the primary system for the first mode is the dominant contribution in the mean square response. The reason could be due to the primary system and nonlinear absorber move in phase at the first mode. The displacement of the primary system presents similar to the single degree of system due to the higher nonlinear stiffness in Figure 4.38(a). The cumulative displacement of the primary system using the nonlinear absorber is also higher at the first mode compared to using a linear absorber.

Mass ratio	Nonlinear stiffness	absorber system			
μ	α	m (kg)	$c\ (\mathrm{N\cdot s/m})$	$k_1\ (\mathrm{N/m})$	$k_3\ (\mathrm{N/m^3})$
0.01	1.56×10^{-3}	1.26×10^{-3}	1.70×10^{-2}	8.93×10^{2}	8.93×10^{8}
0.02	7.80×10^{-4}	2.52×10^{-3}	3.40×10^{-2}	1.79×10^{3}	8.93×10^{8}
0.03	5.20×10^{-4}	3.78×10^{-3}	5.10×10^{-2}	2.68×10^{3}	8.93×10^{8}
0.04	3.90×10^{-4}	5.04×10^{-3}	6.79×10^{-2}	3.57×10^{3}	8.93×10^{8}
0.05	3.12×10^{-4}	6.30×10^{-3}	8.49×10^{-2}	4.47×10^{3}	8.93×10^{8}
0.06	2.60×10^{-4}	7.56×10^{-3}	1.02×10^{-1}	5.36×10^{3}	8.93×10^{8}
0.07	2.23×10^{-4}	8.82×10^{-3}	1.19×10^{-1}	6.25×10^{3}	8.93×10^{8}
0.08	1.95×10^{-4}	1.01×10^{-2}	1.36×10^{-1}	7.15×10^{3}	8.93×10^{8}
0.09	1.74×10^{-4}	1.13×10^{-2}	1.53×10^{-1}	8.04×10^{3}	8.93×10^{8}
0.1	1.56×10^{-4}	1.26×10^{-2}	1.70×10^{-1}	8.93×10^{3}	8.93×10^{8}

Table 4.11 The secondary system parameters are estimated for the model predictions ($k_3 = 8.93\times10^{8}\ \left(\mathrm{N/m^3}\right)$).

Mass ratio	Nonlinear stiffness	absorber system			
μ	α	m (kg)	$c\ (\mathrm{N\cdot s/m})$	$k_1\ (\mathrm{N/m})$	$k_3\ (\mathrm{N/m^3})$
0.01	1.56	1.26×10^{-3}	1.70×10^{-2}	8.93×10^{2}	8.93×10^{11}
0.02	7.80×10^{-1}	2.52×10^{-3}	3.40×10^{-2}	1.79×10^{3}	8.93×10^{11}
0.03	5.20×10^{-1}	3.78×10^{-3}	5.10×10^{-2}	2.68×10^{3}	8.93×10^{11}
0.04	3.90×10^{-1}	5.04×10^{-3}	6.79×10^{-2}	3.57×10^{3}	8.93×10^{11}
0.05	3.12×10^{-1}	6.30×10^{-3}	8.49×10^{-2}	4.47×10^{3}	8.93×10^{11}
0.06	2.60×10^{-1}	7.56×10^{-3}	1.02×10^{-1}	5.36×10^{3}	8.93×10^{11}
0.07	2.23×10^{-1}	8.82×10^{-3}	1.19×10^{-1}	6.25×10^{3}	8.93×10^{11}
0.08	1.95×10^{-1}	1.01×10^{-2}	1.36×10^{-1}	7.15×10^{3}	8.93×10^{11}
0.09	1.74×10^{-1}	1.13×10^{-2}	1.53×10^{-1}	8.04×10^{3}	8.93×10^{11}
0.1	1.56×10^{-1}	1.26×10^{-2}	1.70×10^{-1}	8.93×10^{3}	8.93×10^{11}

Table 4.12 The secondary system parameters are estimated for the model predictions ($k_3 = 8.93\times10^{11}\ \left(\mathrm{N/m^3}\right)$).

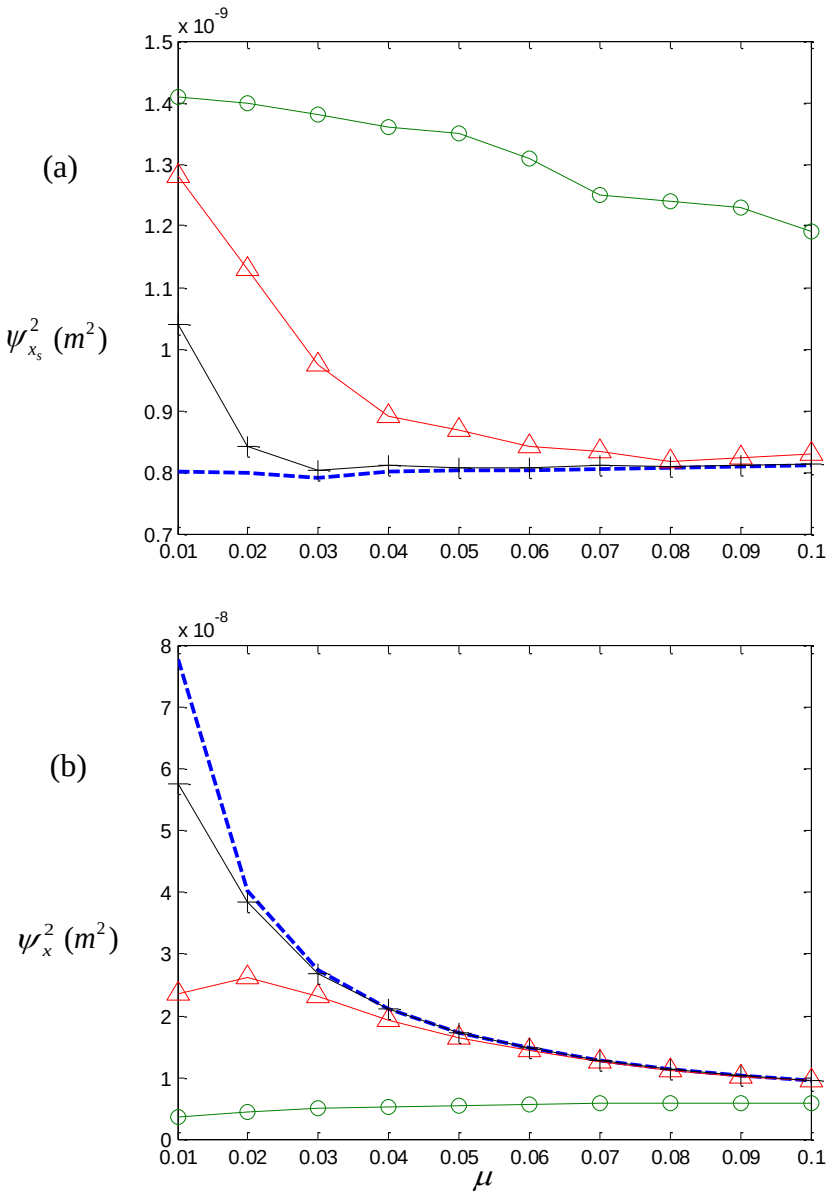

Figure 4.33 The effect of the mass ratio μ and for various values of nonlinear stiffness on the (a) primary and (b) absorber system mean square displacement response. The random input rms force amplitude is 0.5 N. ($\omega_0 = 1$ and damping $\zeta_s = 0.01$ and $\zeta = 0.008$). Linear absorber is dashed line and nonlinear absorber stiffness are $k_3 = 8.93\times10^8\ \left(\mathrm{N/m^3}\right)$ ('+'), $k_3 = 8.93\times10^9\ \left(\mathrm{N/m^3}\right)$ ('Δ') and $k_3 = 8.93\times10^{11}\ \left(\mathrm{N/m^3}\right)$ ('o').

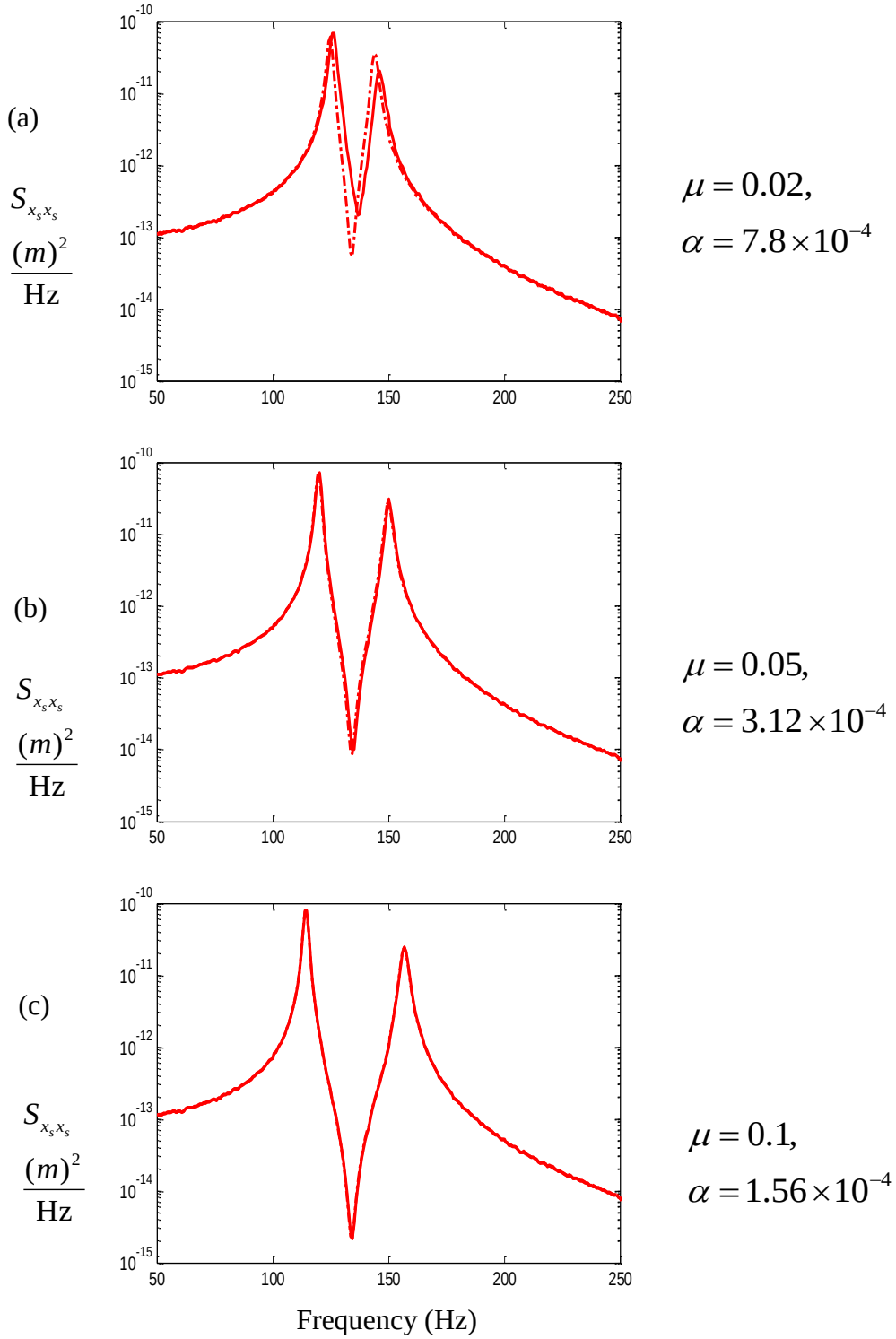

Figure 4.34 The effect of the mass ratio on the primary system displacement PSD. The random input rms force amplitude is 0.5 N. (The 'tuned' frequency $\omega_1/\omega_s = 1$ and damping $\zeta_s = 0.01$, $\zeta = 0.008$). The response for the system with the linear absorber is given by the dashed-dotted line, the solid line is the nonlinear absorber. (a) $\mu = 0.02$, (b) $\mu = 0.05$ and (c) $\mu = 0.1$.

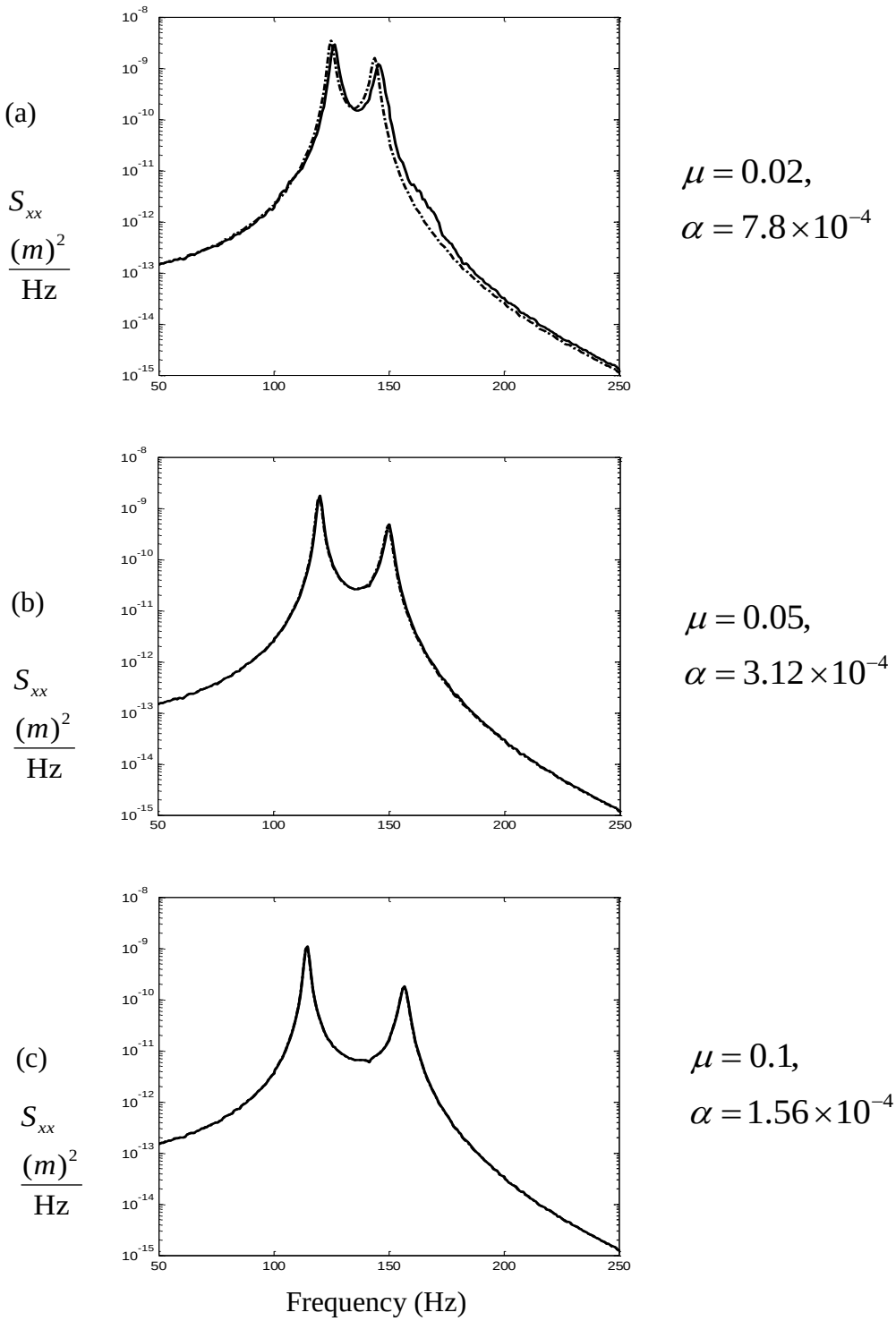

Figure 4.35 The effect of the mass ratio on the secondary system displacement PSD. The random input rms force amplitude is 0.5 N. (The 'tuned' frequency $\omega_1/\omega_s = 1$ and damping $\zeta_s = 0.01$, $\zeta = 0.008$). The response for the system with the linear absorber is given by the dashed-dotted line, the solid line is the nonlinear absorber. (a) $\mu = 0.02$, (b) $\mu = 0.05$ and (c) $\mu = 0.1$.

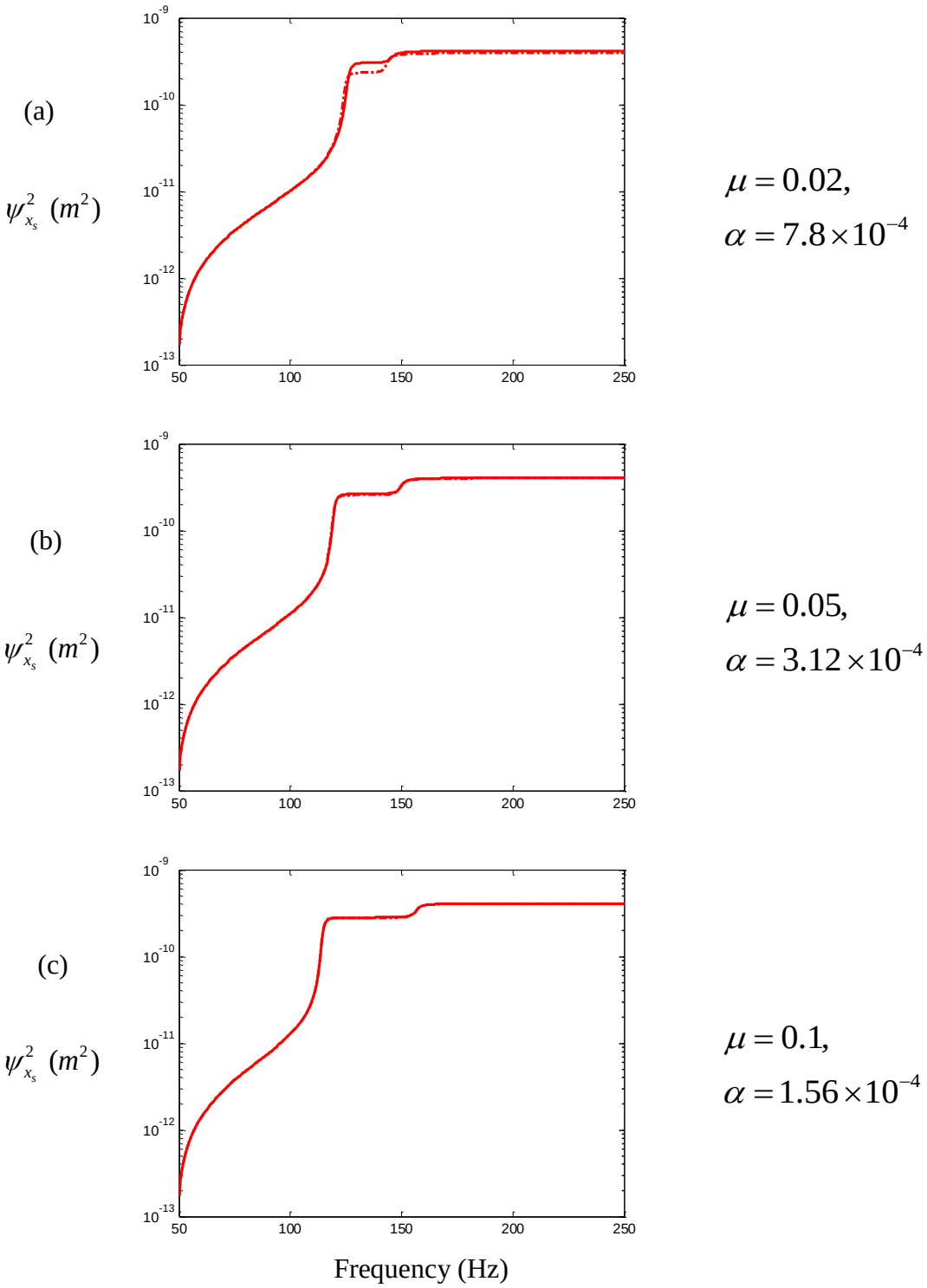

Figure 4.36 The effect of the mass ratio on the primary system cumulative mean square displacement. The random input rms force amplitude is 0.5 N. (The 'tuned' frequency $\omega_1/\omega_s = 1$ and damping $\zeta_s = 0.01$, $\zeta = 0.008$). The response for the system with the linear absorber is given by the dashed-dotted line, the solid line is the nonlinear absorber. (a) $\mu = 0.02$, (b) $\mu = 0.05$ and (c) $\mu = 0.1$.

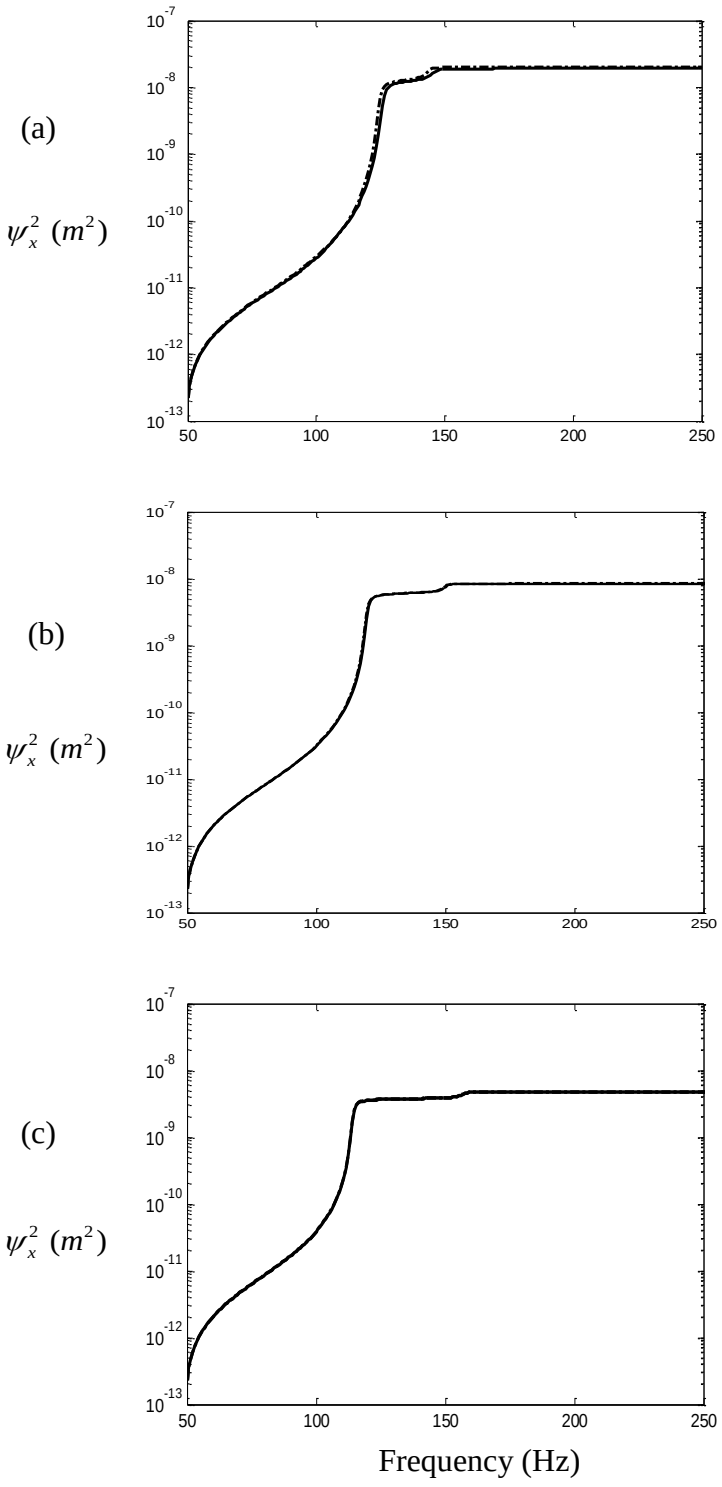

Figure 4.37 The effect of the mass ratio on the secondary system cumulative mean square displacement. The random input rms force amplitude is 0.5 N. (The 'tuned' frequency $\omega_1/\omega_s = 1$ and damping $\zeta_s = 0.01$, $\zeta = 0.008$). The response for the system with the linear absorber is given by the dashed-dotted line, the solid line is the nonlinear absorber. (a) $\mu = 0.02$, (b) $\mu = 0.05$ and (c) $\mu = 0.1$.

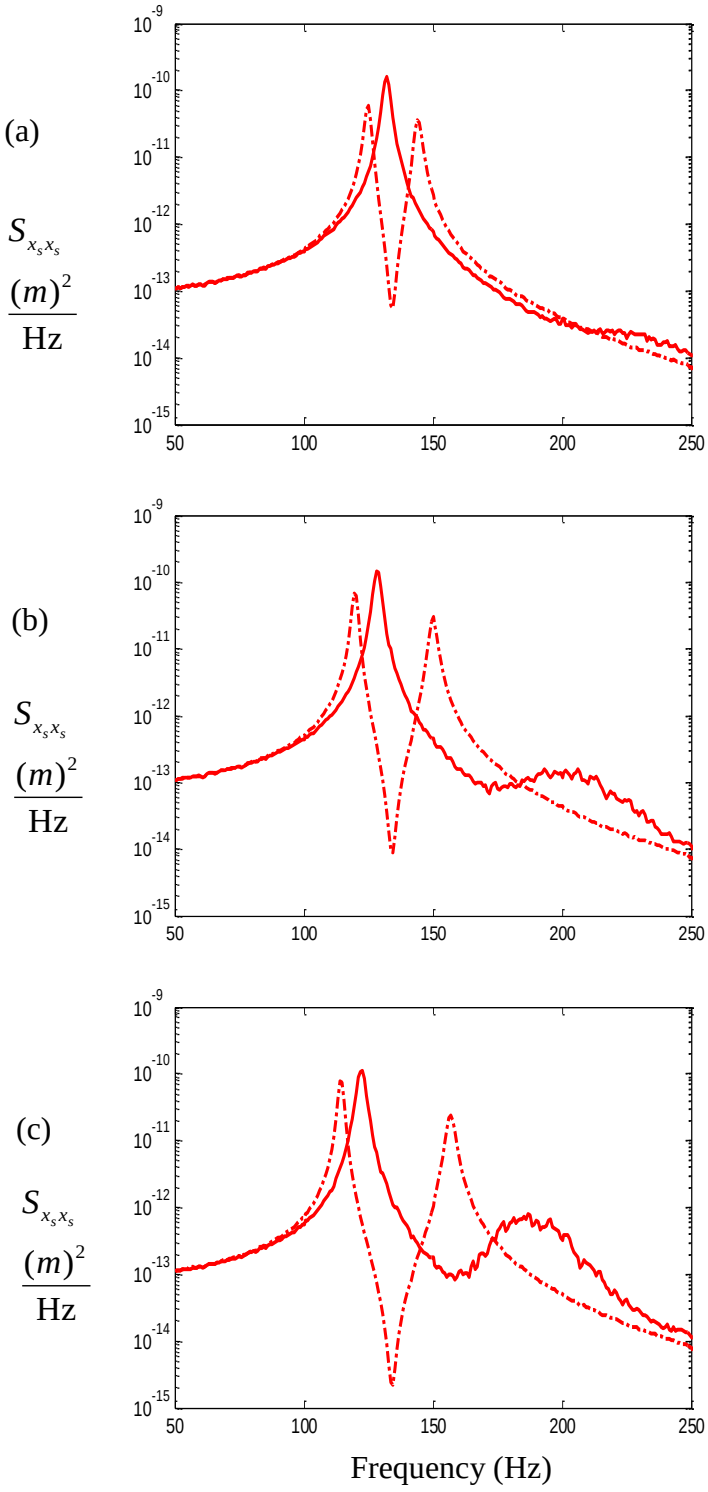

Figure 4.38 The effect of the mass ratio on the primary system displacement PSD. The random input rms force amplitude is 0.5 N. (The 'tuned' frequency $\omega_1/\omega_s = 1$ and damping $\zeta_s = 0.01$, $\zeta = 0.008$). The response for the system with the linear absorber is given by the dashed-dotted line, the solid line is the nonlinear absorber. (a) $\mu = 0.02$, (b) $\mu = 0.05$ and (c) $\mu = 0.1$.

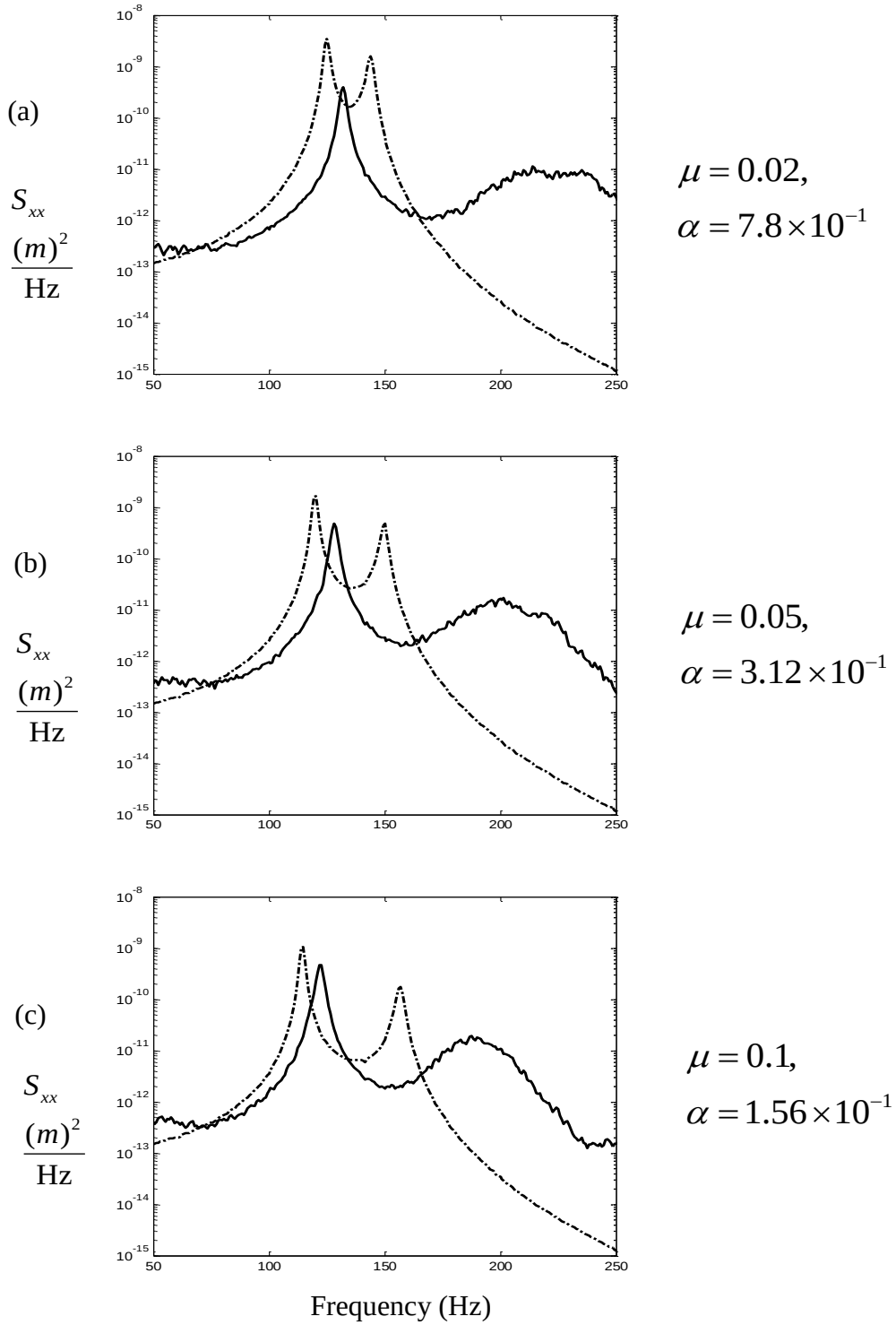

Figure 4.39 The effect of the mass ratio on the secondary system displacement PSD. The random input rms force amplitude is 0.5 N. (The 'tuned' frequency $\omega_1/\omega_s = 1$ and damping $\zeta_s = 0.01$, $\zeta = 0.008$). The response for the system with the linear absorber is given by the dashed-dotted line, the solid line is the nonlinear absorber. (a) $\mu = 0.02$, (b) $\mu = 0.05$ and (c) $\mu = 0.1$.

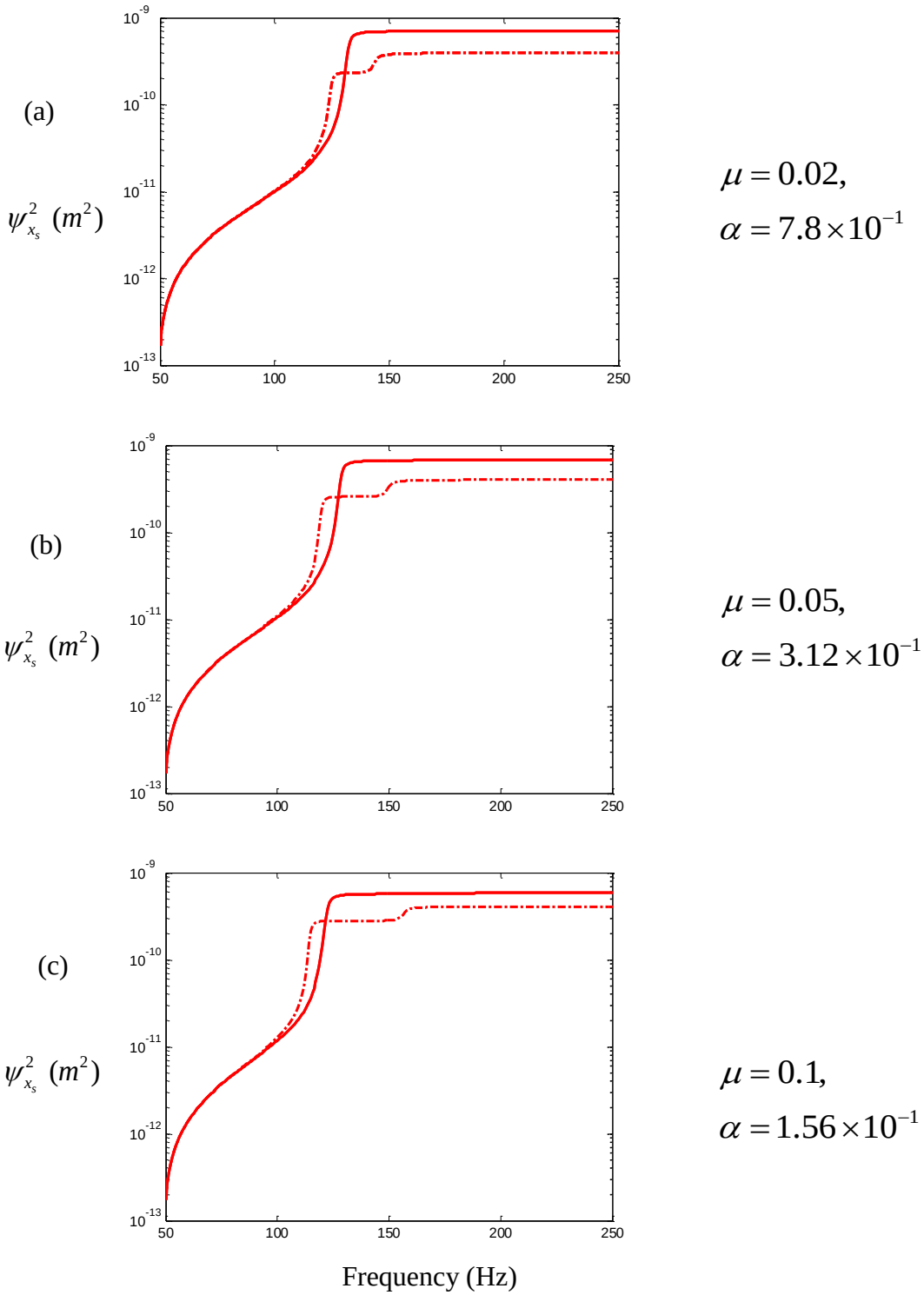

Figure 4.40 The effect of the mass ratio on the primary system cumulative mean square displacement. The random input rms force amplitude is 0.5 N. (The 'tuned' frequency $\omega_1/\omega_s = 1$ and damping $\zeta_s = 0.01$, $\zeta = 0.008$). The response for the system with the linear absorber is given by the dashed-dotted line, the solid line is the nonlinear absorber. (a) $\mu = 0.02$, (b) $\mu = 0.05$ and (c) $\mu = 0.1$.

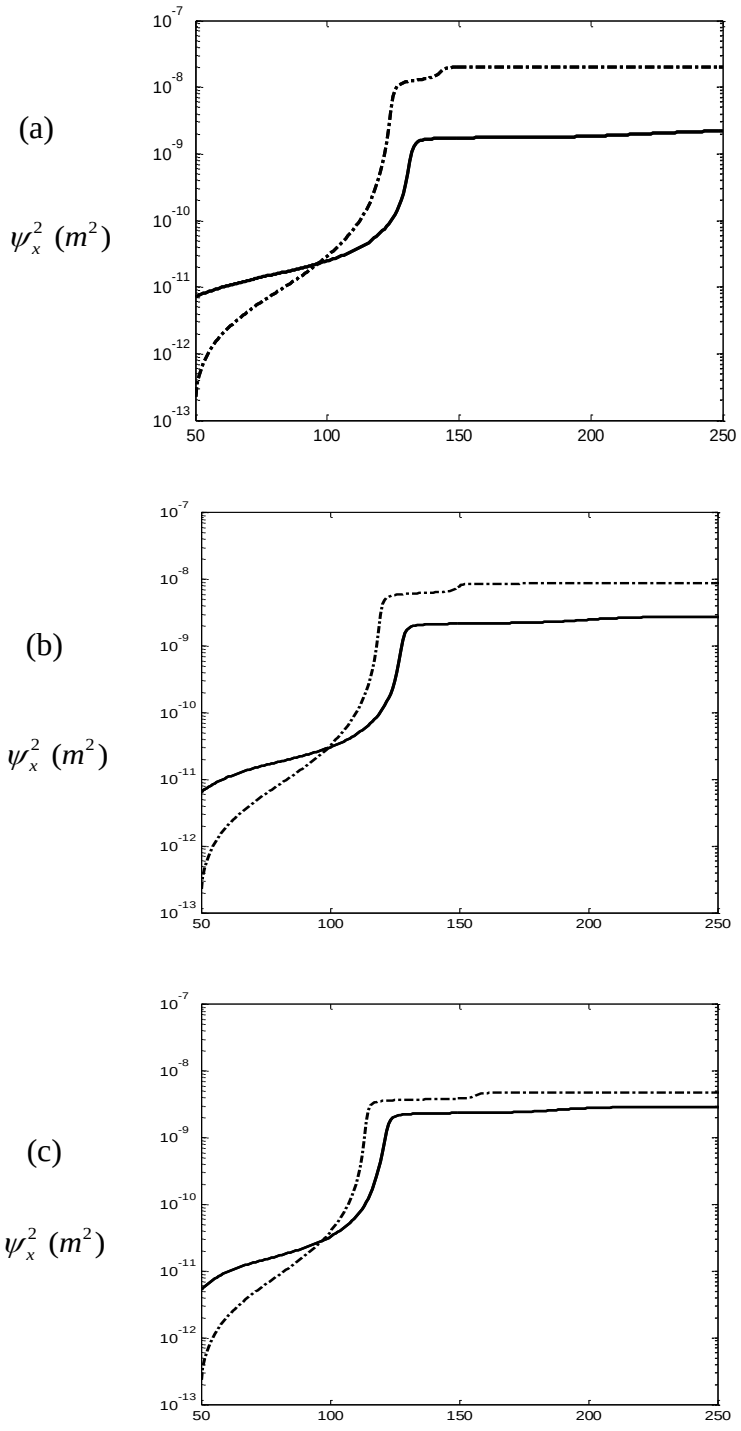

Figure 4.41 The effect of the mass ratio on the secondary system cumulative mean square displacement. The random input rms force amplitude is 0.5 N. (The 'tuned' frequency $\omega_1/\omega_s = 1$ and damping $\zeta_s = 0.01$, $\zeta = 0.008$). The response for the system with the linear absorber is given by the dashed-dotted line, the solid line is the nonlinear absorber. (a) $\mu = 0.02$, (b) $\mu = 0.05$ and (c) $\mu = 0.1$.

4.7 Conclusions

This chapter presented random vibration simulations and subsequent statistical and frequency analysis of the simulated time history. The physical phenomenon lying underneath such dynamic behaviour was of main interest in this chapter. The effects of the random input amplitude, nonlinear stiffness (α), absorber damping ratio (ζ) and mass ratio (μ) on the vibration response were presented by considering a range of parameter values. The results obtained indicate that the mentioned above parameters have a significant effect on the vibration response. The key results presented in this chapter are as follows:

For some ranges of the non-dimensional parameters, for high random input force amplitudes applied to the primary system, the nonlinear absorber provided significant nonlinear behaviour and produced a higher mean square primary system displacement compared to a conventional linear absorber. The cumulative mean square displacement of the primary system using the nonlinear absorber is also higher than when using the linear absorber. In addition, the nonlinear absorber produced a much broader PSD for the primary and secondary response at the second mode, resulting in a larger vibration response at higher frequencies.

For a low nonlinear stiffness, the nonlinear absorber produces the same mean square primary system displacement compared to a linear absorber case. For a high nonlinear stiffness, the nonlinear absorber has a higher mean square primary system displacement compared to a linear absorber. Hence the use of a high stiffness nonlinearity does not improve the vibration reduction compared to the linear absorber case in term of the rms response. The difference between the linear and the nonlinear absorber follows a general trend with the nonlinear absorber reduces a broader PSD of the primary and secondary system responses at the second mode and a vibration response at higher frequency. In addition, the nonlinear absorber produces a higher displacement response PSD in the primary system at the first mode compared to the linear absorber case.

As the damping in the nonlinear absorber is increased, the mean square primary system displacement is higher than when using a conventional linear absorber. For the mean square displacement of the secondary system, the nonlinear absorber response remains lower compared to the linear absorber.

For a nonlinear absorber with a low mass ratio, a higher mean square primary system displacement occurs compared to using a linear absorber with the same level of mass. On increasing the mass ratio then the mean square of primary system displacement using the nonlinear absorber will reduce and eventually is similar to using a linear absorber. The higher mass ratios actually result in a smaller nonlinear nondimensional stiffness as it is defined. When the nonlinear stiffness is higher, the nonlinear absorber again produces a higher mean square primary system displacement compared to the behaviour using a linear absorber with the same level of linear stiffness and mass.

For some range of parameter values, the nonlinear absorber under random excitation produces undesirable increasing in the mean square response of the primary system compared to a linear absorber. This means that the nonlinear absorber still needs to be selected and optimized with the best parameters for the particular application, so as to ensure that one obtains a reduced vibration response of the primary system.

Chapter 5

Experimental validation: design and measurement of a nonlinear dynamic vibration absorber

For harmonic excitation, described in chapter 2, the equations of motion were derived for the main structural system installed with an NDVA. Mathematical expressions for the frequency response curves of the structural system were subsequently determined. Chapter 3 investigated the effect of the nonlinear vibration absorber parameters (e.g., nonlinear stiffness, damping ratio, mass ratio and frequency ratio) on the vibration reduction. Chapter 4 uses a statistical analysis to investigate the effect of the nonlinear absorber parameters on the vibration reduction using broadband random input. Experimental validation is presented in this chapter for both harmonic and random excitation for comparison with the analytical and numerical results produced.

A nonlinear absorber was designed and attached to a cantilever beam which was excited by a shaker. The support frame and cantilever beam can be considered and modelled at low frequency as a linear single degree-of-freedom system. The nonlinear absorber is designed to behave as the modelled hardening stiffness vibration absorber described earlier. The overall system is modelled as a nonlinear vibration absorber coupled to a linear system. An aim of the

experimental investigation is to demonstrate the corresponding vibration reduction of the configuration using this particular nonlinear vibration absorber.

5.1 Nonlinear dynamic vibration absorber design and experimental investigation

5.1.1. Implementation of the nonlinear stiffness characteristics

The phenomenon of nonlinear stiffness was reproduced using a thin uniform clamped circular plate undergoing large flexural deflection [79]. The absorber mass was attached at the centre of the thin circular plate. The plate is clamped by a frame on its edges as illustrated in Figure 5.1. The circular plate has a radius r, thickness h, Poisson's ratio ν and Young's modulus of elasticity E. When the mass moves in the vertical direction, the plate bends with a large deflection producing axial strain and a change in length of the midplane axis. This large deflection, producing geometric nonlinearity, is the cause of the nonlinearity in the restoring force and hence effective stiffness of the absorber. The static relationship between the applied static force f at the centre of the circular plate and the deflection at that point has been obtained when ν is equal to 0.3 [79]

$$0.217\frac{fr^2}{Eh^4} = \frac{y}{h} + 0.443\left(\frac{y}{h}\right)^3 \tag{5.1}$$

Equation (5.1) can be written as

$$f = k_1 y + k_3 y^3 \tag{5.2}$$

where $k_1 = \dfrac{Eh^3}{0.217r^2}$ and $k_3 = \dfrac{0.443Eh}{0.217r^2}$ are the corresponding stiffness coefficients.

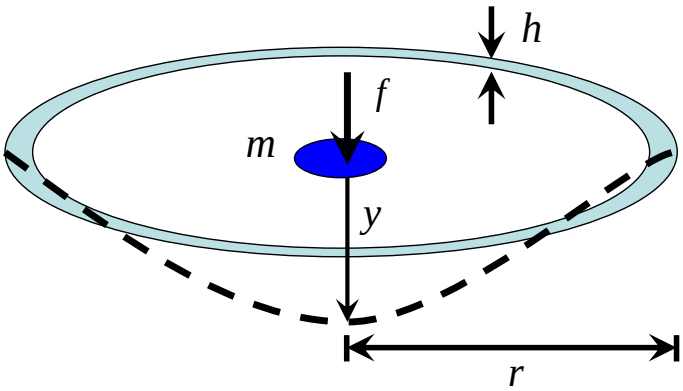

Figure 5.1. Schematic representation of a nonlinear vibration absorber using a thin circular plate.

5.1.2 Description of the combined system with the nonlinear absorber

The practical implementation of the nonlinear vibration absorber is shown in Figures 5.2-5.4. Photographs are shown in Figures 5.2-5.3 and a schematic representation is shown in Figure 5.4. A CAD diagram is given in Appendix B for the actual manufactured rig. A mass m was attached to the thin plate, which is itself bolted to a cantilever beam by a support frame. The spring characteristics between the absorber mass and the support frame are due to the thin circular plate, which can be modelled as the stiffnesses k_1 and k_3 and for small dissipation effects a viscous damper c was introduced. The thickness of the plate or shim and the attached mass can be altered and these have a large effect on the nonlinear absorber characteristics. In addition, the length of the cantilever beam also can be altered, so it is possible to consider different primary system natural frequencies. For large dynamic deformations a hypothesis was made that the absorber would be nonlinear. The cantilever beam was excited by an electro-dynamic shaker. The support frame and beam structure without the absorber can be modelled at low frequencies as a linear system comprising a spring k_s, a viscous damper c_s and a mass m_s. Applying a constant amplitude current at each frequency to the shaker, then one could measure a constant force amplitude using a force gauge. The excitation force can be modelled as a constant amplitude harmonic force, applied to the primary system mass as shown in Figure 5.4. For the random excitation case, a constant white noise random excitation force is applied to the cantilever beam. A force gauge is also included to monitor and control the applied force and for acquisition of the actual applied force.

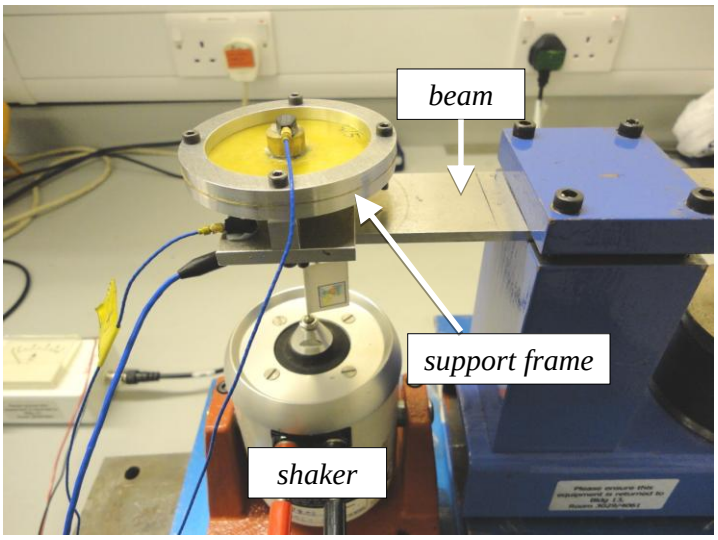

Figure 5.2 Photograph of the actual experimental system consisting of a nonlinear absorber attached to a cantilever beam excited by an electro-dynamic shaker.

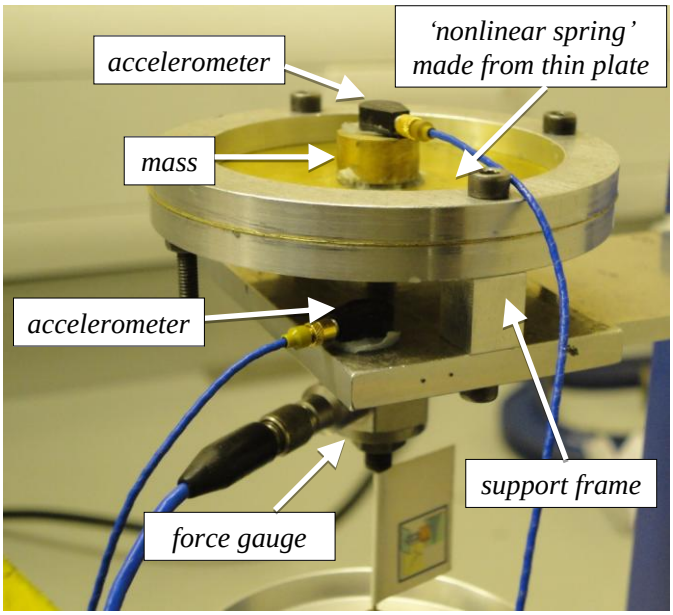

Figure 5.3 Photograph showing the details of the nonlinear system.

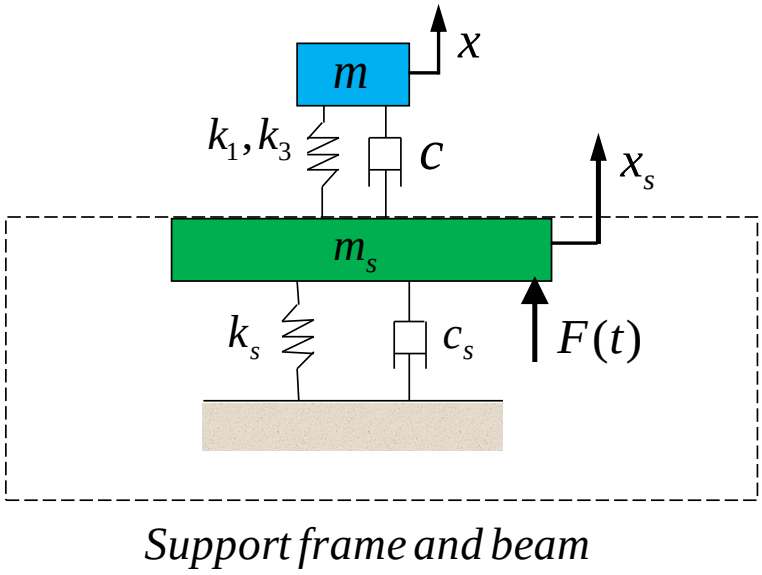

Figure 5.4 Schematic representation of a nonlinear absorber attached to a cantilever beam system excited by a shaker.

5.2 Experimental procedure and results: harmonic excitation

The schematic diagram of the experimental setup is shown in Figure 5.5. The electro-dynamic shaker was driven by a signal generator producing a stepped-sine signal. The accelerometers (PCB type 352C22) were attached to the support frame structure and to the mass of the absorber to measure the system response, while the oscilloscope was used to observe the system response. The data was acquired using a DataPhysics frequency analyser connected to the computer.

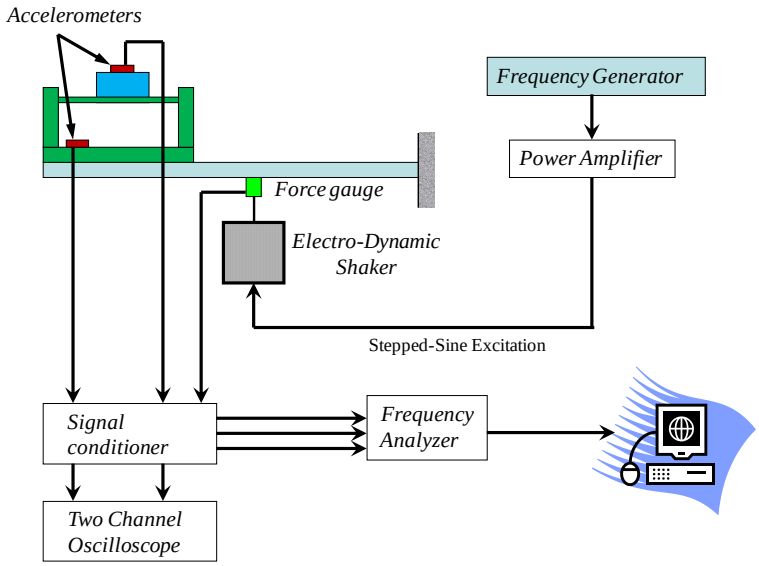

Figure 5.5 Schematic diagram of the instrumentation setup used for the laboratory tests under harmonic excitation.

5.2.1 Experimental procedure

A preliminary test was implemented to broadly investigate the dynamic behaviour of the system. For each test, the shaker had a different force amplitude. In the high force amplitude test, a slow frequency sweep (where the force gauge recorded a constant amplitude voltage and hence force amplitude) was applied from 100 Hz to about 225 Hz and the response of the system was observed using the oscilloscope. The first resonance was monitored at around 123 Hz, with large vibrational amplitudes in both systems. In addition, the first resonance peak was difficult to measure due to the light damping in the cantilever beam. When the frequency was increased beyond this, the effective tuned frequency was observed at about 183 Hz. In this frequency region the vibration of the primary system was a minimum. However, a second resonance occurred at about 213 Hz, where only the vibration of the absorber mass was large. This was followed by a sudden decrease in the motion of the mass of absorber; a jump-down in

the response. The frequency was then slowly swept down from this high frequency back to the low frequency. A sudden increase in the amplitude was observed at a frequency of about 199 Hz, again only for the mass of the absorber (a jump-up). In the low force amplitude test, a response behaviour was observed that is approximately similar to a linear system. The first resonance, effective tuned frequency and second resonance were found to occur at around 125 Hz, 160 Hz and 172 Hz respectively. The jump-up and jump-down frequencies did not occur. It is noted that the preliminary test used a voltmeter to observe the change in the response of the system. This initial experiment did not allow any data to be captured.

For the measured data presented, the shaker was driven at discrete frequencies for the system with the thin plate, corresponding to the cases described above. The excitation frequency was increased from 100 Hz to 225 Hz, in 1 Hz increments, and then decreased to 100 Hz with the same frequency decrements. The amplitude of the excitation force was maintained at a constant level for all excitation frequencies, by manually adjusting the power amplifier so that the output voltage of the force gauge was 127 mV and 12.7 mV respectively. This corresponded to an equivalent force of 1.12 N and 0.11 N respectively. At each frequency, once the system was at steady-state, five seconds of acceleration time histories were captured using a DataPhysics frequency analyser connected to a PC. Subsequently, the acceleration of the support frame and beam structure and the absorber were measured, and then this data was processed to give the displacement. The data is presented in terms of the absolute displacement x_s of the primary system and the absolute displacement x of the absorber. The Fourier series coefficients were extracted from these time histories and the amplitude of the first harmonic of each data set is plotted at the corresponding excitation frequency.

5.2.2 Experimental results

In Figures 5.6(a)-(b), the response of the system for which the forces have low and high amplitudes respectively. At low force amplitude, the data points in each graph are dashed-dotted lines. At high force amplitude, the data points in each graph are denoted by '+' for increasing frequency and '•' for decreasing frequency respectively. The non-harmonic (NH) responses at the corresponding excitation frequencies are given by the symbol 'o'. The NH responses are those for which the amplitudes of the other harmonics exceed 5% of the amplitude of the

excitation frequency in the response. The time response and corresponding Fourier series coefficients for the system will be presented later.

The response of the primary system X_s is plotted in Figure 5.6(a). The frequency bandwidth was determined when $|X_s| \le |X_0|$ in that frequency range, where X_0 is the corresponding static extension of the linear spring represented by the cantilever beam for the same magnitude static load. The response $X_s/F = X_0/F = 1/k_s$ is the thin solid horizontal line shown in the figures. It can be seen that the first resonance frequency and effective tuned frequency occur at about 125 Hz and 160 Hz for the low excitation amplitude and 123 Hz and 183 Hz for the high amplitude force cases, respectively. The nonlinear system attached to the cantilever beam structure has a significant effect on its response. In addition, the corresponding jump-down frequencies occur at about 199 Hz and at approximately 213 Hz for the high force amplitude case. It is noted that a non-harmonic response occurred at the jump-down frequency at 199 Hz. However, jump-up and jump-down did not occur for the low force amplitude. In Figure 5.6(b), which shows the response of the absorber X , in addition to the peak associated with the first resonance frequency of the primary system, a jump-down and a jump-up frequency can also be observed for the high force input amplitude. In addition, Figures 5.7(a)-(b) show the corresponding phase of the responses with respect to the excitation. The corresponding phase responses of each data were measured using a digital phase meter. However, the phase of the responses could not be produced in the frequency ranges from 175 to 201 (Hz), which is due to the non-harmonic response in this frequency ranges.

For excitation at 100, 120 and 150 (Hz), the amplitudes of other harmonics in the response did not exceed 5% compared to the fundamental amplitude. This is illustrated by the time histories shown in Figures 5.8-10. A harmonic response could not be achieved at excitation frequencies of 177, 182 and 195 (Hz), see Figures 5.11-13. This observation corresponds to the parts of the curve identified by the symbol $'0'$ at 177, 182 and 195 (Hz) in Figures 5.6(a)-(b). It is also noted that the corresponding time histories for the excitation force were not a harmonic. This unexpected feature will affect the response of the entire system. In order to minimize the effect of the feedback of the system response on the excitation system, a vibration control system needs to be used in future tests.

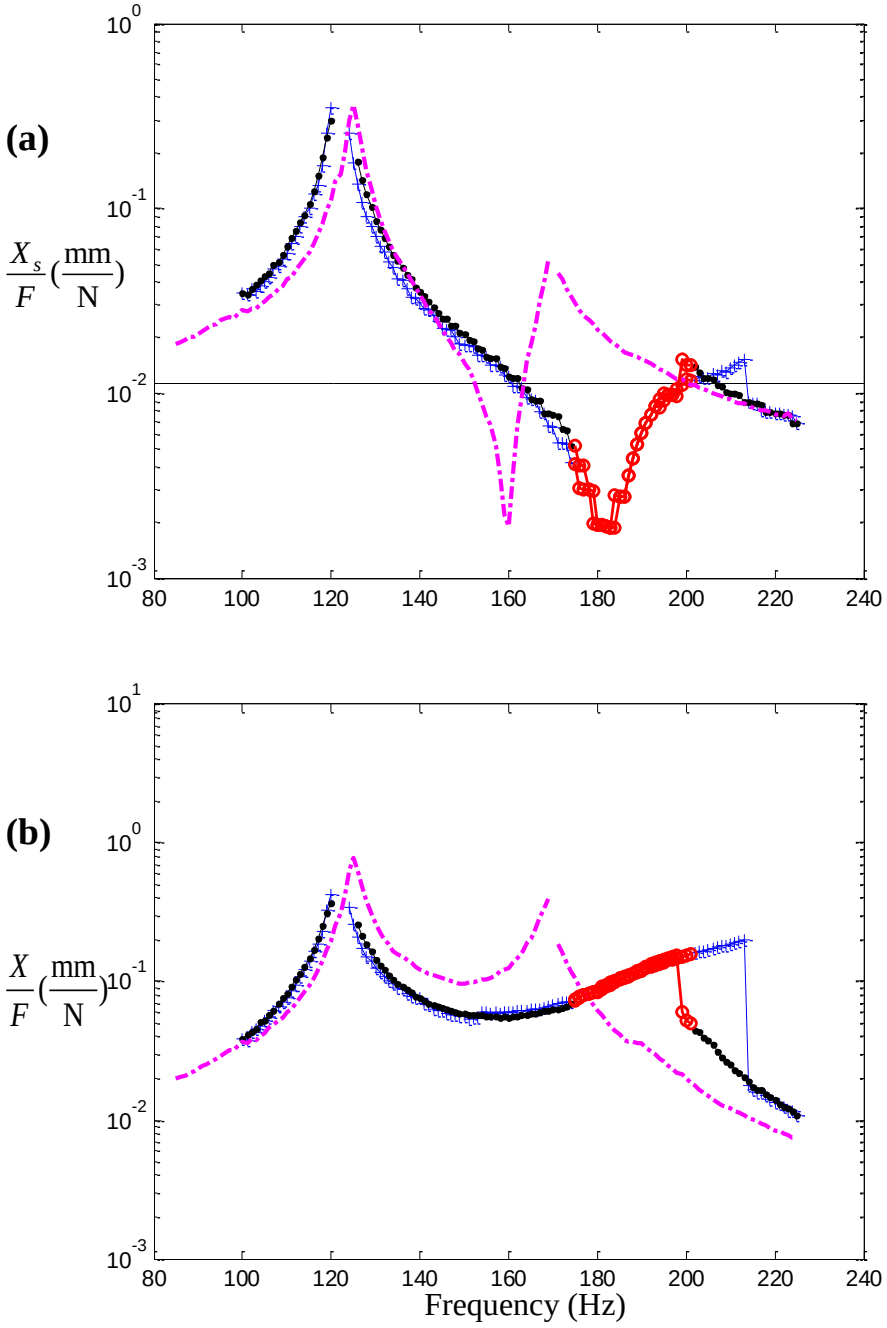

Figure 5.6 Comparison of the measured frequency response curves for the system whose properties are given in Table 5.2. Plate thickness 0.2 (mm): (a) Absolute displacement of the primary system, (b) Absolute displacement of the absorber. Low force amplitude for $F = 0.11\,\text{N}$ (dashed-dotted line). High force amplitude for $F = 1.12\,\text{N}$: increasing frequency ('+'), decreasing frequencies given by the symbol ('•'). The response is not harmonic (NH) at the corresponding excitation frequencies given by the symbol ('o'). The thin solid horizontal line is the static equivalent response which is used to determine the vibration reduction bandwidth.

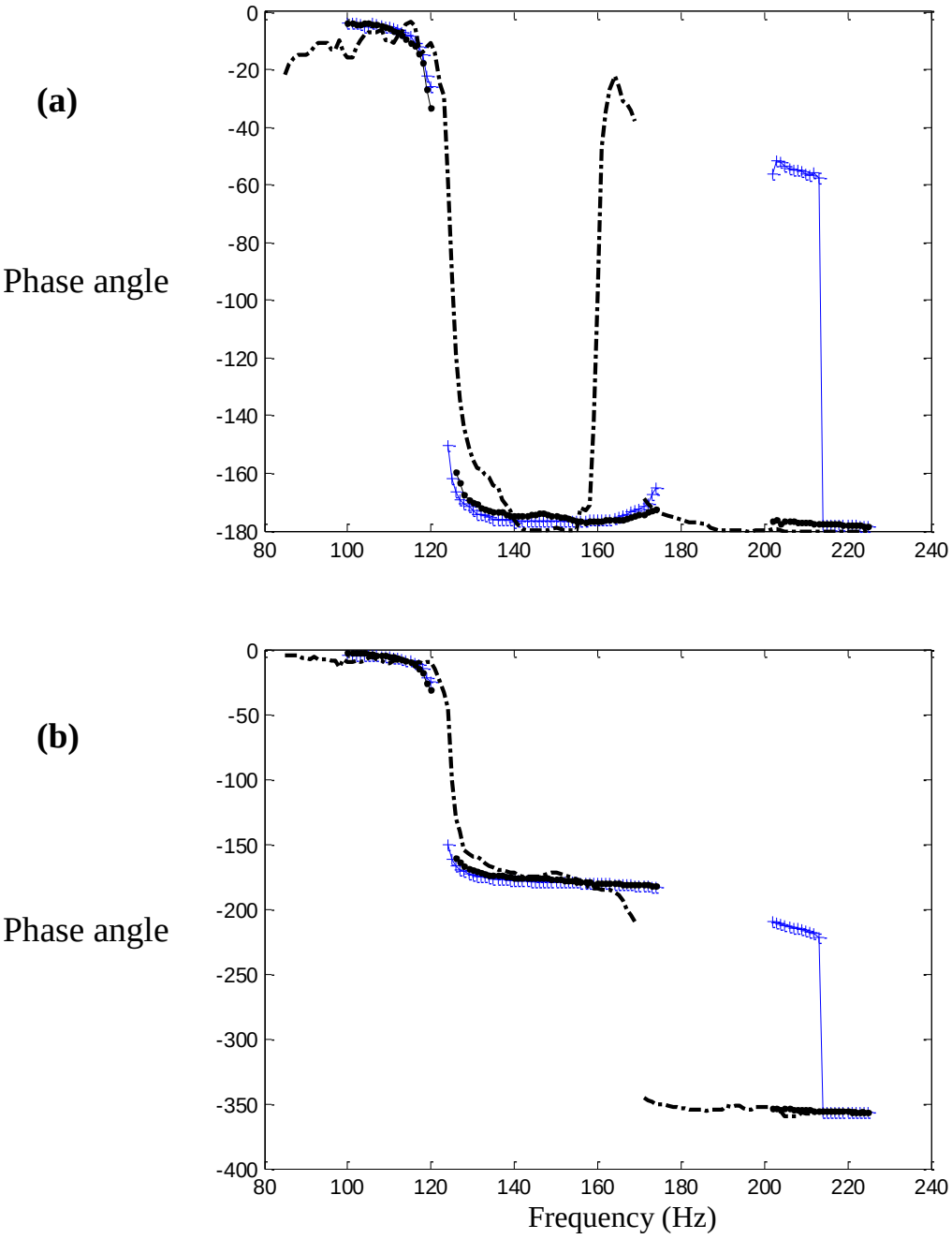

Figure 5.7 Comparison of the phase for measured frequency response curves. The system properties are given in Table 5.2. Plate thickness 0.2 (mm): (a) Phase of the primary system, (b) Phase of the absorber. Low force amplitude for $F = 0.11\ \mathrm{N}$ (dashed-dotted line). High force amplitude for $F = 1.12\ \mathrm{N}$: increasing frequency ('+'), decreasing frequency ('•').

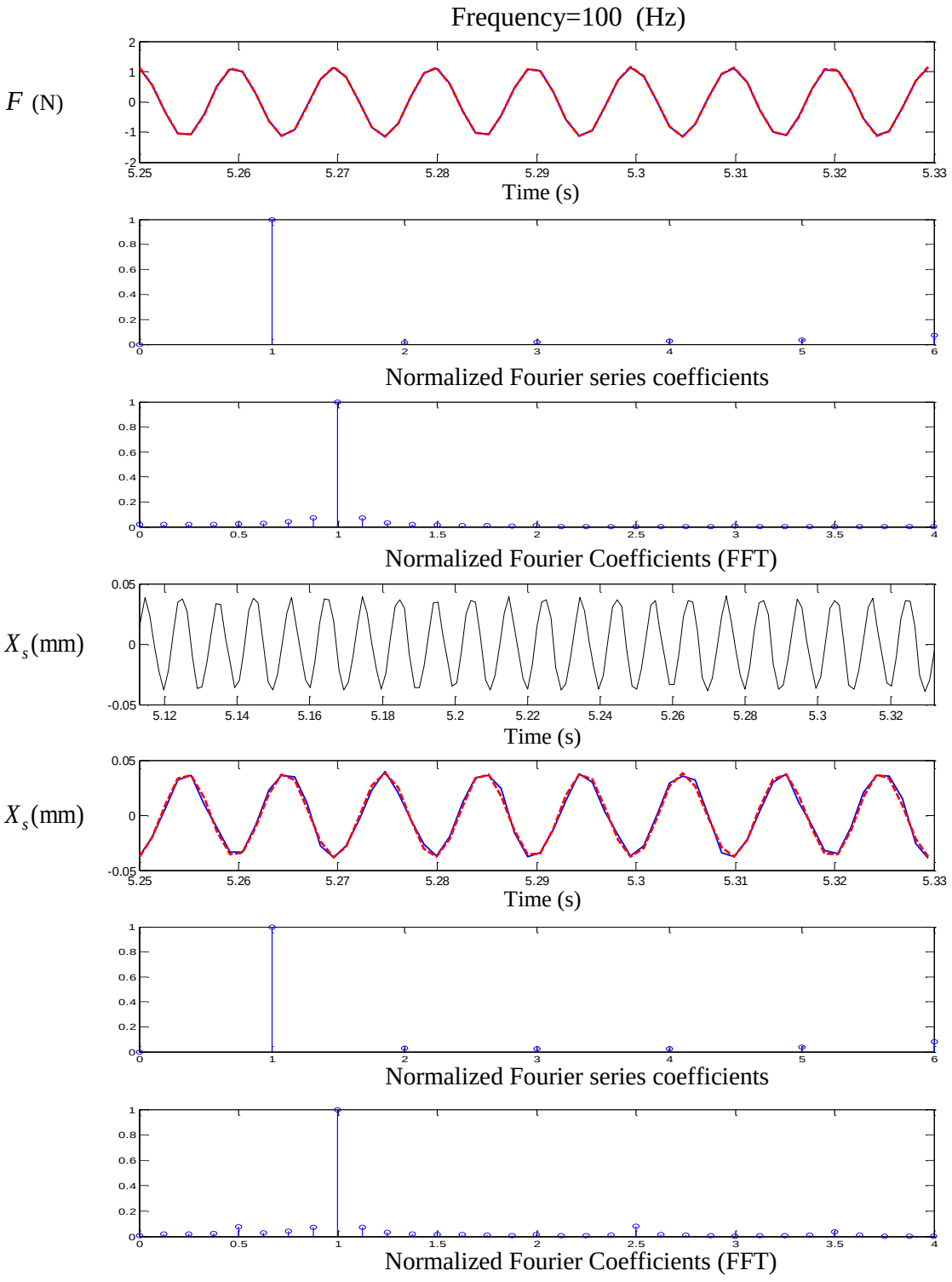

Figure 5.8 Time response and corresponding Fourier series coefficients for the primary system frequency response curves and input force. (linear tuned frequency $\omega_0 = 1.17$, nonlinear absorber stiffness $\gamma = 2.37\times10^{-3}$, mass ratio $\mu = 5.11\times10^{-2}$ and damping $\zeta_s = 5.95\times10^{-3}$, $\zeta = 1.18\times10^{-2}$). The actual response from numerical integration of the measured displacement is the solid line and the first-harmonic approximation is the dashed line. The corresponding excitation frequency is 100 (Hz).

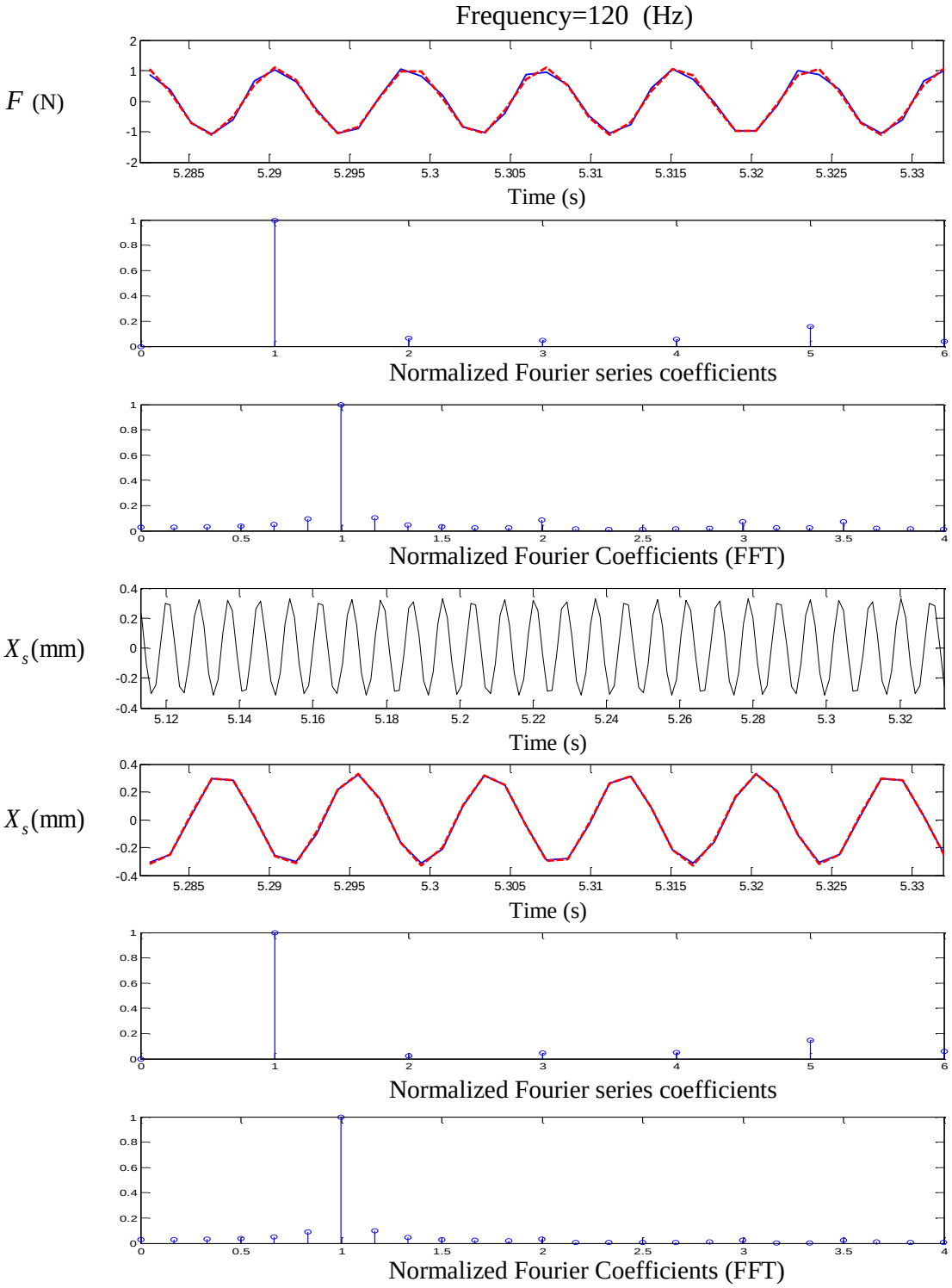

Figure 5.9 Time response and corresponding Fourier series coefficients for the primary system frequency response curves and input force. (linear tuned frequency $\omega_0 = 1.17$, nonlinear absorber stiffness $\gamma = 2.37\times10^{-3}$, mass ratio $\mu = 5.11\times10^{-2}$ and damping $\zeta_s = 5.95\times10^{-3}$, $\zeta = 1.18\times10^{-2}$). The actual response from numerical integration of the measured displacement is the solid line and the first-harmonic approximation is the dashed line. The corresponding excitation frequency is 120 (Hz).

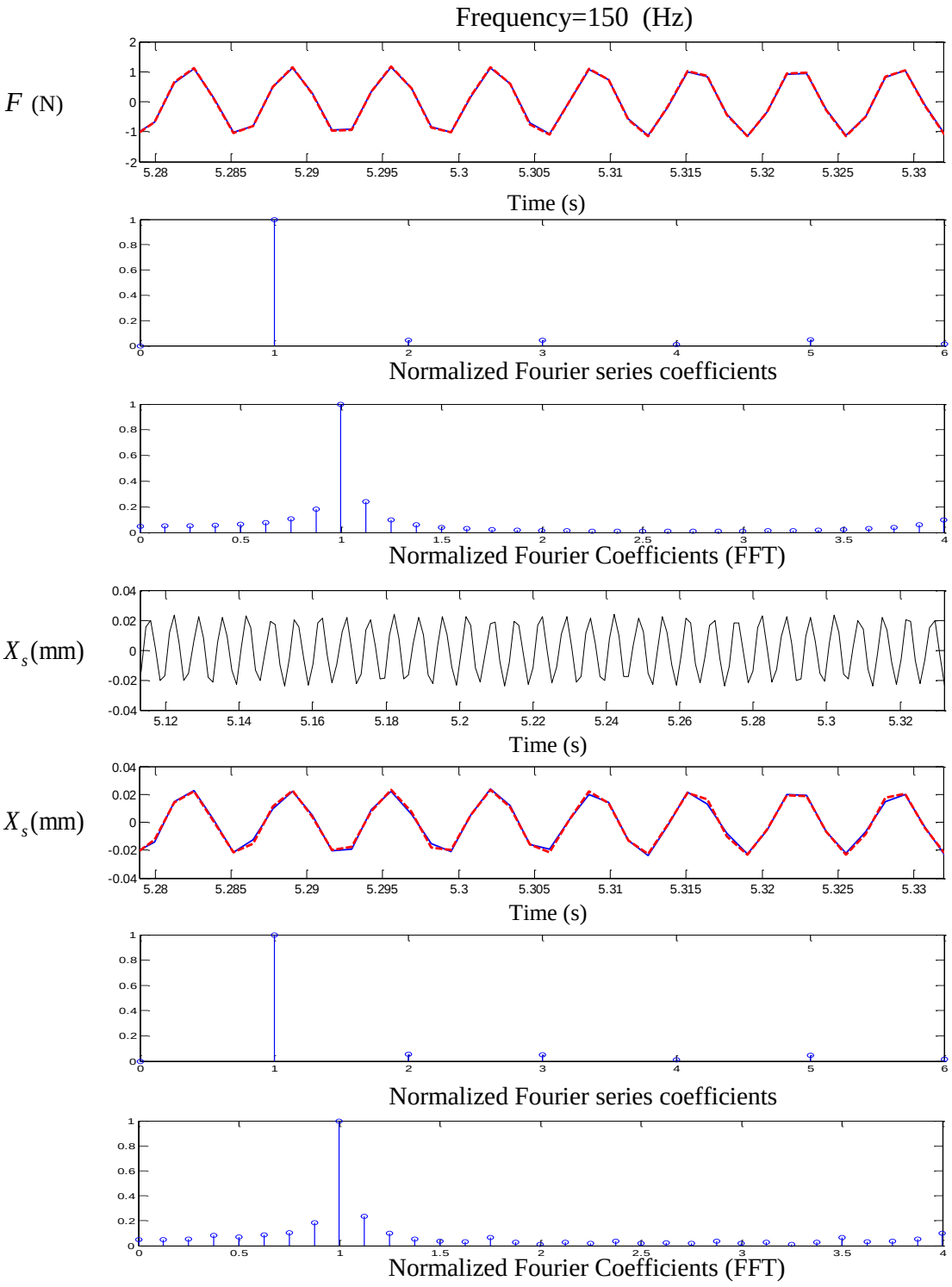

Figure 5.10 Time response and corresponding Fourier series coefficients for the primary system frequency response curves and input force. (linear tuned frequency $\omega_0 = 1.17$, nonlinear absorber stiffness $\gamma = 2.37\times10^{-3}$, mass ratio $\mu = 5.11\times10^{-2}$ and damping $\zeta_s = 5.95\times10^{-3}$, $\zeta = 1.18\times10^{-2}$). The actual response from numerical integration of the measured displacement is the solid line and the first-harmonic approximation is the dashed line. The corresponding excitation frequency is 150 (Hz).

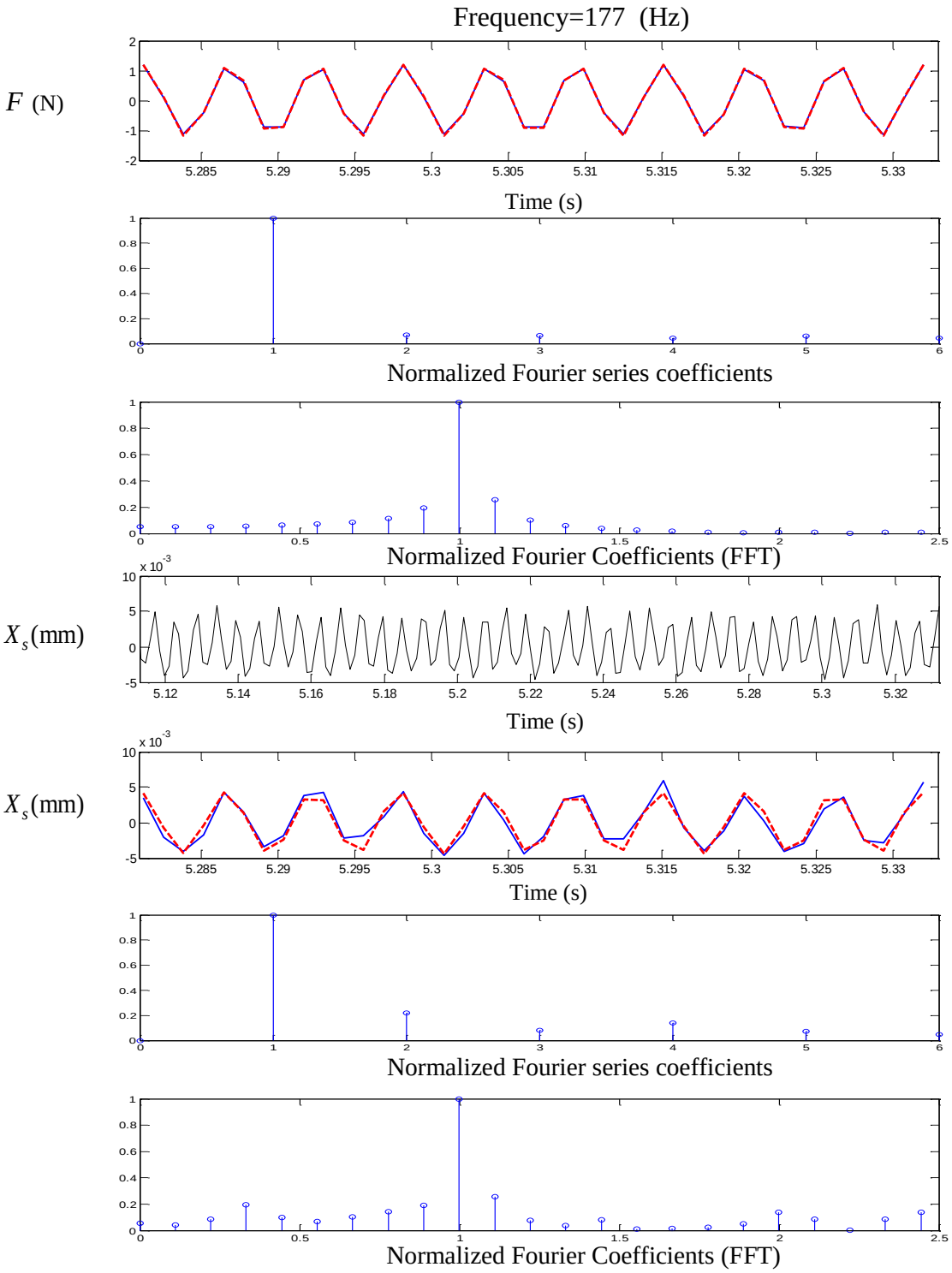

Figure 5.11 Time response and corresponding Fourier series coefficients for the primary system frequency response curves and input force. (linear tuned frequency $\omega_0 = 1.17$, nonlinear absorber stiffness $\gamma = 2.37 \times 10^{-3}$, mass ratio $\mu = 5.11 \times 10^{-2}$ and damping $\zeta_s = 5.95 \times 10^{-3}$, $\zeta = 1.18 \times 10^{-2}$). The actual response from numerical integration of the measured displacement is the solid line and the first-harmonic approximation is the dashed line. The corresponding excitation frequency is 177 (Hz).

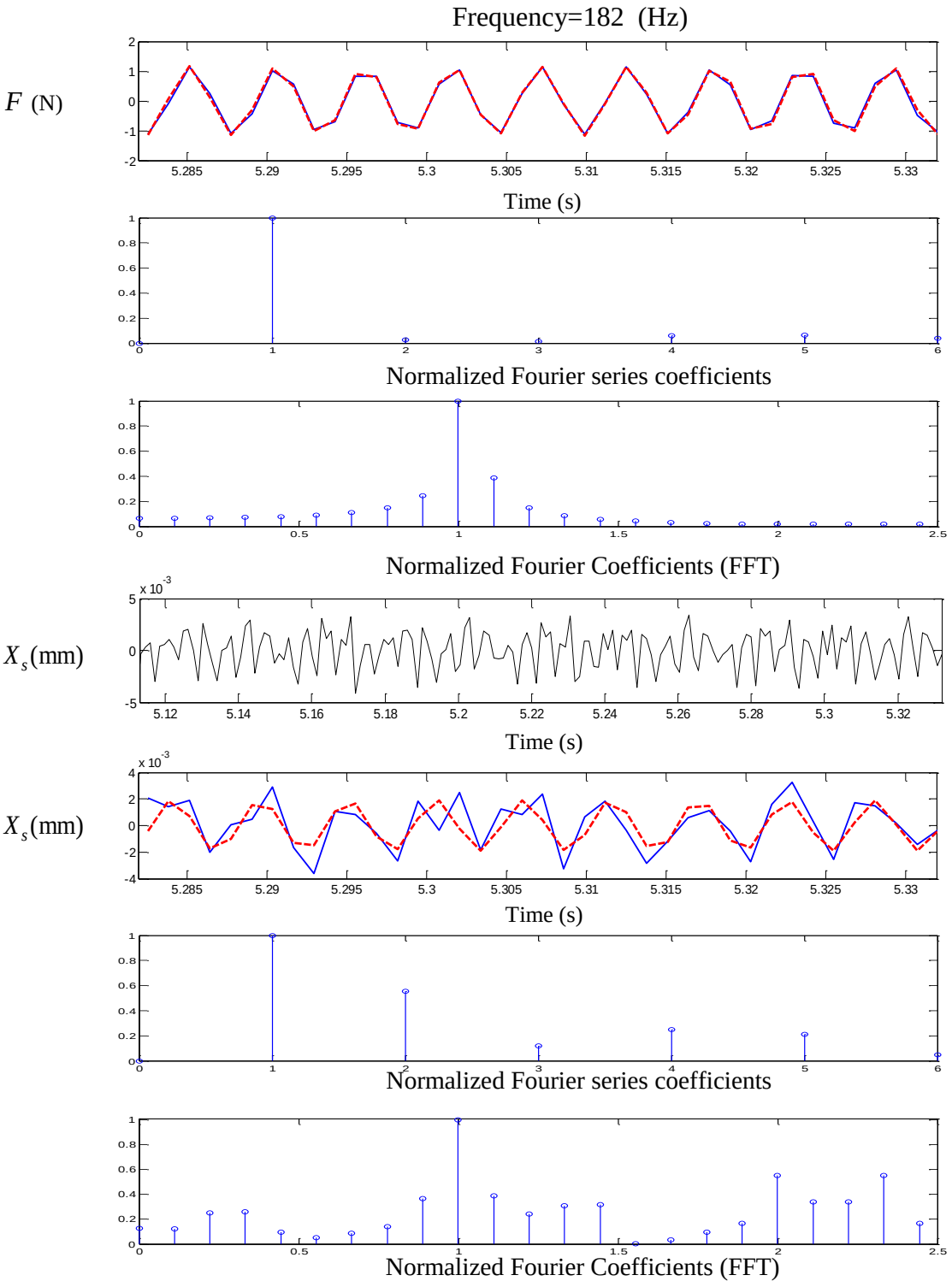

Figure 5.12 Time response and corresponding Fourier series coefficients for the primary system frequency response curves and input force. (linear tuned frequency $\omega_0 = 1.17$, nonlinear absorber stiffness $\gamma = 2.37 \times 10^{-3}$, mass ratio $\mu = 5.11 \times 10^{-2}$ and damping $\zeta_s = 5.95 \times 10^{-3}$, $\zeta = 1.18 \times 10^{-2}$). The actual response from numerical integration of the measured displacement is the solid line and the first-harmonic approximation is the dashed line. The corresponding excitation frequency is 182 (Hz).

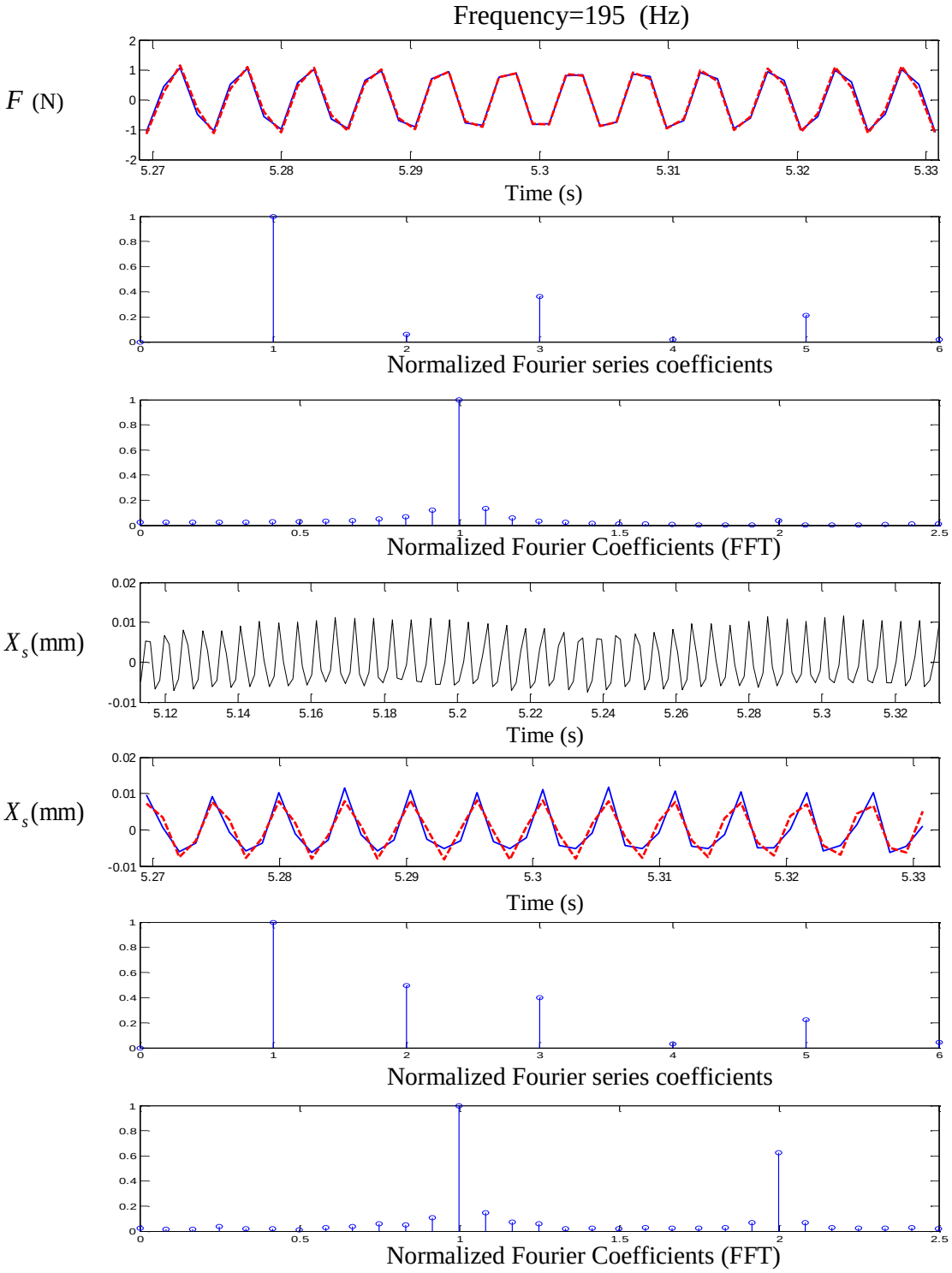

Figure 5.13 Time response and corresponding Fourier series coefficients for the primary system frequency response curves and input force. (linear tuned frequency $\omega_0 = 1.17$, nonlinear absorber stiffness $\gamma = 2.37 \times 10^{-3}$, mass ratio $\mu = 5.11 \times 10^{-2}$ and damping $\zeta_s = 5.95 \times 10^{-3}$, $\zeta = 1.18 \times 10^{-2}$). The actual response from numerical integration of the measured displacement is the solid line and the first-harmonic approximation is the dashed line. The corresponding excitation frequency is 195 (Hz).

5.2.3 Parameter estimation and model validation

The cantilever beam was made of aluminium with a total length $L = 0.09$ m, cross-sectional area $A = 0.04\ \text{m} \times 0.004\ \text{m}$, density ρ=2700 kg/m^3 and Young's modulus $E = 70$ GN/m^2. In addition, the circular plate was made of brass with thickness 0.2×10^{-3} m, area $A = \pi (0.026)^2$ m^2, density ρ=8500 kg/m^3 and Young's modulus $E = 110$ GN/m^2. The parameters for the systems tested were required in order to compare the experimental results with the model predictions. These parameters (m_s, c_s, k_s, m, c, k_1, k_3) were measured independently and were estimated as follows.

The Frequency Response Function (FRF) of the support frame attached to the cantilever beam without the absorber was measured using pseudo random force measurements. The primary system parameters (mass m_s, damping c_s and stiffness k_s) were estimated by fitting a theoretical single degree of freedom FRF to the experimental FRF and this is shown in Figure 5.14. In addition, the mass of the absorber m was measured directly. The value for the viscous damping coefficient c of the nonlinear absorber was estimated separately through the half power points method at low amplitude [2]. Moreover, the stiffnesses k_1 and k_3 of the nonlinear absorber were estimated using the measurements of the static displacement for applied static loads presented in Figure 5.15-16. The estimated parameters are listed in Table 5.1-2. The equivalent system parameters for the equation of motion written in the non-dimensional form of Equations (2.6a,b) are listed in Table 5.3. It is noted that the system was designed such that by simply adjusting the thickness of the plate, in the vibration absorber, the linear and nonlinear stiffness of the absorber could be varied. The value of nonlinearity selected was $\gamma \le 2.42 \times 10^{-3}$, i.e. for $F \le 1.13$, in order to produce responses with the amplitudes of the harmonic orders of the excitation frequency do not exceeding 5% compared to the amplitude of the response at the excitation frequency. The predicted frequency response curves for the absolute displacement of primary and absorber systems are presented in Figures 5.17-18.

	m_s (kg)	c_s (N · s/m)	k_s (N/m)	Input harmonic force F (N)
Low force amplitude	126×10^{-3}	1.26	8.93×10^{4}	0.11
High force amplitude				1.12

Table 5.1 The primary system parameters are estimated by fitting the FRF to the experimental test using a pseudo random force.

m (kg)	c (N · s/m)	k_1 (N/m)	k_3 (N/m^3)
6.44×10^{-3}	0.14	5.69×10^{3}	6.9×10^{10}

Table 5.2 The absorber system parameters are estimated the experimental test using the half power points method for c and static load measurement for k_1 and k_3.

	μ	ω_0	γ	ζ_s	ζ
Low force amplitude	5.11×10^{-2}	1.17	2.29×10^{-5}	5.95×10^{-3}	1.18×10^{-2}
High force amplitude			2.37×10^{-3}		

Table 5.3 Equivalent non-dimensional system parameters for the model predictions.

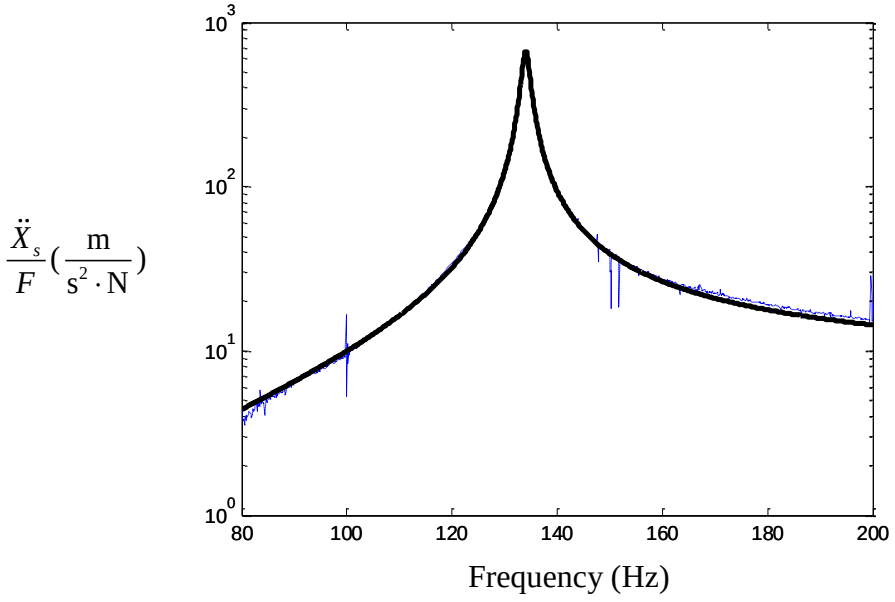

Figure 5.14 The measured frequency response curve for the support frame and beam structure using a pseudo random force. Measured result (dashed line), curve fitting (solid line).

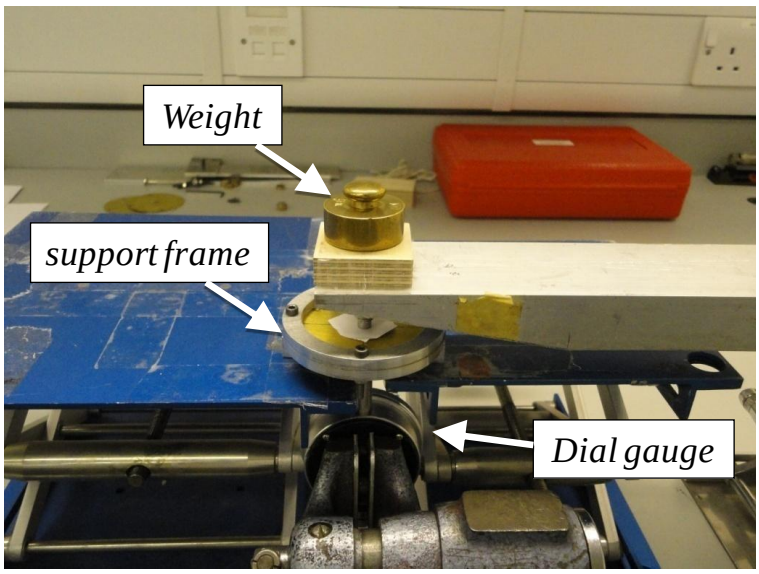

Figure 5.15 Photograph of the actual static load applied and static displacement measured with a dial gauge.

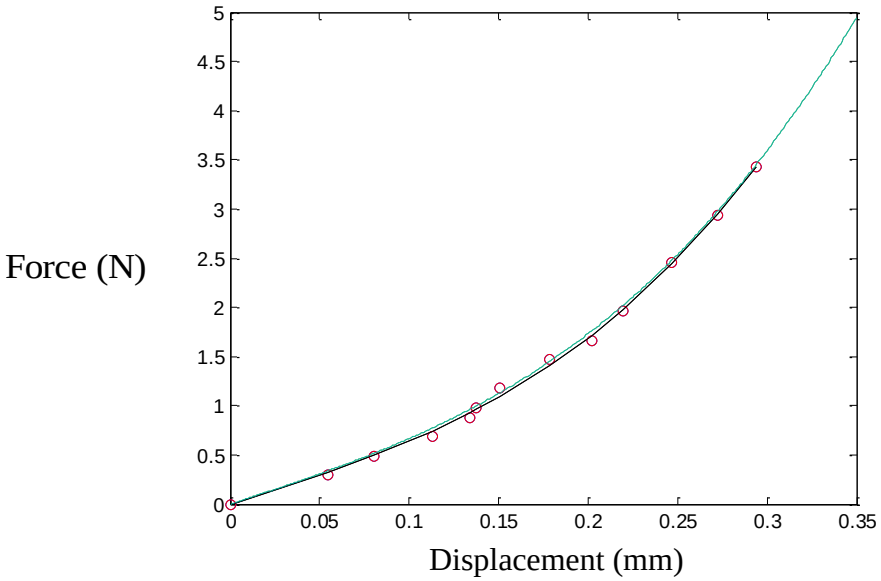

Figure 5.16 Force–displacement characteristic of the shim thickness 0.2 (mm) under static loads. Measured results ('$\circ$'), curve fitting for $f = k_1 y + k_3 y^3$ to estimate the coefficients (k_1, k_3) for the nonlinear regression for the static displacement (y) (solid line) and circular plate theory prediction [79] (dashed line).

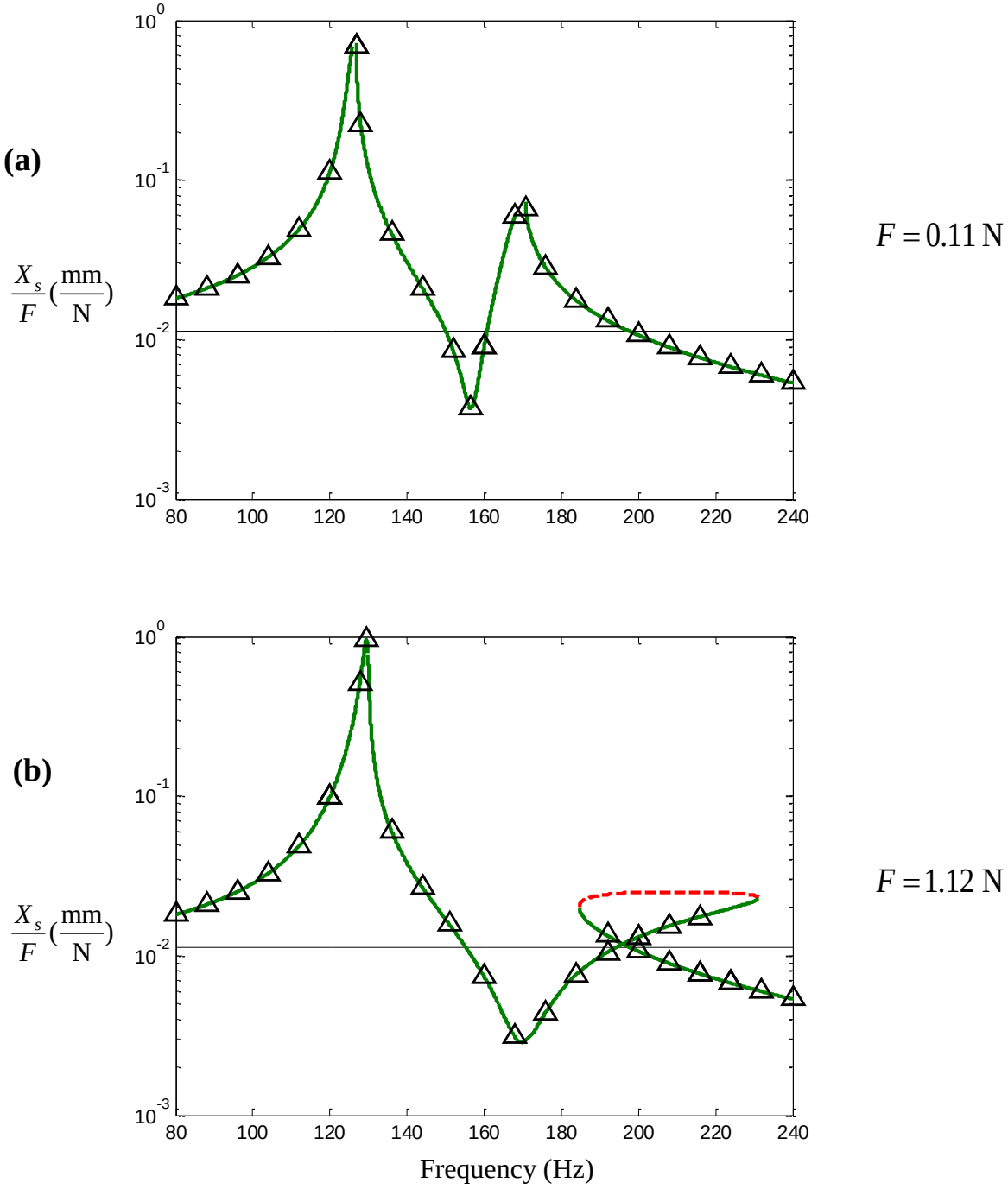

Figure 5.17 The predicted (HBM solution) frequency response curves for the absolute displacement of primary system whose properties are given in Table 5.3. Plate thickness 0.2 (mm): (a) Low force amplitude for $F = 0.11$ N and (b) High force amplitude of $F = 1.12$N. HBM solutions: stable solution (solid line), unstable solution (dashed line). Direct numerical integration of the predicted displacement response at the excitation frequency are shown by the symbol ($'\Delta'$).

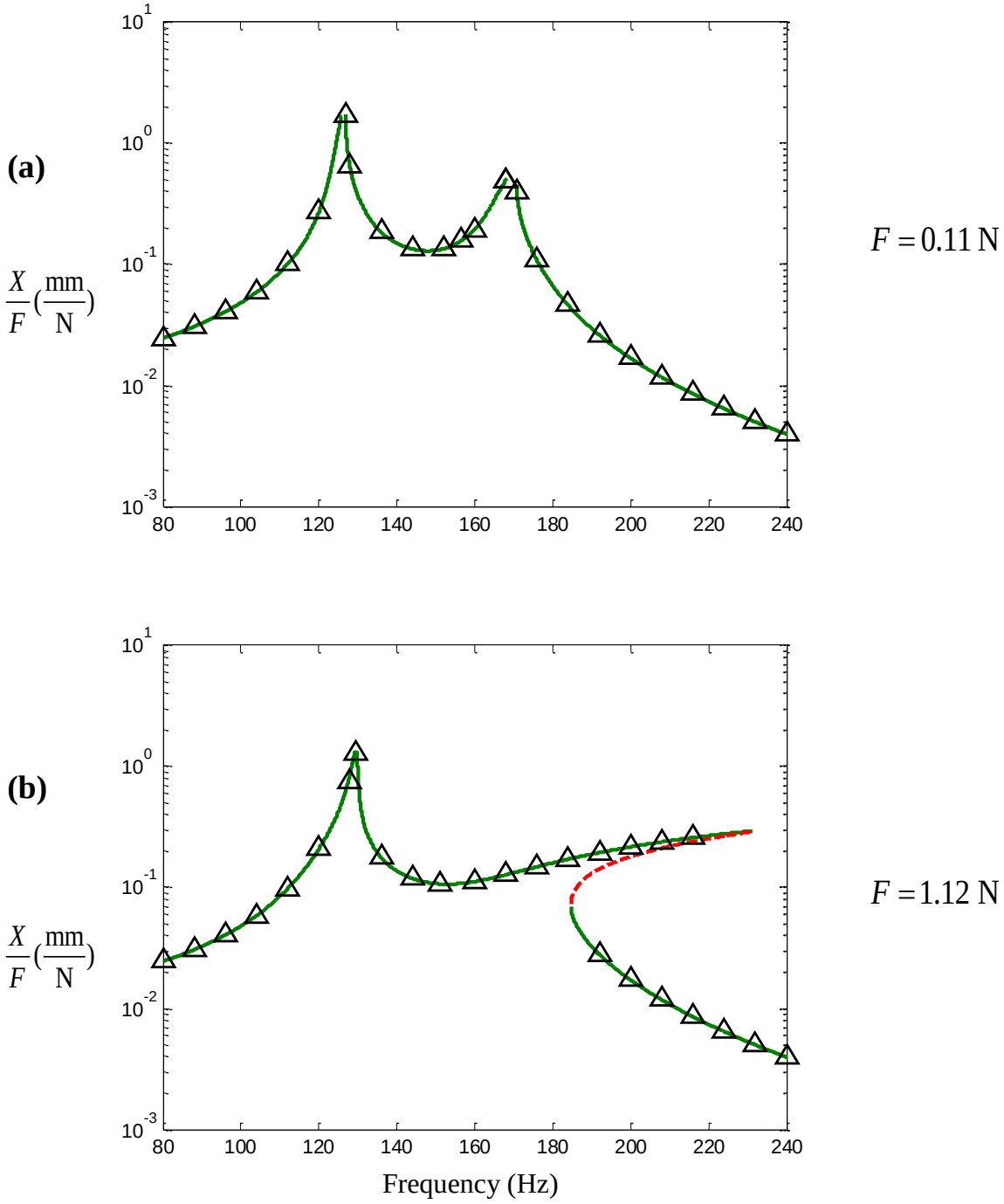

Figure 5.18 The predicted (HBM solution) frequency response curves for the absolute displacement of absorber whose properties are given in Table 5.3. Plate thickness 0.2 (mm): (a) Low force amplitude for $F = 0.11$ N and (b) High force amplitude of $F = 1.12$N . HBM solutions: stable solution (solid line), unstable solution (dashed line). Direct numerical integration of the predicted displacement response at the excitation frequency are shown by the symbol ($'\Delta'$).

Examining Figures 5.19, the high force input amplitude applied for the case of a nonlinear absorber produces a much wider vibration reduction bandwidth on the primary system compared to the low force input amplitude. The numerical parameters for the system are given in Table 5.3. The frequency response curves described by Equations (2.18) and (2.20) are shown in Figure 5.19-20. In addition, Figures 5.21-22 show the corresponding phase of the responses with respect the excitation. In Table 5.4, for the approximate HBM solution, the predicted bandwidth for vibration reduction is increased by about 311% and 188% for the increasing and decreasing input frequency cases, respectively, compared to the low amplitude 'linear' case. From the measurements, the corresponding reduction bandwidth is increased by about 30% and 10% for the increasing and decreasing input frequency cases, respectively. The measured results for the NDVA did not produce a much wider effective vibration reduction bandwidth compared to the predicted values. A reason found is that the harmonic response at the excitation frequency could not be obtained over the frequency range from 175 to 201 Hz. Other harmonics are present in the response, so that the HBM expressions are not a sufficiently accurate representation of the real behaviour around these frequencies. The time response and corresponding Fourier series coefficients for the excitation force were shown in section 5.2.2. Some studies from others [36, 37] also present this vibration behaviour and response.

In Table 5.5, in the low force amplitude test, the first resonance frequency peak in the experimental results occur at about 125 Hz compared to the approximate HBM solution at about 126 Hz, these correspond to an error of approximately 1 %. In addition, the effective tuned frequency occurs at about 160 Hz, compared to the approximate HBM solution at about 157 Hz. This difference in the tuned frequency is 2 %. In the high force amplitude test, the first resonance and effective tuned frequencies in the measurement results were found to occur at 123 Hz and 183 Hz respectively. Those results were compared to the approximate HBM solution at 128 Hz and 169 Hz respectively, these correspond to an error of approximately 4 % and 8.3 %. In the high force amplitude test, the first resonance and effective tuned frequencies produce larger differences compared to the approximate HBM solution. The reason for this could be possibly due to the stiffness parameter of the absorber k_1 was changed. It is suspected to be that the geometry of the thin plate being bolted on the circular ring for different tensions and material properties of the thin plate are affected by environmental factors such as temperature change.

In Figures 5.19(b), the measurement results did not contain the branch of the frequency response of the primary system at the lowest and highest jump-down frequencies. This reason could be probably due to the high amplitude of vibration of the primary and absorber system masses, which made it difficult to obtain this region using the actual experimental rig [66].

HBM solution	Bandwidth for increasing frequency (Hz)	Bandwidth improvement (%)	Bandwidth for decreasing frequency (Hz)	Bandwidth improvement (%)
Low force amplitude	9		9	
High force amplitude	37	311	28	188
Measurements	Bandwidth for increasing frequency (Hz)	Bandwidth improvement (%)	Bandwidth for decreasing frequency (Hz)	Bandwidth improvement (%)
Low force amplitude	10		10	
High force amplitude	13	30	11	10

Table 5.4 Comparison of the predicted and measured vibration reduction bandwidth due to the NDVA on the primary system frequency response curves.

HBM solution	Ω_{r1}	Ω_{r2}	Ω_t
Low force amplitude	126	170	157
High force amplitude	128	231	169
Measurements	Ω_{r1}	Ω_{r2}	Ω_t
Low force amplitude	125	170	160
High force amplitude	123	213	183

Table 5.5 Comparison of the predicted and measured resonance and effective tuned frequencies on the primary system frequency response curves.

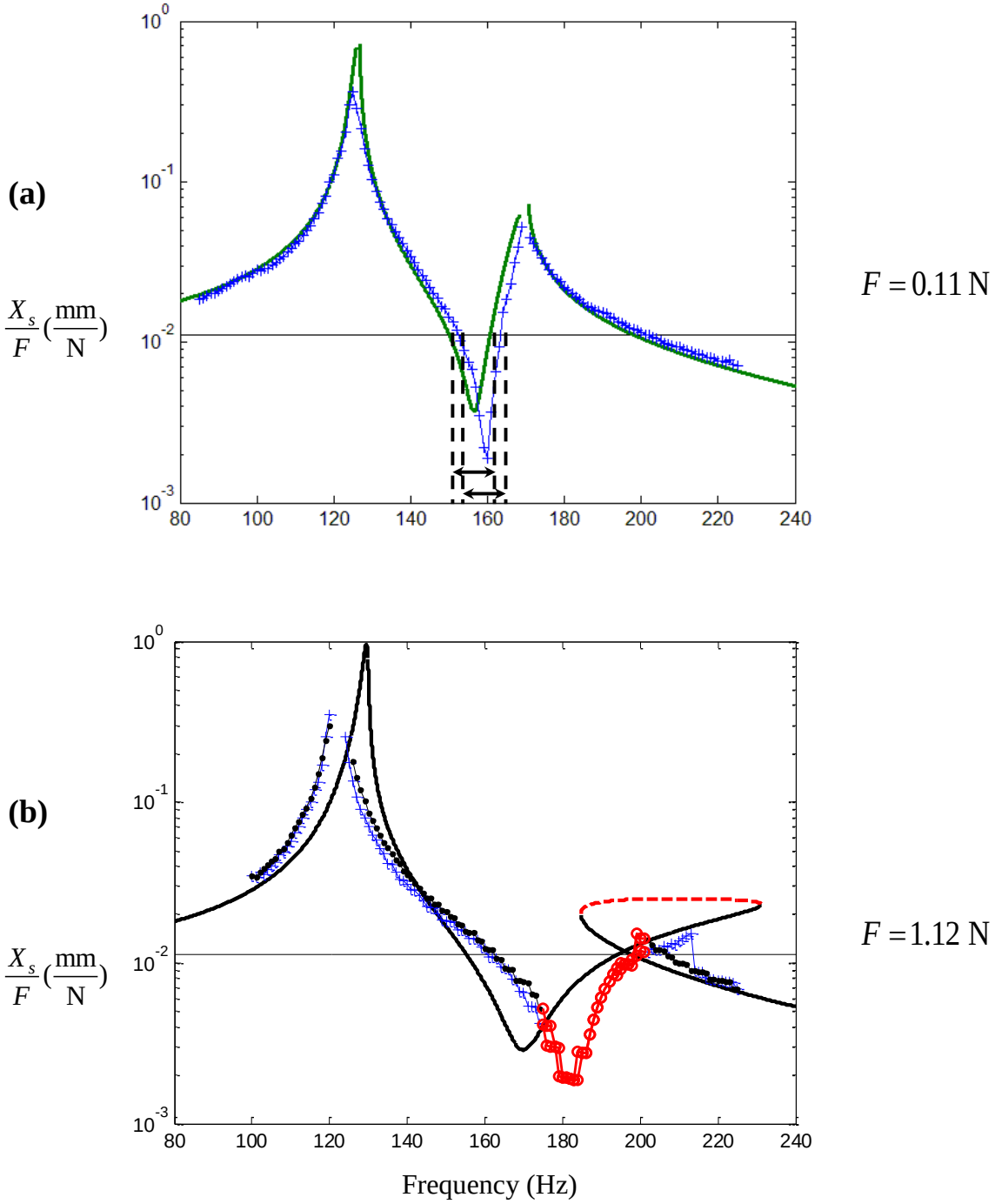

Figure 5.19 Comparison of the predicted (HBM solution) and measured frequency response curves for the absolute displacement of primary system whose properties are given in Table 5.3. Plate thickness 0.2 (mm): (a) Low force amplitude for $F = 0.11$ N and (b) High force amplitude of $F = 1.12$N . HBM solutions: stable solution (solid line), unstable solution (dashed line). Measured results: increasing frequency ('+'), decreasing frequency ('●'). The response is not harmonic (NH) at the corresponding excitation frequencies given by the symbol ('o').

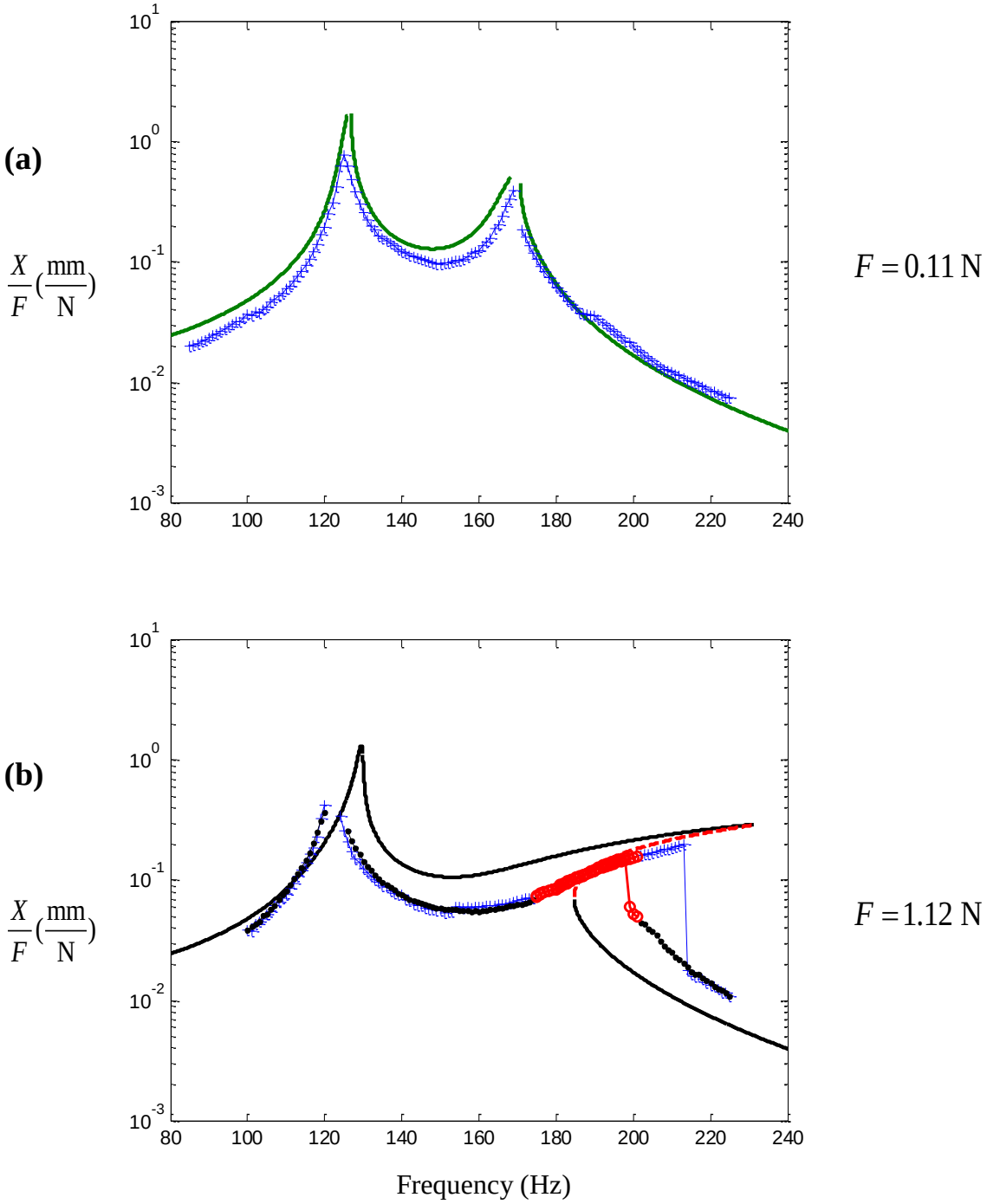

Figure 5.20 Comparison of the predicted (HBM solution) and measured frequency response curves for the absolute displacement of the absorber whose properties are given in Table 5.3. Plate thickness 0.2 (mm): (a) Low force amplitude for $F = 0.11\,\text{N}$ and (b) High force amplitude of $F = 1.12\text{N}$. HBM solutions: stable solution (solid line), unstable solution (dashed line). Measured results: increasing frequency ('+'), decreasing frequency ('•'). The response is not harmonic (NH) at the corresponding excitation frequencies given by the symbol ('o').

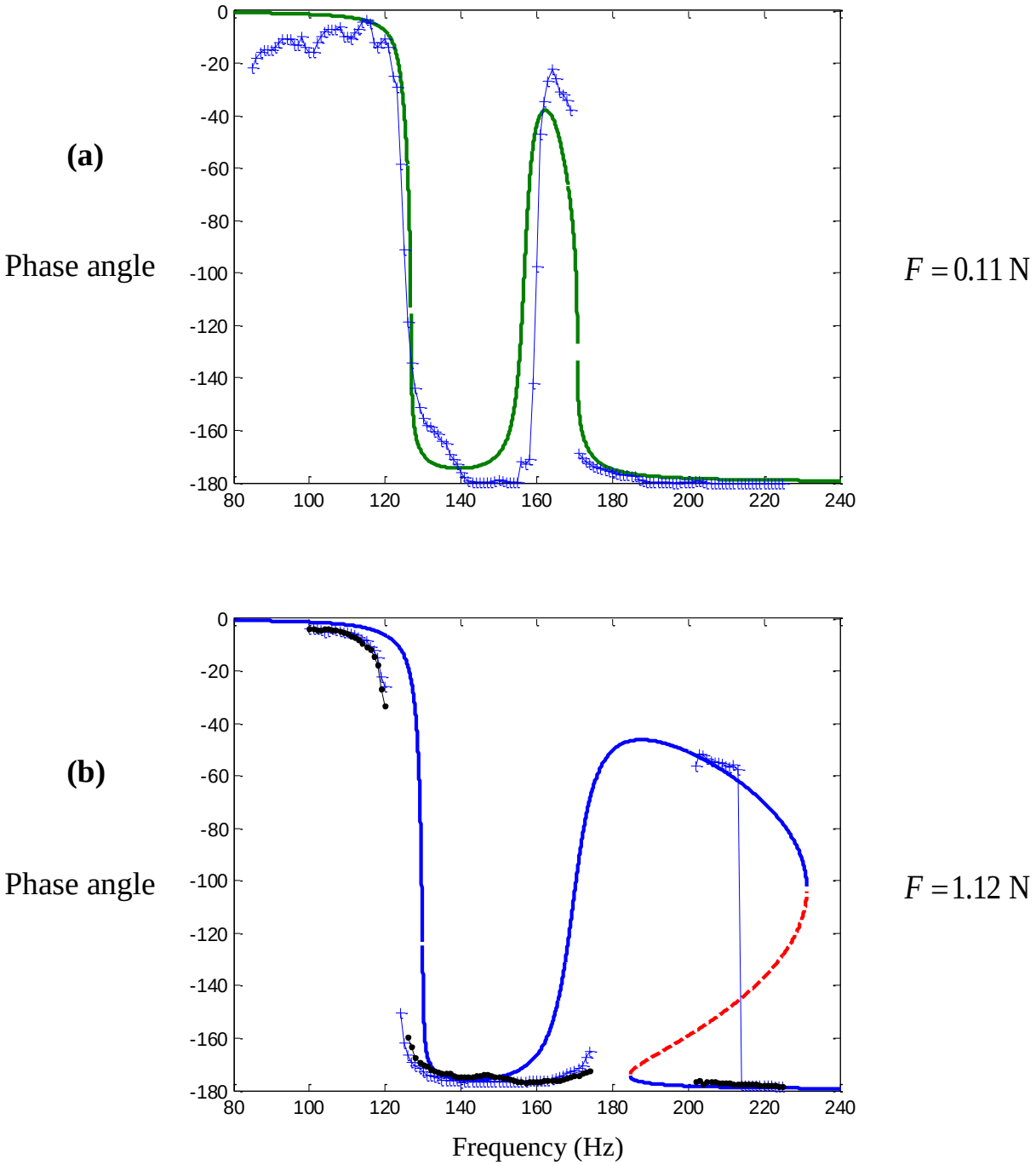

Figure 5.21 Comparison of the predicted (HBM solution) and measured frequency response curves for the phase of primary system whose properties are given in Table 5.3. Plate thickness 0.2 (mm): (a) Low force amplitude for $F = 0.11$ N and (b) High force amplitude of $F = 1.12$N . HBM solutions: stable solution (solid line), unstable solution (dashed line). Measured results: increasing frequency ('+'), decreasing frequency ('•').

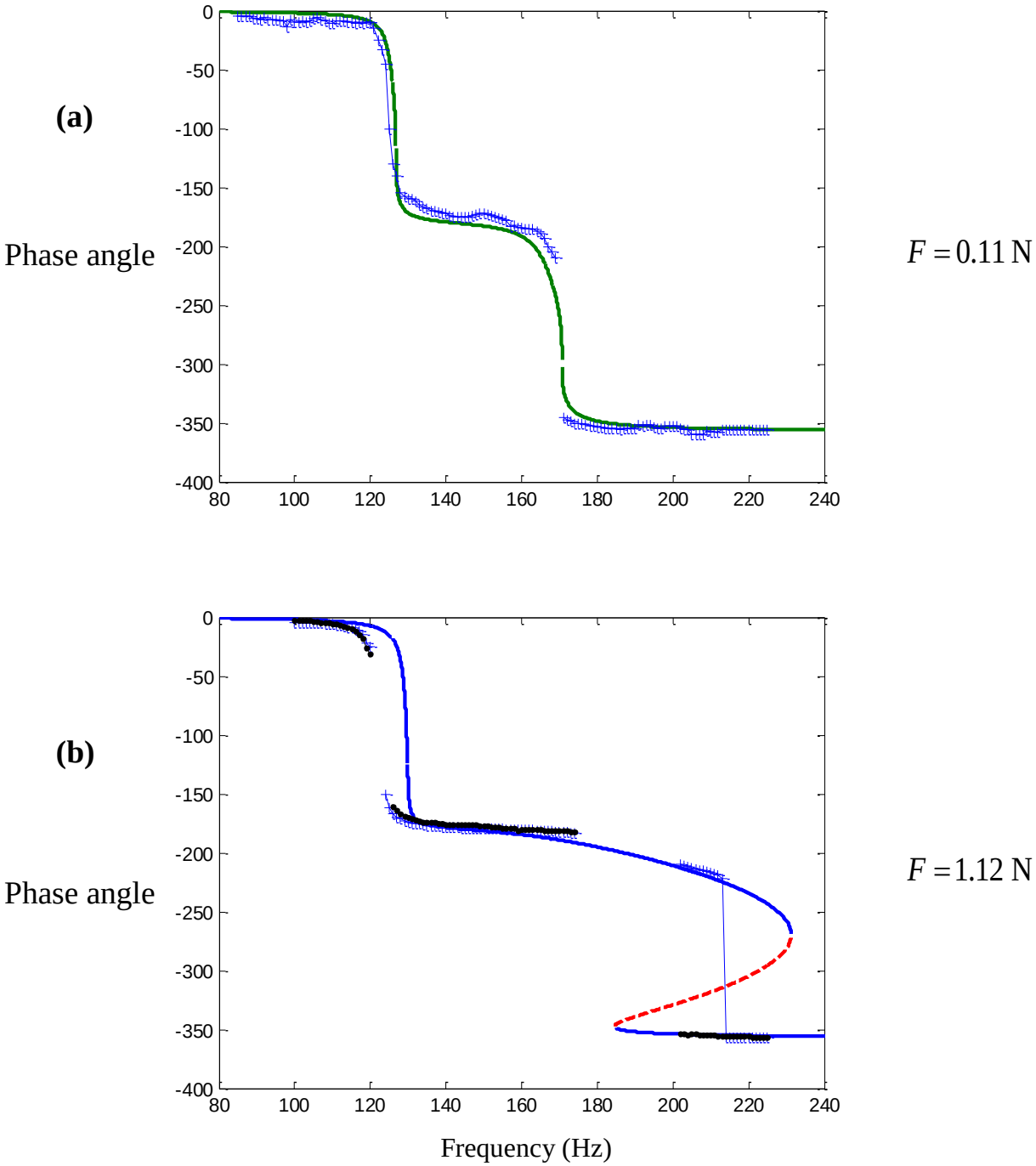

Figure 5.22 Comparison of the predicted (HBM solution) and measured frequency response curves for the phase of the absorber whose properties are given in Table 5.3. Plate thickness 0.2 (mm): (a) Low force amplitude for $F = 0.11$ N and (b) High force amplitude of $F = 1.12$N. HBM solutions: stable solution (solid line), unstable solution (dashed line). Measured results: increasing frequency ('+'), decreasing frequency ('●').

5.3 Experimental procedure and results: random excitation

The schematic diagram of the experimental apparatus used in the testing is shown in Figure 5.23. A signal generator and a random vibration equalizer control system (LMS Test Lab) produced a random white noise signal to drive the electro-dynamic shaker. For the measured data, the accelerometers and oscilloscope were used to measure and observe the system response respectively. Low-pass filtering was used to eliminate any aliasing effect in the measured sampled data. The data acquisition was captured using a data acquisition frequency analyser (LMS Test Lab) connected to a PC.

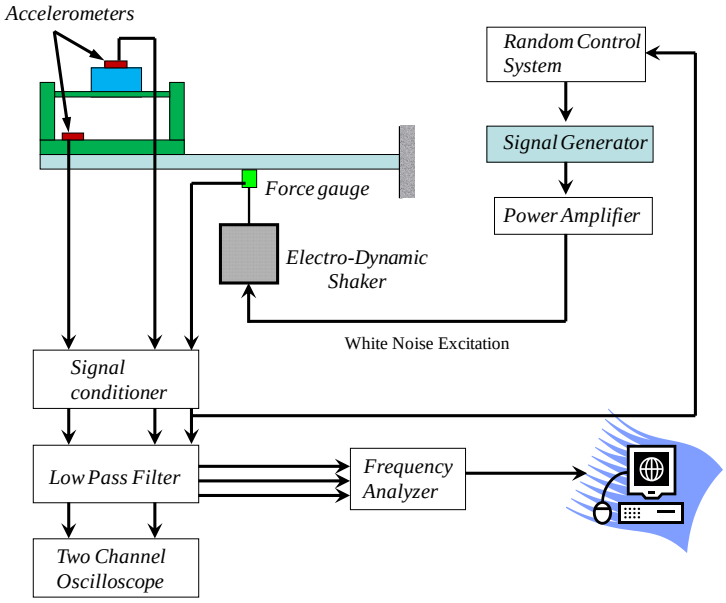

Figure 5.23 Schematic diagram of the instrumentation setup used for the laboratory tests under random excitation.

The measured time domain data included the input force amplitude produced by the shaker and the acceleration responses of the primary system and absorber, respectively. For each test, the shaker had a different force amplitude. The amplifier and control system used were configured so that the shaker produced rms force amplitudes of 0.17, 0.32 and 0.78 N. The shaker force output was controlled to produce a flat force amplitude power spectral density (PSD) with a bandwidth from 50 to 250 Hz shown in Figure 5.24. The data record length was 20.48 s with a sample rate of 800 Hz (with a Nyquist frequency of 400 Hz). The measurement data was repeated 20 times.

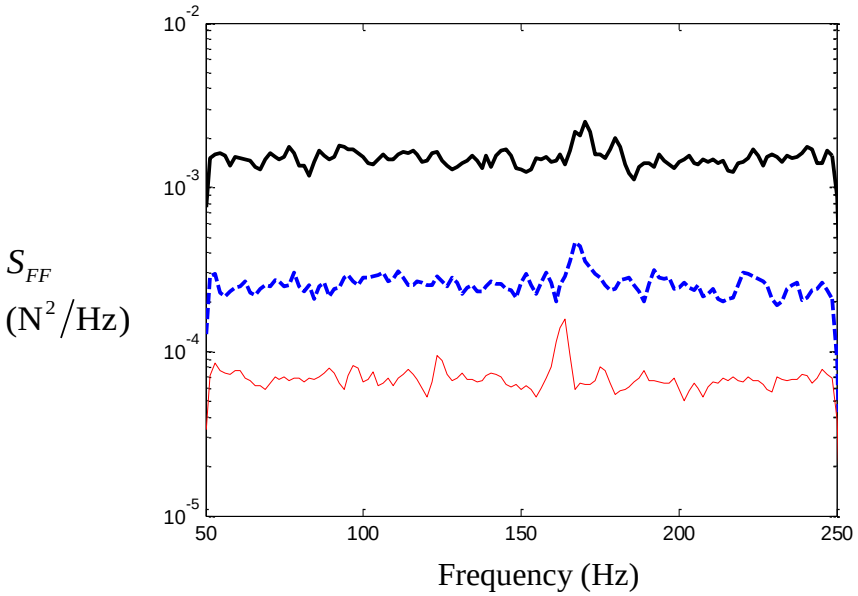

Figure 5.24 Comparison of the measured excitation PSD for signals whose rms force amplitudes are 0.17 N (thin line), 0.32 N (dashed line) and 0.78 N (thick line).

5.3.1. Parameter estimation and model validation

The corresponding experimental data and estimated system parameters (m_s, c_s, k_s, m, c, k_1, k_3) for the experimental tests were described previously. Using the above parameters, the natural frequencies of the primary system and absorber can be calculated.

For the random tests, the record length of the time history data was 20.48 s with a sample rate of 800 Hz (with a Nyquist frequency of 400 Hz). The linear beam structure system with attached nonlinear absorber was excited with a flat white noise random force input from 50 to 250 Hz. The input random time history was obtained from the specified PSD using the Inverse Fourier Transform. The corresponding procedure was described in section 4.1.2. The spectrum was zero padded above the maximum input frequency to 400 Hz to ensure a smooth time history that could be linearly interpolated while running the ODE solver. A 0.64s time record with a corresponding 1.56 Hz frequency spacing was used. The excitation was investigated for signals whose rms force amplitudes were 0.17, 0.32 and 0.78 N. The measured and estimated PSD of the random input are shown in Figure 5.25. The compared spectrum level is within ± 3 dB over the bandwidth.

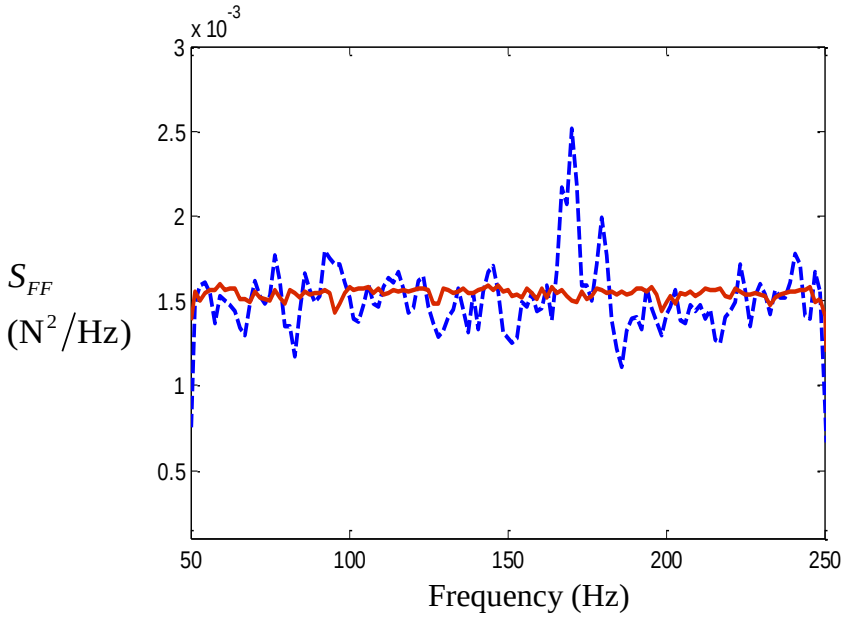

Figure 5.25 Comparison of the measured and predicted force excitation PSD for a rms force amplitude of 0.78 N . Measured result (dashed line), predicted solution (thick line).

5.3.2 Comparison with theoretical predictions

The experimental measurements and numerical predictions were obtained for both the random input and response data. The nonlinear absorber responses are investigated in both the frequency and time domains. The time series are often studied by observing the system mean square response and PSD. The PSD is a measure of the frequency content of the total process [60]. It has also been shown that the response of a system can be satisfactorily investigated by studying the mean square response [80]. The PSD and coherence can help to identify the response of the nonlinear system.

5.3.2.1 Statistical analysis of the time domain responses

For the time domain analysis, it is possible to determine the basic response statistics (i.e. the mean, variance, mean square, skew and kurtosis). The time domain analysis for the vibration reduction produced by the nonlinear absorber considered a determination of the statistical moments. The numerical parameters for the system are given in Table 5.1-2 and the dynamic response described by Equations (4.24a,b).

In Tables 5.6-7, the acceleration response of the primary system and absorber show the possible effect of the nonlinear behaviour of the system, indicated by a kurtosis value less than 3. In Figure 5.26(a), the mean square primary system acceleration for the nonlinear absorber is higher compared to the linear absorber case when the force input amplitudes are $\sigma_F = 0.32$ N and $\sigma_F = 0.78$ N. In addition, comparison of the mean square primary system acceleration of the nonlinear absorber, the predicted solutions are higher compared to the measured results. It can also be found that, for the predicted solutions, the acceleration response PSD of the primary system at the first mode is much higher compared to the measured results shown in Figure 5.28. This is in agreement in that the acceleration response PSD in the first mode is the main contribution to the mean square response. The cumulative mean square acceleration of the primary system from the numerical predictions also produces a higher response than the measured result in Figure 5.30.

In Figure 5.27, the standard deviation of the primary system acceleration with an attached nonlinear absorber did not produce a proportional increase as the input rms of the force increased. The acceleration response exhibits a nonlinear behaviour due to the nonlinear absorber. In addition, the standard deviation of the primary system acceleration using the nonlinear absorber is higher compared to the linear absorber for higher force amplitudes $\sigma_F \geq 0.32$ N. For the standard deviation acceleration of the absorber, the nonlinear absorber response is lower compared to the linear absorber response.

For some range of values for the nonlinear absorber, the primary system response appears to exhibit a detrimental effect at increased input force magnitudes. Hence a negative effect for vibration control. This means that the nonlinear absorber still needs to be designed for the particular application, with the best parameters for reducing the vibration response of the primary system.

Input force	Measurements				Predictions			
σ_F (N)	$\mu_{\ddot{x}_s}$ (m/s^2)	$\psi^2_{\ddot{x}_s}$ $((m/s^2)^2)$	$\iota_{\ddot{x}_s}$	$\kappa_{\ddot{x}_s}$	$\mu_{\ddot{x}_s}$ (m/s^2)	$\psi^2_{\ddot{x}_s}$ $((m/s^2)^2)$	$\iota_{\ddot{x}_s}$	$\kappa_{\ddot{x}_s}$
0.17	-1.4×10^{-3}	62.8	2.8×10^{-2}	2.9	-1.1×10^{-4}	55.8	1.1×10^{-3}	3.0
0.32	2.7×10^{-3}	149.5	4.5×10^{-2}	3.4	-1.6×10^{-4}	234.6	-8.2×10^{-4}	2.9
0.78	3.5×10^{-4}	877.5	7.4×10^{-2}	3.0	-4.4×10^{-3}	1631	1.4×10^{-4}	2.8

Table 5.6 Comparison of the measured and predicted mean, mean square, skewness and kurtosis of the acceleration response on the primary system whose properties are given in Tables 5.1-2.

Input force	Measurements				Predictions			
σ_F (N)	$\mu_{\ddot{x}}$ (m/s^2)	$\psi^2_{\ddot{x}}$ $((m/s^2)^2)$	$\iota_{\ddot{x}}$	$\kappa_{\ddot{x}}$	$\mu_{\ddot{x}}$ (m/s^2)	$\psi^2_{\ddot{x}}$ $((m/s^2)^2)$	$\iota_{\ddot{x}}$	$\kappa_{\ddot{x}}$
0.17	8.7×10^{-4}	761.1	-1.7×10^{-2}	3.3	-1.3×10^{-3}	741.2	8.2×10^{-4}	3.0
0.32	5.1×10^{-3}	1675	-2.0×10^{-2}	4.0	-1.6×10^{-3}	2691	2.3×10^{-3}	3.0
0.78	9.8×10^{-3}	8262	-2.5×10^{-2}	3.4	-1.3×10^{-2}	12880	7.1×10^{-3}	3.3

Table 5.7 Comparison of the measured and predicted mean, mean square, skewness and kurtosis of the acceleration response of the absorber mass whose properties are given in Tables 5.1-2.

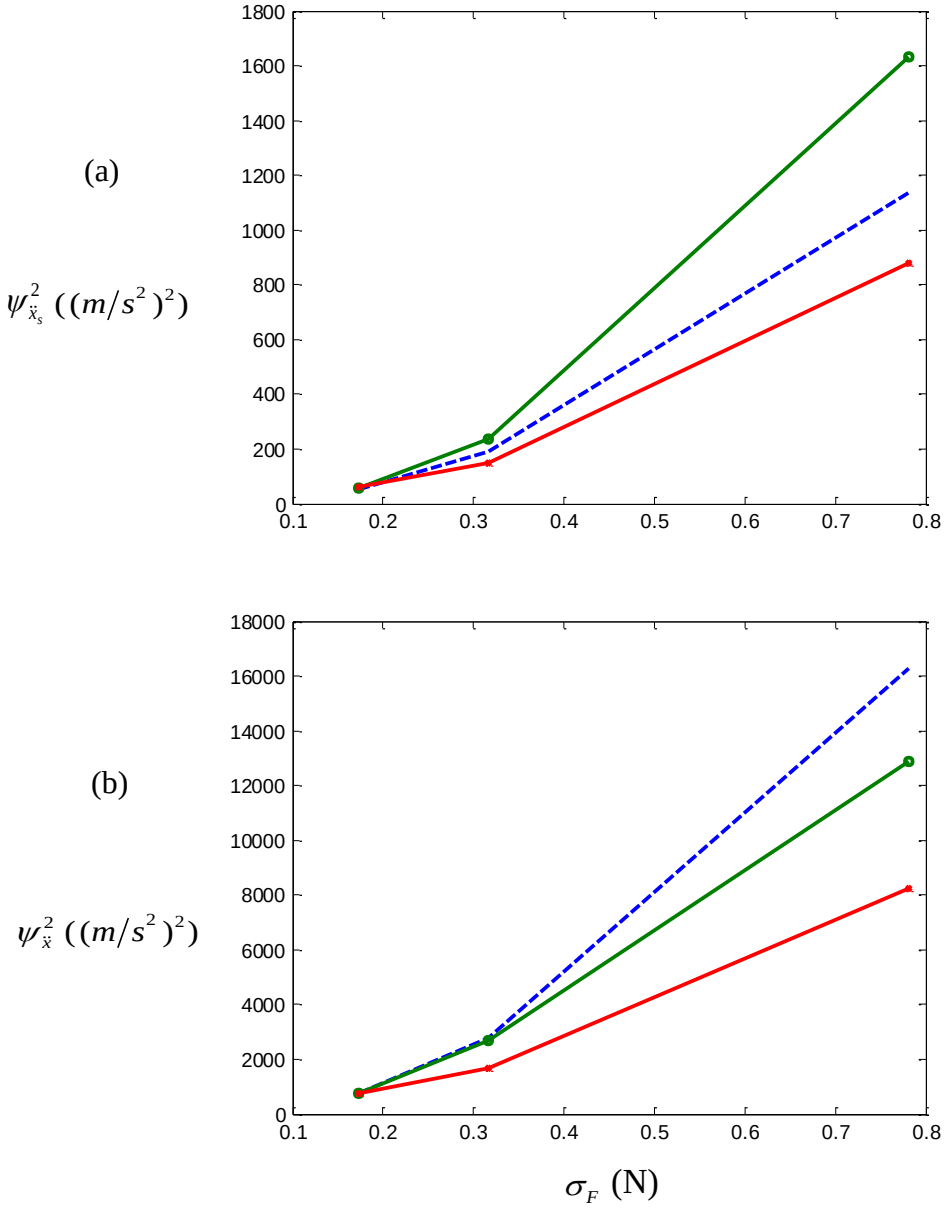

Figure 5.26 Comparison of the predicted and measured mean square acceleration for (a) the primary system and (b) the absorber whose properties are given in Tables 5.1-2. Plate thickness 0.2 (mm): the corresponding overall rms force amplitudes are $\sigma_F = 0.17$ N, $\sigma_F = 0.32$ N and $\sigma_F = 0.78$ N. The linear absorber for predicted solution is dashed line. The nonlinear absorber for the predicted solution ('o') and measured result ('×').

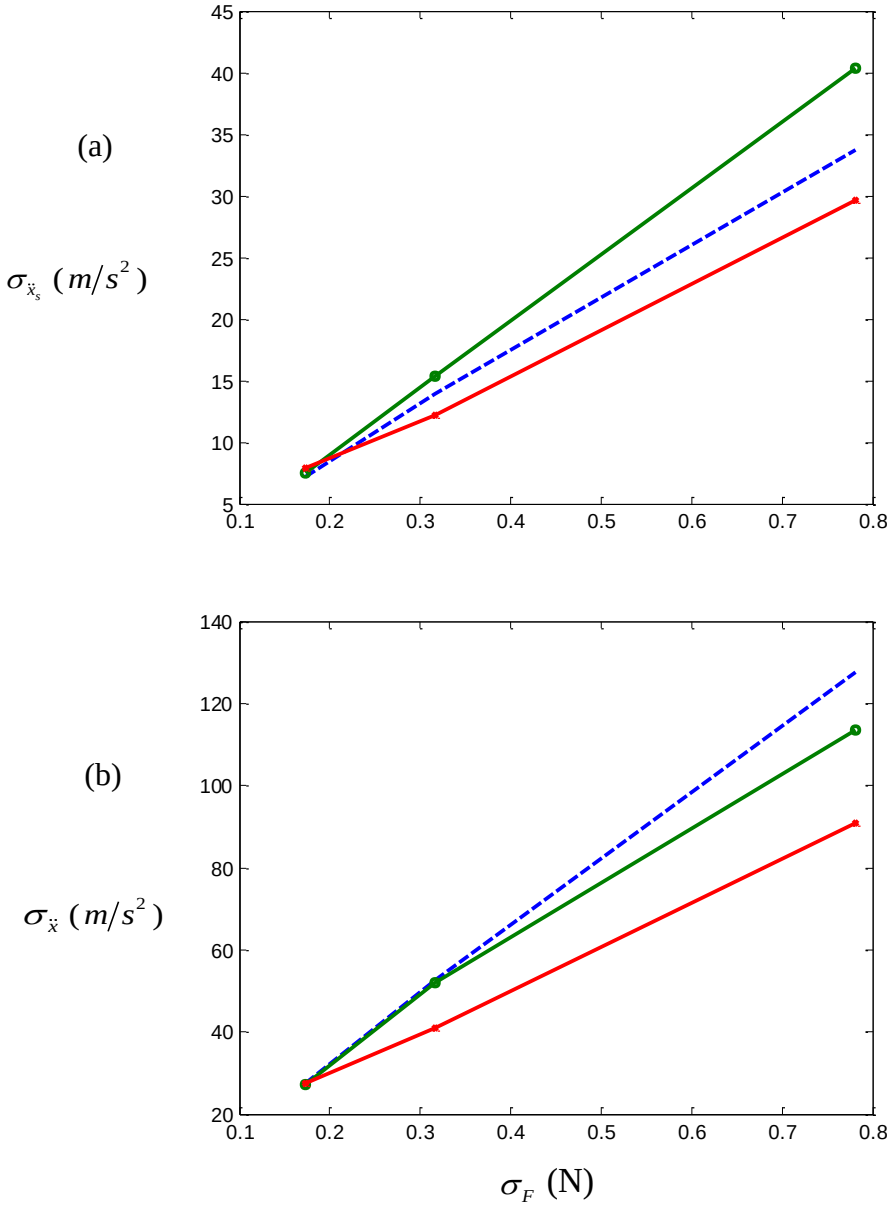

Figure 5.27 Comparison of the predicted and measured standard deviation acceleration for (a) the primary system and (b) the absorber whose properties are given in Tables 5.1-2. Plate thickness 0.2 (mm): the corresponding overall rms force amplitudes are $\sigma_F = 0.17$ N, $\sigma_F = 0.32$ N and $\sigma_F = 0.78$ N. The linear absorber for predicted solution is dashed line. The nonlinear absorber for the predicted solution ('o') and measured result ('×').

5.3.2.2 Frequency domain comparison

The numerical parameters for the system are given in Table 5.1-2 and the dynamic response described by Equations (4.24a,b). The acceleration response spectral density function (PSD) for the primary system and absorber are presented in Figures 5.28-29. The sample size chosen for the PSD estimates was 0.64 s, which resulted in a frequency resolution f of 1.56 Hz. The PSD estimates were made using a Hanning window, 67% overlap of the windowed data [78] and a sample rate of 800 Hz resulting in 512 points for the FFT and 256 frequency domain points. The resolution f of 1.56 Hz was chosen as a compromise between the number of averages and frequency resolution (see Section 4.1.3). In this case, the number of averages was chosen as 32.

The high force input amplitude applied produces a much broader PSD for the primary and absorber response at the second mode. Also, it results in a larger vibration response at higher frequencies compared to the low force input amplitude. The reason for this could be possibly due to the nonlinear stiffness effect. For high force amplitude, the effect on the primary system acceleration response is to shift the first resonance, the effective tuned frequency and the second resonance to higher frequencies compared to the low force amplitude. The second mode of the primary system does not obviously exhibit a resonance or peak response compared to low force excitation. These responses show a nonlinear effect compared to the linear absorber case. The measured first resonance and effective tuned frequencies are different compared to the numerical predictions. One reason could be due to the stiffness parameter of the absorber k_1 changing. It is suspected that the geometry of the thin plate being bolted to the circular ring for different tensions and material properties are affected by environmental factors, such as room temperature changes. For the high force amplitude test, comparison of the mean square primary system acceleration showed that the predictions were higher than the measured results. The cumulative mean square acceleration of the primary system from the numerical simulations are also higher than the measured result, as seen in Figure 5.30.

The coherence functions show where it is likely that the vibration absorber behaves quite linearly and is able to account for most of the response at the low force input amplitude, i.e. see Figure 5.32-33. However, the coherence response does not fair as well for the high force input amplitude, which might result from extraneous measurement noise or more likely significant nonlinear response in the output due to the nonlinear absorber behaviour. For low force input amplitude applied on the primary system, the coherence response for a lightly damped system

does not present good values at the resonances and effective tuned frequencies due to bias errors. The bias error can be reduced by improving the resolution of the FRF estimates, i.e. the frequency resolution bandwidth should be reduced which requires more time history data.

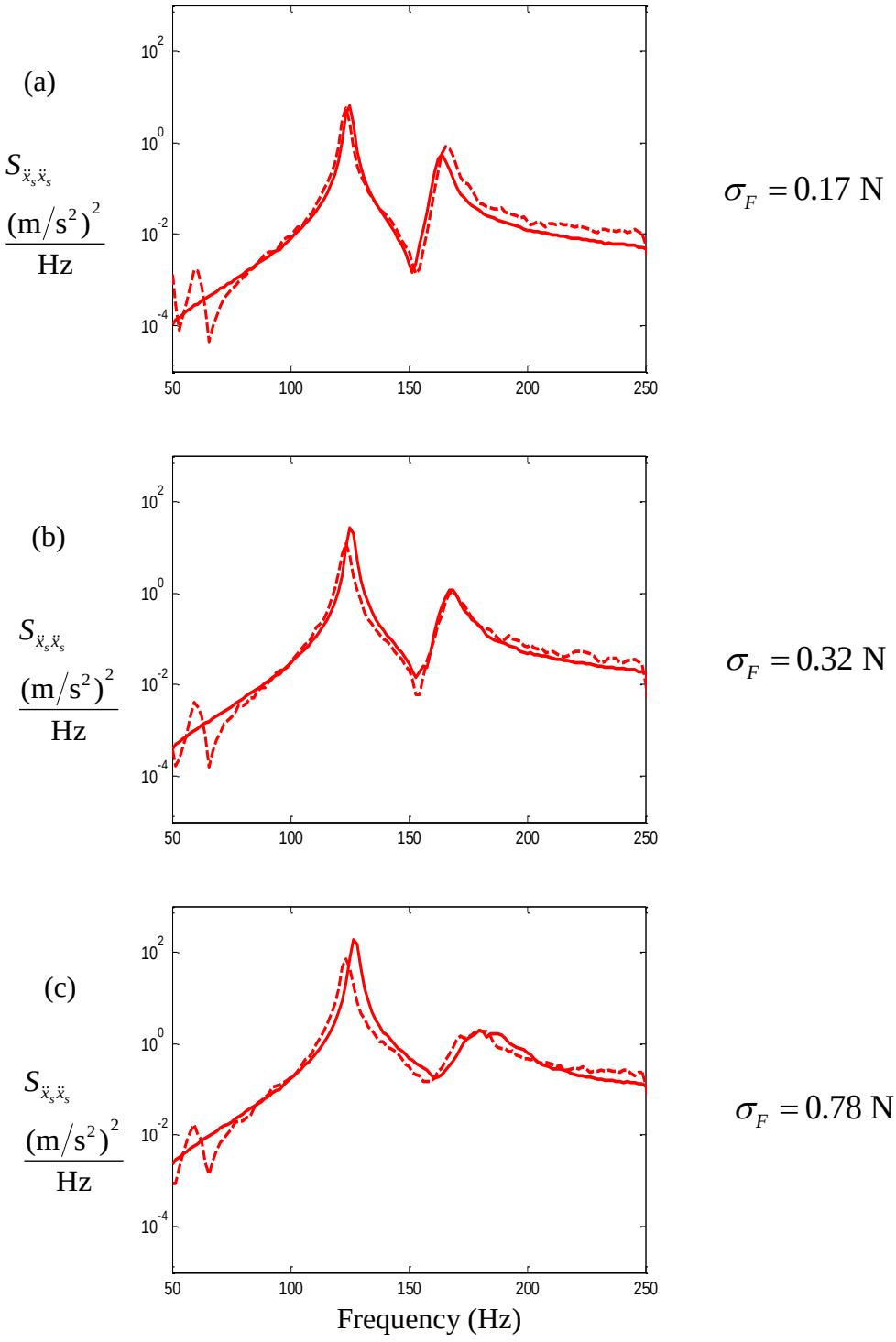

Figure 5.28 Comparison of the predicted and measured acceleration PSD for a primary system whose properties are given in Tables 5.1-2. Plate thickness 0.2 (mm): the corresponding overall rms force amplitudes are (a) $\sigma_F = 0.17$ N, (b) $\sigma_F = 0.32$ N and (c) $\sigma_F = 0.78$ N. The predicted response solution is given by the solid line. The measured response is the dashed line.

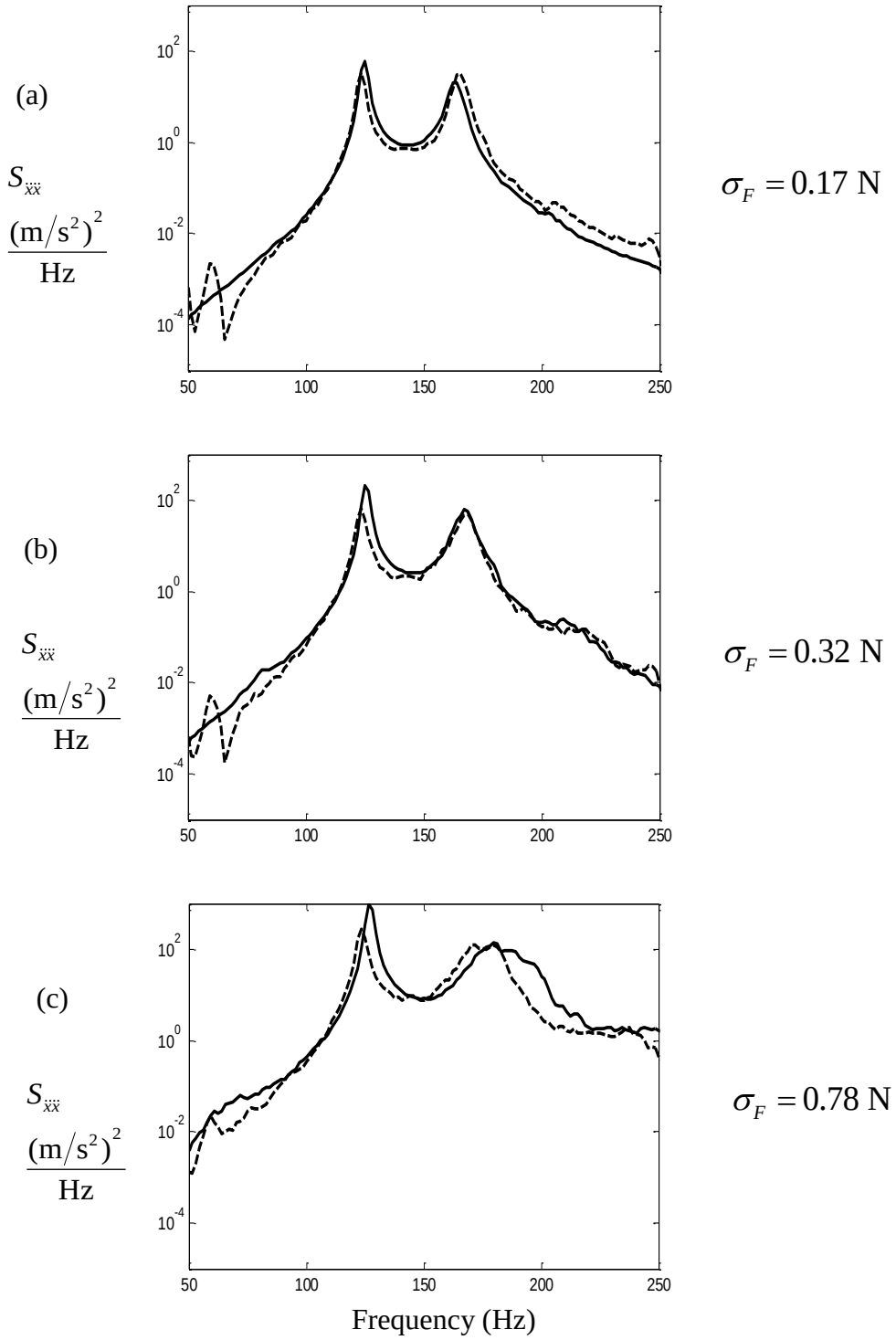

Figure 5.29 Comparison of the predicted and measured acceleration PSD for an absorber whose properties are given in Tables 5.1-2. Plate thickness 0.2 (mm): the corresponding overall rms force amplitudes are (a) $\sigma_F = 0.17$ N, (b) $\sigma_F = 0.32$ N and (c) $\sigma_F = 0.78$ N. The predicted response solution is given by the solid line. The measured response is the dashed line.

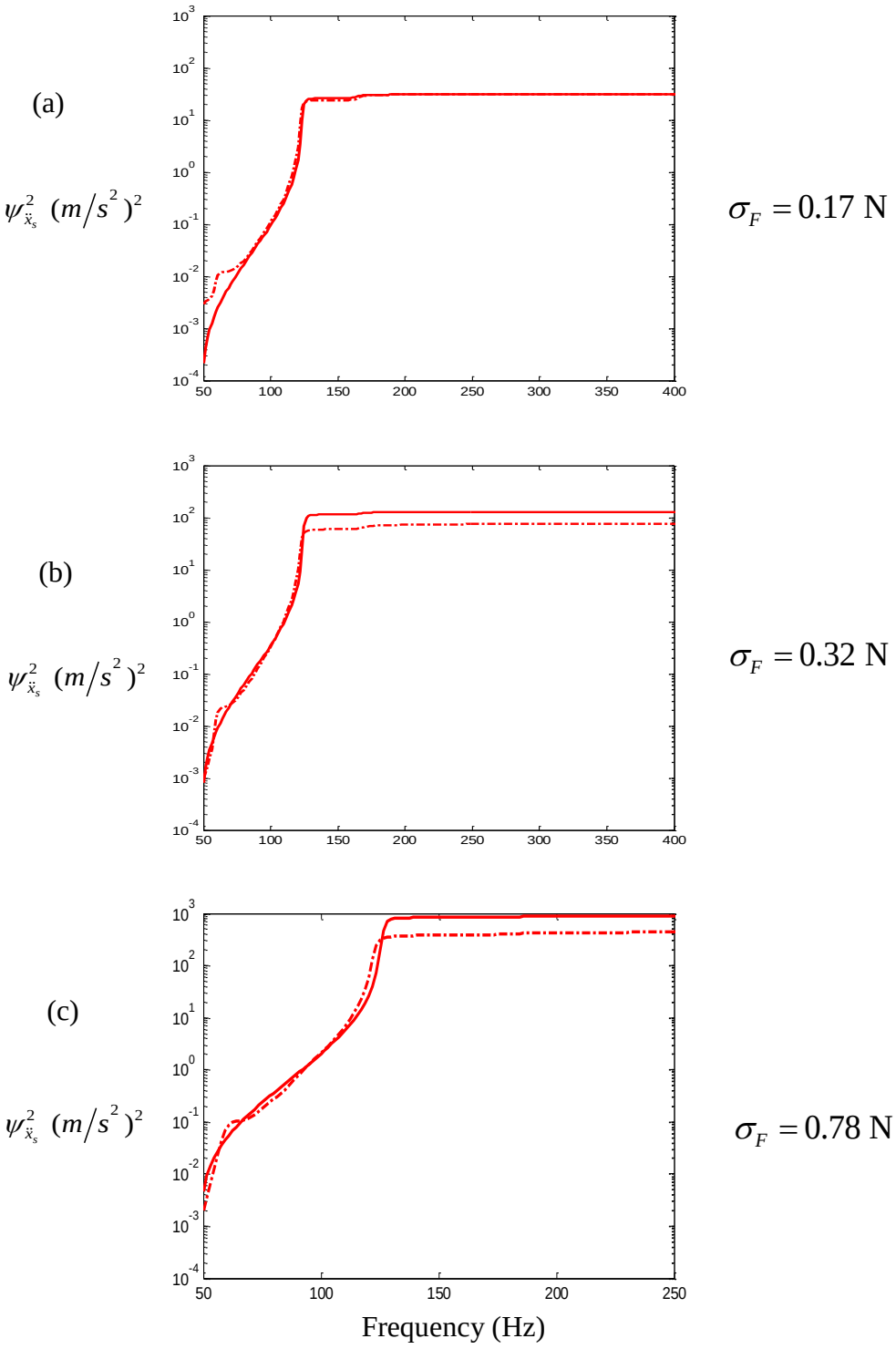

Figure 5.30 Comparison of the predicted and measured cumulative mean square acceleration of the primary system whose properties are given in Tables 5.1-2. Plate thickness 0.2 (mm): the corresponding overall rms force amplitudes are (a) $\sigma_F = 0.17$ N, (b) $\sigma_F = 0.32$ N and (c) $\sigma_F = 0.78$ N. The predicted response solution is given by the solid line. The measured response is the dashed line.

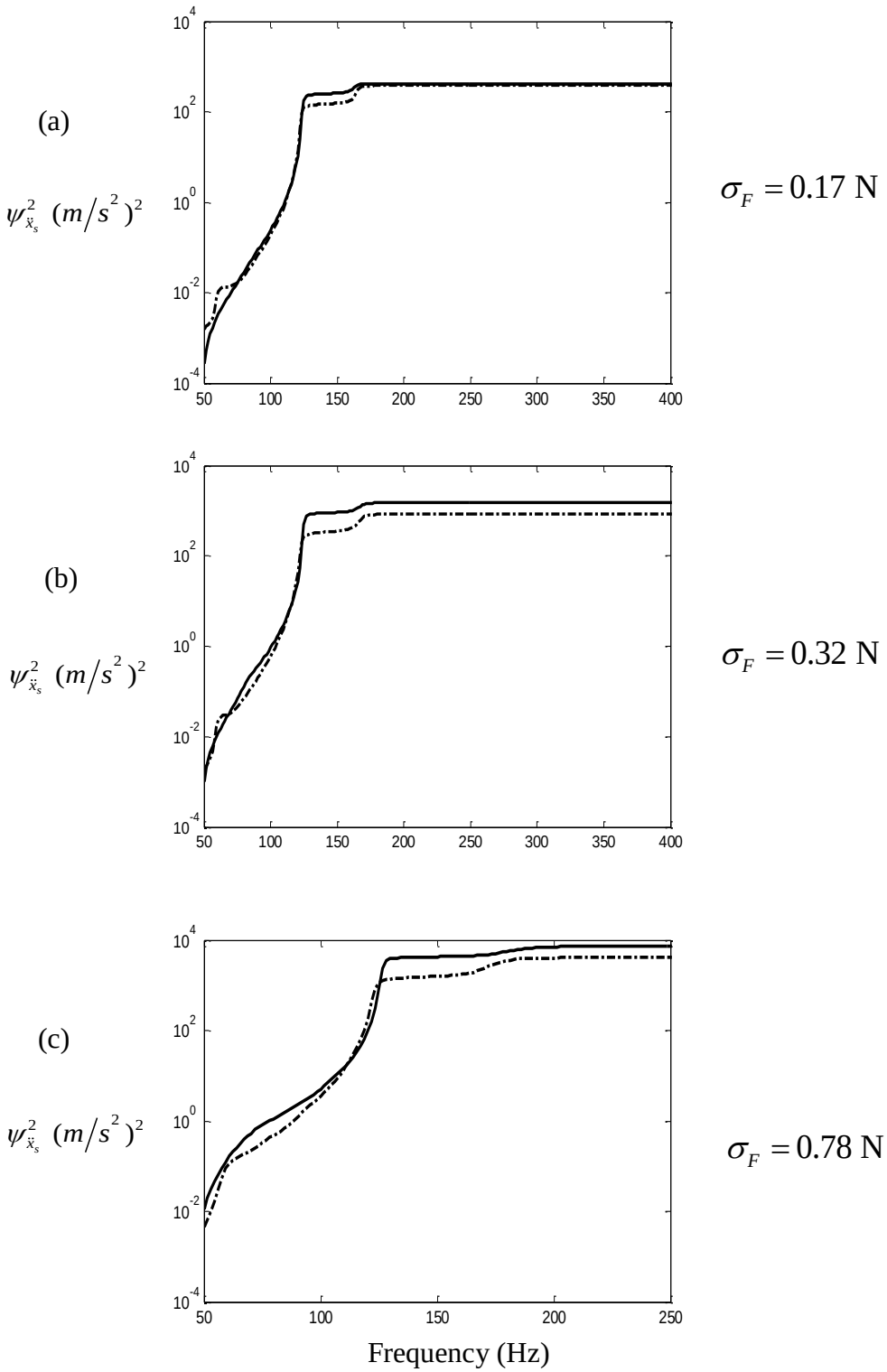

Figure 5.31 Comparison of the predicted and measured cumulative mean square acceleration of the absorber whose properties are given in Tables 5.1-2. Plate thickness 0.2 (mm): the corresponding overall rms force amplitudes are (a) $\sigma_F = 0.17$ N, (b) $\sigma_F = 0.32$ N and (c) $\sigma_F = 0.78$ N. The predicted response solution is given by the solid line. The measured response is the dashed line.

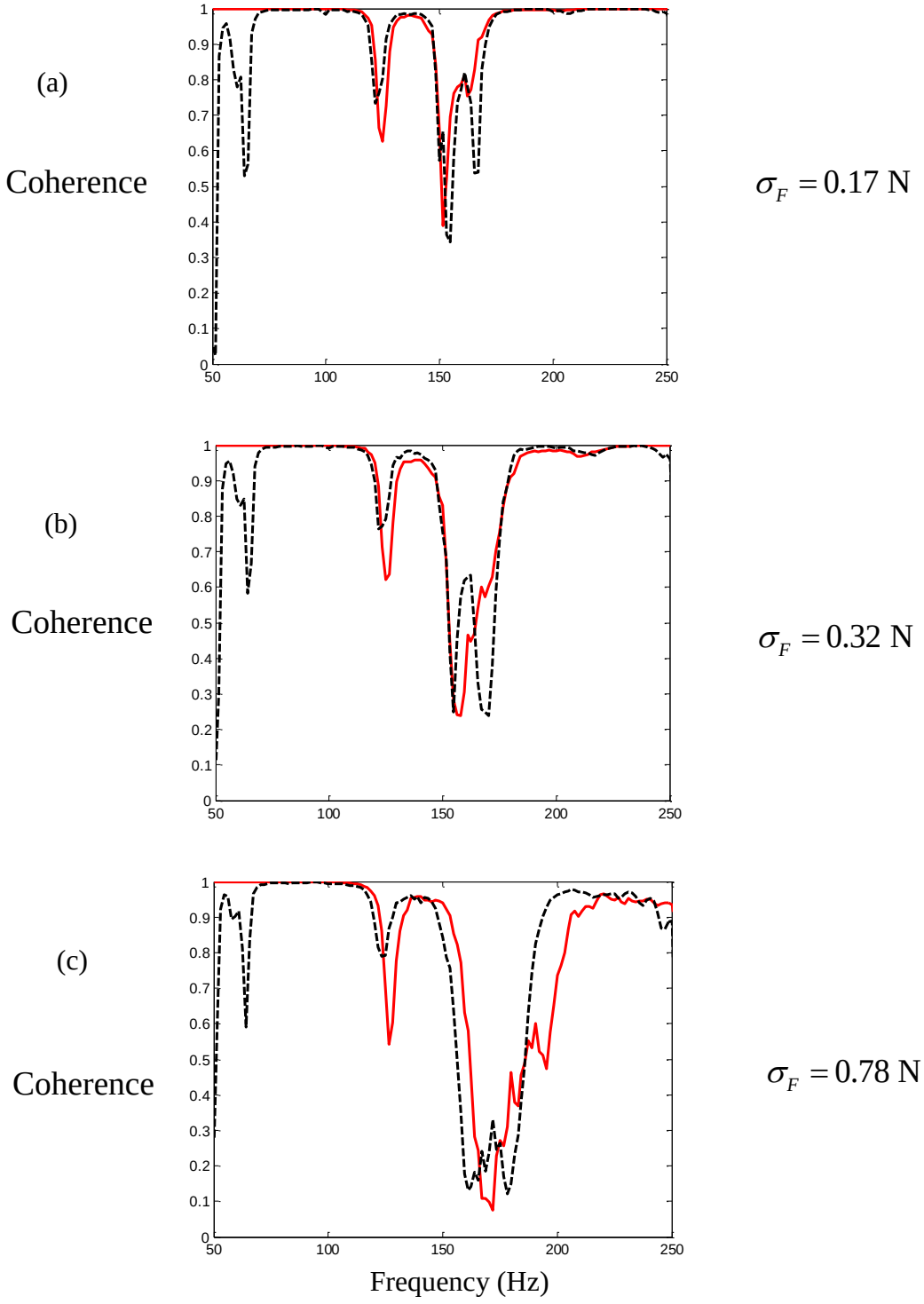

Figure 5.32 Comparison of the predicted and measured coherence for the primary system response. The system properties are given in Tables 5.1-2. Plate thickness 0.2 (mm): the corresponding overall rms force amplitudes are (a) $\sigma_F = 0.17$ N, (b) $\sigma_F = 0.32$ N and (c) $\sigma_F = 0.78$ N. The predicted response solution is given by the solid line. The measured response is the dashed line.

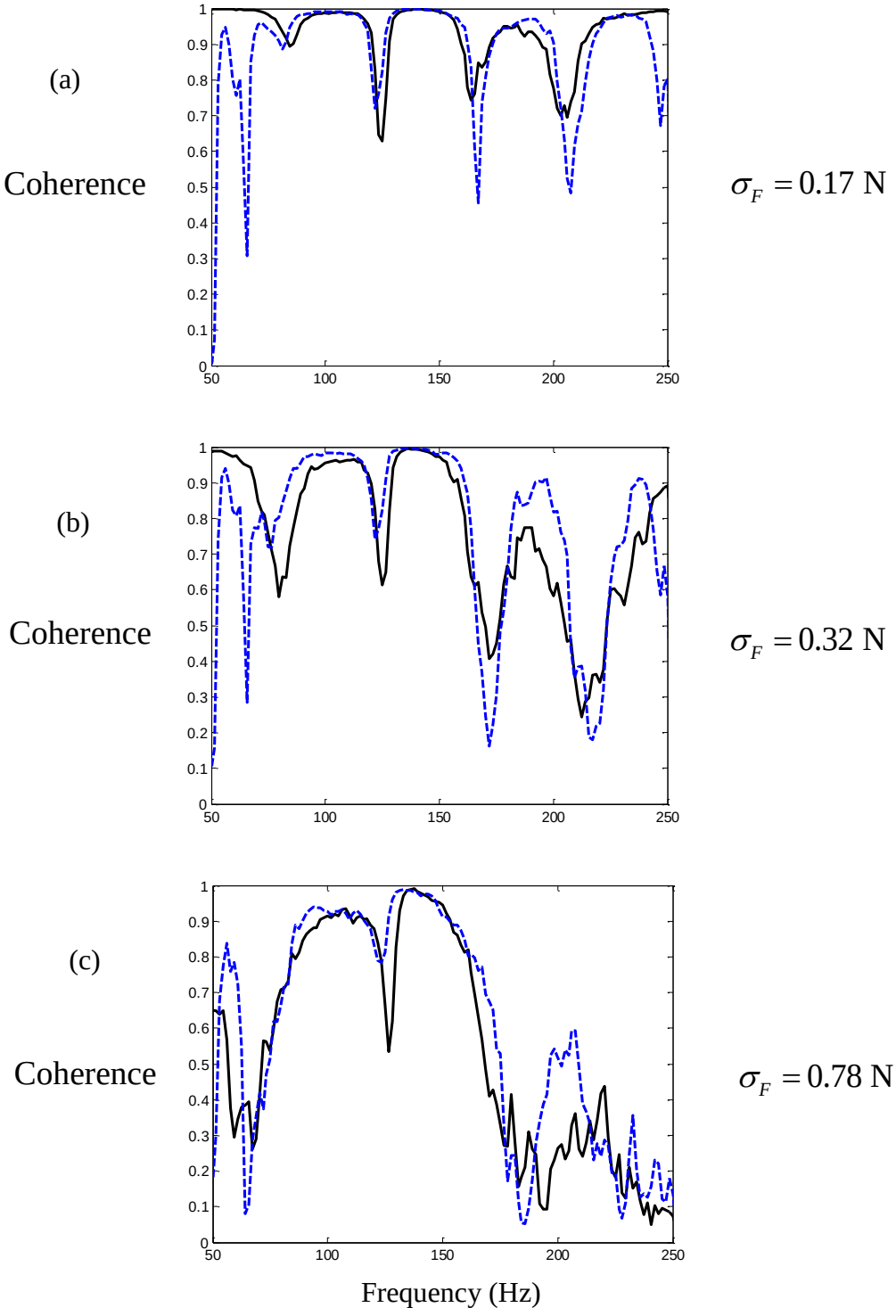

Figure 5.33 Comparison of the predicted and measured coherence for the absorber response. The system properties are given in Tables 5.1-2. Plate thickness 0.2 (mm): the corresponding overall rms force amplitudes are (a) $\sigma_F = 0.17$ N, (b) $\sigma_F = 0.32$ N and (c) $\sigma_F = 0.78$ N. The predicted response solution is given by the solid line. The measured response is the dashed line.

5.4 Conclusions

A comprehensive experimental study of a passive nonlinear vibration absorber attached to a primary structure under harmonic and random excitations has been presented. The nonlinearity of the absorber was due to the particular geometrical configuration of the attached plate undergoing a large amplitude response. Experimental results have been presented to compare with the numerical solutions of the previously derived model.

For harmonic excitation, the bandwidth reduction for the nonlinear absorber was determined and compared to the linear case previously presented in chapters 2 and 3. For comparison of measurements and HBM predictions, there was good agreement in frequency responses for the low force amplitude test. For the high force amplitude test, the frequency responses were not similar. In this latter scenario, the first resonance and effective tuned frequencies of the primary system presented the differences between measurements and HBM predictions. The reason for this could be possibly due to the stiffness parameter of the absorber was changed. It is suspected to be that the geometry of the thin plate being bolted on the circular ring for different tensions and material properties of the thin plate are affected by environmental factors such as temperature change. The measured results for the NDVA did not produce a much wider effective vibration reduction bandwidth as those predictions. One reason found is that the response at some frequencies was not harmonic. The response contained other frequencies, so that the HBM expressions do not accurately represent the actual solution. In addition, the excitation force time histories were not always purely harmonic. In order to minimize the effect of the system at the applied forcing, a control system for the excitation should be used in future tests. The measurement results also did not contain the branch of the frequency response of the primary system at the lowest and highest jump-down frequencies. This reason could be probably due to the high amplitude of vibration of primary and absorber system masses, which made it difficult to obtain this region using the actual experimental rig.

For random excitation, in view of the analytical approach limitations, the measurements provided additional numerical response functions and quantities such as values for the mean square responses, PSDs and coherence. The Power Spectral Densities show the frequency content of the measured and predicted input and response. The nonlinear effects in the system response are presented in the frequency domain. The response PSD is shown to possess a shift and broadening of the frequency content. However, the mean square response only provides an

overall single value as a measure for the total response. In order to understand the variation or changes in the response by statistical analysis, the probability density function (PDF) of the response time histories could be used in the future. For the low force amplitude test, the measurement results produced good agreement with numerical predictions. For the high force amplitude test, the measurement results did not produce similar results compared to the predictions. In this latter scenario, for comparison of the mean square primary system acceleration showed that the predictions were higher than measured results. The predictions also presents higher cumulative mean square acceleration of the primary system at the first mode compared to measured results. This is in agreement in that the cumulative mean square acceleration of the primary system for first mode is the main contribution in the mean square response. The first resonance, effective tuned and second resonance frequencies of the primary system display differences compared to the numerical predictions. It is likely that the stiffness parameter of the absorber changes during the time behaviour from its estimation using static tests compared to during the dynamic testing. The geometry of the thin plate may be affected by environmental factors such as temperature changes. For some values of the nonlinear absorber parameters, the primary system response appears to undergo a detrimental effect compared to using linear absorber for increased force input magnitudes. This means that the nonlinear absorber still needs to be selected for the particular application with the best parameters for reducing the vibration response of the primary system for the specified excitation levels.

Chapter 6

Conclusions and Recommendations

6.1 Conclusions

Many researchers are interested in and have investigated the nonlinear vibration absorber. This thesis has been concerned with the way in which nonlinearity produced by the nonlinear absorber stiffness can be put to good use in a vibration absorber. The reasons for the preference of this passive approach are to be found in the cost, simplicity and reliability of this type of absorbers. The effect of the nonlinear vibration absorber parameters on the vibration response was investigated. The results of this research are summarized in the following.

For harmonic excitation

- The approximate analytical expressions (HBM method) which describe the behaviour for different parameters of nonlinear absorber under harmonic excitation have been derived. The relationship between the bifurcation curves and the frequency response curves was investigated. In addition, the stability characteristics of the periodic steady state solution were analyzed by Floquet theory.

- There are some values of the parameters, e.g. for the nonlinear stiffness, for which harmonic responses do not occur for harmonic excitation. These limits have been explored and quantified. Where the response is non harmonic, the analysis has produced a Fourier series or transform representation of the response time histories where appropriate. The frequency response curves which need to identify the range of corresponding frequencies for non-harmonic response.

- The nonlinear absorber has a much wider effective bandwidth compared to a conventional linear absorber. Compared to the linear absorber, the nonlinearity has the effect of shifting the second resonance peak to a higher frequency away from the effective tuned frequency, improving the robustness of the device to mistune. For the

linear absorber this can be achieved by adding mass to the absorber, so in some way the nonlinearity has the same beneficial effect as adding to the absorber mass.

- The lower the damping in the nonlinear absorber, the effective bandwidth is slightly increased compared to the linear absorber with the same level of damping. However, larger damping in the nonlinear absorber generally produces a wider frequency vibration reduction bandwidth compared to the linear absorber. When damping in the nonlinear absorber is further increased above a certain value though, there appears to be no effective vibration bandwidth. In engineering applications, it is desirable to have a large vibration reduction bandwidth, so that the damping in the absorber needs to be quite small.

- For larger absorber to primary system mass ratios, the vibration reduction bandwidth for the nonlinear absorber is not significantly different than that for a linear absorber. The linear absorber can also produce a broader vibration reduction bandwidth by adding mass to the absorber.

- The nonlinear absorber has a slightly wider vibration reduction bandwidth compared to the linear case for the same effective tuned frequency for the same mass ratio and damping.

- For a hardening stiffness nonlinear absorber design, the limitation on the value of the nonlinear stiffness parameter should be identified first. In order to produce an effective vibration bandwidth, the limitation on the value of the damping and the mass were determined. The larger the damping and the heavier the mass in the nonlinear absorber, a much wider effective vibration bandwidth will be produced compared to using a linear absorber with the same damping and mass levels.

<u>For random excitation</u>

- The simulations and subsequent statistical and frequency analysis were conducted for the nonlinear absorber. Dependent upon the level of nonlinearity and the amplitude of

the random input force applied to the primary system, the nonlinear absorber can produce a nonlinear behaviour. This can result in a higher vibration response of the primary system compared to that produced when using a linear absorber.

- For a low nonlinear stiffness, the nonlinear absorber produces the same mean square primary system displacement compared to a linear absorber case. For a high nonlinear stiffness, the nonlinear absorber has a higher mean square primary system displacement compared to a linear absorber. The use of a high stiffness nonlinearity does not improve the vibration reduction compared to the linear absorber case.

- As the damping in the nonlinear absorber is increased, the mean square primary system displacement is higher than when using a conventional linear absorber.

- For a nonlinear absorber with a low mass ratio, a higher mean square primary system displacement occurs compared to using a linear absorber with the same level of mass. On increasing the mass ratio then the mean square of primary system displacement using the nonlinear absorber will reduce and eventually is similar to using a linear absorber. The higher mass ratios actually result in a smaller nonlinear nondimensional stiffness as it is defined. When the nonlinear stiffness is higher, the nonlinear absorber again produces a higher mean square primary system displacement compared to the behaviour using a linear absorber with the same levels of linear stiffness and mass.

- Based on the NDVA parameters, for some range of the parameters, the nonlinear absorber under random excitation produces undesirable levels for the mean square primary system displacement compared to using a linear absorber. This means that the nonlinear absorber still needs to be selected for the particular application with the best parameters for reducing the vibration response of the primary or main system.

Measurements

- For comparison of measurements and HBM predictions, there was good agreement in frequency responses for the low force amplitude test. For the high force amplitude test, the frequency responses were not similar. In this latter scenario, the first resonance and effective tuned frequencies of the primary system presented large differences between measurements and HBM predictions. The reason for this could be possibly due to the stiffness parameter of the absorber was changed. It is suspected to be that the geometry of the thin plate being bolted on the circular ring for different tensions and material properties of the thin plate are affected by environmental factors such as temperature change. The NDVA measured results did not produce a much wider effective vibration reduction bandwidth compared to the predicted bandwidth. One reason found is that the harmonic response at the excitation frequency could not be achieved for some frequency ranges. Other harmonics contribute to the response, so that the HBM expression is not sufficiently accurate around these frequencies. In addition, the force excitation time histories were not purely harmonic and showed some variation. This unexpected feature will affect the response of the entire system. In order to minimize the effect of the practical system dynamics on the applied excitation system, a control system is required to ensure a harmonic input in future tests.

- For random excitation, the corresponding nonlinear response of the system is presented in the frequency domain. The response PSD is shown to possess a shift and broadening of the frequency content. However, the mean square response only provides an overall single value and measure of the response. In order to understand the variation or changes in the response by statistical analysis, the probability density function of the response time histories could be used in the future. In the low force amplitude test, the measurement results produced good agreement with numerical predictions. For the high force amplitude test, the measurement results did not produce similar results compared to the predictions. In this latter scenario, for comparison of the mean square primary system acceleration showed that the predictions were higher than measured results. The first resonance, effective tuned and second resonance frequencies of the primary system show some differences compared to the numerical predictions. A reason could be due to the stiffness parameter of the absorber which might change due to the geometry of the thin plate on the tensions varying due to environmental factors, such as temperature changes and expansion. For a range of parameters of the nonlinear absorber, the primary

system response did not show any advantage for increased input magnitudes. This means that the nonlinear absorber still needs to be selected, for the particular application, with the best parameters for reducing the vibration response of the primary system.

6.2 Recommendations for Future Work

The research presented in this thesis has improved the understanding of the characteristics and effects of the NDVA and its physical parameters on the vibration reduction. Experimental validation has also taken place. This study has also highlighted several issues discussed below which are thought to be worthy of further study:

For harmonic excitation

1. The numerical results for the vibration reduction bandwidth and effective tuned frequency have been obtained in previous studies. However, the mathematical expressions for the vibration reduction bandwidth and effective tuned frequency have not been investigated. A recommendation is to determine the effect of NVDA parameters on the vibration reduction bandwidth and effective tuned frequency with, if possible, analytical expressions.

2. For the primary system with attached nonlinear absorber, the jump-up and jump-down frequencies produce a sudden (discontinuous) change of the amplitude of the system response. The frequencies at which these jumps occur depend upon whether the frequency is increasing or decreasing. An approximate analytical approach in the determination of the jump-up and jump-down frequencies and the corresponding vibration amplitudes of the NDVA could be considered.

For random excitation

3. In Chapter 4, a numerical technique have been presented to investigate the dynamic behaviour of nonlinear vibration absorber. However, an approximate analytical expressions of nonlinear system for mean square response under random excitation has not been studied.

Measurements

- The nonlinear absorber system was designed to tune the nonlinear stiffness and change the mass of the absorber. However, the nonlinear absorber was not designed so that tuning the damping in the absorber is possible. Further research could be carried out on this issue.

Appendix A

Stability analysis for the periodic solutions

The equations of motion in non-dimensional form are given by (2.8a,b)

$$(1+\mu)y_s'' + 2\zeta_s y_s' + y_s - \mu w'' = \cos(\Omega\tau) \qquad \text{(A1a,b)}$$
$$w'' + 2\zeta\omega_0 w' + \omega_0^2 w + \gamma w^3 = y_s''$$

The stability of the calculated periodic solutions $y_s(\tau)$ and $w(\tau)$ given by equations (2.9a,b) is calculated by applying Floquet theory [65, 81, 82]. The first perturbation of the periodic solutions $y_s(\tau) = \mathrm{Y}_{s_0}(\tau)$ and $w(\tau) = W_{1_0}(\tau)$ are given by introducing the small perturbations $\varepsilon_s(\tau)$ and $\varepsilon(\tau)$

$$y_s(\tau) = \mathrm{Y}_{s_0}(\tau) + \varepsilon_s(\tau) \qquad \text{(A2a,b)}$$
$$w(\tau) = W_{1_0}(\tau) + \varepsilon(\tau)$$

Substituting equations (A2a,b) into equations (A1a,b) and taking the linear terms for the perturbations $\varepsilon_s(\tau)$ and $\varepsilon(\tau)$ one obtains

$$(1+\mu)\varepsilon_s'' + 2\zeta_s\varepsilon_s' + \varepsilon_s - \mu\varepsilon'' = 0 \qquad \text{(A3a,b)}$$
$$\varepsilon'' + 2\varsigma\omega_0\varepsilon' + \omega_0^2\varepsilon + 3\gamma W_{1_0}^2\varepsilon = \varepsilon_s''$$

According to Floquet theory, equations (A3a,b) possess solutions of the form

$$\varepsilon_s(\tau)=e^{\lambda\tau}u_s(\tau),\ \varepsilon(\tau)=e^{\lambda\tau}u(\tau) \qquad \text{(A4a,b)}$$

where $u_s(\tau)$ and $u(\tau)$ are periodic functions with period $\mathrm{T}=2\pi/\Omega$, which is the period of $\mathrm{Y}_{s_0}(\tau)$ and $W_{1_0}(\tau)$ and λ is the eigenvalue. The stability depends upon the real parts of the egienvalues λ being negative.

Time derivatives of equations (A4a,b) yields

$$\varepsilon_s'=\lambda e^{\lambda\tau}u_s+e^{\lambda\tau}u_s',\ \varepsilon'=\lambda e^{\lambda\tau}\mathrm{u}+e^{\lambda\tau}u' \qquad \text{(A5a,b)}$$

$$\varepsilon_s''=\lambda^2 e^{\lambda\tau}u_s+2\lambda e^{\lambda\tau}u_s'+e^{\lambda\tau}u_s'',\ \varepsilon''=\lambda^2 e^{\lambda\tau}u+2\lambda e^{\lambda\tau}u'+e^{\lambda\tau}u''$$

(A6a,b)

Substituting Equations (A4a,b)-(A6a,b) into Equations (A3a,b) gives

$$(1+\mu)u_s''+\left(2\lambda(1+\mu)+2\zeta_s\right)u_s'+\left(1+2\zeta_s\lambda+(1+\mu)\lambda^2\right)u_s - \mu u''-2\mu\lambda u'-\mu\lambda^2 u=0$$

$$-u_s''-2\lambda u_s'-\lambda^2 u_s +u''+\left(2\lambda+2\zeta\omega_0\right)u'+\left(\lambda^2+2\zeta\omega_0\lambda+\omega_0^2+3\gamma W_{1_0}^2\right)u=0$$

(A7a,b)

In order to solve equations (A7a,b) a Fourier series expansion of $u_s(\tau)$ and $u(\tau)$ are expanded which produces

$$u_s(\tau)=p_1\cos(\Omega\tau)+p_2\sin(\Omega\tau) \qquad \text{(A8a,b)}$$

$$u(\tau)=q_1\cos(\Omega\tau)+q_2\sin(\Omega\tau)$$

where $p_1,\ p_2,\ q_1,\ q_2$ are the Fourier coefficient of the first order expansion

Time derivatives of equations (A8a,b) yields

$$u_s'(\tau)=\Omega(-p_1\sin(\Omega\tau)+p_2\cos(\Omega\tau)),\ u'(\tau)=\Omega(-q_1\sin(\Omega\tau)+q_2\cos(\Omega\tau)) \qquad \text{(A9a,b)}$$

$$u_s''(\tau)=\Omega^2(-p_1\cos(\Omega\tau)-p_2\sin(\Omega\tau)),\ u''(\tau)=\Omega^2(-q_1\cos(\Omega\tau)-q_2\sin(\Omega\tau))$$

(A10a,b)

Substituting equations (A8a,b)- (A10a,b) into equations (A7a,b) and equating the coefficient of each harmonic on both sides gives

$$\begin{pmatrix}-(1+\mu)\Omega^2 p_1+\left(2\lambda(1+\mu)+2\zeta_s\right)\Omega p_2+\left(1+2\zeta_s\lambda+(1+\mu)\lambda^2\right)p_1\\ +\mu\Omega^2 q_1-2\mu\lambda\Omega q_2-\mu\lambda^2 q_1\end{pmatrix}\cos(\Omega\tau)+$$

$$\begin{pmatrix}-(1+\mu)\Omega^2 p_2-\left(2\lambda(1+\mu)+2\zeta_s\right)\Omega p_1+\left(1+2\zeta_s\lambda+(1+\mu)\lambda^2\right)p_2\\ +\mu\Omega^2 q_2+2\mu\lambda\Omega q_1-\mu\lambda^2 q_2\end{pmatrix}\sin(\Omega\tau)=0$$

$$\begin{pmatrix} +\Omega^2 p_1 - 2\lambda\Omega p_2 - \lambda^2 p_1 \\ -\Omega^2 q_1 + \left(2\lambda + 2\zeta\omega_0\right)\Omega q_2 + \left(\lambda^2 + 2\zeta\omega_0\lambda + \omega_0^2 + 3\gamma W_{1_0}^2\right) q_1 \end{pmatrix} \cos(\Omega\tau) +$$

$$\begin{pmatrix} +\Omega^2 p_2 + 2\lambda\Omega p_1 - \lambda^2 p_2 \\ -\Omega^2 q_2 - \left(2\lambda + 2\zeta\omega_0\right)\Omega q_1 + \left(\lambda^2 + 2\zeta\omega_0\lambda + \omega_0^2 + 3\gamma W_{1_0}^2\right) q_2 \end{pmatrix} \sin(\Omega\tau) = 0$$

(A11a,b)

Equations (A11a,b) are multiplied by the terms $\cos(\Omega\tau)$ and $\sin(\Omega\tau)$ separately and integrated. Then, a system of linear homogeneous algebraic equations relating the coefficients p_1, p_2, q_1, q_2 and λ are obtained

$$\left(-(1+\mu)\Omega^2 + 1 + 2\zeta_s\lambda + (1+\mu)\lambda^2\right) p_1 + \left(2\lambda(1+\mu) + 2\zeta_s\right)\Omega p_2 + (\Omega^2 - \lambda^2)\mu q_1 - 2\mu\lambda\Omega q_2 = 0$$

$$-\left(2\lambda(1+\mu) + 2\zeta_s\right)\Omega p_1 + \left(-(1+\mu)\Omega^2 + 1 + 2\zeta_s\lambda + (1+\mu)\lambda^2\right) p_2 + 2\mu\lambda\Omega q_1 + (\Omega^2 - \lambda^2)\mu q_2 = 0$$

$$(\Omega^2 - \lambda^2) p_1 - 2\lambda\Omega p_2 + \left(\lambda^2 + 2\zeta\omega_0\lambda + \omega_0^2 - \Omega^2 + 3\gamma W_{1_0}^2\right) q_1 + \left(2\lambda + 2\zeta\omega_0\right)\Omega q_2 = 0$$

$$2\lambda\Omega p_1 + (\Omega^2 - \lambda^2) p_2 - \left(2\lambda + 2\zeta\omega_0\right)\Omega q_1 + \left(\lambda^2 + 2\zeta\omega_0\lambda + \omega_0^2 - \Omega^2 + 3\gamma W_{1_0}^2\right) q_2 = 0$$

(A12a,b,c,d)

Equation (A12a,b,c,d) is the form of matrix

$$\begin{bmatrix} A_1 & A_2 & \mu A_3 & -\mu A_4 \\ -A_2 & A_1 & \mu A_4 & \mu A_3 \\ A_3 & -A_4 & A_5 & A_6 \\ A_4 & A_3 & -A_6 & A_5 \end{bmatrix} \begin{bmatrix} p_1 \\ p_2 \\ q_1 \\ q_2 \end{bmatrix} = 0 \qquad \text{(A13)}$$

where

$$\mathrm{A}_1 = (1+\mu)\lambda^2 + 2\zeta_s\lambda - (1+\mu)\Omega^2 + 1,\ \mathrm{A}_2 = 2\Omega\left(\lambda(1+\mu) + \zeta_s\right),\ \mathrm{A}_3 = \Omega^2 - \lambda^2,\ \mathrm{A}_4 = 2\lambda\Omega$$

$$\mathrm{A}_5 = \lambda^2 + 2\zeta\omega_0\lambda + \omega_0^2 - \Omega^2 + 3\gamma W_{1_0}^2,\ \mathrm{A}_6 = \left(2\lambda + 2\zeta\omega_0\right)\Omega$$

Substituting for μ, ζ_s, ζ, ω_0, Ω and $W_{1_0}^2$ values into A_1 to A_6 in equation (A13). Then, the determinant of the coefficient matrix of this system is set equal to zero, i.e.

$$\begin{vmatrix} A_1 & A_2 & \mu A_3 & -\mu A_4 \\ -A_2 & A_1 & \mu A_4 & \mu A_3 \\ A_3 & -A_4 & A_5 & A_6 \\ A_4 & A_3 & -A_6 & A_5 \end{vmatrix} = 0 \qquad \text{(A14)}$$

A governing equation for the values of are given by λ of equation (A15) can then be obtained

$$B_8\lambda^8 + B_7\lambda^7 + B_6\lambda^6 + B_5\lambda^5 + B_4\lambda^4 + B_3\lambda^3 + B_2\lambda^2 + B_1\lambda + B_0 = 0 \quad \text{(A15)}$$

The actual numerical values of λ result in two possible scenarios, namely that the system is either stable or unstable. If all of the eigenvalues λ lie in the left half of the complex plane, i.e. the real parts of λ are negative, then the periodic solution is stable. Otherwise, it is unstable if any eigenvalues lie in the right half plane.

Appendix B

Design of the nonlinear vibration absorber

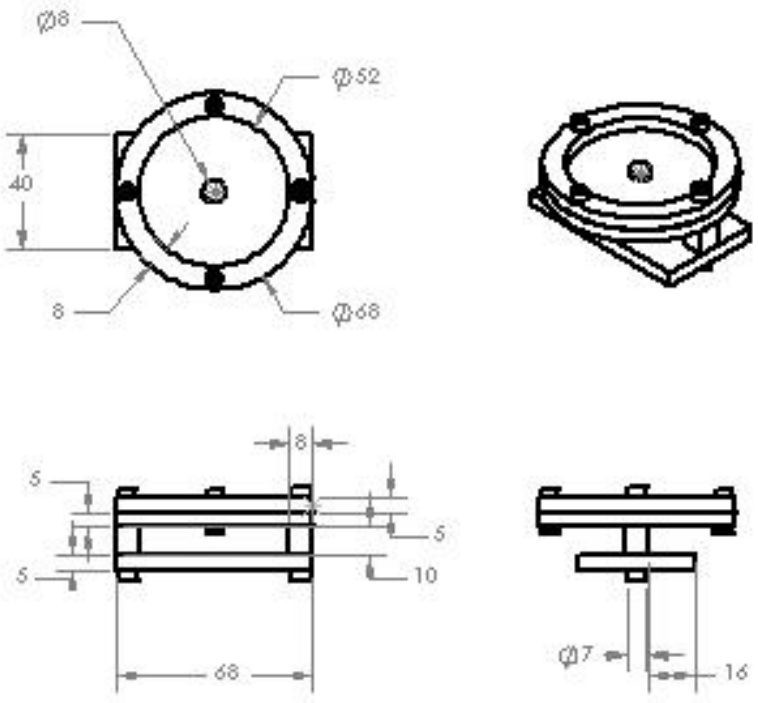

Figure B.1. Schematic diagram of the nonlinear vibration absorber for the actual rig manufactured. The support frame structure and the shim are made of aluminium and brass, respectively.

Reference:

1. Piersol, A.G., T.L. Paez, and C.M. Harris, *Shock and Vibration Handbook*. 6th ed. 2010, New York: McGraw-Hill.
2. Mead, D.J., *Passive vibration control*. 1998, New York: Wiley.
3. Franchek, M.A., Ryan, M. W. and R.J. Bernhard, *Adaptive passive vibration control.* Journal of Sound and Vibration, 1996. **189**(5): p. 565-585.
4. Fuller, C.R., S.J. Elliott, and P.A. Nelson, *Active control of vibration*. 1996, London: Academic Press. xii, 332 p.
5. Karnopp, D.C., M.J. Crosby, and R.A. and Harwood, *Vibration control using semi-active force generators.* Transactions of the American Society of Mechanical Engineers, Journal of Engineering for Industry, 1974. **96**(2): p. 619–626.
6. Jiang, X., McFarland, D. M., Bergman, L.A. and A.F. Vakakis, *Steady State Passive Nonlinear Energy Pumping in Coupled Oscillators: Theoretical and Experimental Results.* Nonlinear Dynamics, 2003. **33**(1): p. 87-102.
7. Fahy, F. and J. Walker, *Advanced applications in acoustics, noise, and vibration*. 2004, London ; New York: Spon Press. xiii, 640 p.
8. *http://blogs.saschina.org/chemicalparadigms/2011/02/*. date: 01/2013.
9. *http://www.sonus.nl/dutch/vakgebieden/trillingen/zouthb.html*. date: 12/2012.
10. Braun, S., D.J. Ewins, and S.S. Rao, *Encyclopedia of Vibration*. 2002, San Diego ; London: Academic.
11. Den Hartog, J.P., *Mechanical vibrations*. Dover books on engineering. 1985, New York: Dover Publications. xi, 436 p.
12. Ozer, M.B. and T.J. Royston, *Extending Den Hartog's Vibration Absorber Technique to Multi-Degree-of-Freedom Systems.* Journal of Vibration and Acoustics, 2004. **127**(4): p. 341-350.
13. Jordanov, I.N. and B.I. Cheshankov, *Optimal design of linear and non-linear dynamic vibration absorbers.* Journal of Sound and Vibration, 1988. **123**(1): p. 157-170.
14. Ormondroyd, J. and J.P. Den Hartog, *The theory of the dynamic vibration absorber.* Transactions of the American Society of Mechanical Engineers, 1928. **50** p. A9-A22.
15. Roberson, R.E., *Synthesis of a nonlinear dynamic vibration absorber.* Journal of the Franklin Institute, 1952. **254**(3): p. 205-220.

16. Hunt, J.B. and J.C. Nissen, *The broadband dynamic vibration absorber*. Journal of Sound and Vibration, 1982. **83**(4): p. 573-578.

17. James, M.L., *Vibration of mechanical and structural systems : with microcomputer applications*. 2nd ed. 1994, New York, NY: HarperCollins College Publishers. xi, 660 p.

18. Thomson, W.T. and M.D. Dahleh, *Theory of vibration with applications*. 5th ed. 1998, Upper Saddle River, N.J.: Prentice Hall. xiii, 524 p.

19. Newland, D.E., *An introduction to random vibrations and spectral analysis*. 2nd ed. 1984, London ; New York: Longman. xxvi, 377 p.

20. Soong, T.T. and M. Grigoriu, *Random vibration of mechanical and structural systems*. 1993, Englewood Cliffs, N.J.: PTR Prentice Hall. xiii, 402 p.

21. McConnell, K.G., *Vibration testing : theory and practice*. 1995, New York ; Chichester: Wiley. xviii, 606 p.

22. Pipes, L.A., *Analysis of a non-linear dynamic vibration absorber*. Transactions of the American Society of Mechanical Engineers: journal of applied mechanics, 1953. **20**: p. 515-518.

23. Kovacic, I. and M.J. Brennan, *The Duffing equation : nonlinear oscillators and their phenomena*. 2011, Chichester, West Sussex, U.K. ; Hoboken, N.J.: Wiley. xvi, 369 p.

24. Arnold, F.R., Stanford, and Calif, *Steady-state behaviour of systems provided with non-linear dynamic vibration absorbers.* Transactions of the American Society of Mechanical Engineers: journal of applied mechanics, 1955. **22**: p. 487-492.

25. Lawrence, N.V., *Introduction to Experimental Nonlinear Dynamics: A Case Study in Mechanical Vibration*. 1th ed. 2000, Cambridge: Cambridge University Press 272 p.

26. Nissen, J.C., K. Popp, and B. Schmalhorst, *Optimization of a non-linear dynamic vibration absorber*. Journal of Sound and Vibration, 1985. **99**(1): p. 149-154.

27. Rice, H.J. and J.R. McCraith, *Practical non-linear vibration absorber design.* Journal of Sound and Vibration, 1987. **116**(3): p. 545-559.

28. Natsiavas, S., *Steady state oscillations and stability of non-linear dynamic vibration absorbers.* Journal of Sound and Vibration, 1992. **156**(2): p. 227-245.

29. Zhu, S.J., Y.F. Zheng, and Y.M. Fu, *Analysis of non-linear dynamics of a two-degree-of-freedom vibration system with non-linear damping and non-linear spring.* Journal of Sound and Vibration, 2004. **271**(1-2): p. 15-24.

30. Gendelman, O.V., E. Gourdon, and C.H. Lamarque, *Quasiperiodic energy pumping in coupled oscillators under periodic forcing.* Journal of Sound and Vibration, 2006. **294**(4-5): p. 651-662.

31. Gourdon, E., Alexander, N. A., Taylor, C. A., Lamarque, C. H. and S. Pernot, *Nonlinear energy pumping under transient forcing with strongly nonlinear coupling: Theoretical and experimental results.* Journal of Sound and Vibration, 2007. **300**(3-5): p. 522-551.

32. Gendelman, O., Y. Starosvetsky, and M. Feldman, *Attractors of harmonically forced linear oscillator with attached nonlinear energy sink I: Description of response regimes.* Nonlinear Dynamics, 2008. **51**(1): p. 31-46.

33. Starosvetsky, Y. and O. Gendelman, *Attractors of harmonically forced linear oscillator with attached nonlinear energy sink. II: Optimization of a nonlinear vibration absorber.* Nonlinear Dynamics, 2008. **51**(1): p. 47-57.

34. Sun, C., Eason, R. P., Nagarajaiah, S. and A.J. Dick, *Hardening Düffing oscillator attenuation using a nonlinear TMD, a semi-active TMD and multiple TMD.* Journal of Sound and Vibration, 2013. **332**(4): p. 674-686.

35. Miller, H.M. and J.R. Gartner, *Tunable nonlinear vibration absorber.* American Society of Mechanical Engineers, 1975.

36. Yamakawa, I., S. Takeda, and H. Kojima, *Behavior of a new type dynamic vibration absorber consisting of three permanent magnets.* Bulletin of the Japan Society of Mechanical Engineers, 1977. **20**: p. 947-954.

37. Kojima, H. and K. Nagaya, *A Study on the Torsional Dynamic Vibration Absorber Consisting of Rare-earth Magnets.* Bulletin of JSME, 1983. **26**(214): p. 611-618.

38. Patil, N.S. and A.K. Mallik, *Experimental investigation of the response of a harmonically excited hard Duffing oscillator.* Pramana, 2007. **68**(1): p. 99-104.

39. Gatti, G., M.J. Brennan, and I. Kovacic, *On the interaction of the responses at the resonance frequencies of a nonlinear two degrees-of-freedom system.* Physica D: Nonlinear Phenomena, 2010. **239**(10): p. 591-599.

40. Rice, H.J., *The assymmetric non-linear vibration absorber*. 1985, National University of Ireland.

41. Nayfeh, A.H. and L.D. Zavodney, *Experimental Observation of Amplitude- and Phase-Modulated Responses of Two Internally Coupled Oscillators to a Harmonic Excitation.* Journal of Applied Mechanics, 1988. **55**(3): p. 706-710.

42. Balachandran, B. and A.H. Nayfeh, *Observations of modal interactions in resonantly forced beam-mass structures.* Nonlinear Dynamics, 1991. **2**(2): p. 77-117.

43. Rice, H.J., *Combinational ínstability of the non-linear vibration absorber.* Journal of Sound and Vibration, 1986. **108**(3): p. 526-532.

44. Shaw, J., S.W. Shaw, and A.G. Haddow, *On the response of the non-linear vibration absorber.* International Journal of Non-Linear Mechanics, 1989. **24**(4): p. 281-293.

45. Gatti, G. and M.J. Brennan, *On the effects of system parameters on the response of a harmonically excited system consisting of weakly coupled nonlinear and linear oscillators.* Journal of Sound and Vibration, 2011. **330**(18–19): p. 4538-4550.

46. Malatkar, P. and A. Nayfeh, *Steady-State dynamics of a linear structure weakly coupled to an essentially nonlinear oscillator.* Nonlinear Dynamics, 2007. **47**(1): p. 167-179.

47. Malatkar, P. and A. Nayfeh, *Authors' response to the rebuttal by A.F. Vakakis and L.A. Bergman of Steady state dynamics of a linear structure weakly coupled to an essentially nonlinear oscillator, Vol. 47, 2007, pp. 167–179.* Nonlinear Dynamics, 2008. **53**(1-2): p. 169-171.

48. Vakakis, A.F., A.N. Kounadis, and I.G. Raftoyiannis, *Use of non-linear localization for isolating structures from earthquake-induced motions.* Earthquake Engineering & Structural Dynamics, 1999. **28**(1): p. 21-36.

49. Vakakis, A.F., Manevitch, L. I., Gendelman, O. and L. Bergman, *Dynamics of linear discrete systems connected to local, essentially non-linear attachments.* Journal of Sound and Vibration, 2003. **264**(3): p. 559-577.

50. Gourdon, E., Alexander, N. A., Taylor, C. A., Lamarque, C. H. and S. Pernot, *Nonlinear energy pumping under transient forcing with strongly nonlinear coupling: Theoretical and experimental results.* Journal of Sound and Vibration, 2007. **300**(3–5): p. 522-551.

51. Robson, J.D., *An introduction to random vibration*. Edinburgh University publications science and mathematics texts, 5. 1963, Edinburgh,: University Press. viii, 150 p.

52. Lin, Y.K., *Probabilistic theory of structural dynamics*. 1976, Huntington, N.Y.: R. E. Krieger Pub. Co. xi, 368 p.

53. Cicek, I., *Vibration absorbers for flexible structures under random excitation: theory and experiments*. 1999, Texas Tech University. p. 284.

54. Cicek, I. and A. Ertas, *Experimental investigation of beam-tip mass and pendulum system under random excitation.* Mechanical Systems and Signal Processing, 2002. **16**(6): p. 1059-1072.

55. Lee, W.K. and D.S. Cho, *Damping effect of a randomly excited autoparametric system.* Journal of Sound and Vibration, 2000. **236**(1): p. 23-31.

56. Tondl, A., *Autoparametric resonance in mechanical systems*. 2000, Cambridge, UK ; New York: Cambridge University Press. x, 196 p.

57. Rüdinger, F., *Tuned mass damper with nonlinear viscous damping.* Journal of Sound and Vibration, 2007. **300**(3–5): p. 932-948.

58. Sun, J.Q. and C.S. Hsu, *Cumulant neglect closure method for nonlinear systems under random excitation.* ASME Journal of Applied Mechanics, 1987. **54**: p. 649- 655.

59. Ibrahim, R.A., Y.J. Yoon, and M. Evans, *Random excitation of nonlinear coupled oscillators.* Nonlinear Dynamics, 1990. **1**(1): p. 91-116.

60. Cuvalci, O., Ertas, A., Ekwaro-Osire, S. and I. Cicek, *Non-linear vibration absorber for a system under sinusoidal and random excitation: experiments.* Journal of Sound and Vibration, 2002. **249**(4): p. 701-718.

61. F. Petit, M. Loccufier, and D. Aeyels, *Feasibility of nonlinear absorbers for transient vibration reduction* in *Proceedings of ISMA 2010* 2010, KU Leuven: Leuven.

62. Gatti, G., I. Kovacic, and M.J. Brennan, *On the response of a harmonically excited two degree-of-freedom system consisting of a linear and a nonlinear quasi-zero stiffness oscillator.* Journal of Sound and Vibration, 2010. **329**(10): p. 1823-1835.

63. Kojima, H. and H. Saito, *Forced vibrations of a beam with a non-linear dynamic vibration absorber.* Journal of Sound and Vibration, 1983. **88**(4): p. 559-568.

64. Clough, R.W. and J. Penzien, *Dynamics of structures*. 1975, New York: McGraw-Hill. xxii, 634 p.

65. Nayfeh, A.H. and D.T. Mook, *Nonlinear oscillations*. Pure and applied mathematics. 1979, New York: Wiley. xiv, 704 p.

66. Brennan, M.J. and G. Gatti, *The characteristics of a nonlinear vibration neutralizer.* Journal of Sound and Vibration, 2012. **331**(13): p. 3158-3171.

67. Schmidt, G. and A. Tondl, *Non-linear vibrations*. 1986, New York: Cambridge University Press. 420 p.

68. Worden, K. and G.R. Tomlinson, *Nonlinearity in structural dynamics: detection, identification, and modelling.* Bristol [England] ; Philadelphia: Institute of Physics. xix, 2001: p. 659.

69. Hamdan, M.N. and T.D. Burton, *On the Steady State Response and Stability of Non-Linear Oscillators Using Harmonic Balance.* Journal of Sound and Vibration, 1993. **166**(2): p. 255-266.

70. Dickenstein, A. and I.Z. Emiris, *Solving polynomial equations : foundations, algorithms, and applications*. Algorithms and computation in mathematics,. 2005, Berlin ; New York: Springer. xiii, 424 p.

71. Lambert, J.D., *Numerical methods for ordinary differential systems : the initial value problem*. 1991, Chichester: Wiley. x, 293 p.

72. Troger, H. and A. Steindl, *Nonlinear stability and bifurcation theory : an introduction for engineers and applied scientists*. 1991, New York: Springer-Verlag. xi, 407 p.

73. Vakakis, A. and L. Bergman, *Rebuttal of "steady state dynamics of a linear structure weakly coupled to an essentially nonlinear oscillator" by P. Malatkar and A.H. Nayfeh.* Nonlinear Dynamics, 2008. **53**(1-2): p. 167-168.

74. Shin, K. and J.K. Hammond, *Fundamentals of signal processing for sound and vibration engineers*. 2008, Chichester, England ; Hoboken, NJ: John Wiley & Sons. x, 403 p.

75. Sweitzer, K.A., *Random vibration response statistics for fatigue analysis of nonlinear structures*. 2006, PhD thesis, University of Southampton, UK: Southampton. p. P.207.

76. Bendat, J.S., *Nonlinear Systems Techniques and Applications*. 1998, New York: John Wiley & Sons.

77. Bendat, J.S. and A.G. Piersol, *Random data : analysis and measurement procedures*. 3rd ed. Wiley series in probability and statistics. Texts and references section. 2000, New York ; Chichester: Wiley. xvii, 594 p.

78. Randall, R.B., *Frequency Analysis* 3rd edition ed. 1987: Bruel & Kjaer.

79. S. Timoshenko, S.W.-K., *Theory of plates and shells*. 1959, McGraw-Hill: New York. p. 580.

80. Lutes, L.D. and S. Sarkani, *Stochastic analysis of structural and mechanical vibrations*. 1997, Upper Saddle River, N.J.: Prentice Hall. x, 509 p.

81. Hayashi, C., *Nonlinear oscillations in physical systems*. [Rev. and enl. ed. 1964, New York,: McGraw-Hill. xii, 392 p.

82. Ali H. Nayfeh, B.B., *Applied Nonlinear Dynamics: Analytical, Computational, and Experimental Methods*. 1995, New York: Wiley. 700 p.